

**A non-linear
Reduced Order Methodology
applicable to
Boiling Water Reactor
Stability Analysis**

Zur Erlangung des akademischen Grades
Doktor der Ingenieurwissenschaften
der Fakultät für Maschinenbau
Karlsruher Institut für Technologie (KIT)

genehmigte
Dissertation

von

Dipl.-Math. techn. Dennis Paul Prill

Hauptreferent:
Korreferent:

Prof. Dr.-Ing. habil. Andreas G. Class
Prof. Dr. rer. nat. habil. Ulrich Maas

Tag der mündlichen Prüfung: 06.Dezember 2013

Good character is not formed in a week or a month. It is created little by little, day by day. Protracted and patient effort is needed to develop good character.

(HERACLITUS)

VORWORT

Die vorliegende Arbeit entstand während meiner Tätigkeit als Promotionsstudent der AREVA GmbH am Institut für Kern- und Energietechnik (IKET) des Karlsruher Institut für Technologie (KIT). Die Arbeit wurde im Rahmen der AREVA Nuclear Professional School (ANPS) gefördert und von Herrn Prof. Dr.-Ing. habil. Andreas G. Class betreut. Im Rahmen dieser Arbeit wurde ich von zahlreichen Personen unterstützt, wofür ich mich an dieser Stelle bedanken möchte.

Herrn Prof. Dr.-Ing. habil. Andreas G. Class danke ich besonders für die Anregung zu dieser Arbeit, die wissenschaftliche Förderung, die stets vorhandene Diskussionsbereitschaft und für die Übernahme des Hauptreferates. Zahlreicher Gedankenaustausch hat erst zum Erfolg dieser Arbeit beigetragen.

Für die freundliche Übernahme des Korreferates gebührt mein ganz besonderer Dank Herrn Prof. Dr. rer. nat. habil. Ulrich Maas vom Institut für Technische Thermodynamik (ITT). Bei Frau Prof. Dr.-Ing. Bettina Frohnäpfel des Institutes für Strömungslehre bedanke ich mich die Übernahme des Prüfungsvorsitzes.

Bei Herrn Dr.-Ing. Franz Wehle der AREVA GmbH möchte ich mich herzlichst für die vielen Diskussionen und Anregungen bedanken. Die Unermüdlichkeit in der Erörterung technischer und wissenschaftlicher Fragestellungen hat maßgeblich zum Erfolg dieser Arbeit beigetragen. Des Weiteren möchte ich mich bei Herrn Prof. Dr.-Ing. Thomas Schulenberg, dem Institutsleiter des IKETs, für die Möglichkeit bedanken, diese Arbeit im Rahmen der ANPS an seinem Institut fertig zustellen. An dieser Stelle gebührt auch ein herzlichstes Danke der AREVA GmbH für die Finanzierung und die Zusammenarbeit.

Für die stetige Hilfsbereitschaft und das hervorragende Arbeitsklima möchte ich mich bei all meinen Kolleginnen und Kollegen im IKET bedanken. Besonders bedanken möchte ich mich bei Markus Stokmaier für die unzähligen Diskussionen. Nicht zu vergessen ist Dr.-Ing. Christian Bruzzese, welcher mir immer mit Rat und Tat zur Seite stand. Ganz besonders möchte ich auch allen danken, die an der Korrektur meiner Arbeit teilnahmen, u.a. Dr.-Ing. Christian Bruzzese, Stephan Gabriel, Christoph Schneider, Markus Stokmaier und Mathias Viellieber.

Ein besonderer Dank gilt meiner Familie für die Unterstützung und den Zuspruch während der Zeit meines Studiums und darüber hinaus. Mein größter Dank allerdings gebührt Christine, die mich in den vergangenen Jahren, auch in schwierigen Phasen, unterstützt, angetrieben und aufgemuntert hat. Ohne sie wäre dies alles nicht möglich gewesen.

Karlsruhe,
im Dezember 2013

Dennis Paul Prill
Karlsruher Institut für Technologie (KIT)

KURZFASSUNG

Das Stabilitätsverhalten von Siedewasserreaktoren (SWRs) ist geprägt durch die thermohydraulische Kopplung zwischen Leistung, Massenstrom und Dichteverteilung, welche durch die neutronenphysikalische Rückkopplung noch verstärkt wird. Bei niedrigen Massenströmen und hohen Leistungen kann in Verbindung mit ungünstigen Leistungsverteilungen der SWR zu instabilen Betriebszuständen neigen, welche Leistungsoszillationen auslösen können. Nur durch detaillierte Kenntnis und sorgsame Analyse der zugrunde liegenden Wechselwirkungen können solche instabilen Betriebszustände vermieden werden.

Eine umfassende Analyse der relevanten Einflussgrößen des nichtlinearen Verhaltens von SWRs ist erst durch den Einsatz ordnungsreduzierter Modelle (ROMs) möglich, welche darüber hinaus auch bezüglich der Rechenzeit großen Vorteile bieten. In der Reaktordynamik gibt es bisher keine allgemeine und automatisierte Methodik um hochdimensionale ROMs detailgetreuer SWR-Modelle abzuleiten. In dieser Arbeit wird eine systematische und in sich geschlossene modellordnungsreduzierende (MOR) Methodik entwickelt, welche allgemein auf verschiedenste dynamische Probleme anwendbar ist und im Speziellen auf das Stabilitätsverhalten von SWRs.

Die Grundlage der Methodik basiert auf Expertenwissen, welches sowohl durch betriebliche, experimentelle, als auch durch numerische Transienten gegeben sein kann, und diese Daten in eine optimale Gestalt (Basisfunktionen) überführt. Die Methodik ist größtenteils automatisiert und liefert den Rahmen zur Reduzierung beliebig komplexer Systeme mit überschaubarem Aufwand. Sie ist als Quellcode in Matlab implementiert und koppelt kommerzielle Software verschiedenster Art. Der gitterfreie Ansatz dieser Methodik reduziert ein komplexes System zu einem ROM, welches in der Lage ist, nichtlineare Effekte zu erfassen. Eine optimale Wahl von Basisfunktionen wird dabei durch die sogenannte Proper Orthogonal Decomposition (POD) bereitgestellt. Ein zuverlässiges und stabiles ROM ist durch wohldefinierte Kalibrierungsschritte erreicht.

Um die Validierung und Verifikation im Hinblick auf eine SWR-Anwendung sicherzustellen, werden repräsentative Testbeispiele systematisch untersucht. Das erste Beispiel hat dabei nichtlinearen und dispersiven Charakter. Ein weiteres generisches Zwei-Zonen-Modell behandelt den transienten Übergang zwischen zwei verschiedenen Gebieten. Zusätzlich werden zwei stark nichtlineare Systeme analysiert: Der Durchflussreaktor (tubular reactor), welcher Arrhenius-Reaktionsterme und Wärmeverluste aufweist, zeigt empfindliches Systemverhalten bezüglich sich zeitlich verändernden Randbedingungen. Weiterhin wurde ein Naturkonvektionskreislauf ausgewählt, dessen dynamisches Verhalten durch Grenzzyklen gekennzeichnet ist, was die validationsrelevante Ähnlichkeit zur SWR-Dynamik sicherstellt.

Aufbauend auf diesen essentiellen Grundlagen, werden in dieser Arbeit erste grundlegende Implementierungsschritte hin zu einem SWR-POD-ROM erarbeitet. Hierbei bilden die thermohydraulischen Erhaltungsgleichungen die Basis für die Modellierung des homogenen Gleichgewichtsmodells (HEM).

ABSTRACT

Thermal-hydraulic coupling between power, flow rate and density, intensified by neutronics feedback are the main drivers of boiling water reactor (BWR) stability behavior. High-power low-flow conditions in connection with unfavorable power distributions can lead the BWR system into unstable regions where power oscillations can be triggered. This important threat to operational safety requires careful analysis for proper understanding.

Analyzing an exhaustive parameter space of the non-linear BWR system becomes feasible with methodologies based on reduced order models (ROMs), saving computational cost and improving the physical understanding. Presently within reactor dynamics, no general and automatic prediction of high-dimensional ROMs based on detailed BWR models are available. In this thesis a systematic self-contained model order reduction (MOR) technique is derived which is applicable for several classes of dynamical problems, and in particular to BWRs of any degree of details.

Expert knowledge can be given by operational, experimental or numerical transient data and is transferred into an optimal basis function representation. The methodology is mostly automated and provides the framework for the reduction of various different systems of any level of complexity. Only little effort is necessary to attain a reduced version within this self-written code which is based on coupling of sophisticated commercial software. The methodology reduces a complex system in a grid-free manner to a small system able to capture even non-linear dynamics. It is based on an optimal choice of basis functions given by the so-called proper orthogonal decomposition (POD). Required steps to achieve reliable and numerical stable ROM are given by a distinct calibration road-map.

In validation and verification steps, a wide spectrum of representative test examples is systematically studied regarding a later BWR application. The first example is non-linear and has a dispersive character. Another generic model treats transient transition between two different regions. Additionally, two strongly non-linear systems are analyzed: The tubular reactor (TR), including an Arrhenius reaction term and heat losses, yields sensitive system response on transient boundary conditions. A simple natural convection loop is considered due to its dynamical similarities to BWRs. It exhibits bifurcations resulting in limit cycles.

This thesis further covers a first mandatory step towards a BWR-POD-ROM focusing on elementary thermal-hydraulics described by the homogeneous equilibrium model (HEM).

PUBLICATIONS

This doctoral thesis is based on following publications of the last three years:

1. D.P. Prill, A.G. Class, and M. Stokmaier. Methodology of reduced order modeling applying proper orthogonal decomposition of BWR fuel assemblies applied to introductory examples. Proceedings in Applied Mathematics and Mechanics (PAMM), 12 (1), 2012. URL <http://onlinelibrary.wiley.com/doi/10.1002/pamm.201210109/abstract;jsessionid=A83C749FD1BEA6E9C1DBFB1826530167.d04t03>
2. D.P. Prill and A.G. Class. Analysis of Non-linear BWR Stability Behavior Applying Proper Orthogonal Decomposition. In Annual Meeting on Nuclear Technology, Stuttgart, Germany, May 2012
3. D.P. Prill and A.G. Class. Application of reduced order modeling to BWR fuel assemblies. In The 9th International Conference on Nuclear Thermal Hydraulics, Operations and Safety (NUTHOS-9), Kaohsiung, Taiwan, September 2012
4. D.P. Prill and A.G. Class. Progress of non-linear proper orthogonal decomposition reduced order modeling for BWR fuel assemblies. In European Nuclear Conference (ENC), Manchester, United Kingdom, December 2012. URL <http://www.euronuclear.org/events/enc/enc2012/transactions/ENC2012-transactions-plant-operations.pdf>
5. D.P. Prill, A.G. Class, and M.J. Stokmaier. Report on grid-free pool model. In Thermal Hydraulics of Innovative Nuclear Systems (THINS) WP2 - Deliverable D2.1.07, 2013
6. D.P. Prill and A.G. Class. Non-linear Proper Orthogonal Decomposition Reduced Order Modeling: Bifurcation Study of a Natural Convection Circuit. Proceedings in Applied Mathematics and Mechanics (PAMM), 13, 2013
7. D.P. Prill and A.G. Class. Semi-automated POD-ROM non-linear analysis for future BWR stability analysis. Annals of Nuclear Energy, 2013. URL <http://www.sciencedirect.com/science/article/pii/S0306454913006063>
8. D.P. Prill and A.G. Class. Predictions by the Proper Orthogonal Decomposition reduced order methodology regarding non-linear BWR stability. In Annual Meeting on Nuclear Technology, Berlin, Germany, May 2013
9. D.P. Prill and A.G. Class. Verification of non-linear Proper Orthogonal Decomposition Reduced Order Modeling for BWR Fuel Assemblies. In 21th International Conference on Nuclear Engineering (ICONE21), number 16434, Chengdu, China, July 29- August 2 2013
10. A.G. Class and D.P. Prill. Semi-automatic reduced order models from expert defined transients. In American Physical Society: 66th Annual Meeting of the APS Division of Fluid Dynamics, November 24-26 2013
11. D.P. Prill, A.G. Class, and M.J. Stokmaier. On Grid-free pool models using proper orthogonal decomposition based reduced order models. In International Workshop on Thermal Hydraulics of Innovative Nuclear Systems (THINS), Modena, Italy, January 20-22 2014. (abstract accepted)

CONTENTS

Preface	iv
Abstract (german)	vi
Abstract (english)	viii
Publications	x
Contents	xiii
Nomenclature	xv
1 Introduction	1
1.1 Subject of this thesis	1
1.1.1 Fundamental issue	1
1.1.2 Particular issue regarding boiling water reactors	1
1.2 On general approaches for stability analysis of boiling water reactors	3
1.3 Aim of this thesis	4
1.4 Outline of this thesis	7
2 Boiling water reactor models	9
2.1 Detailed boiling water reactor model	10
2.1.1 Applied commercial codes	10
2.2 Simplified BWR model	11
2.2.1 Instabilities	11
2.2.2 Description	14
2.3 Simplified reduced BWR models	14
2.3.1 Recent developments	14
2.3.2 Summary of significant details	15
2.3.3 Currently applied stability analysis	17
2.4 Towards a new BWR ROMing agenda	18
2.4.1 Discussion of recent developments	18
2.4.2 Towards a BWR reduced order modeling agenda	19
3 Towards an optimal choice of reduction method	23
3.1 Spectral methods	24
3.1.1 Trial functions	24
3.1.2 Weighted residual approaches	24
3.1.3 About the optimality of test and trial functions	24
3.2 Currently applied decomposition methods in modal order reduction	25
3.2.1 Dynamic mode decomposition	25
3.2.2 Proper orthogonal decomposition	26
3.2.3 Discussion	28

3.3	Proposed methodology	29
4	Codes and Methods	31
4.1	Full order model solution	32
4.1.1	COMSOL Multiphysics	32
4.1.2	General partial differential equation formulation	32
4.1.3	Boundary conditions	33
4.1.4	Finite element method	33
4.1.5	Weak formulation	34
4.1.6	Independence of the numerical scheme	34
4.2	Verification of the implementation of the full order model	34
4.2.1	Linear stability analysis	35
4.2.2	The eigenvalue solver	36
4.2.3	Linear stability map	37
4.3	Proper orthogonal decomposition procedure to attain reduced order models	37
4.3.1	Attaining full order model data	38
4.3.2	Spectral expansion by proper orthogonal decomposition	38
4.3.3	Galerkin Projection	40
4.3.4	Stability preserving for continuous projections	42
4.3.5	Anti-Aliasing	45
4.3.6	Higher order derivatives	46
4.3.7	Calibration road map	46
4.4	Code structure sketches	46
4.5	Errors	47
5	Validation and Verification	53
5.1	Soliton waves	55
5.1.1	Model and properties	55
5.1.2	Reduced order models of shallow water waves	57
5.1.3	Performance	60
5.2	Free surface waves after a diffusor	64
5.2.1	Two-zone model	64
5.2.2	Full order model implementation	66
5.2.3	Proper orthogonal decomposition analysis	67
5.2.4	Two-zone reduced order model	68
5.3	Natural convection in a closed circuit	72
5.3.1	Configuration	73
5.3.2	Conservation equations	73
5.3.3	Verification of the implementation	77
5.3.4	Non-linear characteristics	78
5.3.5	POD based ROM for the NCC	82
5.3.6	Two NCC-POD-ROM transients	85
5.3.7	Conclusions	88
5.4	Tubular reactor	89
5.4.1	Full order model data	89
5.4.2	Discretization	91
5.4.3	Analysis of different kernel choices	91
5.4.4	Reconstructions: mean excluded (ANA:a)	94
5.4.5	Prediction Capabilities: mean excluded (ANA:a)	99
5.4.6	Reconstructions: mean included (ANA:b)	101

5.4.7	Prediction Capabilities: mean included (ANA:b)	103
5.4.8	Conclusions	104
6	Towards BWR-application	107
6.1	Thermal-hydraulic system	108
6.1.1	Characterization of the fluid	108
6.1.2	Fluid properties	110
6.1.3	Derivation of the equation system	111
6.1.4	Non-dimensional groups	118
6.2	Implementation and verification	119
6.2.1	Solberg Experiment	120
6.2.2	Implementation	120
6.2.3	Validation	121
6.3	Application of the POD-ROM methodology	122
6.3.1	Perturbation of a linear stable operation point	122
6.3.2	Snapshot basis	124
6.3.3	Comparison of oscillation modes	124
6.3.4	A reformulation of the HEM	126
6.3.5	HEM-POD-ROM system	128
6.3.6	Results	129
6.3.7	Discussion	131
7	Conclusions and recommendation for future work	133
	Appendix	
A	Implementation of the dynamic mode decomposition	137
B	Further enhancements of proper orthogonal decomposition reduced order models	139
B.1	Multi variable expansion by tensor decomposition	139
B.2	Boundary conditions within a variational problem	140
B.3	Inner product choices	140
B.4	Aliasing	140
C	Reformulation of the homogeneous equilibrium model based on an auxiliary equation	143
	Bibliography	147

NOMENCLATURE

ACRONYMS

1D	<i>one-dimensional</i>
2D	<i>two-dimensional</i>
3D	<i>three-dimensional</i>
ADS	<i>accelerator driven system</i>
APRM	<i>average power range monitor</i>
BIFDD	<i>bifurcation formulae for delay-differential system</i>
BWR	<i>boiling water reactor</i>
CC	<i>correlation coefficient</i>
CFD	<i>computational fluid dynamics</i>
CHF	<i>critical heat flux</i>
DAE	<i>differential algebraic equation</i>
DFM	<i>drift flux model</i>
DMD	<i>dynamic mode decomposition</i>
DNS	<i>direct numerical simulation</i>
DWO	<i>density-wave oscillation</i>
EV	<i>eigenvalue</i>
EVD	<i>eigenvalue decomposition</i>
FA	<i>fuel assembly</i>
FDE	<i>functional differential equation</i>
FDM	<i>finite differences method</i>
FE	<i>finite element</i>
FEM	<i>finite element method</i>
FOM	<i>full order model</i>
HEM	<i>homogeneous equilibrium model</i>
HOSVD	<i>higher-order singular value decomposition</i>
HPLWR	<i>high performance light water reactor</i>
KATHY	<i>multi-function thermal-hydraulic test loop in Karlstein</i>
KdV	<i>Kortweg-de-Vries</i>
LES	<i>large eddy simulation</i>
LPRM	<i>local power range monitor</i>
ME	<i>maximum error</i>
MOR	<i>model order reduction</i>
NCC	<i>natural convection in a closed circuit</i>
NPCH	<i>phase-change number</i>
NSUB	<i>sub-boiling number</i>
ODE	<i>ordinary differential equation</i>
PDE	<i>partial differential equation</i>
PDO	<i>pressure-drop oscillation</i>
PID	<i>proportional-integral-derivative</i>

POD	<i>proper orthogonal decomposition</i>
POI	<i>point of interest</i>
POM	<i>proper orthogonal mode</i>
RMSE	<i>root mean square error</i>
ROM	<i>reduced order model</i>
SCRAM	<i>safety control rod axe man</i>
SIMPLE	<i>semi-implicit method for pressure linked equations</i>
SOTA	<i>state-of-the-art</i>
SVD	<i>singular value decomposition</i>
TOBI	<i>time domain analysis of BWR instability</i>
TR	<i>tubular reactor</i>
WST	<i>water steam table</i>

GENERAL SYMBOLS

$\langle \cdot, \cdot \rangle$	<i>inner product</i>
$\langle \cdot, \cdot \rangle_{H^1}$	<i>continuous H^1 inner product</i>
$\langle \cdot, \cdot \rangle_{L^2}$	<i>continuous L^2 inner product</i>
$\langle \cdot, \cdot \rangle_{\Omega}$	<i>integration over domain Ω</i>
$\langle \cdot, \cdot \rangle_T$	<i>integration over domain T</i>

LATIN SYMBOLS

A	<i>flow cross-section or arbitrary matrix associated with an equation system</i>
a	<i>$a = (\alpha_1, \dots, \alpha_r)$ matrix of coefficients or constant wave speed</i>
A_0	<i>linearized equation matrix</i>
\tilde{A}	<i>matrix depending on amplitudes α_i and on time</i>
A_{x-s}	<i>cross-sectional flow area</i>
B	<i>arbitrary matrix associated with an equation system</i>
B_0	<i>linearized equation matrix</i>
\tilde{B}	<i>boundary operator</i>
C	<i>arbitrary vector associated with an equation system</i>
C_i	<i>inlet concentration</i>
c_p	<i>specific heat capacity of an incompressible fluid</i>
\overline{CC}	<i>temporal mean of correlation coefficient</i>
CC	<i>correlation coefficient at time t</i>
d	<i>diameter</i>
D_1	<i>parameter in the KdV-diffusor setup</i>
D_2	<i>parameter in the KdV-diffusor setup</i>
d_a	<i>damping (mass) coefficient</i>
D_H	<i>hydraulic diameter</i>
dA	<i>volume element</i>
Δh_{SUB}	<i>inlet sub-cooling</i>
$\partial p / \partial \varphi$	<i>pressure gradient</i>
dS	<i>surface element</i>
E	<i>quantity representing energy conservation in KdV</i>
e	<i>inner energy</i>
e_a	<i>mass coefficient</i>

F	$F_i = \langle f, \phi_i \rangle$ matrix of source term projections
f	source term
\tilde{F}	matrix depending on amplitudes α_i and on time
\tilde{f}	source function not depending on u
f_w	friction force
f_{w0}	friction transfer coefficient
G	source or mass flux term
g	local gravity
g_{eff}	vertical gravitational component
H	regional $H(x)$ or temporal $H(t)$ jump function (KdV) or substitution for heat transfer within energy equation (NCC)
h	enthalpy, contour of the upper wall of the diffusor, water depth or boundary values
h_0	initial height of the diffusor
h_{in}	inlet enthalpy
h_w	heat transfer coefficient
K	control parameter
K_0	fundamental kernel for data only
K_1	fundamental kernel for first derivatives only
K_2	fundamental kernel for second derivatives only
K_s	generalized modified Sobolev kernel
\tilde{K}_s	generalized modified Sobolev kernel
k_x	volume force in x -direction
\mathbf{L}	$\mathbf{L}_{ij} = \langle \mathcal{L}\phi_i, \phi_j \rangle$ matrix of linear projections
L	length of the flow channel
l	reduction level or radius of the circuit
L_e	length of the reactor
\mathcal{L}	linear differential operator
m	number of spatial grid points or quantity representing mass conservation in KdV or slope of the diffusor
\mathbf{N}	$\mathbf{N}_i(a) = \langle \mathcal{N}(\sum_{i=1}^r \alpha_i \phi_i), \phi_j \rangle$ matrix of non-linear projections
N	number of soliton solutions
\mathbf{n}	normal vector
n	number of snapshots
\mathcal{N}_2	(non-linear) quadratic operator
\mathcal{N}_3	(non-linear) cubic operator
\mathcal{N}	non-linear operator
\tilde{N}	grid element of discretization of FEM
$\mathcal{O}(i)$	order of i
p	pressure or quantity representing momentum conservation in KdV
p_0	inlet pressure
p_d	dynamic pressure
P_f	wetted perimeter
P_H	heated perimeter
p_{loss}	enforced constant pressure drop of the channel
P_m	form (shape) or Ansatz function of FEM
\dot{Q}	combination of all source terms (depending on φ)
\dot{q}	volumetric power distribution (depending on φ)
\tilde{Q}	dimensionless parameter for source term
\bar{q}'	uniform power profile

R	<i>constraint</i>
r	<i>Dirichlet boundary condition or truncation criterion</i>
r^C	<i>truncation criterion for concentration field</i>
r^T	<i>truncation criterion for temperature field</i>
r^u	<i>truncation criterion for velocity field</i>
\overline{RMSE}	<i>temporal mean of root mean square error</i>
$RMSE$	<i>root mean square error at time t</i>
T	<i>temporal domain or (dimensionless) temperature distribution</i>
t	<i>(dimensionless) time</i>
T_0	<i>temperature of the incompressible fluid</i>
T_{end}	<i>length of time interval</i>
t_h	<i>temporal step size</i>
T_i	<i>inlet temperature</i>
T_w	<i>wall temperature</i>
u	<i>single dependent variable, snapshot, nondimensional height (KdV), flow velocity in x-direction</i>
u'	<i>fluctuation field</i>
U_i	<i>coefficients of FEM</i>
u_M	<i>approximate numerical solution truncated at M</i>
u_r	<i>approximate numerical solution truncated at r</i>
u_s	<i>speed of sound</i>
\tilde{u}	<i>dimensionless flow velocity (NCC) or density-weighted cross-sectional averaged velocity</i>
\tilde{u}_i	<i>i-th eigenfunction, left singular vector</i>
\tilde{u}_{in}	<i>inlet velocity</i>
u_x	<i>first derivative of u with respect to x</i>
u_{xx}	<i>second derivative of u with respect to x</i>
v	<i>specific volume, velocity in y-direction or substitution for u_{xx}</i>
\dot{V}	<i>inlet volume flow depending on time</i>
\tilde{v}_i	<i>i-th eigenfunction, right singular vector</i>
\vec{f}	<i>volume force</i>
\vec{v}	<i>velocity vector $\vec{v} = (u, v)^T$</i>
w	<i>velocity in z-direction</i>
X	<i>quality</i>
x	<i>spatial position</i>
d	<i>depth of the KdV-diffusor setup</i>
x_g	<i>time-dependent interface</i>
x	<i>dimensionless axial distance</i>
x_h	<i>spatial grid</i>

GREEK SYMBOLS

α	<i>small arbitrary constant (KdV) or fluid-wall parameter (NCC)</i>
α_0	<i>thermal expansion of the incompressible fluid</i>
α_i^T	<i>i-th temporal function for temperature</i>
α_i^u	<i>i-th temporal function for velocity</i>
α_i	<i>i-th temporal function</i>
β	<i>heating parameter</i>
β^0	<i>heat input value where two solutions branch off symmetrically</i>

β_{all}	<i>complete heat input value for a un/rotated system</i>
β^*	<i>heat input value for Hopf bifurcation point where the stable steady state solution becomes unstable with respect to oscillatory disturbances</i>
β_1^*	<i>heat input value for Hopf bifurcation point where the preferred solution becomes unstable</i>
β_2^*	<i>heat input value for Hopf bifurcation point where the isolated solution becomes unstable</i>
β^{HO}	<i>heat input value for homoclinic orbit</i>
β^{LP}	<i>heat input value/limit point for change of direction of the preferred steady state solution</i>
δ	<i>tilting/symmetry angle</i>
$\delta_{\partial\Omega}$	<i>indicator function marking the boundary $\partial\Omega$</i>
ΔT	<i>forcing temperature $\Delta T = T_H(\varphi) - T_C(\varphi)$</i>
$\nabla \cdot$	<i>divergence operator</i>
ε	<i>mean height of the roughness of underlying steel</i>
ε_0	<i>generalized Sobolev weight for kernel K_0</i>
ε_1	<i>generalized Sobolev weight for kernel K_1</i>
ε_2	<i>generalized Sobolev weight for kernel K_2</i>
η	<i>height of the free surface</i>
$\eta + h$	<i>elevation of the surface above the bottom</i>
Γ	<i>diagonal matrix of penalty parameters $(\Gamma^1, \Gamma^2), \dots$</i>
γ	<i>surface tension (KdV) or activation energy (TR)</i>
Γ^C	<i>penalty parameters for concentration field</i>
Γ^T	<i>penalty parameter for temperature</i>
$\tilde{\Gamma}$	<i>conservative flux vector</i>
Γ^u	<i>penalty parameter for velocity</i>
ρ_0	<i>density of the incompressible fluid</i>
Λ	<i>eigenvalues of a linearized problem or substitution within energy equation</i>
λ_0	<i>thermal conductivity of the incompressible fluid</i>
λ_i	<i>eigenvalue</i>
Λ_{Im}	<i>complex part of eigenvalue</i>
Λ_{Re}	<i>real part of eigenvalue</i>
λ_{th}	<i>thermal conductivity</i>
μ	<i>dynamic viscosity or heat transfer coefficient (TR)</i>
μ_i	<i>eigenvalue</i>
μ_L	<i>Lagrangian multiplier</i>
∇	<i>gradient, Nabla operator</i>
ν	<i>kinematic viscosity or heat of reaction (TR)</i>
ν_0	<i>kinematic viscosity of the incompressible fluid</i>
$\tilde{\nu}$	<i>arbitrary test function</i>
Ω	<i>subdomain or spatial domain</i>
$\partial\Omega$	<i>boundary of the subdomain Ω</i>
ϕ	<i>dissipation function</i>
ϕ_i^T	<i>i-th proper orthogonal mode for temperature</i>
ϕ_i^u	<i>i-th proper orthogonal mode for velocity</i>
ϕ_i	<i>i-th proper orthogonal mode, spatial component</i>
π	<i>non-dimensional pressure</i>
ψ	<i>vector of unknowns</i>
ψ_0	<i>steady-state solution of the vector of unknowns</i>
$\tilde{\psi}$	<i>eigenfunctions</i>

ρ	<i>density</i>
σ	<i>normal stress</i>
σ_i	<i>i-th singular value</i>
φ	<i>space coordinate of the circuit</i>
τ	<i>dimensionless parameter for temperature or amplitude of the symmetric τ-periodic solution</i>
τ	<i>shear stress</i>
2τ	<i>amplitude of the symmetric 2τ-periodic solution</i>
$2^n\tau$	<i>amplitude of the symmetric $2^n\tau$-periodic solution</i>
$3\tau^+$	<i>amplitude of the mirror symmetric $3\tau^+$-periodic solution</i>
$3\tau^-$	<i>amplitude of the mirror symmetric $3\tau^-$-periodic solution</i>
ϑ_i	<i>Ansatz functions of the FEM</i>
ξ	<i>Darcy-Weisbach friction factor</i>

INDICES

f	<i>saturated liquid</i>
g	<i>saturated steam</i>
H	<i>heated part of flow channel</i>
i	<i>spatial coordinate $i = \{1, 2, 3\} = \{x, y, z\}$ or index</i>
j	<i>index</i>
k	<i>index</i>
$-$	<i>cross-sectional averaged quantity</i>
$'$	<i>local deviation of a cross-sectional averaged quantity</i>
\sim	<i>density-weighted cross-sectional averaged</i>

CHARACTERISTIC NUMBERS

Da	<i>Damköhler number</i>
Fr	<i>Froude number</i>
Λ_{EU}	<i>Euler number</i>
Ma	<i>Mach number</i>
N_{PCH}	<i>phase-change number</i>
N_{SUB}	<i>sub-cooling number</i>
Pe_h	<i>Peclet number for heat transfer</i>
Pe_m	<i>Peclet number for mass transfer</i>
Pr	<i>Prandtl number</i>
Re	<i>Reynolds number</i>

1 INTRODUCTION

1.1 SUBJECT OF THIS THESIS

1.1.1 FUNDAMENTAL ISSUE

Technological progress can be attributed to a constant urge of gaining insight into increasingly difficult structures and processes. Mankind's unique gifts of accurately analyzing, simplifying and restructuring principles since essential mechanisms are revealed, contribute to detailed knowledge and reliable operation. The general systematic methodology, that is subject of this thesis, reflects this natural approach. It transforms a complex dynamical system into a simple form by analysis. Characteristic behavior is preserved up to a prescribed accuracy goal, and an appropriate simple model is built up in the end. The reduced model is the basis for further analysis and discovery of relevant physical mechanisms.

Complex dynamical systems in industry and research can have sophisticated geometries. Their underlying dynamics can be subject to various interaction of multiple physics. Even simple systems can be affected by non-linear effects. For instance, a closed loop that is filled with a fluid having a heat source at the bottom and a sink at the opposite side. By constantly heating up the circuit, a stable fluid flow can be established without a preferred direction. Accordingly, fluid flows either clockwise or counter-clockwise. By tilting the circuit, a preferred fluid flow direction is chosen. However, this stable flow loses its stability while increasing the heat input at some point. Then, complex chaotic non-linear flow behavior is seen which is characterized by a transition between a faster and slower flow of the fluid but also times where the flow direction might reverse. Depending on the tilting of the geometry and the heat input, flow behavior might resonate or saturate, or even have chaotic transient behavior [40, 41]. Closed dynamical loops play an important role in various industrial applications: In plant construction for power stations in general, or in particular for boiling water reactors (BWRs). This particular system is subject of this thesis. Its system characteristics give a specification of requirements in the derived methodology within this thesis.

The principle technical question that rises so far is whether transient chaotic behavior can partially be accepted within operation, or if it should be strictly forbidden as system security might be violated. An answer to this question can only be given by a model that, on the one hand represents the complex system with sufficient depth, and on the other hand is simple enough such that a vast number of important operational transients can be analyzed. The derived methodology within this thesis helps to derive such reliable simple models.

1.1.2 PARTICULAR ISSUE REGARDING BOILING WATER REACTORS

The boiling water reactor (BWR) is a typical light water reactor. In this complex nuclear system, the heating is provided by a nuclear chain reaction (nuclear fission) in the so-called fuel rods. They are clustered in fuel assemblies (FAs) that are wrapped by boxes. These are placed in the reactor pressure vessel which is of cylindrical form with a hemispherical shape on the top and bottom. Its interior is depicted within Fig. 1.1 and is supplemented by a qualitatively radial power distribution

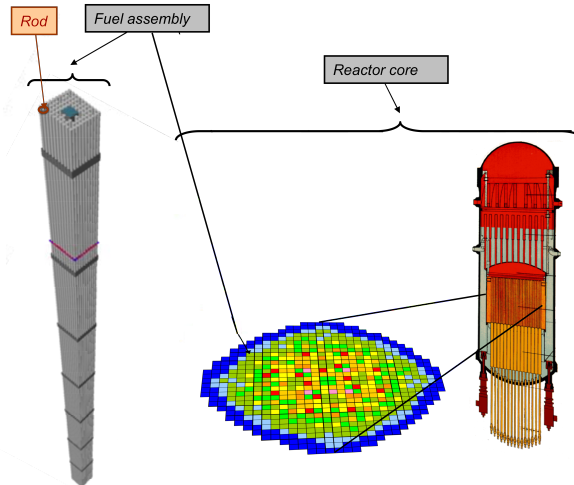


Figure 1.1.: Scheme of the interior of a boiling water reactor: fuel rod, fuel assembly, qualitatively radial power distribution and reactor core [1].

of the reactor core. Circulating water, the so-called moderator, is consecutively heated until boiling. The generated steam is dried in the upper part of the reactor vessel and directed to the turbine. The water is then re-injected into the reactor vessel. A closed-loop setup is established. The core of a modern boiling water reactor (BWR) is loaded by up to 800 fuel assemblies (FAs) with up to 112 fuel rods which consist of low-enriched uranium fuel. Already from a geometrical point of view, the BWR core has immense dimensions including an exceedingly complex and fine-detailed structure.

Furthermore, the BWR system is marked by various involving physical disciplines. The main drivers of BWR stability behavior are characterized by the multiple thermal hydraulic interactions between power, flow rate, and density, reinforced by the neutronics feedback. The tight coupling between the neutronics and the thermal-hydraulics is marked by the void and Doppler feedback reactivities. It is schematically presented in Fig. 1.2.

Due to the boiling process within the BWR, it is subject to two-phase flow. This means that the density distribution of water in the core is never homogeneous and never stationary. It includes shifting water properties with not only heat transfer changes, but also variations in neutrons moderation. Time-varying shifts in thermo-hydraulics and neutronics with corresponding length scales of the size of the reactor itself and their feedback channels as well as time constants are what needs to be carefully dealt with in BWR stability analysis.

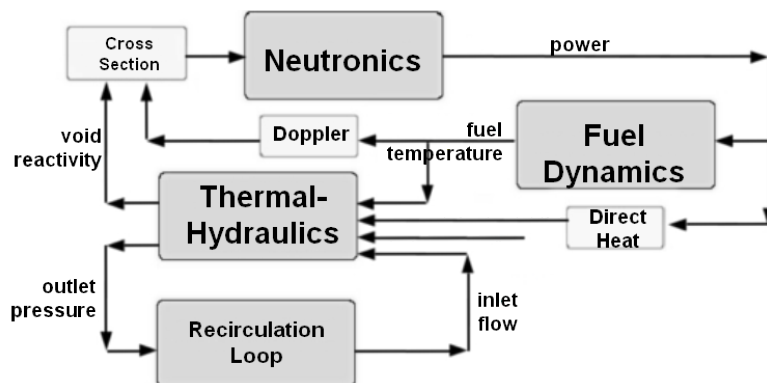


Figure 1.2.: Feedback system in a BWR, redraw of March-Leuba et al. [80].

High-power low-flow conditions in connection with unfavorable power distributions can lead the BWR system into unstable regions where power oscillations can be triggered [27]. System control and performance can therefore be decreased. This important threat to operational safety requires careful analysis for proper understanding.

Unexpected non-linear instability events in various BWR plants, e.g. LaSalle II in 1988 [27], emphasize the major safety relevance and the existence of parameter regions with unstable behavior. During operation at a stable operating point, an erroneous valve opening results in a rapidly growing power oscillation of 25% – 50% with a period of 2 - 3 seconds after 5 minutes. After 7 minutes a safety control rod axe man (SCRAM) was triggered. Other similar BWR instability events have been reported [27], e.g. Oskarshamn II in 1990. Instability events may jeopardize fuel cladding integrity by exceeding the critical heat flux (CHF) leading to dry-out. The essential question of how oscillating behavior can be avoided is addressed by operating utilities and vendors, as well as scientific institutions.

1.2 ON GENERAL APPROACHES FOR STABILITY ANALYSIS OF BOILING WATER REACTORS

Reactors are designed to avoid typical oscillations by design. Additionally, appropriate operating procedures are defined in the operation handbook. These design rules assure admissible reactor operation conditions based on numerous stability experiments, numerical calculations and analytical methods.

Special experiments as well as recorded operational transients are used to calibrate physical models. A model of coupled non-linear partial differential equations (PDEs) is able to represent the non-linear physics and all relevant instability mechanisms of the BWR. Nevertheless, an exhaustively analysis of the non-linear BWR system is expensive due to the huge parameter space. Numerous calculations are required for entirely characterizing the stability and oscillation phenomena of a BWR including non-linear behavior and strong coupling.

State-of-the-art (SOTA) solving strategies, used by vendors and science, are illustrated in Fig. 1.3 and explained below.

- **Level of details (horizontal):**

The treatment of the detailed BWR dynamics is visualized in the box to the very left. Detailed BWR models have a high level of sophistication depending on the applied commercial or industrial software. In general, system codes are applied, simplifying physics and geometry by modeling complete FAs in an one-dimensional (1D) formulation. Proceeding from that point by geometrical considerations, a simplification is achieved, for instance by a reduction to a small number of considered FAs. These so-called simplified BWR models are represented in the center box. By further mathematical and phenomenological considerations, underlying physics of simplified BWR models can be further reduced. In general, transformations rely on various (and often restricted) reduction methods. Simplified reduced BWR models are depicted in the very right box. They focus on the most dominant effects with respect to geometry, neutronics and thermal-hydraulics. Due to the number of different types of simplified reduced BWR models, a distinction can be given by the applied geometry, physical sub-models and/or the mathematical reduction method. Note, that from the left to the right the degree of details of the BWR model is strongly reduced.

- **Analysis types (vertical):**

For any type, i.e. detailed, simplified or reduced simplified BWR models, by an expert choice

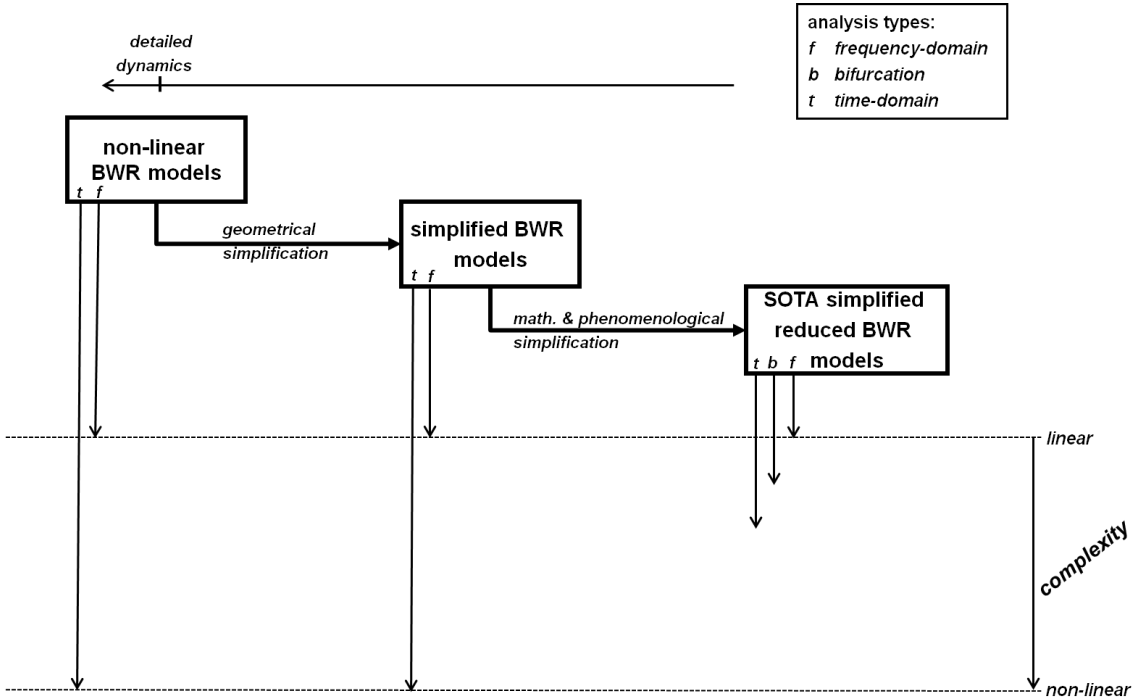


Figure 1.3.: Currently applied models and methods for stability analysis of a BWR.

of transient, the non-linear temporal response of the system can be examined using time-domain analysis. Depending on the level of detail, this can be a rather time-consuming procedure. Frequency domain analysis linearizes the PDEs around the steady-state operating point. It is a rather quick tool but belongs to linear methods and reduces analysis complexity enormously. However, it is applicable to systems of any level of details. Only for low-dimensional state-of-the-art simplified reduced BWR models, the stability character can directly be derived by bifurcation analysis tools. These are methods of non-linear dynamics applicable to ordinary differential equations (ODEs). They can locate various types of stability behavior and continue solution orbits. This enables systematic studies of dynamical models and characterization of system stability relevant parameters [28, 29, 31, 52]. Bifurcation tools might also vary in analysis complexity. Up to now, for a complete non-linear stability analysis of a BWRs, a time-domain analysis of a detailed BWR model is necessary.

1.3 AIM OF THIS THESIS

The level of details is an essential attribute for a reliable BWR model. An accurate numerical system needs to take into account both, geometrical as well as physical details. Expert knowledge strongly influences the accuracy of a model and is hence of vital importance. The choice of operation transients and experiments for calibration of physical models is crucial.

Efforts regarding simplified BWR models are based on simplified physics and drastically reduced geometry. Here, expert knowledge is based on phenomenological decisions.

Time-domain and frequency-domain analyses are powerful tools that allow treating models of any kind. Nevertheless, depending on the level of details, time-domain codes can be rather time-consuming procedures. Moreover, frequency-domain codes linearize around a steady-state operating point and reduce analysis complexity enormous. The step from a simplified model to a simplified

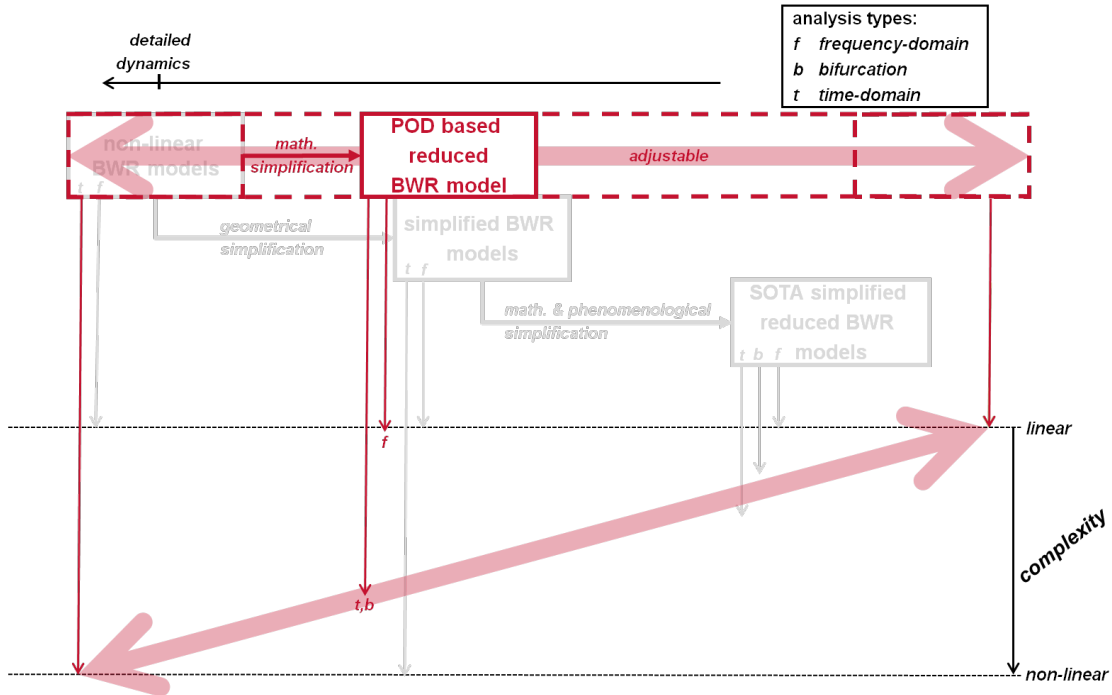


Figure 1.4.: Proposed strategy for attaining proper orthogonal decomposition based reduced order model of BWRs - an adjustable methodology and applicable to detailed or geometry simplified models.

reduced model is generally taken by various types of mathematical reduction methods on the basis of selected operating point information. However, applied methods are often restricted and cannot be adapted to BWR models with higher level of sophistication. Nevertheless, as models have low-dimension, bifurcation tools can be applied to investigate their non-linear stability character.

This motivates the need of an extended methodology based on a general and systematic model order reduction (MOR) technique, yielding an accurate low-cost simulation tool for either the complete or simplified BWR model (or even any other physical model). The methodology that is applied within this thesis hence should complement to the SOTA presented in Fig. 1.3. Incorporation of this methodology fitted into this graphic would result in a completely general and adjustable methodology shown in Fig. 1.4. These reduced order models (ROMs) of appropriate dimension can be solved either by time-domain or frequency-domain analysis but also by bifurcation analysis. Moreover, they can be based on various experimental or numerical data sets. Presently within reactor dynamics, no automatic predictions for such high-dimensional ROMs are available.

OBJECTIVES OF THIS THESIS

Thus, the present thesis has the following **main objective**:

- Development of a general model order reduction (MOR) methodology.

In particular, the methodology should be applicable to BWRs but also to various other types of systems. Moreover, the methodology has to **full-fill** following **fundamental requirements**:

- Generality.
- Ability for complete automation.
- Inclusion of expert knowledge by various operational, experimental as well as numerical data sets.
- Applicability to time-domain, frequency as well as bifurcation analysis.

PROPOSED METHODOLOGY

The proposed methodology is illustrated in Fig. 1.5. It consists of well-defined processing steps. Relevant data selected by an expert choice of transient is exploited. This data is obtained from trajectories of experiments, numerical integration or analytical derivations reflecting the dynamics of the system. The key element of the methodology is the proper orthogonal decomposition (POD) algorithm, which is the essential technique in the mathematical data analysis. The proper orthogonal decomposition (POD) provides a method defining the best approximating subspace to a given set of data. It detects relevant states (modes) which are hidden in transient data. Proper orthogonal modes are extracted and serve as ansatz functions within a Galerkin spectral approach, yielding a reduced order model (ROM).

Note, a complex, time-consuming system which involves numerical difficulty, is mostly automatically transferred to a simplified non-linear ROM which is efficiently solvable. Accordingly, analyzing the system with respect to non-linear stability phenomena becomes feasible with a prescribed accuracy goal. Further investigations like bifurcation analysis, obtaining stability maps, can be achieved.

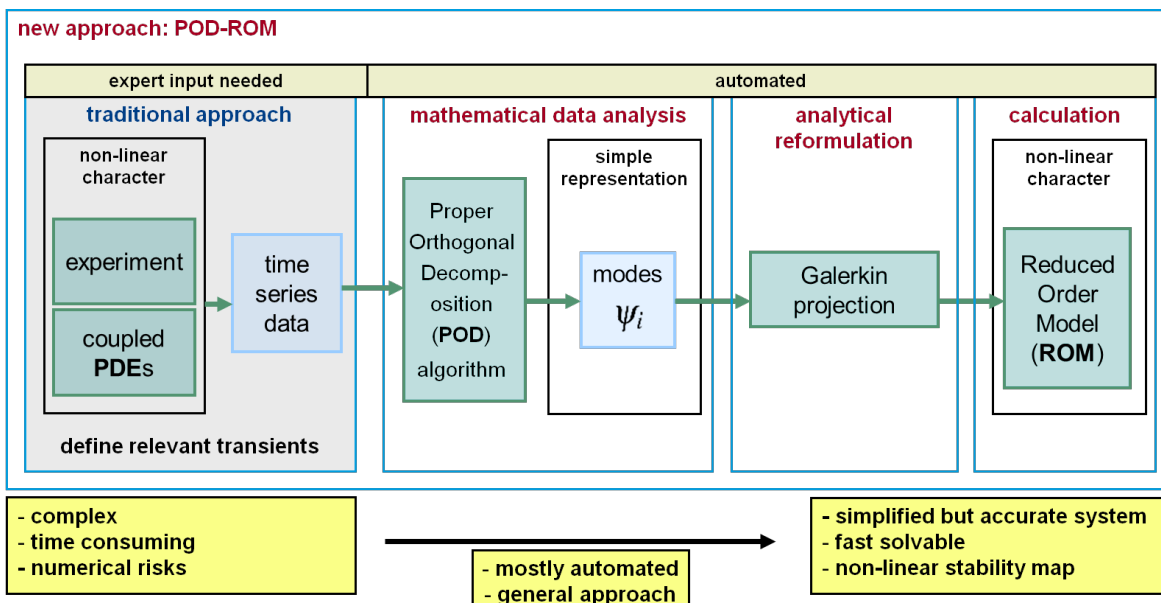


Figure 1.5.: Flow chart of the proposed methodology based on proper orthogonal decomposition.

1.4 OUTLINE OF THIS THESIS

The present thesis is arranged as follows:

Chapter 2: In this chapter, the necessity of a general model order reduction (MOR) methodology based on a systematic technique is motivated and presented in more detail. It follows the description of detailed BWR models towards phenomenological (geometrical) simplified models, and analyzes aspects of these methodologies and further innovative approaches.

Chapter 3: Up to now within reactor dynamics, methodologies generating efficient and minimal ROMs are not available and regarding industrial operation, an automated self-contained methodology is crucial. Within this chapter, the route towards an optimal reduction method is established by introducing so-called spectral methods. By a review of two heavily applied decomposition methods that make use of the underlying dynamics of a system, the so-called proper orthogonal decomposition (POD) is selected and the general methodology is presented.

Chapter 4: This chapter presents a detailed description of the numerical codes and methods used within this thesis. Throughout this thesis, data is generated by the commercial code COMSOL[®] which is introduced in this chapter. Beside focusing on the verification of implementations, this chapter is also occupied with linear stability analysis using the internal COMSOL[®] eigenvalue solver and an external MATLAB[®] routine. A description of the applied POD based ROMing strategy is given in detail. The complete methodology is further summarized and the proposed POD calibration road-map explained. The self-written code structure is presented at the end.

Chapter 5: Within the scope of the envisioned BWR-ROM for stability analysis, a wide spectrum of verification and qualification examples is explored in this chapter. It refers to important validation steps yielding a reliable strategy for deriving ROMs. In particular, four problems are treated that are well-chosen regarding a later BWR application. The first problem is chosen due to its non-linear and dispersive character. By a second problem, questions are treated concerning POD based ROMs with instationary transition between two different regions. A third problem is chosen due to its dynamical similarities compared to BWRs. Last but not least, a system featuring a complex non-linear dynamical behavior is considered as an equivalent test case for perturbation investigations of the BWR system, i.e. against pump trips etc., violating the inlet and outlet conditions. Here, the derived methodology is validated and verified for oscillating phenomena caused by external conditions.

Chapter 6: This chapter gives a first step towards a future BWR-ROM. It considers a thermal-hydraulic equation system that is chosen demonstrating the advantages of the POD-ROM methodology. Although it is not the most sophisticated model to apply for BWR thermal-hydraulics, from a mathematical point of view it already consists of certain hurdles. This chapter includes a mathematical derivation of the underlying thermal-hydraulic system. The implementation is further verified by a comparison to experimental results within a linear stability map. Based on a transient that passes through the boundary of this linear stability map, the route towards a POD based ROM is presented. Focus is put on distinct steps of the POD-ROMing strategy. Questions concerning a suitable snapshot basis are treated, as well as further issues regarding whether appropriate transients for POD based ROMs can robustly be chosen without defining a specific transient history.

Chapter 7: The results of this thesis are summarized and a outlook is given regarding further studies.

2 BOILING WATER REACTOR MODELS

This chapter starts with a short review of detailed boiling water reactor (BWR) models and their simulation. Based on a phenomenological description of possible instabilities within the two-phase BWR system, (geometrical) simplified BWR models are introduced. A further review of the state-of-the-art (SOTA) of simplified reduced BWR models is given and yields a classification. Currently used stability analysis methods are described as well. A discussion about aspect of these methodologies and innovative approaches, motivates the need of an extended methodology based on a systematic model order reduction (MOR) technique, yielding an accurate low-cost simulation tool of either the complete BWR or simplified BWR models. Presently within reactor dynamics, no automatic predictions for such high-dimensional reduced order models (ROMs) are available. Accordingly, the last part explains how the proposed methodology complements the SOTA and fits into Fig. 2.1.

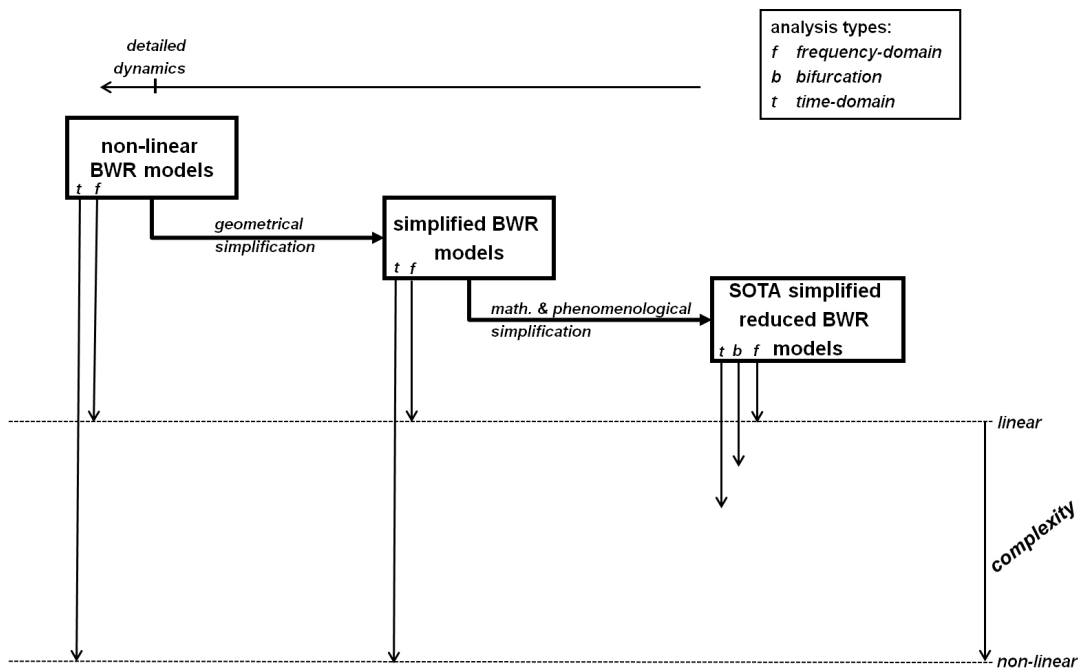


Figure 2.1.: Currently applied models and methods for stability analysis of a BWR.

2.1 DETAILED BOILING WATER REACTOR MODEL

High-power low-flow conditions in connection with unfavorable power distributions can lead the BWR system into unstable regions where power oscillations can be triggered. This important threat to operational safety requires careful analysis for proper understanding.

2.1.1 APPLIED COMMERCIAL CODES

An exhaustively analysis of the non-linear BWR system is very expensive due to the huge parameter space. Various numerous calculations are required for entirely characterizing the stability and oscillation phenomena of a BWR including non-linear behavior and strong coupling.

SYSTEM CODES

Non-linear analysis is usually carried out using industrial or commercial software tools. System codes with a high level of sophistication, i.e. RAMONA, TRACE-PARCS, RELAP-5-PARCS, RETRAN, EPA, SABRE, TRAB, TOSDYN-2, STANDY, SPDA, ATHLET-QABOX/QUBOX and ATHLET-DYN3D are specifically designed to examine the dynamical behavior of the BWR system in time-domain [81, 141]. Since decades, they are applied and improved for analyzing the dynamical behavior of nuclear systems. They can handle complex mathematics that describe the physics of the core such as thermal-hydraulics, neutronics, heat transfer and also the steam line flow dynamics. Moreover, they are based on an accurate core and ex-core geometry and have special models for the down comer, lower and upper plenums, the risers, pumps and the steam dome. Special models for plant protection systems, safety injections and control systems are also included.

Efforts of research and industry of the past half century yield on system codes with a sophisticated degree of accuracy. Various experiments and operational transients are analyzed to improve code reliability. Examples can be given by the multi-function thermal-hydraulic test loop in Karlstein (KATHY) operated by AREVA GmbH since 1993 for instance. It delivers extremely valuable experimental data to full-scale electrical heated fuel assembly (FA) experiments [6]. Occurring BWR neutronic feedbacks can be simulated by the test facility. Stability tests treat linear as well as non-linear behavior [142] and improve time-domain codes, such as RAMONA5-FA and others.

System codes are capable to describe thermal-hydraulics as well as (coupled) neutronics covering a wide spectrum of transients and accident scenarios. Most instability types can be handled, i.e. BWR, parallel channel, density wave instabilities or pressure-drop oscillations. In general, thermal instabilities due to the lack of descriptions of transition and film boiling cannot be analyzed [9].

A huge number of system codes prohibits a detailed description of a single physical model hereafter. A general view on system codes is based on open literature, i.e. RAMONA descriptions [100, 125, 140] among others. In general, neutronics are represented by simplified two-group diffusion theory. They are simulated in three-dimensional (3D) on a coarse finite-difference mesh representing each individual FA with additional empirical expressions. For each neutronic node, fuel thermodynamics calculate the heat flux to the cladding. Heat conduction in the fuel pin is only based on radial direction. Thermal-hydraulics consist, depending on the system code, on three, four or six equation, (non-)homogeneous, (non-)equilibrium, one-dimensional (1D) two-phase flow models with additional constitutive equations. Acoustics are in general disregarded. This system is extended by various special models for pumps, steam generators, condensers and many more. Although system codes are limited through numerical methods and mesh resolution, they satisfactorily predict the 3D interaction between thermal-hydraulics and neutronics within the core, as well as the impact of primary and secondary systems within the whole nuclear power plant.

FREQUENCY CODES

Codes like LAPUR, NUFREQ or FABLE, are rarely used frequency-domain codes and are based on a linearization about the steady-state. A complete description of such codes can be found in [81]. For instance, MATSTAB [56] is based on the thermal-hydraulic model of RAMONA-3B and the 3D neutronic model of POLCA. Core-wide and regional oscillations can be studied and analyzed in frequency-domain. Although these codes are rather quick tools accomplishing linear stability behavior, they belong to linear methods and diminish the system complexity enormous. Note that a complete stability analysis needs the application of time-domain codes [33].

2.2 SIMPLIFIED BWR MODEL

Time-domain analysis, stability experiments and operating experience demonstrate that the most encountered BWR instabilities are either of channel flow or of coupled neutronic-thermalhydraulic type [81]. Both belong to a certain fundamental instability, the so-called density-wave oscillation (DWO). A detailed review of all instability phenomena is beyond the scope of this section. However, a short review of possible two-phase flow and BWR instabilities should provide the reader a feeling of the most important stability features, especially in terms of geometry and physics, relevant for a (geometrical) simplified BWR model description (and later derived reduced versions, see Sec. 2.3).

2.2.1 INSTABILITIES

Thermally induced two-phase flow instabilities are of concern for various industrial fields, such as chemical-processing, steam generators, refrigeration plants, thermo siphons, re-boilers and also includes BWR operation. Boiling, condensation as well as adiabatic flows are the basis for instabilities. They depend on design features, flow, controlling and special feedback mechanisms [9, 61, 98]. In the following with the view to BWRs, instabilities will be categorized in two groups:

- neutronically decoupled cases (i.e. two-phase flow instabilities),
- and coupled cases (i.e. BWR instabilities).

TWO-PHASE FLOW INSTABILITIES

In 1973, two-phase flow instabilities were reviewed by Bouré et al. [9]. They classified different types and distinguished between different stability analysis methods. In 1993, Lahey Jr. and Moody [68] published a book about thermal-hydraulics of boiling water nuclear reactors. Summaries of analysis methods for different types of instability phenomena are given among others. On the basis of Bouré et al. [9], a more comprehensive classification of types of instabilities is given by Lahey Jr. et al. [69] and Bergles [7]. Also, Ortega Gómez [98] described relevant thermal-hydraulic instability phenomena concerning supercritical reactors, i.e. in particular the high performance light water reactor (HPLWR). Kakac and Bon [61] gave a review about thermally induced flow instability in two-phase flow systems in 2008. Similar to Bouré et al., they distinguished between different types and the mathematical modeling of instabilities. Correspondingly, a classification of two-phase flow instabilities, having constant heat input, will be given according to Bouré et al. [9], Kakac and Bon [61] and also Lahey Jr. and Moody [68] in the following.

A linear stable steady flow is given, provided that by a perturbation the new operating condition tends asymptotically towards the previous. If small perturbations damp than the steady-state flow is linear stable. A steady-state flow is subject to a static instability since by a small perturbation

another steady-state is not possible. Then, the original operating point is a stable equilibrium point. A flow is subject to a **dynamic instability** due to interactions between delayed feedbacks of inertia of the flow and compressibility, or multiple feedbacks such as flow rate, pressure-drop or changes in density evoked by time-varying heat input [9, 61]. A first classification is hence given by distinction into static and dynamic instabilities:

- The first type can be explained by steady-state laws. Static instabilities result in different steady-states or periodic behavior. They can be characterized by flow excursion (Ledinegg) instability, flow pattern transition instability or bumping, geysering, or chugging.
- To predict the threshold of dynamic instabilities, **time-dependent** systems are needed for analyzing. They manifest in an interaction of inertia and feedback mechanism. Fundamental dynamic instabilities can be characterized as: density-wave type oscillations and acoustic (or pressure-wave) type oscillations. Their mechanism can be explained by the time delay of propagation of a disturbance and an immediately feedback when arriving at the end of the configuration. At this, two different types of disturbance transport processes can be clearly distinguished: pressure/acoustic and void/density waves. Both types are present in systems but they act on different scales. Due to their dissimilar order of magnitude of wave velocities, a distinction is possible.

A flow instability is fundamental if only one mechanism triggers the process. Instead compound instabilities are triggered by several elementary mechanisms. The various flow instabilities are classified in Tab. 2.1.

Table 2.1.: Classification of instabilities and some physical types, extract of Bouré et al. [9].

class	type	mechanism	characteristics
1. static instabilities			
1.1 fundamental static	Ledinegg instability	slope of the (internal) channel demand (pressure-drop versus flow rate) curve is negative and steeper than the (external) loop supply curve and multiple intersects	flow undergoes sudden large amplitude excursion to a new, stable operating condition
2. dynamic instabilities			
2.1 fundamental dynamic	acoustic oscillations	resonance of pressure waves	high frequency (10 – 100Hz) related to time required for pressure wave propagation in system
	density wave oscillation	delay and feedback effects in relationship between flow rate, density, and pressure drop	low frequency (1Hz) related to transit time of a continuity wave
2.2 compound dynamic as secondary phenomena	pressure drop oscillations	flow excursion initiates dynamic interaction between channel and compressible volume	very low frequency periodic process (0.1Hz)
2.3 compound dynamic as primary phenomena	parallel channel instability	interaction among small number of parallel channels	various modes of flow redistribution
	BWR instability	interaction of void reactivity coupling with flow dynamics and heat transfer	strong only for a small fuel time constant and under low pressures

Fluctuations in a single unstable channel have approximately no effect on the total core [98]. Within a single-channel **density-wave oscillation (DWO)**, thermal-hydraulics can be considered as neutronically decoupled. Analyzing channel thermal-hydraulic flow instabilities, with constant heat input in time, the DWO is one of the most commonly encountered flow instabilities in two-phase systems. It scales with the time needed for water to pass through the core and is also named enthalpy wave

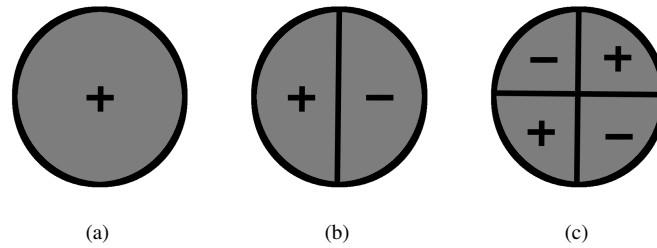


Figure 2.2.: Oscillation modes for the coupled neutronic-thermohydraulic instability type based on March-Leuba [80]: (a) fundamental, (b) first azimuthal, (c) second azimuthal.

oscillation. The physics of this phenomenon is well understood. For certain operating conditions the system becomes unstable since a time-delay exists between heat transfer, resulting in density changes, and an immediate pressure drop feedback. The ratio of pressure losses in the high density region and in the low-density region is the dominant trigger for that oscillatory behavior. The moving of the boiling boundary is often referred to as the deeper reason of a DWO [98]. The manifestation of density-wave instabilities are self-excited oscillations of flow variables [67].

Another neutronically decoupled case is given by the compound dynamic **parallel channel instability**. It can be analyzed by two identical flow channels connected by an upper and lower plenum. This setup is significant for BWR operation as local out-of-phase oscillations of a few FAs can be analyzed.

BWR INSTABILITIES

The BWR features a **strongly coupled** multi-physical system. Main drivers of BWR stability behavior are interactions between power, flow rate and density, intensified by neutronics feedback, such as void and Doppler feedback reactivities. Based on observed oscillation modes, March-Leuba [80] published a SOTA review on coupled thermal-hydraulic/neutronic instabilities in BWRs in 1992. Three main types of instabilities could be identified that are triggered by different physical phenomena:

- channel thermal-hydraulic instabilities,
- coupled-neutronic/thermal-hydraulic (also so-called BWR or reactivity) instabilities,
- control system instabilities.

The latter gives a rather low frequency oscillation and are triggered by malfunctions of control rods, recirculation pumps, valves, reactor controllers and so on. Note, that other types of instabilities can be released through malfunctions. Channel thermal-hydraulic instabilities (see above) can be treated without neutronics. The coupled neutronic/thermal-hydraulic instability is also called **reactivity instability** and includes interaction of the neutronic reactivity feedbacks in addition to density wave oscillations. General types of reactivity instabilities are illustrated in Fig. 2.2 and named:

- core-wide reactivity instabilities,
- out-of-phase reactivity instabilities.

Within a core-wide reactivity instability all the FAs oscillate in-phase across the reactor. This oscillation mode is also called fundamental mode. Out-of-phase oscillations, such as the first and second azimuthal mode, are characterized through different power risings in different regions. In general, modes up to the **first azimuthal mode** can be observed in BWRs.

2.2.2 DESCRIPTION

For a deeper understanding of non-linear stability behavior of a BWR, suitable models with a sufficiently small number of degrees of freedom are crucial. This motivates developments of distinct types of charmingly simplistic models facing conflicting objectives: On the one hand, the BWR feedback system is complex; accordingly, the stability behavior of the reduced version should be highly complex. On the other hand, the system should be as simple as possible in order to distinguish physical mechanisms. Such models are referred to as simplified BWR models.

Based on a short review of BWR instabilities given in Sec. 2.2.1, feasible phenomenological reduction is pointed out and a strategy for a minimum BWR setup concerning **geometry** is identified:

- The dynamics of a simplified BWR model should rely on a **time-dependent** description of **coupled** thermal-hydraulics, heat transfer and neutronics. The coupling of these three physical disciplines are essential to capture flow channel thermal-hydraulic instabilities, in particular the **density wave oscillation** as well as **coupled-neutronic/thermal-hydraulic instabilities**. It is outlined that neutronic modes up to the **first azimuthal mode** play a dominant role in BWR stability. This implies at least a **parallel channel** setup of **two** involved channels. Including neutronics modes up to the second azimuthal mode for instance involves already a four channel setup. In general, only one spatial expansion is considered for fuel assemblies and simulations are realized in 1D. Detailed thermal-hydraulics, heat transfer and neutronic models as well as models for the recirculation system can be adopted from system codes.

Although detailed BWR models are simplified by geometrical consideration, detailed time-domain analysis is nevertheless computational expensive due to the huge parameter spaced of a BWR. Moreover, yielding a better non-linear understanding for coupling mechanism and characterizing non-linear instability behavior by bifurcation tools, such as bifurcation formulae for delay-differential system (BIFDD) [52], AUTO-07p [31] and MatCont [28, 29], requires further reduction to a system of ordinary differential equations (ODEs).

2.3 SIMPLIFIED REDUCED BWR MODELS

Due to the different underlying physics behind simplified BWR models, SOTA reduced versions can be attained by specific-applicable mathematical methods. Hereafter, a short review is given concerning most important historical and current simplified BWR models with no claim to comprehensiveness. Focus is given to the underlying physics and applied model order reduction methodologies which leads to a classification and a discussion about their application limits. In the end, recently applied stability analysis is discussed.

2.3.1 RECENT DEVELOPMENTS

Achard et al. [2] investigated thermally induced flow instability in boiling channels by the homogeneous equilibrium model (HEM). They attained two functional differential equations (FDEs) by **analytical** studies. The thermal-hydraulic model has been extended by Rizwan-Uddin and Dorning [112] to a drift flux model (DFM). A system of complicated non-linear integro-differential equations was attained and its stability investigated.

March-Leuba et al. [79, 82] **integrated** a simple thermal-hydraulics model over two nodes and based on one-point neutron point-kinetics and one-node heat transfer, they derived a phenomenological reduced order model for describing BWR dynamics. In 1986, the model was enhanced in [83] by a two-node heat transfer approximation. Note that phase variables are discretized by a (**Galerkin**) **nodal approach**, i.e. a direct integration between two nodes.

Clausse and Lahey [21] and Lahey Jr. [67] developed a simple ODE model for thermal-hydraulics by applying a weighted-residual-like **variational approach** [64] assuming a linear space dependence of enthalpy in the single and two-phase region within the HEM. Approximations lead to three ODEs [64]. In general, this method can be applied to a sophisticated high-number of axial sub-regions.

Later, this approach was enhanced by quadratic profile assumptions for single-phase enthalpy and two-phase quality using also the HEM by Karve et al. [63]. The simple model was adopted and extended by Karve et al. [64] by point-kinetics to attain a simplified dynamical system which describes the BWR dynamics by non-linear ODEs.

Dokhane et al. [33] developed a model for simulating DWOs in a heated two-phase channel, based on the DFM. By **variational principles** with quadratic profiles they attained five ODEs. The later derived enhanced BWR model has taken into account two heating channels. Dokhane et al. [32, 34] derived a two-channel ROM consisting of 22 ODEs. The thermal-hydraulics are modeled by a DFM based on ideas of [63]. The neutron kinetics model, used by Miró et al. [88] among others, is derived from two-energy group diffusion equations and based on the assumption that the neutron flux can be **expanded in terms of Λ -modes**. Only two dominant modes are contained in the final neutron kinetics model. The fuel rod is modeled separately in the two axial regions of single-phase and two-phase flow and consists of three distinct radial regions. Based on the ideas of Karve et al. [64], a **variational principle** on the basis of **quadratic profiles** is applied to the thermal-hydraulic and heat transfer model.

The approach of Dokhane et al. was continued by Lange et al. [72]. They enhanced the BWR model by the implementation of a recirculation loop model. In [70, 71, 73] they developed the RAM-ROM approach where integrated BWR system codes, in particular RAMONA, and simplified BWR models are used as complementary tools. Recently, the ROM model was enhanced addressing four parallel heated channels [37] and neutronics consisting of three dominant modes.

In 2006, Farawila and Pruitt [42, 43] focused on the study of the non-linear behavior of a BWR system undergoing power oscillations of the global and regional type. They **analytically** derived a fourth-order ROM where the thermal-hydraulic equation is of van-der-Pol type. As only a single boiling channel is modeled, they proposed a road-map towards several parallel channels.

In 2008, Wehle et al. [141] developed a ROM for non-linear stability analysis of the BWR applicable for stability analysis in the non-linear regime. The basis of the TOBI (time domain analysis of BWR instability) model [141] is the simplified BWR system. TOBI respects the interaction between the time-dependent single-phase and two-phase regions. It includes a single node lumped fuel heat transfer model and point kinetics. It has shown to be accurate in describing limit cycles and allows stability analysis in the non-linear regime, where even high amplitude oscillations with inlet flow reversal may occur [141]. The physical model description of TOBI is strongly simplified but its application leads to overall good results. An investigation [141] showed that the model could be qualified based on multi-function thermal-hydraulic test loop in Karlstein (KATHY) stability measurements and by comparison to the licensed code RAMONA.

2.3.2 SUMMARY OF SIGNIFICANT DETAILS

Section 2.3.1 illustrates that simplified reduced BWR models drastically differ in various physical descriptions and reduction strategies. Obviously, this affects the number of degrees of freedom

and accuracy. In general, underlying models are based on partial differential equations (PDEs) that are transformed to a set of low-dimensional ODEs. General, often used, physical models (a) and mathematical reduction strategies (b) are summarized below:

- **Thermal-hydraulics:**

- (a) Depending on the degree of sophistication of the model, either three or four equation-based thermal-hydraulics are applied. Two-phase flow is characterized either by the homogeneous equilibrium model (HEM), the slip-flow model, the drift-flux model and never by the two-fluid-six-equation model. The homogeneous model treats the two-phases as mixture with equal velocity and temperature assumption. Within the slip-flow model, the two phases are artificially segregated and most commonly assumes thermal equilibrium for both phases traveling at mean velocity. The drift flux model approximates the two-fluid model. It takes the relative velocity of the two phases into account.
- (b) An integration over the different axial nodes applying a Galerkin nodal approach (assuming one or two nodes only) and/or applying the variational principle with up to quadratic profile assumptions for each region yields a set of ODEs.

- **Heat conduction:**

- (a) In general, the heat transfer model is based on following assumptions. Depending on the thermal-hydraulic model, there are up to two axial regions: the single-phase and two-phase region. Only radial heat conduction is assumed. There are distinct radial regions, namely the fuel pellet, the gap and the cladding. Heat conduction is considered azimuthally symmetric. The volumetric heat generation is time-dependent.
- (b) In general a two or three point formulation is used. Either integration over different regions or applying the variational principle with quadratic Ansatz functions yield a set of low-dimensional ODEs.

- **Neutronics:**

- (a) Neutronics are either based on simple point kinetic approximations (1) of the diffusion equation or the two-group diffusion equation (2) itself.
- (b-1) Provided that the reactor point-kinetics approximation is used, it directly gives a set of ODEs, describing the behavior of neutrons and (up to six) delayed neutron precursors. It includes the total reactivity feedback which is the sum of void reactivity, calculated as weighted average over the axial length, and Doppler reactivity feedback.
- (b-2) The two neutron-energy group diffusion equation is generally applied with only one delayed neutron precursors group. Here, only different processing steps yield a set of ODEs: The reactor is discretized in a certain amount of nodes. A nodal collocation method is then applied which expands the neutron flux in terms of Legendre polynomials, which permits discretization of the spatial part of the equation, and yield already a set of ODEs denoted by (*). The eigenvalues of the static problem of (*) is solved to attain so-called Λ -modes. By the adjoint static problem, adjoint Λ -modes are also attained. Note that a static assumption only involves static time-independent cross-sections. Applying up to three dominant (fundamental, first and second azimuthal) Λ - modes within a mode expansion included into (*) and projecting on the adjoint modes, yield a set of simple ODEs. Note that this set of equations includes dynamic mode feedback reactivities. They can be divided into void and Doppler feedbacks. By a first calculation of Λ -modes to the static problem (*) and by an additional perturbed static problem (in void and fuel temperature), they can be achieved by a special routine.

- **Recirculation loop:**

It consists of a lower and upper plenum, steam generators, dryers, jet pumps and the down comer. In general, models of the recirculation loop considers all components as a single path with variable flow areas at same mass flow rate. This results in a fixed total pressure with respect to time and can be related to the inlet velocity.

2.3.3 CURRENTLY APPLIED STABILITY ANALYSIS

A selection of operating point information is the basis in SOTA approaches for analyzing the stability behavior of simplified reduced BWR models. As reduced simplified BWR models have low-dimension, additionally bifurcation tools can be applied to attain their non-linear stability character.

A summary of applied stability analysis methods is given in the following:

- **Time-domain-analysis:**

The ODE system can directly be solved by time-domain analysis. Expert-chosen transients or selected operation points are analyzed.

- **Frequency-domain-analysis:**

The frequency-domain method, also referred to as linear stability analysis, is a well-established method for stability analysis. Applying first order perturbation theory to a steady-state solution, a Jacobian can be attained whose eigenvalues (EVs) provide information about the stability of the steady-state: A ODE system is linearized about the steady-state. The Jacobian is directly given. The system becomes unstable if the real part of the EVs becomes negative when increasing the bifurcation parameter. This method is linear and hence additional numerical integration around the neutral stability boundary becomes necessary to determine the non-linear behavior.

- **Hopf bifurcation theory:**

Hopf theory can be applied for studying amplitudes and frequencies of oscillations. A Hopf bifurcation point is characterized by a conjugate complex pair of EVs. Based on Hopf [55] a branching off periodic solutions exists particularly at this point. The Hopf theorem, also referred to as Poincaré-Andronov-Hopf bifurcation theorem, deduces the nature of this bifurcation as sub- or supercritical. For instance, semi-analytical bifurcation approaches investigate dynamical systems using the bifurcation analysis code of Hassard [52]: bifurcation formulae for delay-differential system (BIFDD). BIFDD calculates for a given set of ODEs the critical Hopf-bifurcation parameter, frequencies and also the amplitudes of these oscillations.

Note that inherent limitations arise due to the use of local phenomena (i.e. the steady-state). As time-domain analysis is the only way to completely study the non-linear response [30], also numerical integration of the ODE system needs to be conducted.

Note that all simplified reduced BWR model solutions need further justification by time integration employing system codes. Authors of [70, 71, 73] developed the RAM-ROM approach where integrated BWR system codes, in particular RAMONA, and simplified BWR models are used as complementary tools. Local bifurcation analysis using BIFDD was validated by RAMONA calculations.

2.4 TOWARDS A NEW BWR ROMING AGENDA

2.4.1 DISCUSSION OF RECENT DEVELOPMENTS

BIFURCATION ANALYSIS

Studying dynamics of physical systems was and still is an attractive field. Stability analysis of nearly every physical system [61] was improved by historical achievements in mathematics. A recent review of different types of existing stability analysis methods can be found in [61] summarizing different approaches in two-phase flow stability analysis. It is stated that highly non-linear approaches for characterizing dynamical behavior are already available. For example, it was pointed out that the Lyapunov method was already applied to a parallel channel mock-up investigating pressure-drop oscillations (PDOs) and DWOs.

SOTA bifurcation analysis tools such as [31], solve continuation and bifurcation problems and can detect bifurcations which not necessarily must be of Hopf type and hence allows achieving full non-linear stability maps. Note that innovative bifurcation investigations need a precise non-linear ROM containing ODEs.

SIMPLIFIED REDUCED BWR MODELS

Summarizing the efforts regarding simplified BWR models, more and more accurate physics are involved, such as a drift flux representation of thermal-hydraulics, the two-group-diffusion equation, a sufficient heat conductive model and a reliable recirculation model. The geometry choice of up to four channels is drastically reduced regarding a detailed BWR core but it is phenomenological justified.

Taking the step from a simplified model to a simplified reduced model by applied mathematical reduction methods (mentioned in Sec. 2.3.1 and Sec. 2.3.2), it is notable that there is room for further improvement. This will be shortly discussed hereafter and motivates the need of an extended, systematic reduced order methodology:

(1) **Grid independence**

A variational formulation of the thermal-hydraulics takes into account two axial sub-domains in addition to a quadratic profile assumption. Stability analysis of a super-critical light water reactor, namely the HPLWR, was investigated in [94–98] by a finite element method (FEM) based code. Note that the FEM is similar to variational formulations by nature. Grid independent results of a complete FA could only be attained by a spatial resolution of 240 nodes where shape (Ansatz) functions of order four and five have been employed.

- **Taking grid-independent modes as basis for a variational type of method could supplement SOTA methods.**

(2) **Transient information**

Within the nodal modal method for the neutron diffusion equation, a static problem is solved to attain the so-called Λ -modes. Ansatz functions for variational formulations of the thermal-hydraulics and heat conduction are assumed to be quadratic.

- **Building up a variational type of method based on Ansatz functions (modes) calculated by transient information would lead to shape functions with physical justification.**

(3) **Grid spacers and reversal flow**

Assuming several grid spacers distributed along the axial direction of a FA. A minimum pres-

sure loss is realized by intelligent positioning of spacers. Right before the grid spacer dry-out is barely avoided and strong wetting takes place afterwards. Changing the operation condition of a reactor, unstable limit cycles with inlet reverse flow may occur [141]. Note that in those cases enthalpy profile variation especially along the spacers is by far not simple.

- **Ansatz functions based on sophisticated physical information being reducible to more sophisticated geometry would overcome inherent restrictions and enrich accuracy of a variational type of method.**

(4) **Adaptiveness to multi-space dimensions**

Simulation of complex geometries can contribute to a better understanding of hidden physical mechanisms.

- **Variational types of reduction methods handling sophisticated multi-space information would include multi-dimension effects and enhance the level of details.**

2.4.2 TOWARDS A BWR REDUCED ORDER MODELING AGENDA

Keeping in mind identified steps for possible improvement of Sec. 2.4.1, a quick review of innovative non-linear reduction approaches in various types of fields reveals the importance of Galerkin spectral approaches based on an optimal choice of basis functions derived by a certain decomposition method, the so-called proper orthogonal decomposition (POD).

A precise ROM making many transient runs quick and affordable would be a valuable tool for getting a stability description, also applicable in the non-linear region, leading to a deeper understanding of the system's stability. Further investigations like bifurcation analysis, attaining non-linear stability maps, can then be achieved.

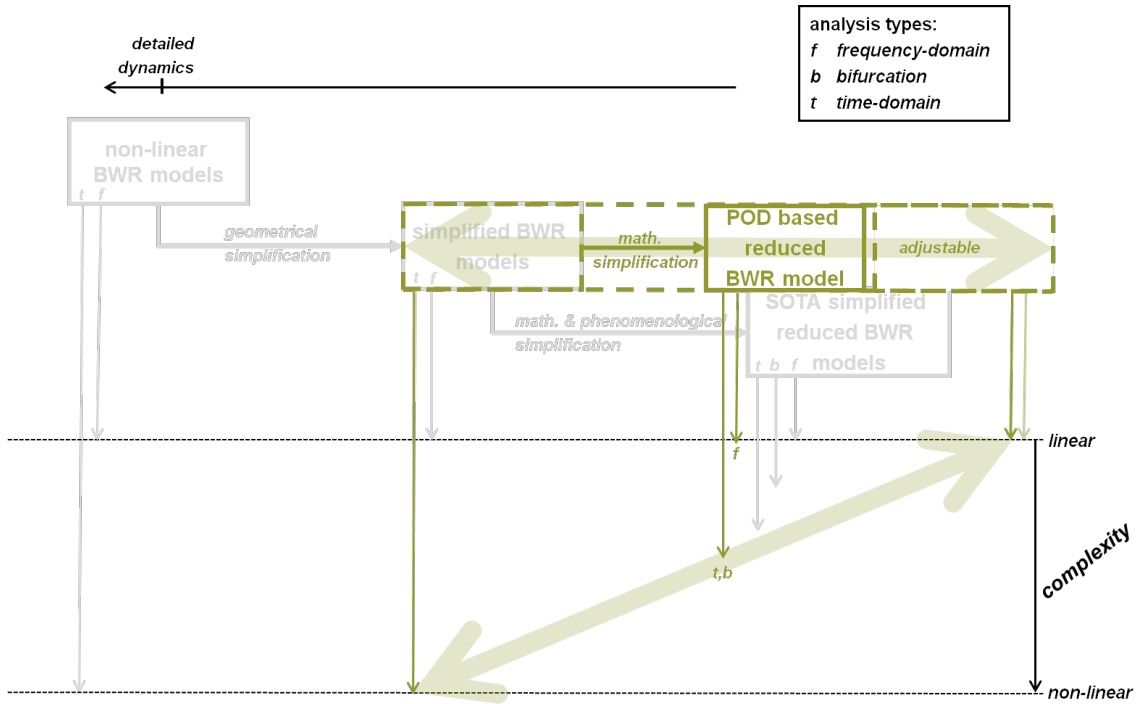
- A promising result was published in [40, 41] by Ehrhard and Müller. The dynamical system of a natural convection in a closed circuit (NCC) was reduced to a set of non-linear ODEs by a **Galerkin spectral approach** and analytical Ansatz functions. A methodology based on Fourier series is difficult to apply for complex geometry. In addition, the modal shapes are independent of the underlying physical system.
- Merzari et al. [87] talked about proper orthogonal decomposition (POD) of the flow in a T-junction. Merzari and Ninokata [86] investigated flow in a tight lattice-rod bundle. For extremely tight configurations there exist large-scale periodic flow oscillations. The proper orthogonal decomposition (POD) has been used with snapshots of a large eddy simulation (LES) flow field to obtain the most **energetic modes** of turbulence. This analysis highlighted traveling waves in the stream-wise direction and hence gives **additional insight** into the structure of flow oscillations.
- In 1992, Kirby [65] stated that Fourier- or Chebyshev-based spectral Galerkin methods make no use of underlying system dynamics. Intuitively, this does not yield an optimal representation of dynamics. However, an **optimal basis** is given by the proper orthogonal decomposition (POD). Establishing the proper orthogonal decomposition (POD) on additional information, such as the flow field and higher-order derivatives, yields even more efficient reduced order models (ROMs). Based on the Kuramoto-Sivashinsky equation, he derived a **minimal ROM**.
- In 2006, a large scale upper ocean model was reduced by a set of basis functions derived by the POD [13]. The root mean square error (RMSE) of the reduced model is less than 1% regarding the averaged upper ocean layer thickness.

- Buchan et al. [11] applied the proper orthogonal decomposition (POD) for calculating eigenvalue problems in **reactor physics** application and highlighted its potential. He stated that the method is general and adaptable to other fields as well. In general, it requires time-dependent data of transient simulations of dynamical systems.

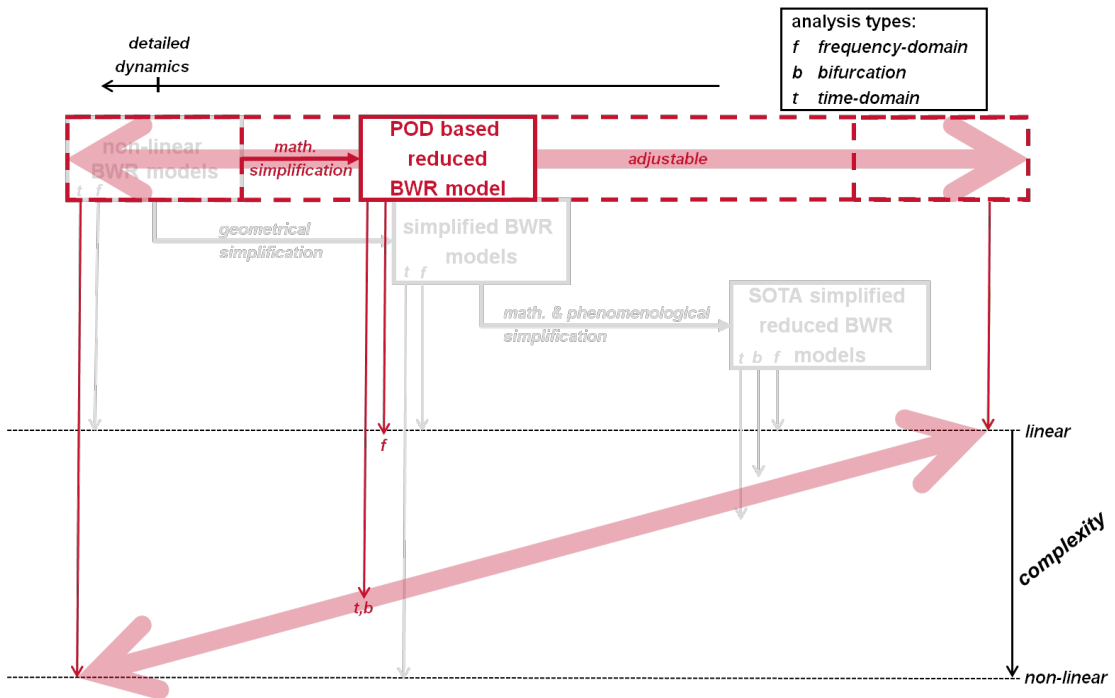
This underlines that POD based ROMs have potential in nuclear and other fields of application. Model order reduction (MOR) based on Galerkin projection is a highly flexible and general methodology. It reveals often hidden physical information. The level of accuracy for a POD based ROM is completely adjustable and depends on the number of most energetic modes that are retained in the reduced system. Moreover, it yields a minimal system by its optimal basis choice. The mismatch between the reduced order model and the original model completely depends on the number of involved modes. Note that depending on the given transient data, the methodology can be considered grid-independent. It incorporates transient data. Complex geometrical setups affecting physical behavior are inherently captured. It is adaptable to multi-space dimensions.

Figure 2.3(a) and 2.3(b) illustrates the advantages of systematic MOR based on POD. It can be applied either to the detailed or simplified BWR model (or to any other physical model). This technique yields non-linear a BWR-POD-ROM with a prescribed accuracy goal. The precision of the ROM is completely adjustable and depends of the number of included proper orthogonal modes (POMs). This is marked by the two large thick arrows within both figures. This optimal low-dimensional ROM, representing the whole coupled BWR system, can be solved either by time-domain or frequency-domain analysis but also by bifurcation analysis.

A low-cost simulation tool based on POD, representing the coupled BWR system, would be of great advantage. Up to now, within reactor dynamics, no automatic predictions for such efficient minimal ROMs are available. Regarding industry, an automated self-contained ROM-POD methodology is required that is based on a wide spectrum of validation and verification examples.



(a)



(b)

Figure 2.3.: Proposed strategy for attaining proper orthogonal decomposition based reduced order model of BWRs - an adjustable methodology and applicable to geometry simplified (a) or detailed (b) models.

3 TOWARDS AN OPTIMAL CHOICE OF REDUCTION METHOD

For achieving a non-linear stability map of a boiling water reactor (BWR), various numerical calculations are necessary due to its huge parameter space. This generates significant interest in low-cost simulation tools that represent the coupled boiling water reactor (BWR) system as accurate as possible with the absolute necessary demand on keeping its dynamical structure. By reviewing current reduced order methodologies applied in the scope of BWRs (see Sec. 2.4.1), the need of an extended, systematic reduced order methodology catches the eye.

Up to now within reactor dynamics, methodologies generating efficient and minimal reduced order models (ROMs) are not available and regarding industrial operation, an automated self-contained methodology is crucial. Commonly, so-called spectral methods are applied to construct general types of reduced order models (ROMs). More recently, they are enhanced by an optimal basis choice of so-called trial or test functions, yielding efficient ROMs.

The aim of the proceeding chapter is to give a brief overview of spectral methods. Based on a general classification of spectral methods, optimal choices of basis functions are discussed. Two of them are of particular importance for identifying coherent structures. Based on recently published literature, a comparison is given and one method is selected, the so-called proper orthogonal decomposition (POD). Finally, the general methodology for establishing ROMs based on an optimal basis function choice by the proper orthogonal decomposition (POD) is presented.

3.1 SPECTRAL METHODS

Spectral methods are often applied for solving differential equations numerically. Various methods are available that differ in the choice of trial and test functions as well as in how boundary conditions are implemented. Newly, optimal choices of basis functions enrich this class of technique. The following section contributes to a better classification of the spectral method applied throughout this thesis.

3.1.1 TRIAL FUNCTIONS

The fundamental idea of a numerical solution method is to write the solution of an underlying equation system by a sum of varying basis functions, the so-called approximation or trial functions. Depending on the trial function, general classes of numerical techniques can be derived, for instance the finite differences method (FDM) or finite element method (FEM). Both use local polynomials of low degree [49]. However, spectral methods make use of trial functions having global representation with certain special properties. Typically, several analytical functions are utilized, i.e. (complex, sinus or cosinus) Fourier-types or global polynomials of Chebyshev- or Legendre-types [12].

3.1.2 WEIGHTED RESIDUAL APPROACHES

The choice of coefficients in the derived expanded equations can be solved directly (as in the case of the FDM) or by projection to weighting or so-called Ansatz/test functions (as in the case of the FEM). Implementation of spectral methods are accomplished by various different classes of weighted residual approaches that can be distinguished by the choice of test functions [12, 19, 49]:

- **Tau method:**
Within the Tau method, test and trial functions are identical chosen. Trial functions do not necessarily fulfill the boundary condition and hence they need to be imposed. In general, they are enforced by additional equations.
- **Collocation method:**
Functions are zero but at one collocation point. This is formulated by Dirac-delta functions. The differential equation is only formulated at distinct collocation points. Again, this system is degenerated and boundary conditions must be imposed.
- **Galerkin method:**
The general idea of this method is to expand the solution in terms of a linear combination of polynomials fulfilling the boundary conditions.

3.1.3 ABOUT THE OPTIMALITY OF TEST AND TRIAL FUNCTIONS

Spectral methods, based on analytical basis functions, make no use of any information of the underlying system [16, 65]. Intuitively, this do not yield an optimal representation of dynamics and accordingly do not conduct to an efficient and minimal reduced system. Both, experiments and numerical simulations yield on investigations that indentify coherent structure and extract dynamical relevant processes. A question that is adressed in the following deals with the issue if those information can contribute to a more optimal basis.

Methods of computer science within the field of artificial intelligence [8] can contribute to a deeper understanding of the underlying dynamical processes. Especially its sub-discipline, the so-called machine-learning where computers learn from underlying data, is of particular interest. Based on given training data, certain methods can detect complex patterns and allow to take intelligent decisions [8]. Some techniques that have been discussed recently are clustering, kernel methods and

dimensionality reduction methods among others. Recent applications of machine learning are given for example by robotic control, data mining, autonomous navigation, data processing and others.

The field of dimensionality reduction consists of techniques that find a reduced basis to a given data set and establishes a reduced model by a Galerkin (or Tau) method. Such a technique always consists of selection and extraction processes [8]:

- **Selection:**

Feature selection identifies a subset of variables that best defines the data.

- **Extraction:**

Feature extraction transforms the data from high-dimensionality to low-dimensionality.

Various types of techniques are available that differ in the way of data transformation. Two of them are of particular importance regarding the detecting of coherent structure:

- Dynamic mode decomposition (DMD) and
- Proper orthogonal decomposition (POD).

In the following, they will be discussed by reviewing well-chosen literature.

3.2 CURRENTLY APPLIED DECOMPOSITION METHODS IN MODAL ORDER REDUCTION

Two decomposition methods in combination with a Galerkin (or Tau) method received enormous attention in science for constructing general ROMs. In comparison to analytical chosen functions, they yield a more sophisticated basis representing the underlying dynamics of a system. An optimal representation of the system is achieved by only a few basis functions. However, for this purpose transient data is needed. In the following, two heavily used complementary decomposition methods are discussed on the basis of open literature.

3.2.1 DYNAMIC MODE DECOMPOSITION

A recently developed method to attain a model decomposition is the dynamic mode decomposition (DMD) [113, 120]. The DMD is an iterative Arnoldi-like data-based algorithm based on the Koopman operator [18]. This is a linear operator representing the non-linear dynamics without linearization. It extracts dynamical relevant processes from temporal or spatial flow sequences [124] with respect to perturbation dynamics. It is solely data-dependent and an underlying set of equation systems is not needed. Eigenvalues and eigenmodes are extracted based on an approximate linear model. Mode properties, i.e. frequencies and growth rates for instance, can be computed by the magnitude and phase of the modes [18]. A description of an implementation within MATLAB[®] can be found in Appendix A.

Various applications of the DMD can be found in literature [118]. They are based on experimental and numerical data. In the following, some of them are presented in more detail:

- Schmid [119] and Schmid and Pust [121] applied the DMD to a laminar axisymmetric jet. Dynamically relevant coherent structures could be detected. While applying the decomposition to PIV- and image-based flow of a steady and pulsed jet [122, 124], most relevant frequencies and spatial structures have been identified.
- Schmid [120] investigated flow over a square cavity and flow in the wake of a flexible membrane by the DMD. Based on an experiment of a jet between two cylinders he compared the

DMD with the proper orthogonal decomposition (POD) which processes second-order statistics. The DMD isolates distinct frequencies while the POD achieves a decomposition based on spatial orthogonality.

- Another comparison was realized by investigations of flow in a lid-driven cylindrical cavity by Schmid et al. [123]. They remarked that both techniques identified bifurcation points. This underlines the usage of both methods as complementarity techniques.
- By a jet in crossflow, Rowley et al. [113] discovered that for a linear system the DMD modes reduce to global eigenmodes. For periodic systems, modes can be achieved by the discrete temporal Fourier transformation as well. They remarked, that the DMD decouples different frequencies more efficiently than POD.
- In 2012, Chen et al. [18] derived an optimized DMD algorithm which does not depend on numerical sensitivity. It is superior in computing a small number of modes.

3.2.2 PROPER ORTHOGONAL DECOMPOSITION

The book of Schilders et al. [117] presents a summary of general and more specialized model order reduction techniques for linear and non-linear cases. Therein, R. Pinnau describes a technique using the proper orthogonal decomposition (POD) method. It requires solving large eigenvalue (EV) problems for a full matrix. For this reason, in practical computations the so-called method of snapshots is exploited [129].

The POD method [54] is known under different alias names, such as the Karhunen-Lòve decomposition in signal analysis, principal component analysis in statistics, the method of empirical orthogonal functions in geophysical fluid dynamics [13]. It provides a technique for analyzing multidimensional data and transfers a given set of data into an optimal representation. Note that a POD projection converges faster than any other spatial or temporal basis corresponding to the same number of modes [4]. The procedure is solely data dependent and does not need any underlying system equations. The POD is widely used capturing coherent structures which is attained by applying second-order statistics on a correlation tensor [17, 77, 120, 128]. This so-called covariance matrix is derived by correlating the vast number of snapshots. There is a connection between singular value decomposition (SVD) and POD [137]. POD modes capture the most energetic structures [113] having several frequency content but do not provide phase information [120]. Combining the POD with a projection step leads to low-dimensional and efficient models [11]. Due to the search for linear (or affine) subspaces instead of curved sub-manifolds, it is computationally beneficial [111]. It is interesting to note that non-linearities are not unattended. Depending on the non-linear character of the original system also the POD-ROM contains this property.

The POD is heavily applied in various fields of engineering and science, such as data analysis, data compression and model reduction. Note that specific requirements of the POD method apply for different fields of physics [117]. Many authors have employed the POD reduction technique for generating ROMs in several areas, see [53, 131, 136, 144] among others. Applications can be found including natural fields of image processing, data compression, signal analysis, as well as modeling and control of chemical reactors [136], fluids, power grids, wind engineering and also investigations of coherent structures in fluids.

Due to the huge number of material covering POD based ROMs, below only specific literature is mentioned. It is classified by different important issues concerning the derivation of reliable, stable, efficient and minimal ROMs. Some of them have contributed to the proposed POD-ROM methodology (see Sec. 4.3).

- **Comsol-Matlab interface:**

Spronkmans et al. [131] applied the POD for Comsol[®] Multiphysics [23, 25] based partial differential equation (PDE) models. As model reduction techniques are not implemented in Comsol[®], a Matlab[®] [85] code was written. They intended to derive an automated process for model order reduction by POD written in Comsol[®] but their implementation requires extensive manual interaction. Benchmarks have been carried out for a coating process and turbulent flow past a cylinder.

- **Accuracy:**

A large scale upper ocean model [13] showed that ROMs with a minimum error can be attained. These results are also underlined by low order models derived for simulation of variable-density flow and salt transport [148] or models for the dynamics of wall heat transfer in pulsating flow [127]. Other accurate POD based ROMs may be cited here as well.

- **Multi-variable treatment:**

Belzen et al. [136] mentioned that the POD might become complicated in systems with a large number of physical variables. They aimed at finding an optimal projection space from tensor representation of data and illustrated their method by a reduced order model of a tubular reactor (TR) under boundary perturbation. POD-ROMs to single variable expansion are compared to lumped setups. Moreover, results based on higher-order singular value decomposition (HOSVD) and tensor SVD are compared.

- **Boundary conditions / constraints:**

The effect of forcing conditions are only partly visible in POD modes, nevertheless they are not inherited automatically by the ROM and hence need to be imposed [62]. Feßler [44] applied the POD for model order reduction of a catalytic converter. The ROM only included a few equations but nevertheless results are in good agreement. Incorporation of boundary conditions were taken into account by additional modes in this work. Efe and Özbay [38, 39] included free boundary conditions by a control input. Additional to the weak formulation, Kalashnikova and Barone [62] applied a penalty enforcement of boundary conditions. They remarked that a weak formulation can be insufficient. A forcing at the inlet of a ROM was included by Selimefendigil and Polifke [127] by an explicit formulation of an ordinary differential equation (ODE).

- **Stabilization:**

In general, POD-ROMs lack stability and need stabilization to correctly reproduce long-time behavior. A loss of long-term stability is contributed to the truncation of smaller scales. However, various methods are available which overcome this drawback. Gloerfelt [47] focused on reliable POD-ROMing for the application to a two-dimensional (2D) cavity flow. They focused on methods involving optimization, i.e. the penalty method, the inner product choice, mean exclusion/inclusion, but also on calibration using the temporal information between snapshots minimizing the error between full order model (FOM) and ROM data. Also Kirby [65] and Du et al. [36] combated the lack of dissipation by using higher order information in the covariance matrix (i.e. a change of inner product choice). Recently, a Petrov-Galerkin method was introduced by Carlberg [15] to control the stability of a one-dimensional (1D) nonlinear static problem. Here, diffusivity is introduced without tuning or optimization. A new Petrov-Galerkin-POD method has been published by Xiao et al. [147] more recently, where a mixed finite element pair overcome stability concerns.

- **Complex functions:**

In the work of Herkt [53] the highly non-linear behavior of a vehicle tire was simulated using modal order reduction based on POD. She mentioned that POD reduces the effort attaining a solution but function evaluation still requires a high amount of time. It is notable that

surely computational savings achieved by POD can be affected by complex evaluations of non-linear functions [111]. However, savings can be achieved if the reduced models are small enough. Moreover, Kalashnikova and Barone [62] successfully applied best points interpolation to time-consuming non-linear terms within a ROM of a tubular reactor (TR).

- **Quadrature schemes:**

Barone et al. [5] estimate stability by a continuous formulation of the POD-ROM. They noted that these estimates need higher-order numerical quadrature formulas for exactly integration of the inner products.

- **Bifurcation analysis:**

Cazemier et al. [16] derived a POD-ROM of the flow in a square lid-driven cavity. A linear analysis was applied to the reduced system. Furthermore, the stability of periodic solutions was analyzed by Floquet multipliers. The periodic solutions of the dynamical system could be shown to exhibit nearly identical behavior. Some complicated transitions within the bifurcation diagram could not be detected in comparison to direct numerical simulation (DNS) data.

- **Optimization:**

Wlotzka [144] investigated flow past a cylinder modeled by Navier-Stokes. He derived a POD-ROM and optimized the model by a problem specific optimal choice of snapshot positions (data acquisition).

Applications of the POD within the scope of BWRs are scarce, including [86, 87]. Buchan et al. [11] applied the POD for calculating eigenvalue problems in reactor physics application. Wols [146] applied the POD to reconstruct the steady-state reference flux of a 1D accelerator driven system (ADS) model. In 2012, it was shown by Prill et al. [101–103, 108] that attaining a low order model by the POD-ROM-methodology is feasible, also for simple thermal-hydraulics, but further model specific developments need to be carried out for BWRs which is concern of issues of publications [20, 104–107] in 2013 and a submitted publication [110] for 2014.

3.2.3 DISCUSSION

Based on the literature review, a summary of both methods is given by Tab. 3.1. Both methods make use of transient data and do not need any underlying equation system to achieve spatial structure. The recorded snapshot series can be processed either direct or mean/equilibrium subtracted. POD modes capture similar spatial structures than the DMD (Koopman) modes [113]. Nevertheless, POD focuses

Table 3.1.: Comparison of decomposition methods: proper orthogonal decomposition (POD) versus dynamic mode decomposition (DMD).

criterium	POD	DMD
usage of transient data	yes	yes
necessity of an equation system	no	no
data handling	direct, mean-subtracted	direct, mean/equilibrium-subtracted
operator	Koopman (linear operator)	covariance matrix (second-order statistics)
information about the flow	according to energy	according to average contribution over time
- properties of modes	consist of several frequencies	consist of only one frequency
- distinct mode frequency	no	yes
- distinct mode phase	no	yes
convergence	+ faster than any other set with the same number of basis functions	-
bifurcation diagram	yes	yes

on spatial orthogonality and DMD on temporal orthogonality (frequencies). ROMs might benefit from both types. By construction, DMD modes contain only a single frequency and POD modes contain several frequencies. The DMD decouples different frequency components more effectively than the POD. However, this might yield to higher dimensional systems as more frequencies must be included. Note that phase and frequency information is achieved directly by the DMD. Bifurcation diagrams can be achieved by both methods [123] but as the basis is different they possibly differ.

Schmid et al. [123] noted that both methods should be used as complementarity techniques. Both methods have assets and drawbacks. In a study of Noack et al. [91] only a combination of POD, linear stability and shift modes accurately describes incompressible flow around a circular cylinder. Also Morzyński et al. [90] proposed the usage of a hybrid model.

Throughout this thesis only POD based ROMs are considered. The proposed general methodology allows a replacement of the decomposition methods as well as a hybrid usage of two or more decomposition methods. This fundamental methodology will be focused from a general point of view in the following and in all details in Sec. 4.3.

3.3 PROPOSED METHODOLOGY

In contrast to other authors, we are interested in a fully automated process for several PDE inputs investigating different physical systems. A flexible, accurate and easy to handle approach is the usage of the commercial software package Comsol[®] Multiphysics [23, 25]. It is a finite element analysis software environment for the modeling and simulation of physics-based systems and equipped with an interface to Matlab[®] [85]. A ROM is generated based on the "general form" PDE input of Comsol[®] with little user interaction. This approach follows an idea of Cardiff and Kitanidis [14]. Additional Mathematica[®] [145] routines perform the symbolic mathematical manipulation. Matlab[®] is used in POD preprocessing and finally to solve the ROM. A Matlab script calls all the other codes. Fig. 3.1 illustrates the essential steps of the new proposed methodology.

Traditionally equations rely heavily on experimental data. Equations will continuously be calibrated by new experiments which is a time-consuming step. The derived BWR system is then used to investigate the stability behavior which takes immense effort investigating the complete parameter set by several PDE calculations. Nevertheless, complex coherent structure can hardly be discovered.

Data sets, which are obtained from trajectories of experiments, numerical integration or analytical derivations reflecting the dynamics of the system, can serve as basis for time series (so-called snapshots) within the new approach. In the following this data is referred to as the FOM solution.

The key element of the methodology is the POD algorithm, which is the essential technique in the mathematical data analysis. Note that the methodology can also be based on other types of decomposition techniques. The POD provides a method defining the best approximating subspace to a given set of data. It detects relevant (often oscillating) states which are hidden in transient data. These so-called proper orthogonal modes (POMs) have physical meaning and are ranked according to their energy content. By respecting a certain number of modes the spatial and temporal characteristics of the system are reproduced. Both, the essential and low-important POMs can be distinguished by a well-defined truncation criterion. After truncation only dominant POMs are utilized and the approximate solution is defined by a superposition of time-varying magnitudes of POMs.

The Galerkin projection has widely been used in reducing PDEs to ordinary differential equations (ODEs) by projecting onto appropriate basis functions that describe the spatial variations in the solution. This procedure is applicable to any subspace but within the proposed methodology, POMs are used as test functions taking advantage of their orthonormal property. This step is carried out

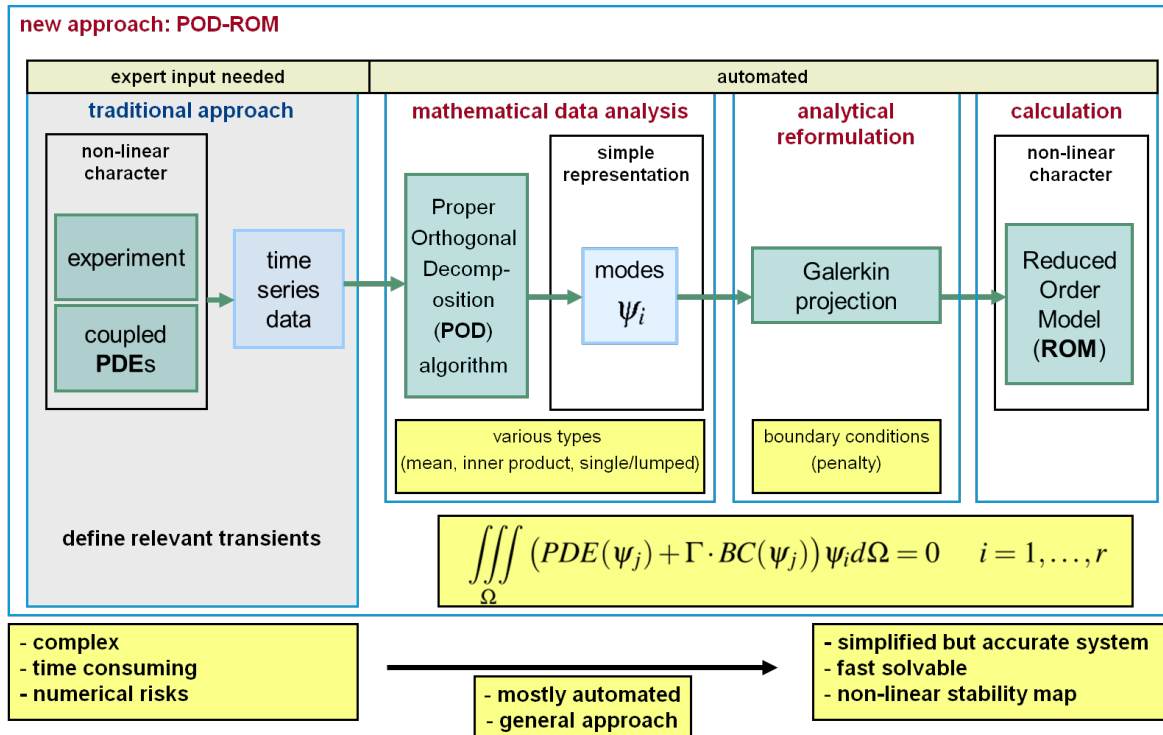


Figure 3.1.: Flow chart of POD-ROMing approach.

completely analytical by symbolic manipulation yielding a low dimensional model of the dynamical system, the so-called POD-ROM.

In general, POD-ROMs losses long-term stability due to the truncation of smaller scales. Various types of methods are available that overcome this drawback, i.e. the penalty method, the inner product choice, mean exclusion/inclusion, but also the treatment of different data sets by a lumped or single variable expansion approach. Boundary or constraint effects, that are only partly visible in POMs, are not automatically inherited by the ROM. They need to be imposed. Accordingly, the proposed methodology equally belongs to Galerkin as well as tau methods.

Note, a complex, time-consuming system which involves numerical difficulty, is mostly automatically transferred to a simplified non-linear ROM which is efficiently solvable. Accordingly, analyzing the system with respect to non-linear stability phenomena becomes feasible with a prescribed accuracy goal. Further investigations like bifurcation analysis, attaining stability maps, can be achieved.

4 CODES AND METHODS

A detailed description of the numerical codes and methods used within the thesis is presented in this chapter.

The first section discusses the generation of the snapshot data by attaining the full order model (FOM) fields within COMSOL[®][23–25]. It focuses on COMSOL[®]'s general partial differential equation (PDE) form, its solution by finite elements, applied boundary conditions and its weak formulation.

Focusing on the verification of this implementation, the next section is occupied with linear stability maps. It presents linear stability analysis using COMSOL[®]'s internal eigenvalue solver. A linear stability map is finally attained by an external MATLAB[®][85] routine.

The strategy to achieve a reliable reduced basis by proper orthogonal decomposition (POD) is pursued in the third section. Here, a detailed description of the POD-based reduced order model (ROM)ing strategy is given. It moreover describes the calculation of proper orthogonal modes (POMs) and problems of long-time stabilization either by choosing different symmetric kernels for the eigenvalue (EV) problem and/or by preserving boundary effects. Methods to avoid anti-aliasing errors are also discussed. It further summarizes the complete methodology and explains the proposed calibration road-map.

The self-written code structure is afterwards presented before global error quantities are introduced in the end.

4.1 FULL ORDER MODEL SOLUTION

Within this thesis, a FOM solution is attained by solving the implemented equation system within the COMSOL Multiphysics[®] software package [23–25]. This section introduces COMSOL[®] from a general point of view. It moreover discusses its general form partial differential equation (PDE) which is used throughout this thesis. The implementation of boundary conditions is then be focused on. COMSOL[®]'s finite element formulation and the reformulation of every strong form into a weak representation is afterwards referred to. The last part deals with the independence of the numerical scheme.

4.1.1 COMSOL MULTIPHYSICS

COMSOL[®] is based on a finite element (FE) formulation [75] and is a toolbox for different kind of physics-based systems. The user is able to define different, up to three-dimensional (3D), spatial geometries and multiple PDEs can act on parts or on the whole geometry domain. There are pre-defined types of PDEs available as well as general types allowing for more flexibility. Three application modes are available: Besides the coefficient form and the general form (also the so-called strong forms), that are both appropriate for non-linear problems [98], there is a very powerful and flexible [25] so-called weak formulation. The general and the coefficient form are equivalent formulations. Depending on the PDE system either one of them is the more adapted form. By default, COMSOL Multiphysics[®] converts each model into weak form representation before solving. After meshing a model can then be solved by internal solver routines. The computational effort strongly depends on the specific system and how it is solved within COMSOL[®]. Numerous numerical solvers are offered. Various analyses methods exist too, e.g. steady-state linear and non-linear, time-dependent and modal analyses among others. After meshing, each element is represented by shape functions of different types up to order five. Depending variables are approximated by a finite number of parameters that characterizes the shape function. The order of the model is equal to the number of degrees of freedom and can easily exceed numbers of thousands. Post-processing routines allow handling and visualization of the data.

4.1.2 GENERAL PARTIAL DIFFERENTIAL EQUATION FORMULATION

As the physical system describing the boiling water reactor (BWR) is highly non-linear, a strong or weak form representation is suitable. The so-called *general form PDE* is appropriate for all types of non-linear problems and is utilized consecutively throughout all types of analysis within this thesis. Note that the coefficient form might also be used in the same manner.

Let us assume u to be a single dependent variable defined on the subdomain Ω . The general form for non-linear PDEs is specified by the following equation system,

$$e_a \frac{\partial^2 u}{\partial t^2} + d_a \frac{\partial u}{\partial t} + \nabla \cdot \tilde{\Gamma} = f, \quad (4.1)$$

where e_a denotes the mass coefficient, d_a the damping (mass) coefficient, $\tilde{\Gamma}$ the conservative flux vector, f the source term and ∇ the Nabla operator and $\nabla \cdot$ the divergence operator.

4.1.3 BOUNDARY CONDITIONS

The Dirichlet boundary condition R specifies the value of a dependent variable on the boundary. This type is also called essential boundary conditions or constraints. The boundary condition in COMSOL[®] is either defined by the constraint R ,

$$0 = R,$$

or the Dirichlet boundary condition r ,

$$\begin{aligned} u &= r, \\ g &= -\mu_L. \end{aligned}$$

For example to constrain u to 7 at the boundary either choose $R = 2 - u$ or $r = 2$. The generalized Neumann boundary condition, the so-called mixed boundary or Robin boundary condition, is defined by

$$-\mathbf{n}\Gamma = G + \left(\frac{\partial R}{\partial u}\right)^T \mu_L \quad (4.2)$$

and specifies the value of a linear combination of the normal flux and the dependent variables on a boundary [25]. A pure Neumann condition is defined by selecting $R = 0$. The Lagrangian multiplier is denoted by μ_L , \mathbf{n} is the normal vector on $\partial\Omega$ and G the source or flux term. Note that without defining of a Dirichlet boundary condition the Neumann condition yields vanishing value, i.e. a no flux condition, due to predefined $G = 0$ within COMSOL[®]. A constraint implementation of the boundary is chosen in the following for all type of systems.

4.1.4 FINITE ELEMENT METHOD

The finite element method (FEM) is based on a discretization of the whole geometry by \tilde{N} grid elements. Ansatz functions ϑ_i are defined on the chosen spatial grid. A linear combination of coefficients U_i and Ansatz functions ϑ_i , or so-called shape function, yields the approximate solution of an unknown

$$u = \sum_{i=1}^{\tilde{N}} U_i \vartheta_i. \quad (4.3)$$

Within this thesis, only Lagrangian shape functions ϑ_i are applied, that have following properties:

- at knot i : $\vartheta_i = 1$.
- at all other knots $j \neq i$: $\vartheta_j = 0$.
- element i has a distinct polynomial order P_m which influences the number of intermediate knots.

In COMSOL[®] notation, the form function is denoted by P_m , where m represents the order of the underlying polynomial. Instead of searching for a solution u , by inserting Eq. (4.3) in the general form PDE yields a search for coefficients U_i , the so-called degrees of freedom.

4.1.5 WEAK FORMULATION

Numerical convergence is directly linked to a precise Jacobian matrix [25]. The following describes the conversion of a strong form into weak formulation. An automatism for both strong formulations, i.e. the coefficient or general form, is provided in COMSOL[®] by default.

The general form PDE of Eq. (4.1) is converted into weak representation by the help of an arbitrary test function \tilde{v} which is defined on the subdomain Ω . Multiplying Eq. (4.1) with this test function and integrating over the subdomain leads to

$$\int_{\Omega} \tilde{v} \left(e_a \frac{\partial^2 u}{\partial t^2} + d_a \frac{\partial u}{\partial t} + \nabla \cdot \tilde{\Gamma} \right) dA = \int_{\Omega} \tilde{v} f dA, \quad (4.4)$$

where dA is the volume element. Applying of the Gaussian integral theorem leads to a formula for integration by parts for multi-dimensions

$$\int_{\Omega} u \nabla \cdot v dV = \int_{\partial\Omega} u v \mathbf{n} dS - \int_{\Omega} v \nabla u dA, \quad (4.5)$$

where dS denotes a surface element. Making use of this mathematical identity and inserting into Eq. (4.4) yields

$$\int_{\Omega} \tilde{v} e_a \frac{\partial^2 u}{\partial t^2} dA + \int_{\Omega} \tilde{v} d_a \frac{\partial u}{\partial t} dA - \int_{\Omega} \nabla v \cdot \tilde{\Gamma} dA + \int_{\partial\Omega} v \tilde{\Gamma} \cdot \mathbf{n} dS = \int_{\Omega} \tilde{v} f dA.$$

A combination with the boundary condition (4.2) leads to the weak formulation applied throughout this thesis:

$$\int_{\Omega} \tilde{v} e_a \frac{\partial^2 u}{\partial t^2} dA + \int_{\Omega} \tilde{v} d_a \frac{\partial u}{\partial t} dA - \int_{\Omega} \nabla v \cdot \tilde{\Gamma} dA - \int_{\partial\Omega} v \left(G + \left(\frac{\partial R}{\partial u} \right)^T \mu_L \right) dS = \int_{\Omega} \tilde{v} f dA. \quad (4.6)$$

4.1.6 INDEPENDENCE OF THE NUMERICAL SCHEME

Shape functions of up to order five are available within COMSOL[®]. They approximate depending variables by a chosen number of parameters. Depending on the physical problem, the order and shape of these functions need to be selected [26]. For example, the later introduced homogeneous equilibrium model (HEM) in Sec. 6.1 requires shape functions of order five for enthalpy and mass equation and of order four for the momentum equation. Only a well-chosen spatial mesh size in agreement to the order of shape functions (degree of freedom) provides independence of the numerical scheme. By an analysis of mesh size refinement and shape order increasing, on the basis of a modal analysis, only a convergent result yields an independent scheme [57, 98].

4.2 VERIFICATION OF THE IMPLEMENTATION OF THE FULL ORDER MODEL

In this thesis, linear stability maps are exploited for verification purposes due to the fact that transient experimental data are only rarely available. Starting with an introduction of linear stability analysis within COMSOL[®], this section presents COMSOL[®]'s eigenvalue solver and the enveloping MATLAB[®] routine, that are applied for attaining the linear stability maps.

Well-behaved linear stability maps are considered as indicators for a decent implementation of the

equation system within COMSOL[®]. A later numerical integration is hence justified and can be used as basis for attaining a ROM. Note that as this method is linear, it cannot represent the full non-linear behavior at the neutral stability map. Verification by transient data, as long as available, needs to be further conducted.

4.2.1 LINEAR STABILITY ANALYSIS

Linear stability analysis in frequency domain is outlined in Fig. 4.1. The frequency-domain method, also referred to as linear stability analysis, is a well-established method for stability analysis. Applying first order perturbation theory to a basic solution, it transfers a non-linear PDE system into a linear system. The perturbation is expressed by a modal approach. Inserting the approach into the linearized system and tackle the solution by finite elements for instance, yields conjugate complex EVs. The system becomes unstable if the real part of the EVs becomes negative when increasing the bifurcation parameter. This method is further focused in the following.

For studying linear stability analysis, a steady-state analysis and a EV study needs to be considered within COMSOL[®]. The overall analysis is performed by the strong form formulation. A general equation system in strong form is assumed, see Eq. (4.1). It can be written in matrix form as

$$A \frac{\partial \psi}{\partial t} + B \frac{\partial \psi}{\partial x} = C. \quad (4.7)$$

The vector of unknowns is given by ψ . Arbitrary matrices and vectors associated with the equation system are denoted by: A , B and C . A solution to this equation system might be attained by a time-domain analysis, which is however a time-consuming procedure. A linear stability analysis is based on the steady-state solution ψ_0 to certain initial and boundary conditions specifying the treated operation point. The steady-state version of Eq. (4.7) reads

$$\frac{\partial \psi_0}{\partial x} = (B^{-1})C. \quad (4.8)$$

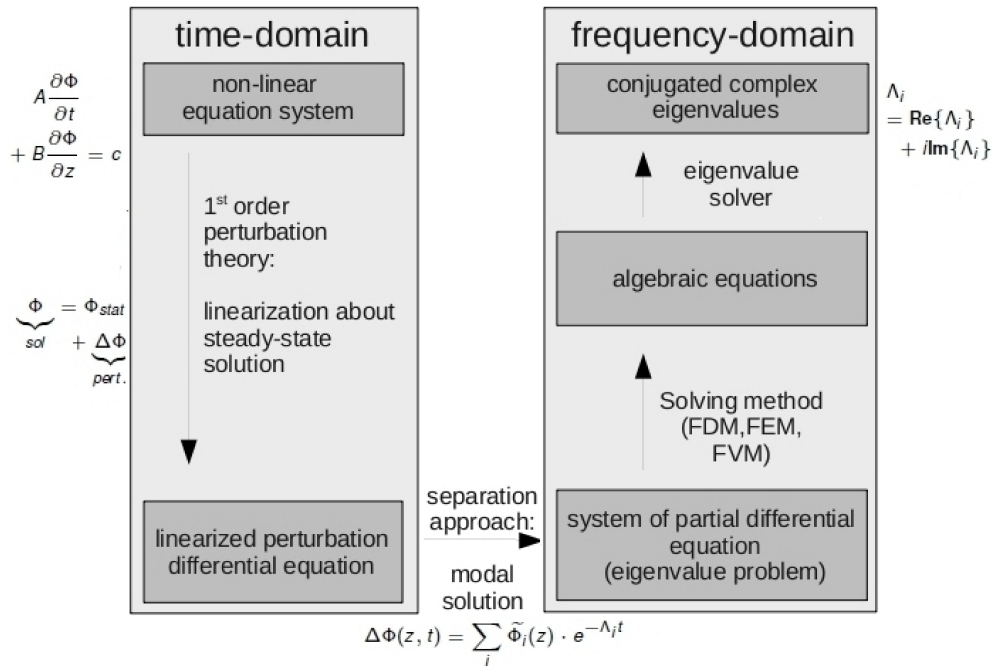


Figure 4.1.: Principles of linear stability analysis in frequency domain.

Equation (4.7) is linearized by the so-called fixed points ψ_0 , i.e. the fully developed flow about the steady-state. The linearized version then reads

$$A_0 \frac{\partial \delta \psi}{\partial t} + B_0 \frac{\partial \delta \psi}{\partial x} = 0, \quad (4.9)$$

where A_0 and B_0 define the linearized equation matrices and a first order perturbation approach,

$$\psi(x, t) = \psi_0(x) + \delta \psi(x, t),$$

has been applied. This perturbation is then expressed as a modal approach:

$$\delta \psi(x, t) = \tilde{\psi}(x) e^{-\Lambda t}.$$

Eigenfunctions are denoted by $\tilde{\psi}$ and complex or real eigenvalues are represented by Λ . Inserting this modal approach into Eq. (4.9) leads to

$$-\Lambda \tilde{\psi} A_0 + \frac{\partial \tilde{\psi}}{\partial x} B_0 = 0,$$

and can be rewritten as EV problem

$$(\Lambda A_0 - \tilde{B}_0) \tilde{\psi} = 0. \quad (4.10)$$

COMSOL's EV routine, which will later be described in Sec. 4.2.2, is used to solve this problem. Its non-trivial solution is given by:

$$\det(\Lambda A_0 - \tilde{B}_0) = 0.$$

It yields various EVs of following type

$$\Lambda = \Lambda_{Re} \pm i \Lambda_{Im},$$

where the real part is given by Λ_{Re} and Λ_{Im} denotes the complex part. The considered fixed point is unstable with respect to small perturbations if a single real EV or a pair of conjugate complex EVs crosses the axis at $\Lambda_{Re} = 0$ [98].

4.2.2 THE EIGENVALUE SOLVER

COMSOL[®]'s EV solver, *mpheig*, is based on the iterative EV algorithm of Arnoldi [3]. In contrast to Lanczos' invented iteration method solving Hermitian matrices, this EV procedure solves general (possibly non-Hermitian) matrices. It is based on Krylov subspaces and takes only a small amount of iterations to give reasonable partial results. The EV algorithm solve the real latent root problem of Eq. (4.10) and is based on ARPACK FORTRAN routines [50]. Its size depends on the chosen nodal discretization and can become rather huge. The algorithm allows treating of extremely large EV problems with a high amount of degrees of freedom.

Conventional iterative methods start with the convergence to the largest dominant latent root for an arbitrary column of $\tilde{\psi}$. Then, the dominant mode is removed and the second dominant mode becomes dominant of the altered matrix. A repetitive application of this procedure leads to all eigenvalues. The total accuracy depends strongly on the accuracy of each step. High numerical costs and slow convergence are expected if roots are not dispersed.

In contrast, by a series of orthogonal function, *mpheig* replaces the solution of the original homogeneous equation by the solution of a reduced order matrix. This matrix is solved in terms of polyno-

mial functions with the help of the orthogonal functions. Thus, EV problems with a high number of degrees of freedom can be solved fast. *mpheig* is verified not only by various examples stated in [25] but also by [48] comparing EVs attained by MATHEMATICA[®] and COMSOL[®] to the Rössler attractor.

4.2.3 LINEAR STABILITY MAP

A MATLAB[®] routine is applied searching for the minimum non-negative EV (the minimum linear stable configuration) by varying bifurcation parameters on a defined direction. For a given operating point the self-written routine checks EVs for a desired grid mesh. By calculating a further refinement, it cross-correlates the EVs and erases non-physical values. It further distinguishes whether a linear stable operation point is present or a linear unstable point. The self-written MATLAB[®] routine is sketched in Fig. 4.2. Searching on distinct parallel lines defined by two user selected operating points, i.e. Q_1 and Q_2 , MATLAB[®]'s *fminsearch* function finds two neutral stable points L_1 and L_2 . Each new line search is defined by

- (a) a distance Δ in the direction of the continuation of the previously found neutral stability points and
- (b) a search for the next neutral stable point L_{i+2} with $i = 1$, in normal direction $n_{i,i+1}$ of the previously found neutral stable points.

By continuing this procedure, the full neutral stability boundary can be found. This neutral stability boundary is marked red within Fig. 4.2.

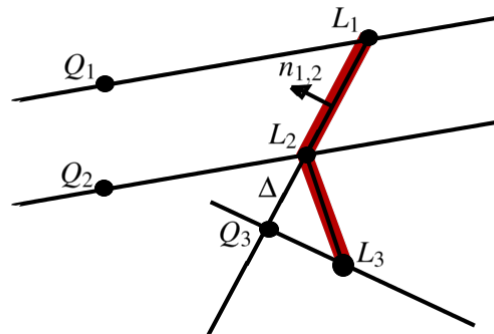


Figure 4.2.: Course of action for attaining linear stability maps by the self-written MATLAB[®] routine.

4.3 PROPER ORTHOGONAL DECOMPOSITION PROCEDURE TO ATTAIN REDUCED ORDER MODELS

This section presents a detailed description of the POD-ROM procedure. It firstly discusses the data generation for attaining the FOM data followed by the calculation of the reduced basis by POD. Part three deals with the problem of long-time stabilization either by choosing different symmetric kernels for the EV problem and/or by preserving boundary effects. A second last part deals with anti-aliasing errors and the last one summarizes the complete methodology and explains the proposed calibration road-map.

4.3.1 ATTAINING FULL ORDER MODEL DATA

A FOM solution can fully be derived using MATLAB[®] routines. Though COMSOL[®]'s solution matrix is not readable within MATLAB[®], data, needed for the decomposition step, is attained by COMSOL[®] to MATLAB[®] interface functions. Data on a user-defined grid can be attained by COMSOL[®]'s *mphinterp* command which translates the unreadable solution matrix to values on the specified spatial grid. Restrictions of spatial derivatives are balanced by highly accurate derivatives, needed for proper orthogonal mode (POM) derivatives within the projection step.

An internal model order reduction is not available within COMSOL[®]. An automatic procedure using the COMSOL[®] to MATLAB[®] interface is of concern for many research topics, see i.e. [131]. However, non of them uses automatic symbolic manipulation to attain their reduced order models and to minimize user interaction. Cardiff and Kitanidis [14] used COMSOL[®]'s general coefficient form PDE as the basis for a general formulation of an inverse problem. Following their idea, our methodology is based on COMSOL[®]'s *general form PDE*, described in Sec. 4.1, doing automatic symbolic manipulation by a self-written MATHEMATICA[®] script.

Increasing the scope of validity range for a dynamical ROM involves collecting data of different representative transients. A multivariate approach collects important transient data and its dedicated goal is to predict system responses not included in the data set [127]. Note, that the validation range of a ROM, going beyond the data basis, needs to be checked for each configuration. In contrast, a monivariate approach just make use of a single transient. ROMs that will be derived within this thesis are based on monivariate data only.

4.3.2 SPECTRAL EXPANSION BY PROPER ORTHOGONAL DECOMPOSITION

A first step on the road to a reduced order model (ROM) relies on the calculation of a reduced basis using the POD for an ensemble of snapshot data, either generated from numerical simulations or experiments. Given this data set of n combined snapshots denoted by $u = \{u(x, t) : x \in \Omega, t \in \{t_1, \dots, t_n\} \subset T\}$ with spatial variable x of the domain Ω and temporal variable t_k ($k = 1, \dots, n$) of the time domain T , the POD is a mathematical tool to attain its related basis which is optimal in the sense that it captures more energy than any other linear basis of same dimension. This energy does not necessarily refer to kinetic energy of the investigated system but rather also to enstrophy and palinstrophy [10], that are measures for the strength of a vorticity and how vorticity is transferred from one direction to another. Detailed discussions referring to the optimality and capturing capabilities can be found in Lumley [78] and Holmes et al. [54]. The POD resembles an optimal, orthogonal, spatial as well as an optimal, orthogonal, temporal basis and the projection converges, in quadratic means, faster than any other spatial or temporal basis corresponding to the same number of modes. This hidden beauty was first discovered by Aubry [4] in 1991.

Basically, the idea of POD is to find the "best" approximation of $u(x, t)$ in terms of n spatial components (i.e. POMs) $\phi_i(x)$, i, \dots, n and temporal functions (i.e. coefficients) $\alpha_i(t)$, i, \dots, n [16]. The approximated numerical solution, denoted by u_M , is represented in terms of a superposition of the temporal variation of the basis functions, i.e.

$$u_M(x, t) = \sum_{i=1}^n \alpha_i(t) \phi_i(x) \quad i = 1, \dots, n,$$

where i represents the index for the mode number truncated at n .

The difference of the projected (approximated) data and the original data will be minimized in the least square sense,

$$\min \int_{\Omega} \int_T \left(u(x, t) - \sum_{i=1}^n \alpha_i(t) \phi_i(x) \right)^2 dt dx,$$

which finally leads to the desired modes [16]. The orthogonality property for both, the modes and temporal functions, i.e. $\langle \alpha_i, \alpha_j \rangle_T = 0 = \langle \phi_i, \phi_j \rangle_{\Omega}$ for $i \neq j$, and insertion into the arbitrary variations of the respectively other set of unknowns $\phi_i(x)$ and $\alpha_i(t)$,

$$\left\langle \left(u - \sum_j \alpha_j \phi_j \right), \alpha_j \right\rangle_T = 0 = \left\langle \left(u - \sum_j \alpha_j \phi_j \right), \phi_j \right\rangle_{\Omega},$$

where the integration over Ω is denoted with $\langle \cdot, \cdot \rangle_{\Omega}$ and over T with $\langle \cdot, \cdot \rangle_T$, leads to a reformulation into Fredholm integral equations of second type [16]:

$$\begin{aligned} \lambda_i \phi_i(x) &= \int_{\Omega} \langle u(x, t), u(x', t) \rangle_T \phi_i(x') dx', \\ \mu_i \alpha_i(t) &= \int_T \langle u(x, t), u(x, t') \rangle_{\Omega} \alpha_i(t') dt'. \end{aligned}$$

These EV problems have self-adjoint and positive semi-definite Hermite kernels where the first integrand is the so-called autocorrelation tensor. Properties, like orthogonality of eigenfunctions and real and positive eigenvalues λ_i and μ_i , are given by the Hilbert-Schmidt theorem. Moreover, a fully recovery of the flow field $u(x, t)$ for $n = \infty$ eigenfunctions is assured. It is common to normalize the spatial eigenfunctions. An EV λ_i can thus be interpreted as the average amount of energy in the direction of the corresponding POD mode [16]. The best approximation will be achieved by ordering the EVs. The solution of the optimization problem is hence reduced to an EV problem. The set of n eigenfunctions corresponding to the n largest EVs is the set of functions that solves the optimization problem.

POD ANALOGY

Having $u_1 = u(x, t_1), \dots, u_n = u(x, t_n) \in \mathbb{R}^m$ snapshots, the corresponding snapshot matrix is denoted by $U \in \mathbb{R}^{n \times m}$. This snapshot field consists of n temporal levels and is available at m spatial grid points. Due to the space-time symmetry of the EV problem there is the choice of two different ways to compute the POMs [138] which enables us to reduce the costs of deriving the correlation matrix. In general, the calculation of eigenvalue decomposition (EVD) for the temporal basis is computationally beneficial. Additionally, there is a third choice due to the similarity between EVD and singular value decompositions (SVDs) [138].

To attain the POMs, one of the following problems need to be solved:

- EVD for $UU^T \in \mathbb{R}^{m \times m}$ if $m < n$:
 $UU^T \tilde{u}_i = \sigma_i^2 \tilde{u}_i$
- EVD for $U^T U \in \mathbb{R}^{n \times n}$ if $m > n$:
 $U^T U \tilde{v}_i = \sigma_i^2 \tilde{v}_i, \tilde{u}_i = \frac{1}{\sigma_i} B \tilde{v}_i$
- SVD for $U \in \mathbb{R}^{n \times m}$:
 $U \tilde{v}_i = \sigma_i \tilde{u}_i$

with EVs $\lambda_i = \sigma_i^2$ and POMs $\phi_i = u_i$. Having identified the cheapest way for the given problem, basically the spatial or temporal grids limit the dimension of the matrix such that the upper limit is equal to the number of snapshots or the number of spatial grid points.

SNAPSHOT BASIS

The choice of the number of snapshots taken from a simulation on a given spatial grid is less obvious. We restrict ourselves to uniform spacings in time. The algorithm does not demand uncorrelated data so that the number of snapshots can be arbitrarily high. However, from a numerical point of view, a reasonable number of snapshots results in smaller EV problems, cheaper costs for computation and possibly in better posed problems [16]. A suitable way to find the best snapshot basis is to regard the convergence of the EV. The eigenspectrum as a function of the number of snapshots can assure, in case of full convergence, that long-wave phenomena are completely covered by the basis.

MEAN FLOW TREATMENT

The POD can also be computed for fluctuation fields

$$u'(x,t) = u(x,t) - \langle u(x,t) \rangle_T$$

which is basically the same if $\langle \langle u(x,t), u(x,t') \rangle_\Omega \rangle_T$ is constant [16]. The mean flow can either be excluded or included from the flow field. Note that a variation of the mean is only possible for the latter which might be of importance for transient and control applications. For each physical problem individually a decision is to take whether to in/exclude the fluctuation fields.

MULTI VARIABLE TREATMENT

Construction of data-based expansions for multi variables $u^{(a)}(x,t), \dots, u^{(q)}(x,t)$, with space coordinates x and time variables t , can be realized in different ways. Fig. 4.3 illustrates these different methods in an overview.

A POD basis can be derived by application of the POD algorithm to each variable field separately (single variable expansion or segregated handling) or for all fields as an entity (lumped variable expansion or coupled handling). The former only includes dominant POMs while the latter also respects composite modes with some small or negligible sub-modes within the ROM. A normalization step is necessary in case of different order of magnitudes of individual variables. A third expansion (coupled variable expansion) treats all fields as a single field. Therefore, only a reduced number of POMs are created. It is not commonly used as main characteristics of variables are lost.

Lumped configurations, treated in [127] for instance, yield good results for a composite mode choices, keeping the coupling of variable fields directly, but at the expense of a higher order ROMs. Throughout this thesis only single variable expansions are applied. Problems of accuracy and robustness are handled by certain inner product choices and a penalty formulation of boundaries. Earlier findings of better performance of lumped-variable expansion can therefore be tackled. Nevertheless, note that tensor approaches, see Appendix B.1 are a suitable alternative for higher dimensional systems with a large number of physical variables.

4.3.3 GALERKIN PROJECTION

In order to get a ROM out of the POMs ϕ_i , the governing system of PDEs needs to be projected onto them with respect to an well-chosen inner product denoted by $\langle \cdot, \cdot \rangle$. The dynamics of the full system will be projected onto the dynamics included in the Ansatz functions within this step.

Let us assume the general governing system of equations for a state vector u of following form:

$$\frac{\partial u}{\partial t} = \mathcal{L}u + \mathcal{N}_2(u, u) + \mathcal{N}_3(u, u, u),$$

where \mathcal{L} is a linear differential operator and \mathcal{N}_2 and \mathcal{N}_3 are (non-linear) quadratic and cubic operators. By neglecting modes with small EV number, the captured energy content is estimated [137] by the first r POMs:

$$l(r) = \frac{\sum_{i=1}^r \lambda_i}{\sum_{i=1}^N \lambda_i},$$

where l is the reduction level defined by the ratio of energy captured by the first r modes to the information content of the ensemble. The reduction level $l \in [0, 1]$ is usually pre-defined by

$$r = \min\{i : l(i) \geq l\}$$

and leads to the truncation criterion r . It is generally set to 99.9% yielding sufficient accuracy. Consequently the reduced approximated numerical solution u_r , the so-called spectral expansion, is represented in terms of a superposition of the temporal variation of the basis functions:

$$u_r(x, t) = \sum_{i=1}^r \alpha_i(t) \phi_i(x),$$

where i the index for the mode number truncated at r . Substituting the ROM solution u_r instead of u into the equation system and applying the Galerkin projection step, by choosing POMs $\phi_j, j = 1, \dots, r$ as Ansatz functions, leads to following system:

$$\left\langle \frac{\partial u_r}{\partial t}, \phi_j \right\rangle = \langle \mathcal{L}u_r, \phi_j \rangle + \langle \mathcal{N}_2(u_r, u_r), \phi_j \rangle + \langle \mathcal{N}_3(u_r, u_r, u_r), \phi_j \rangle.$$

Making use of the orthonormality property within the inner product lead to a set of time-dependent ordinary differential equations of modal amplitudes (i.e. ROM coefficients) that accurately describes

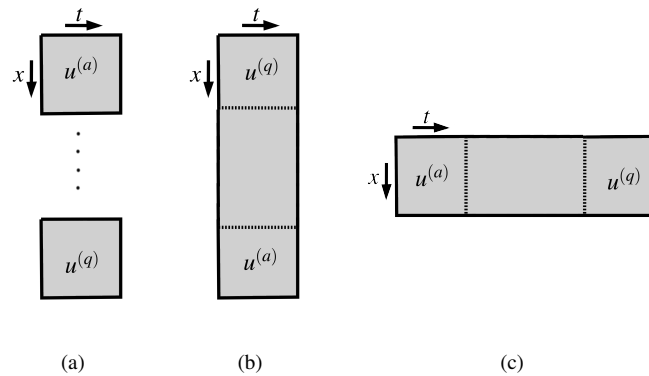


Figure 4.3.: Different multivariable approaches: (a) single variable expansion, (b) lumped-variable expansion, (c) coupled variable expansion.

the flow dynamics of the FOM for limited flow conditions:

$$\begin{aligned} \frac{d\alpha_j}{dt} = \dot{\alpha}_j = & \sum_{l=1}^r \alpha_l \langle \mathcal{L}, \phi_j \rangle + \sum_{l=1}^r \sum_{m=1}^r \alpha_l \alpha_m \langle \mathcal{N}_2(\phi_l, \phi_m), \phi_j \rangle \\ & + \sum_{l=1}^r \sum_{m=1}^r \sum_{n=1}^r \alpha_l \alpha_m \alpha_n \langle \mathcal{N}_3(\phi_l, \phi_m, \phi_n), \phi_j \rangle \quad \text{for } j = 1, 2, \dots, r. \end{aligned}$$

In this case, all amplitudes of non-linearities can be excluded from the inner products such that a simple treatment is possible.

MORE CHALLENGING NON-LINEARITIES

Let us consider a more challenging governing system of following form:

$$\frac{\partial u}{\partial t} = \mathcal{L}u + \mathcal{N}(u) + \tilde{f}$$

where \mathcal{L} is a linear operator and \mathcal{N} is a non-linear operator and \tilde{f} denotes a source function not depending of u . A Galerkin projecting yields an ordinary differential equation (ODE) system of following type:

$$\frac{\partial a}{\partial t} = La + N(a) + F,$$

with $a = (\alpha_1, \dots, \alpha_r)$, $L_{ij} = \langle \mathcal{L}\phi_i, \phi_j \rangle$ for all $i, j = 1, \dots, r$, $F_i = \langle f, \phi_i \rangle$ and $N_i(a) = \langle \mathcal{N}(\sum_{i=1}^r \alpha_i \phi_i), \phi_j \rangle$ with $j = 1, \dots, r$.

Let us assume the inner products of the non-linear term N contain a strong non-polynomial non-linearity. In this case, it is not a priori computable and therefore belongs to online costs that have to be computed at each time step. This is quite expensive so that an alternative way to handle this problem might be best point interpolation [62]. In contrast, we deal with such a system directly as in nuclear applications there are source terms either depending on time and on space and hence our system to solve will have the following type anyway,

$$\tilde{A}(a, t) \frac{\partial a}{\partial t} = \tilde{F}(a, t),$$

where \tilde{A} is a matrix depending on amplitudes α_i and also on time functions and \tilde{F} accordingly. Solving this problem in MATLAB[®] can be realized by the explicit solver routine *ode15s* or the implicit solver *ode15i*, that are capable handling differential algebraic equation and also ODE systems with mass matrix and source terms depending both on time and amplitudes.

4.3.4 STABILITY PRESERVING FOR CONTINUOUS PROJECTIONS

Note that during the symbolic mathematical manipulation a "continuous projection" is applied, where the projection onto basis modes in a continuous inner product is employed instead of the use of a "discrete projection" approach where the semi-discrete representation of the governing equations are projected onto a set of discrete modes in a discrete inner product choice. This is beneficial as numerical analysis techniques employed within spectral methods can be used to stabilize and letting the system converge to the same stability behavior than the original system. The ROM can comprise a certain stability guarantee and an efficient, asymptotically stable reduced version of the non-linear PDE system is attained. This approach is sometimes also referred to as grid-free modeling.

We emphasize that ROMs, constructed by a discrete projection approach without a stability check, can be potentially unstable, see e.g. [62]. Kalashnikova and Barone [62] highlighted that preserving asymptotic stability of the reduced system attained by a Galerkin projection step is closely tied to the choice of the inner product and the formulation and implementation of the boundary conditions. Both are under investigation in the following.

IMPLEMENTATION OF BOUNDARY CONDITIONS

Boundary conditions are only present up to a certain effect in the POMs but are not inherited automatically within the ROM constructed using the continuous Galerkin projection approach [5, 62]. A weak implementation, applying the boundary conditions directly into the boundary integrals arising from integration by parts after projection, can be argued not being accurate close to the boundary. Numerical experiments demonstrate that especially ROMs with mixed type (Robin) boundary conditions have significant errors near the boundary that may grow in time and spoil the solution on the complete domain [62]. Preserving the boundary condition as an own equation leads to a number of constraints and to a differential algebraic equation (DAE) system [131] which is solvable requiring a time-consuming procedure. Methods taking into account extended expansions, i.e. additional modes for each boundary and adjusting their amplitudes, let the ROM diverge [44, 131].

A **weak implementation of the boundary condition** is derived by applying integration by parts for multi-dimensions, see Eq. (4.5). Making use of this identity and deploy it onto the diffusion and/or convection term yields boundary integrals including the boundary conditions of Neumann and/or Dirichlet type,

$$\begin{aligned}\langle \Delta u, v \rangle &= -\langle \nabla u, \nabla v \rangle + \langle \nabla u, v \rangle \Big|_{\partial\Omega}, \\ \langle \nabla u, v \rangle &= -\langle u, \nabla v \rangle + \langle u, v \rangle \Big|_{\partial\Omega}.\end{aligned}$$

Note that the boundary contributions are included by a factor of one. They are not amplified which means that the impact is small. Hence, additionally, based on the energy method, a **penalty-enforcement of boundary conditions** ensures non-destabilizing effects within the ROM and was proposed by Kalashnikova [62]. This penalty enforcement of the boundary conditions rewrites a boundary value problem,

$$\begin{cases} u_t = \mathcal{L}u + \mathcal{N} + f & \text{in } \Omega \\ Bu = h & \text{on } \partial\Omega \end{cases},$$

into following system representation:

$$u_t = \mathcal{L}u + \mathcal{N} + f - \Gamma(\tilde{B}u - h)\delta_{\partial\Omega} \quad \text{in } \Omega \cup \partial\Omega$$

where Γ represents a diagonal matrix of penalty parameters selected such that stability is preserved, \tilde{B} is the boundary operator and h are the boundary values. The indicator function

$$\delta_{\partial\Omega} = \begin{cases} 1, & \text{for } x \in \partial\Omega \\ 0, & \text{otherwise} \end{cases}$$

marks the boundary. In general, the penalty parameters can be derived by a energy method [62] or simply by employing an iteration step which is our preferred choice.

Within our implementation, for a consistent formulation of boundary conditions, diffusion and convection terms are replaced by its equivalent integration by parts formulation but boundary parts are amplified by a penalty parameter which is chosen to be the same as for a penalty formulation. A

further penalty formulation includes the boundary as punitive function. Summarizing this procedure leads to following **penalty amplified weak formulation** keeping the remaining parts of the equation system as it is:

$$\begin{aligned}\langle \Delta u, v \rangle &= -\langle \nabla u, \nabla v \rangle + \Gamma \langle \nabla u, v \rangle \Big|_{\delta\Omega}, \\ \langle u, v \rangle &= -\langle u, \nabla v \rangle + \Gamma \langle u, v \rangle \Big|_{\delta\Omega}.\end{aligned}$$

Note that preferred approaches including boundary conditions leading to systems having no additional unknowns. Taking into account exact boundary conditions within the penalty enforced weak formulation leads to systems having high penalty parameter and to ill-conditioned problems. Further types of boundary implementation possibly performing better, are summarized in Appendix B.2.

WEIGHTED SOBOLEV INNER PRODUCT FOR CALIBRATION

The above derived POD yields a basis that optimally describes a certain data set. As interest lies in matching numerical ROM solutions to original solution trajectories, terms corresponding to derivatives must optimally be approximated. Higher order derivatives, i.e. u_x, u_{xx}, \dots , have not been approximated in the derived procedure hence a convergence, as rapid as the approximation of u , cannot implicitly be assured [65]. Furthermore, a low-dimensional POD-ROM might not be capable describing the original system due to its truncation as low-energy modes, having impact on fine-scale structure, are neglected. Due to this loss of dissipation of energy, long-term stability gets lost. This may be overcome by retaining smaller scales in the model. Enhancing dissipation artificially can be done by another inner product choice to calibrate the ROM [36]. Kirby [65] chooses a inner norm different to an euclid norm for the Kuramoto-Sivashinsky equation due to missing dissipation. Note that for time-varying inflow conditions (perturbations) gradients will be of importance and should be regarded by an optimal inner product choice for the kernel.

Accordingly, a modified minimization problem is solved by

$$\begin{aligned}\lambda_i \phi_i(x) &= \int_{\Omega} K_s(x, t) \phi_i(x) dx, \\ \mu_i \alpha_i(t) &= \int_T \tilde{K}_s(x, t) \alpha_i(t) dt,\end{aligned}$$

where K_s and \tilde{K}_s are the generalized modified Sobolev kernels defined by

$$\begin{aligned}K_s(x, t) &= \varepsilon_0 \langle u(x, t), u(x', t) \rangle_T + \varepsilon_1 \langle u_x(x, t), u_x(x', t) \rangle_T + \varepsilon_2 \langle u_{xx}(x, t), u_{xx}(x', t) \rangle_T, \\ \tilde{K}_s(x, t) &= \varepsilon_0 \langle u(x, t), u(x, t') \rangle_{\Omega} + \varepsilon_1 \langle u_x(x, t), u_x(x, t') \rangle_{\Omega} + \varepsilon_2 \langle u_{xx}(x, t), u_{xx}(x, t') \rangle_{\Omega}.\end{aligned}$$

This preserves the favored symmetry property of the kernel [65]. For reasons of simplification, the following only refers to (untilded) K_s generalized Sobolev kernels. In a simplified denotation, it reads

$$K_s = \varepsilon_0 K_0 + \varepsilon_1 K_1 + \varepsilon_2 K_2,$$

where fundamental kernels will be denoted by $K_0 = \langle u(x, t), u(x', t) \rangle$, $K_1 = \langle u_x(x, t), u_x(x', t) \rangle$ and $K_2 = \langle u_{xx}(x, t), u_{xx}(x', t) \rangle$. The generalized Sobolev weight for kernel K_0 is defined by ε_0 , ε_1 is the generalized Sobolev weight for kernel K_1 and ε_2 denotes the generalized Sobolev weight for kernel K_2 . Sometimes even higher derivatives play an important role within the energy dissipation mechanism. In such a case they need also be included into the kernels.

The energy method can be used to obtain an energy inequality that gives a domain where the temporal growth is bounded in regions where the exact solution are asymptotically stable [62]. This procedure a priori identifies the optimal inner product choice with respect to stability. As this cannot be captured in a general approach for different systems, we instead apply an iteration about the Sobolev inner product weight ε_1 keeping $\varepsilon_0 = 1$ and $\varepsilon_2 = 0$ constant or iterations for weights ε_1 and ε_2 keeping $\varepsilon_0 = 1$ constant.

INNER PRODUCT APPROXIMATIONS

The continuous L^2 inner product $\langle \cdot, \cdot \rangle_{L^2}$ is applied and approximated by a discrete L^2 inner product version

$$\langle u, v \rangle_{L^2} = \int_{\Omega} uv d\Omega \approx \sum_{k=0}^N u(x_k)v(x_k)$$

where $x_0, \dots, x_N \in \Omega$ are spatial discretization points. Further stabilization achievable by Sobolev type inner products $\langle \cdot, \cdot \rangle_{H^1}$, see Appendix B.3, are not considered within this thesis.

CONSEQUENCES

Boundary terms are imposed by a penalty method and artificial dissipation is included by a problem specific inner product. Additional iterative loops for the best boundary penalty parameters Γ and the Sobolev inner product weights are therefore performed. Barone et al. [5] and Kalashnikova and Barone [62] emphasized that for compressible Euler or Navier-Stokes equations the preferable inner product choice is of Sobolev inner product type. Tests need to be carry out if the standard L^2 inner product sufficiently preserve stability for each equation system anew.

4.3.5 ANTI-ALIASING

The POD-ROM belongs to spectral methods following the principle, the higher the order the better the results of the ROM. Unfortunately, this is not always true provided that aliasing effects come into play. Aliasing can be divided into two groups:

Aliasing referring to spatial resolution Fine-scale modes are not regarded. These information should not alias into those POMs which are of interest. This can be ensured by an adequate resolution in space. For particular modes, i.e. Fourier modes, the amount of measurement positions can be calculated by the Nyquist criterion such that the spatial aliasing is minimized. The POD is protected against those aliasing effects by taking into account a certain spatial resolution such that the eigenvalue spectra is fully converge.

Aliasing referring to higher order non-linear terms Multiplications regarding higher order non-linear terms need to be checked carefully. If results of multiplication chains influence unresolved POMs then these contributions will affect amplitudes of important POMs. Small errors within multiplication chains can therefore mislead to a wrong solution. This holds especially for high order non-linear terms and/or terms were state variables are included in exponential functions. Typical aliasing phenomena need to be checked and filtered where appropriate.

This thesis only treats aliasing referring to spatial resolution. Aliasing referring to higher order non-linear terms might be mastered by error controls/filters, see Appendix B.4, but are not treated here.

4.3.6 HIGHER ORDER DERIVATIVES

The approximation of derivatives plays a dominant role for the POD-ROM methodology. Difference schemes will be used within decomposition and reconstruction.

Within this work, the general explicit difference formulas for numerical differentiation derived by Li [76] are used which are effective and of higher order i , i.e. $\mathcal{O}(i)$: First derivatives are at least approximated by $\mathcal{O}(4)$, second derivatives by at least $\mathcal{O}(3)$, third derivatives by at least $\mathcal{O}(2)$ and fourth order derivatives are of $\mathcal{O}(1)$.

Even higher accuracy order can be achieved by respecting functional values at all nodes. These Tschebycheff collocation methods, also so-called Tschebycheff pseudospectral methods, combined with an optimal choice of nodes by Gauß-Lobatto or Gauß-Tschebycheff collocation schemes, are not treated within this thesis.

4.3.7 CALIBRATION ROAD MAP

A novel POD-ROM-calibration road map is proposed and orange-colored in Fig. 4.4. System dynamic predictions for a few representative data sets (gappy data), $ds1, ds2, \dots$, must be treated carefully. A spectral basis is achieved by single variable expansions for each variable field by its own. For a transient analysis the mean flow needs to be considered in/out of the decomposition and reconstruction. Two different types of ROMs will be discussed in the following. Boundary terms are imposed by weak penalty implementation method and artificial dissipation are always included by a problem specific inner product. Two additional iterative loops for the best boundary penalty parameters and the Sobolev inner product weights are hence performed.

Note that this POD-ROM methodology might be enhanced by different expansion methods, modal specific inner product choices within the Galerkin projection, methods including boundary conditions and error controls avoiding aliasing effects. For a more detailed description we refer to Appendix B.

4.4 CODE STRUCTURE SKETCHES

Figure 3.1 already summarizes the methodology of attaining a ROM based on POMs. Different commercial programs are utilized for the different processing steps whereas MATLAB[®] is the controlling program. Attaining full order model (FOM) data is performed by COMSOL[®], the calculation of the reduced POD basis is realized by MATLAB[®], all analytical reformulations and the final calculation of the reduced system matrices are defined by MATHEMATICA[®]. MATLAB[®]'s ODE solver finally determines the system. The coupling interface is realized via the well-established LiveLink without graphical user interface in the case of COMSOL[®] and MATLAB. In contrast, MATHEMATICA[®] is integrated by a system function call, interchanging text files.

The structure of the used main program *comparison* is outlined in Fig. 4.5. Here, the user can define iterative parameter searches. The program further opens the function *start* where four preselected PDE systems can be selected: homogeneous equilibrium model (HEM), Kortweg-de-Vries (KdV), natural convection in a closed circuit (NCC) and tubular reactor (TR). Note that code architecture is straightforward such that different systems can be integrated easily. Moreover, fluid properties are loaded as necessary by a self-written piecewise cubic spline fit of water steam table data of *webbooknist.com*. The user can further distinguish between three types of different analyses. Linear stability analysis being started by *fct_lin_ew_stab_ana*, time analysis either for perturbed or unperturbed systems started by *fct_time_analysis*, and transferring and solving the PDE system as reduced

version by *fct_pod_rom*.

Having started a linear stability analysis by *fct_lin_ew_stab_ana*, involves intelligent line searches by *fminsearch*, see Fig. 4.2. Particular operating points are solved by its EV problem with *model_PDE*. Here, constants, functions and the geometry are defined, initial conditions selected, the PDE system is included and solved for a given mesh by *fct_posteval_sol_comsol_study_steady_state*. Then a linear stability analysis takes place. By a consecutively mesh refinement, EVs without physical meaning are erased. A structural outline is given in Fig. 4.6.

The centerpiece for attaining a ROM by *fct_pod_rom* is based on three main function calls: *model_pde*, *fct_pod_data* and *fct_pod_treatment*. The former function defines the physical system and calculates a steady-state solution before doing a transient analysis by *fct_posteval_sol_comsol_study_time*. The snapshot basis is read into a structure by *fct_pod_data*. Within *fct_pod_treatment* the technical construction of the ROM is realized. *POD_fct* determines the POMs. *fct_odecomponentstring* creates the text input for the MATHEMATICA[®] script call by *PODcoef2*. This script performs all necessary analytical steps within the Galerkin procedure to attain the coefficient matrices for the ODE system in text form. These text files are interpreted within *fct_odecomponentstring* before finally *fct_odesolvesystem* solves the ROM by MATLAB[®]'s *ode15i* routine.

4.5 ERRORS

Only local information is given by plotting time evolutions of FOM to ROM data at a reference location. A global comparison of POD-ROMs is based on quantities referring to the entire domain, i.e. error quantities. These errors, i.e. root mean square error (RMSE), correlation coefficient (CC) and maximum error (ME), will be given in the following. An optimal ROM has smallest \overline{RMSE} by a large as possible \overline{CC} and smallest maximum error (ME).

ROOT MEAN SQUARE ERROR

Let us assume, u determines a certain field that is to be investigated. The root mean square error (RMSE) between the POD-ROM and the true FOM solution at time levels t_j estimates the error of the projection. It is defined by

$$RMSE(t_j) = \left(\frac{1}{m} \sum_{i=1}^m (u_{FOM}(x_i, t_j) - u_{ROM}(x_i, t_j))^2 \right)^{0.5} \quad \forall t_j$$

where m is the total number of axial nodes of the domain and $u_{FOM}(x_i, t_j)$ and $u_{ROM}(x_i, t_j)$ are the distributions at time steps t_j and axial positions x_i . The average RMSE is given by

$$\overline{RMSE} = \frac{1}{n} \sum_{j=1}^n RMSE(t_j)$$

and is a measure for the averaged error. Here, the total number of snapshots is denoted by n . For an optimal system the average RMSE vanishes.

CORRELATION COEFFICIENT

Another error quantity is the correlation coefficient (CC) which describes how the dynamical behavior of the reduced system behaves in comparison to the original system. It is defined by

$$CC(t_j) = \left(\sum_{i=1}^m (u_{FOM}(x_i, t_j) - u_{ROM}(x_i, t_j))^2 \right) \cdot \left(\sum_{i=1}^m u_{FOM}(x_i, t_j)^{0.5} \sum_{i=1}^m u_{ROM}(x_i, t_j)^{0.5} \right)^{-1} \quad \forall t_j$$

The time average CC

$$\overline{CC} = \frac{1}{n} \sum_{j=1}^n CC(t_j)$$

and is a measure for the averaged correlation.

MAXIMUM ERROR

Finally the ME, here referring to the temperature field only, indicates the maximum error on the whole temporal and spatial domain.

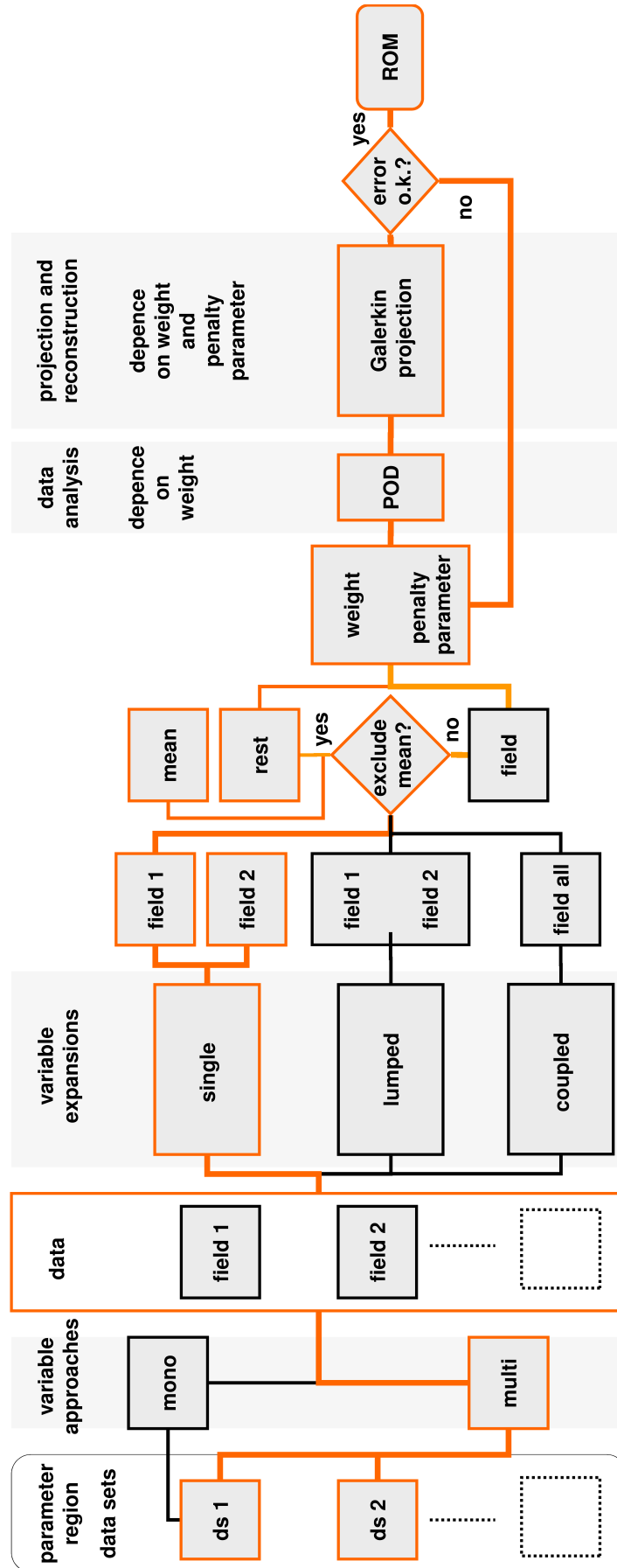


Figure 4.4.: Novel POD-ROM enhancements.

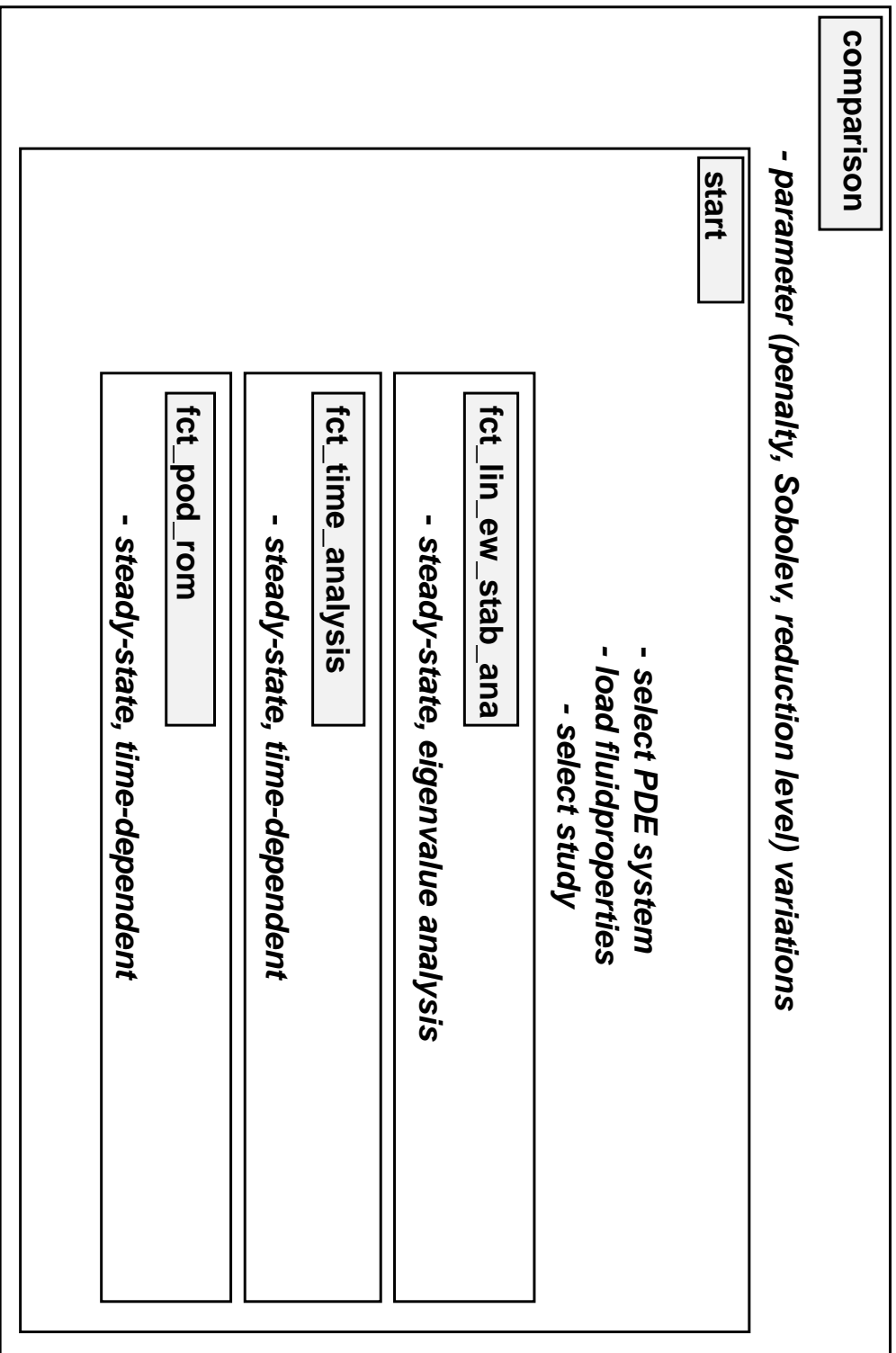


Figure 4.5.: Schematic code structure of the main program.

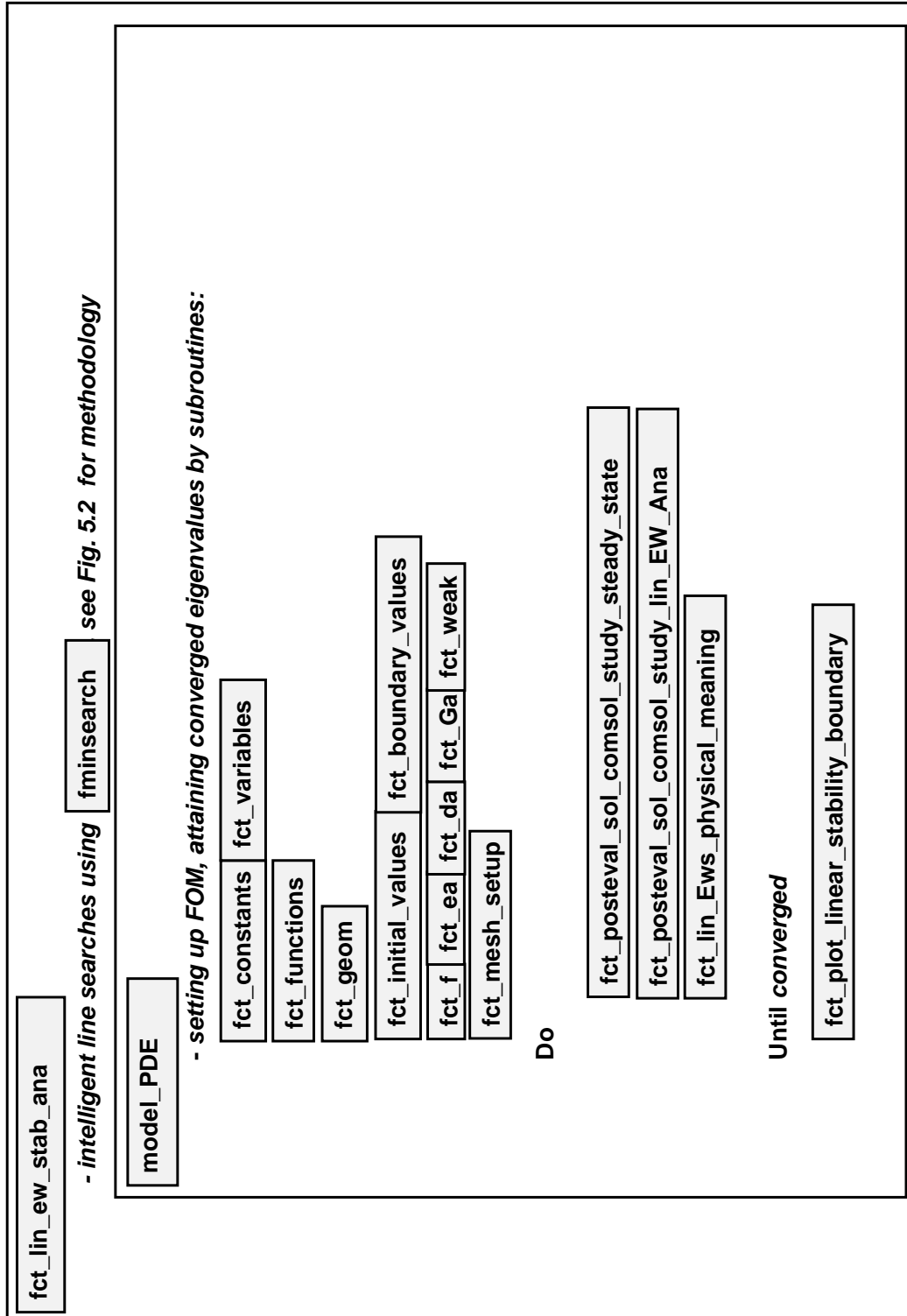


Figure 4.6.: Schematic code structure for attaining linear stability maps.

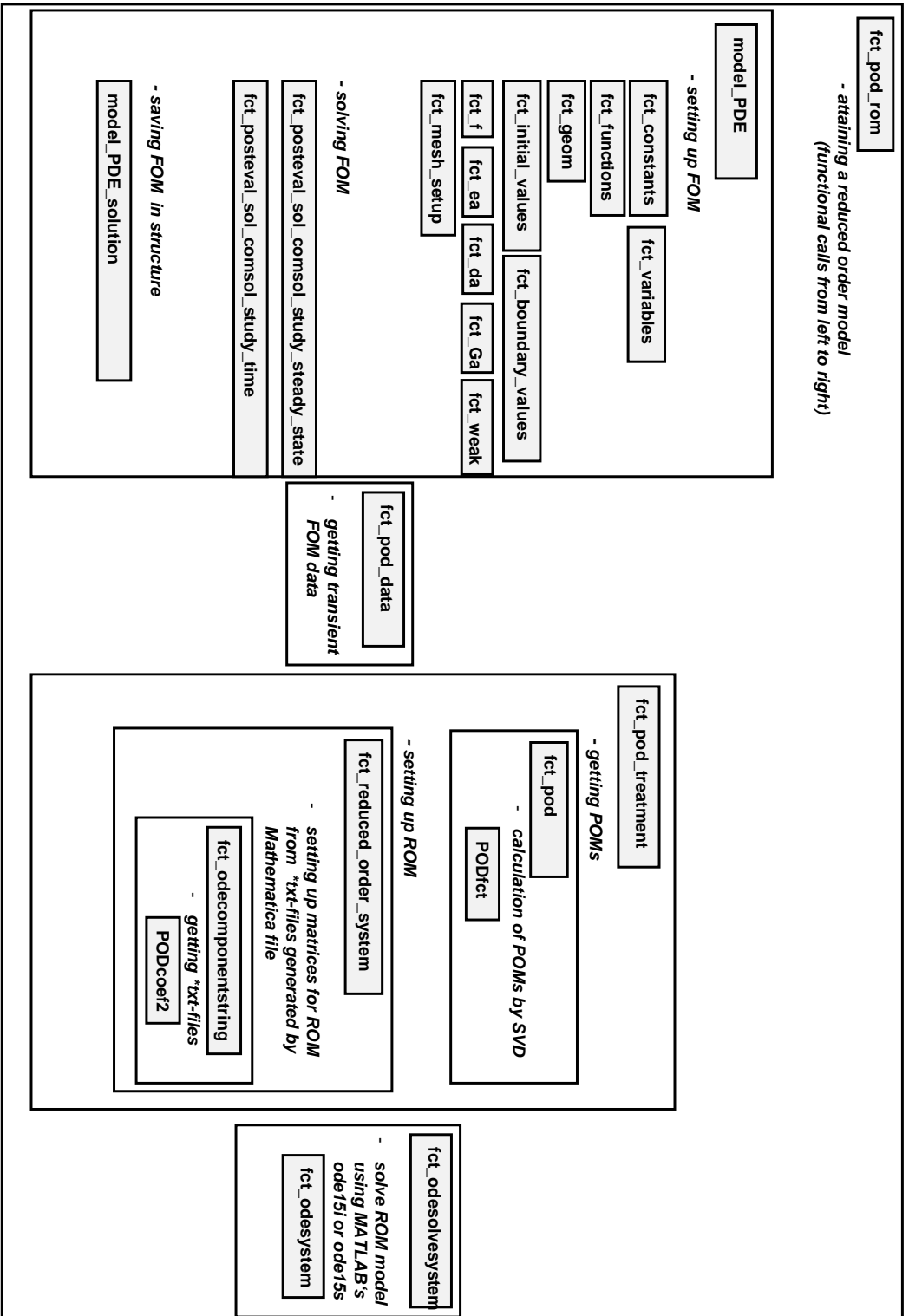


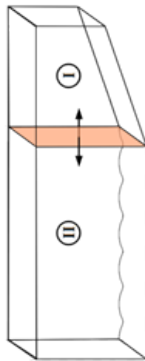
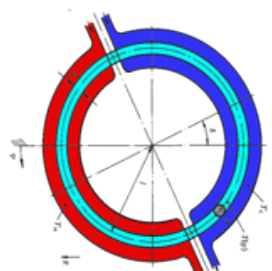
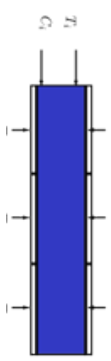
Figure 4.7.: Schematic code structure for solving POD based ROMs.

5 VALIDATION AND VERIFICATION

Within the scope of our envisioned boiling water reactor (BWR) stability analysis, a wide spectrum of verification and qualification examples is exploited, as specific requirements need to be implemented for different proper orthogonal decomposition (POD)-reduced order models (ROMs). This chapter refers to important validation steps illustrated in Tab. 5.1, yielding a reliable strategy for deriving ROMs. A short summary is given below. A more detailed description can be found in each section.

- The Kortweg-de-Vries (KdV) equation describes surface waves in shallow water. In [101, 108] it was shown that the dynamic behavior can be reproduced by a small amount of modes. Important conservation quantities also indicate that reduced order model (ROM) can be applied for stability analysis.
- Channel flow entering a free surface domain by a Kortweg-de-Vries (KdV)-diffusor setup was modeled by Steinbacher [132]. A pressure equation was derived modeling the pressure loss within the diffusor. Moreover, the KdV was transformed to describe pressure waves. Both equations fundamentally differ and applying the POD-ROM methodology to the full problem fails. A constant two-zone setup is shown to be capable of handling time-varying interfaces separating regions where different partial differential equations (PDEs) are valid.
- Based on experiments and modeling of Ehrhard [40] and Ehrhard and Müller [41], verification and validation was given for a natural convection in a closed circuit (NCC)-POD-ROM in [103, 104, 106, 107]. The natural convection in a closed circuit (NCC) represents an adequate qualification example as physics contain strong non-linear effects. Perturbations are imposed by an abrupt change of heat input such that, referring to BWR conditions, this can be compared to neutronic feedback. A comparison of limit cycles attained by [41] and the natural convection in a closed circuit (NCC)-POD-ROM shows that the ROM attains the same amplitude. It is able to correctly predict trajectories in the parameter space which are partially lying outside the subspace covered by the input transient. This is an example of the physics-extrapolating possibility of POD-ROMs.
- Based on a setup of Belzen et al. [136], further validation is realized by the tubular reactor (TR), a system also featuring a complex non-linear dynamical behavior. This example is considered as an equivalent test case for perturbation investigations of the BWR system (i.e. against pump trips etc.) violating the inlet and exit conditions. The whole methodology was validated and verified for oscillating phenomena caused by external conditions in [105]. The robustness of the general approach is demonstrated through application to a perturbed version of a tubular reactor (TR) and is shown to describe both aspects well: the dynamical behavior of the underlying transient and a prediction within a perturbation range not included in the data set. Different stabilized ROMs are reviewed and the road to an optimal ROM is given. By a comparison to results of [136] it is demonstrated that the approach delivers meaningful results.

Table 5.1.: Validation and verification basis of the POD-ROM methodology.

example	geometry	description	achievements
KdV		surface waves in shallow water	dynamical behaviour by a small amount of modes reproduced
KdV diffusor		surface waves after a diffusor	dynamical behaviour by a small amount of modes reproduced
NCC		dynamical behaviour of the fluid	verification and validation against experimental and analytical data and prediction of different operating point possible
TR		evolution of a reactant	verification of the complete methodology

5.1 SOLITON WAVES

Kortweg-de-Vries (KdV) type equations are reasonable examples for POD based ROMs investigations due to their non-linear and dispersive character. Their numerous conserved quantities easily allow comparisons of reduced order models (ROMs) to full order models (FOMs) of perturbed versions.

A general description of the Kortweg-de-Vries (KdV) equation describing solitons, is given in the following. Properties and features of the equation system are referred to. Out of a representative transient choice, a POD based ROM of the non-dimensional KdV equation is further derived in this section. Its performance demonstrates that system dynamics can be reproduced by a few number of proper orthogonal modes (POMs). Moreover, it is shown that, even for substantial perturbed KdV versions, that accurate error results are attained.

5.1.1 MODEL AND PROPERTIES

In 1834 John Scott Russell first discovered a certain type of wave that seems to travel forever [114]. Riding on a horse, he kept watching on a boat traveling up on a small rectangular channel surrounded by walls. The boat suddenly stopped and released a wave. He pursued this wave and observed that it did not change form during time and/or diminish speed. Those properties gave rise to the name of his detection: the so-called soliton (wave).

In general, a soliton is a non-linear wave with the nature of a particle [35]. It follows the superposition principles although the wave itself is highly non-linear. The speed of the wave depends on its height and does not change in time. Non-linear and dispersive effects are evenly balanced. In a collision of two solitons the form is conserved and a phase shift appears. Energy is conserved during interaction due to the remarkable stability property. The stability of various colliding solitons was first observed by Zabusky and Kruskal by computer calculations with sinusoidal initial conditions [149].

Korteweg and de Vries [66] derived the equation, describing the long-time evolution of small-amplitude long-wavelength dispersive waves, also so-called flat shallow water waves, in small channels in its dimensional version in 1895:

$$\frac{\partial \eta}{\partial t} = \frac{3}{2} \sqrt{\frac{g}{h}} \frac{\partial}{\partial x} \left(\frac{1}{2} \eta^2 + \frac{2}{3} \alpha \eta + \frac{1}{3} \sigma \frac{\partial^2 \eta}{\partial x^2} \right).$$

Here, η is a small quantity, $\eta + h$ represents the elevation of the surface above the bottom at a horizontal distance x from the origin of coordinates, α is a small arbitrary constant being related to the exact velocity of the uniform liquid motion and $\sigma = h^3/3 - \gamma h/g\rho$ depends on the water depth h . The surface tension is denoted by γ , the gravitational acceleration by g and ρ represents the density. This system has soliton wave solutions and can be transferred into non-dimensional form to the so-called Kortweg-de-Vries (KdV) equation:

$$\frac{\partial u}{\partial t} - 6u \frac{\partial u}{\partial x} + \frac{\partial^3 u}{\partial x^3} = 0, \quad (5.1)$$

with nondimensional height u . The term uu_x denotes the focusing of the wave and u_{xxx} describes the dispersion. It possesses steady progressing wave solutions, either having wave train or solitary wave form [45]. Solitary wave solutions to Eq. (5.1) can only be observed in rather special cases. The solutions to the KdV equation can be studied by the help of the one-dimensional (1D) Schrödinger equation where inverse scattering transformations yield N soliton solutions [46]. For periodic initial

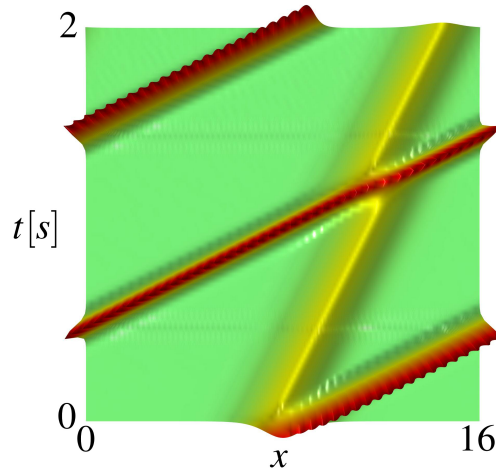


Figure 5.1.: Moving of two solitons with different speed to the right.

values with

$$u(x, 0) = -N(N + 1) \operatorname{sech}^2(x), \quad (5.2)$$

there are exactly N solitons. They can explicitly be stated by

$$u(x, t) = 3a^2 \operatorname{sech}^2\left(\frac{1}{2}a(x - x_0 - a^2t)\right)$$

and are traveling to the right with constant speed a^2 being proportional to their amplitude. The width is inversely proportional to the square root of the speed. Note that the higher the wave the faster it travels. Figure 5.1 illustrates the solution for $N = 2$ on a computational domain of $[0, 16]$ for time instances $t \in [0, 2s]$ with periodic boundary conditions. Note that two solitons are produced and within the collision only a phase shift appears.

Equivalent equation versions to Eq. (5.1), sometimes having various constants and an additional u term, are capable to describe different physical applications [45]. Multiple fluid dynamical applications, besides the description of long water waves in channels of finite depth, and plasma physics are also referred to this equation in articles. Furthermore, solitons play an important role in fiber optics, acoustics of crystal lattices and waves within density-stratified oceans.

There are countable infinite conserved quantities for the KdV equation due to a transformation derived by Gardner [46]. Among others, quantities that represent mass m , momentum p and energy conservation E are given by:

$$m(t) = \int_{\Omega} u(x, t) dx, \quad (5.3a)$$

$$p(t) = \int_{\Omega} \frac{1}{2} u(x, t)^2 dx, \quad (5.3b)$$

$$E(t) = \int_{\Omega} \frac{1}{2} \left(\frac{\partial}{\partial x} u(x, t)^2 \right) + u(x, t)^3 dx, \quad (5.3c)$$

where Ω denotes the spatial domain.

5.1.2 REDUCED ORDER MODELS OF SHALLOW WATER WAVES

Different steps towards a POD based ROM of the KdV are illustrated within this subsection. Starting with the implementation of the full order model (FOM) in COMSOL[®], a POD based ROM is derived by a representative transient choice. Its reconstruction potential is demonstrated and the attained reduced version is used to illustrate that, either for spatial or temporal perturbed versions of the KdV-POD-ROMs, the temporal evolution of conservation quantities yield accurate results.

FULL ORDER MODEL IMPLEMENTATION

Data of a shallow water wave simulation is derived by a transient calculation of the non-dimensional KdV equation in COMSOL[®]:

$$\frac{\partial u}{\partial t} - 6u \frac{\partial u}{\partial x} + \frac{\partial^3 u}{\partial x^3} = 0. \quad (5.1)$$

The computational domain has a length of 2π and periodic boundary conditions. As third and higher order derivatives cannot be evaluated within COMSOL[®] (by a substitution v) the original equation is transformed to the following equation system that is solved within COMSOL[®]:

$$\begin{aligned} \frac{\partial u}{\partial t} + \frac{\partial v}{\partial x} &= 6u \frac{\partial u}{\partial x}, \\ \frac{\partial^2 u}{\partial x^2} &= v. \end{aligned}$$

The transformed equations are subject to periodic boundary conditions:

$$\begin{cases} u|_{x=0} = u|_{x=2\pi}, \\ v|_{x=0} = v|_{x=2\pi}. \end{cases}$$

TRANSIENT CHOICE

Each ROM of the KdV equation is based on the implementation of the following **transient** simulation of $t \in [0, 5s]$ with initial conditions:

$$\begin{aligned} u(x, 0) &= -\sin(x) - 2, \\ v(x, 0) &= +\sin(x). \end{aligned}$$

This "expert" choice of transient is simulated. The spatial grid is well resolved and the grid size is fixed to $x_h = 0.025$. This can be underlined by a comparison of conserved quantities referring to a full order model (FOM) simulation with temporal resolution of $t_h = 0.0025s$. Figure 5.2(a-c) shows the temporal behavior of the simulated FOM conserved quantities. They have been evaluated using COMSOL[®]'s internal numerical integration scheme with order 10. Results are in good agreement with the analytical solution corresponding to the chosen initial conditions:

$$\begin{aligned} m(t) &= \int_0^{2\pi} u(t) dx = \int_0^{2\pi} (-\sin(x) - 2) dx = -4 * \pi \approx -12.5664, \\ p(t) &= \int_0^{2\pi} 0.5 u(t)^2 dx = \int_0^{2\pi} 0.5 (-\sin(x) - 2)^2 dx \approx 14.1372, \\ E(t) &= \int_0^{2\pi} 0.5 u'(t)^2 + u(t)^3 dx \approx -67.5442. \end{aligned}$$

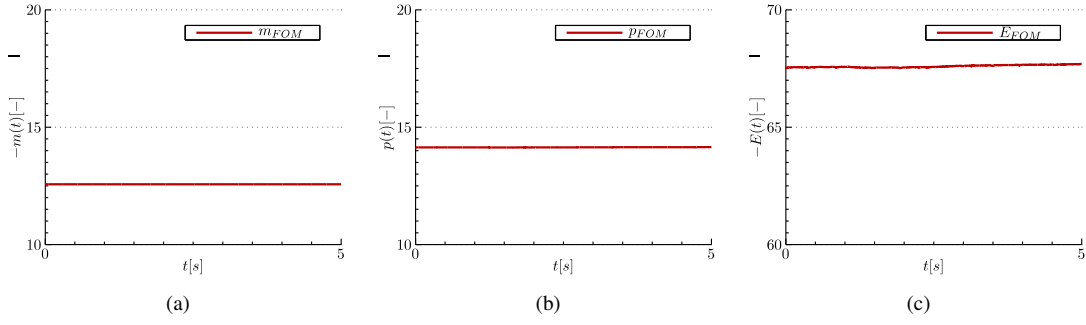


Figure 5.2.: Conservation of mass (a), momentum (b) and energy (c) of full order model.

Note that the finite element method (FEM) is not conservatively formulated by itself. Preserving conservation quantities therefore indicates a sufficient resolution.

EXPERIMENTS

Three different kinds of KdV type experiments will be analyzed in the following. The first experiment (a) is chosen to demonstrate that a reconstruction of the original data can be achieved. This guarantees that dynamics of both, the FOM and ROM, are identical. Experiments (b) and (c) tackle issues of spatial and temporal modifications within the KdV equation. Concerning the BWR scope, this is similar to switches swapping between different flow regimes and/or heat transfer regimes.

- (a) Reconstruction of the original "true" FOM data
- (b) Simulation of a ROM with spatial weakened non-linear term in Eq. (5.1):

$$H(x) \delta u u_x,$$

with

$$H(x) := \begin{cases} -1 & \text{if } x \in [0, 2\pi] \setminus (1, 5) \\ -0.5 & \text{if } x \in (1, 5) \end{cases}$$

and differently chosen initial conditions

$$\begin{aligned} u(x, 0) &= -\sin(x) + 1, \\ v(x, 0) &= +\sin(x). \end{aligned}$$

- (c) Simulation of a ROM temporal weakened non-linear term

$$H(t) \delta u u_x,$$

with

$$H(t) := \begin{cases} 1 & \text{if } t \in [0, 1] \cup [2.5, 5.0] \\ 0 & \text{if } t \in (0.5, 2.5) \end{cases}$$

and same initial conditions as in experiment (a).

Note that spatial and temporal jump functions, i.e. $H(x)$ and $H(t)$, are modeled by smooth hyperbolic tangent functions.

ATTAINING REDUCED ORDER MODELS

The typical transient choice is referred to as FOM solution. Applying the POD algorithm to an ensemble of snapshots for the non-dimensional heights fields u detects relevant system states which are hidden in the transient data. The mean value of the non-dimensional height has been included in the correlation matrix calculations and further ROM achievements. Hence, the first dominant POD mode represents a normalized version of the mean. Due to the spatial grid choice of the FOM, the ROM is also based on the fixed axial grid size of $x_h = 0.025$.

The number of snapshots, necessary for attaining the correlation matrix, is not a priori known. A convergence plot of the dominant eigenvalues (EVs) in Fig. 5.3(a) underlines that a snapshot basis of approximately 2000 is sufficient for fully resolving long-wave phenomena. No significant variation indicate that relevant transient dynamics are not hidden between the time steps. Fine-scale information is therefore captured. Note, that hidden information would lead to jumps within the EVs plot of Fig. 5.3(a). Accordingly, the time step size is fixed to $t_h = 0.0025s$ and applied throughout this section.

Figure 5.3(b) illustrates the eigenspectrum on a semi-logarithmic scale with inserted reduction level of 99.98% and treated temporal mean directly within the snapshot bases. Besides the first EV referring to the normalized version of the mean, coherent structures appear in pairs. This is due to the fact that the autocorrelation matrix is invariant under translation and depends on the difference between the snapshot fields. The associated first ten dominant POMs are represented in Fig. 5.4. The first POM refers to the mean that only slightly varies in space. Higher POMs refer to the moving of the underlying traveling wave. They have sinusoidal form. Always two modes have similar wave number but they are shifted to each other. The higher the mode, the higher the wave number of the sinusoidal form.

By truncating low-importance POMs the essential spatial and temporal characteristics of the system should be preserved. A well-defined truncation criterion should identify r relevant POMs. Using an Ansatz with these r modes and applying the Galerkin method to the system of equations by employing POMs as test functions, determines the desired non-linear ROM-POD. Periodic boundary conditions need not be respected within these ROMs due the periodic nature of the POMs. This procedure maps the physical system of coupled non-linear PDEs to coupled non-linear ordinary differential equations (ODEs).

The analysis, presented in Fig. 5.5, shows the variation of the time-averaged root mean square error

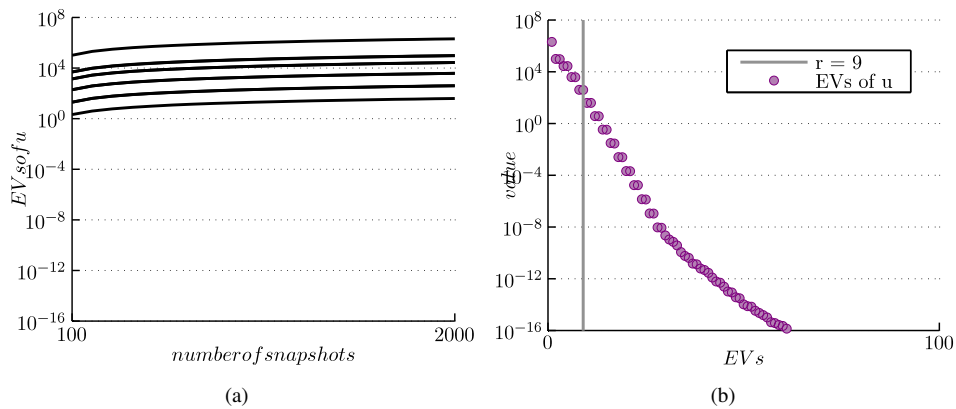


Figure 5.3.: Convergence plot of the first ten eigenvalues of the non-dimensional heights field (a) and the associated eigenspectrum on a semi-logarithmic scale with inserted reduction level and temporal mean included (b) for a snapshot basis of 2000.

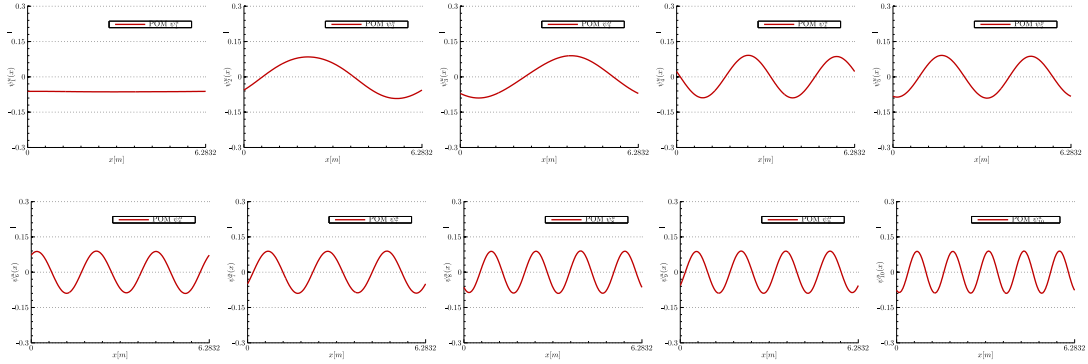


Figure 5.4.: 10 dominant proper orthogonal modes of "true" full order model data to the "expert" KdV transient.

(RMSE) \overline{RMSE} over the rank r representing the reduction level. The RMSE between the POD-ROM and the true FOM solution at time levels t_j estimates the error of the projection. For an optimal POD-ROM the time average RMSE vanishes. Note its non-monotonic decrease after $r = 5$. A reconstruction level of 99.98% is achieved by a truncation criterion of $r = 9$, which was previously also marked in Fig. 5.3(b). The averaged RMSE yields a value of $\overline{RMSE} = 8.845\%$. Due to numerical errors, a fully vanishing temporal RMSE can never be achieved.

5.1.3 PERFORMANCE

EXPERIMENT (A)

The potential to recover the solution of the FOM is illustrated in Fig. 5.6. Full order model (FOM) data is marked in red and reduced order model (ROM) data is colored in blue within all comparing graphs. In Fig. 5.6(a), the dynamics are well-reproduced for the non-dimensional heights at the position $x = \pi$. Given the time evolution of two global error quantities in Fig. 5.6(b)-(c), the RMSE and correlation coefficient (CC) demonstrate that small long-time destabilization effects are hidden in (a). Note that from a numerical point of view, the system response is stable and the increasing error is attributed to the upcoming phase shift. Global conserved quantities, illustrated in Fig. 5.6(d-f), underline that mass and momentum is conserved during the ROM calculation. Energy is also conserved but at a different level comparing to the FOM. This can be addressed to the differently applied

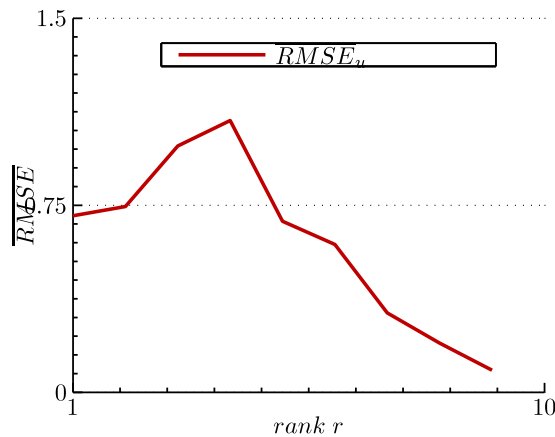


Figure 5.5.: Time averaged root mean square error (RMSE) for varying KdV reduced order model (ROM) ranks.

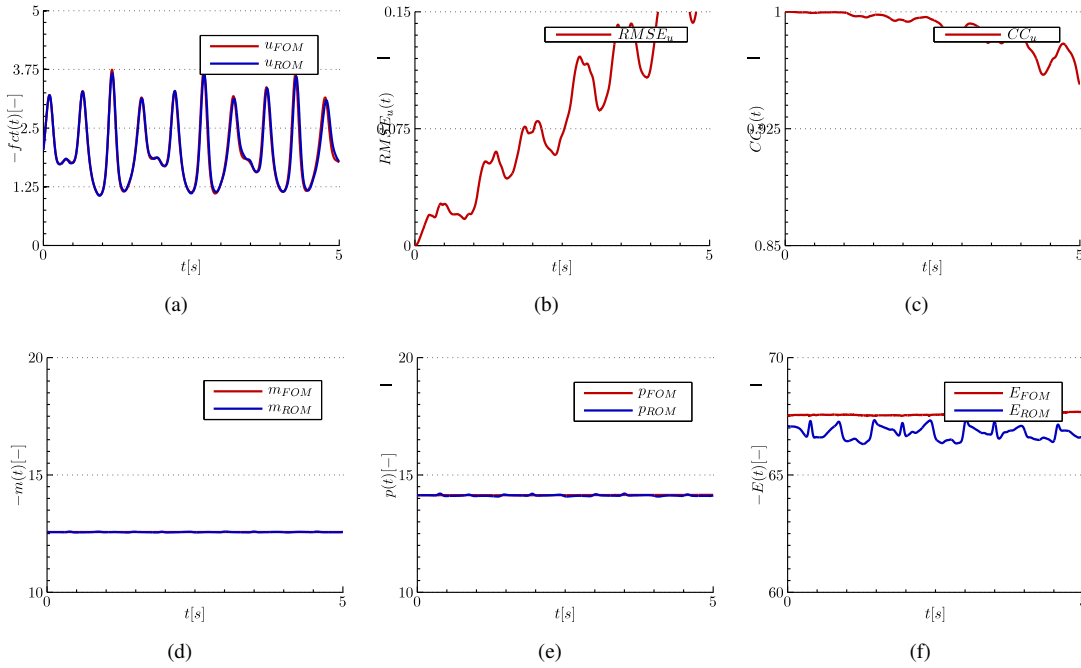


Figure 5.6.: Experiment (a): Time evolution of non-dimensional height at $x = \pi$ (a), root mean square error (b), correlation coefficient (c) and global conserved quantities (d-f).

numerical integration scheme: *trapz* within MATLAB[®] using the trapezoidal rule and having order two in comparison to the COMSOL[®] integration scheme having order ten.

EXPERIMENT (B) AND (C)

KdV experiments having spatial and temporal weakened non-linear terms are illustrated in Fig. 5.7 and Fig. 5.8. Both experiments substantially change the KdV equation. Accordingly, conserved quantities of the unperturbed KdV equations are no longer preserved. A transient behavior is expected instead.

Within the spatial perturbed experiment (b), local and global results demonstrate that system dynamics are well-reproduced besides a small phase shift. Again in all comparing graphs, full order model (FOM) data is marked in red and data referring to the ROM is colored in blue. As the non-linear term is modified at $x \in [1, 5]$ and fully retained in the rest of the domain, Fig. 5.7(a) shows a fundamental different temporal behavior than in experiment (a). Dynamics are preserved but an increasing phase shift is visible in the end of the transient. This also holds true for error quantities, being illustrated in Fig. 5.7(b-c). Global conserved quantities in Fig. 5.7(d-f) present the same underlying dynamics including the phase shift. The error in comparison to the FOM solution increases as the numerical integration scheme within MATLAB[®] is different to the scheme in COMSOL[®].

Local and global results of the temporal perturbed experiment demonstrate that system dynamics are well-reproduced besides a small phase shift which is clearly visible in Fig. 5.8(b-c). Again, colors of comparing graphs are chosen as above. Within this simulation, the non-linear term is completely switched off after 1s and fully switch on again after 2.5s. It is remarkable that a system behavior, not included in the underlying data set, can be reproduced within this time period and afterwards (Fig. 5.8(a)). Note that conserved quantities (Fig. 5.8(d-f)) are comparable to FOM data, besides the already aforementioned effects of different internal integration strategies.

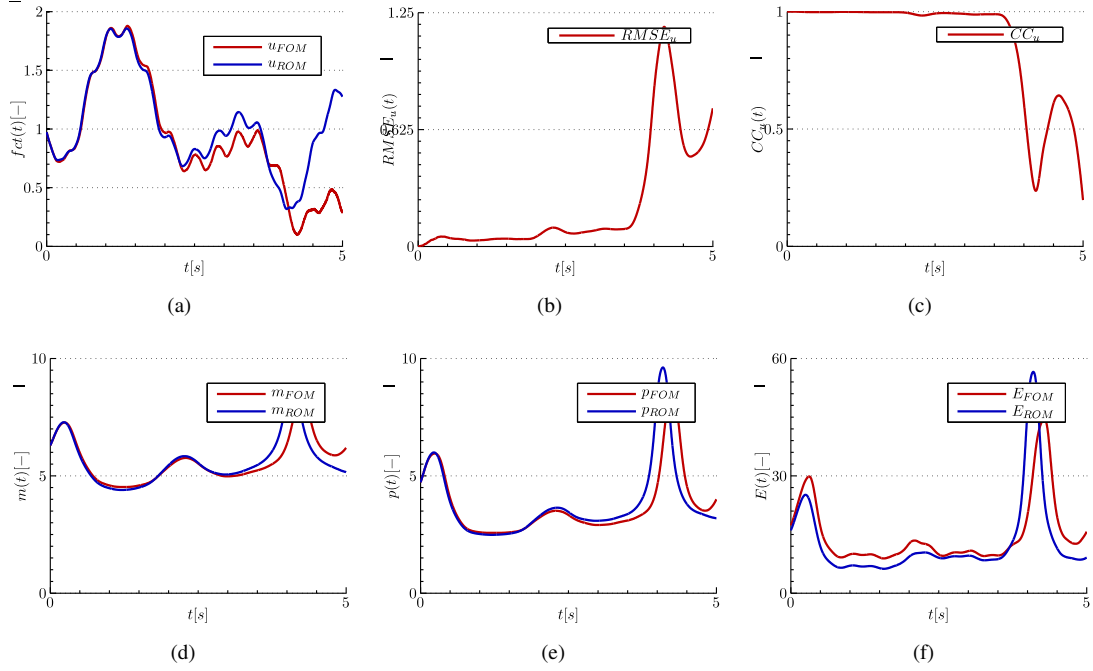


Figure 5.7.: Experiment (b): Time evolution of non-dimensional height at $x = \pi$ (a), root mean square error (b), correlation coefficient (c) and global conserved quantities (d-f).

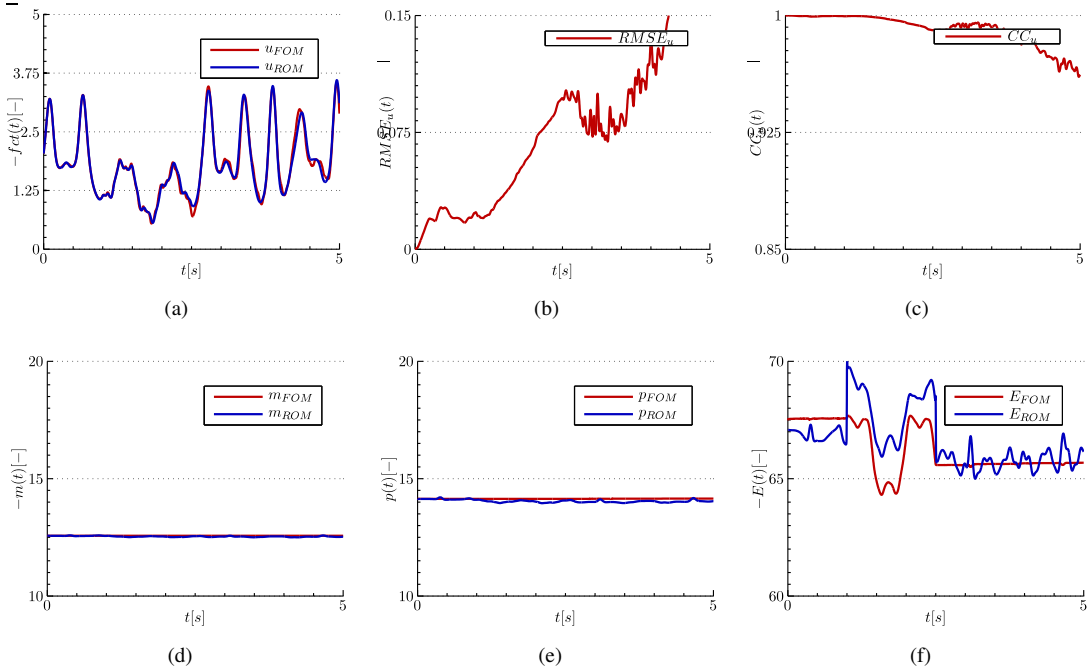


Figure 5.8.: Experiment (c): Time evolution of non-dimensional height at $x = \pi$ (a), root mean square error (b), correlation coefficient (c) and global conserved quantities (d-f).

CONCLUSIONS

Although, long-time system behavior of the ROM is not in phase to the FOM for a unperturbed version of the KdV equation (experiment (a)) stability results are not affected. A verification is given by the temporal distribution at $x = \pi$, where no overshooting is visible. Experiment (b) and (c) demonstrate that attention has to be paid to the validation range of a ROM. Perturbing the system and tracking the response is closely related to stability analysis. An expert choice of transient to build up a reliable data basis is necessary. In both investigated cases, conserved and global error quantities of the underlying transient show dynamical similarities to the true solution. Nevertheless, there is a pronounced phase shift within both investigated spatial or temporal perturbed versions of the KdV-POD-ROMs.

Remaining errors of conserved quantities of the ROMs can be addressed to the usage of MATLAB[®]'s internal trapezoidal numerical integration routine *trapz* of second order. COMSOL[®]'s internal numerical interpolation rely on a interpolation order of ten. No additional error is expected as derivatives within the energy conservation Eq. (5.3c) are approximated by a higher order derivative scheme of Li [76].

5.2 FREE SURFACE WAVES AFTER A DIFFUSOR

Single-phase sub-cooled water enters the reactor in BWR core. Due to nuclear fission, water is heated up within fuel elements and a two-phase flow is achieved at some position. Due to varying inlet conditions, e.g. on the basis of changing inlet sub-coolings and/or occurring pressure or density oscillations among others, the phase-change position is time-dependent. The transition between one-phase flow and two-phase flow can be smooth but also rather sharp. By modeling thermal-hydraulics with a homogeneous equilibrium model (HEM) for instance, sharp transitions are expected without considering of sub-cooled boiling. In addition, they are possibly instationary.

By a generic two-zone model, derived by Steinbacher [132] in a master thesis, questions concerning POD based ROMs with instationary transition between two different regions have been treated. The channel flow entering a free surface domain is modeled by a KdV-diffusor setup. A pressure equation is derived for modeling the diffusor pressure loss. The KdV, describing shallow water waves, has been used to characterize the pressure distribution after the diffusor. By a sinusoidal inlet mass flow, the break-off point of the shallow water wave is triggered to be instationary. Both equations have fundamental differences and applying the POD-ROM methodology to the full problem fails.

The following section describes the geometry and the model of the KdV-diffusor setup. By investigating proper orthogonal modes (POMs) of the complete region, three different zones are identified, namely the diffusor, the transition and the free surface region. Due to the modeling by equations of different character, the proposed strategy of [132] is utilized in this section to handle the time-varying interface employing a constant two-zone setup. Finally, improvements will be discussed concerning this static setup choice.

5.2.1 TWO-ZONE MODEL

Treating instationary transitions between two different regions is modeled by a time-varying generic two-zone model with different physical behavior. It is sketched in Fig. 5.9 and was derived in [132]. It consists of two different regions, the diffusor (I) and the free surface region (II), separated by a time-dependent interface x_g (marked orange). The channel setup has a length of 25 units and only a small depth d . The contour of the upper wall of the diffusor is denoted by h and depends on its position x . It has an initial height of h_0 and a constant slope m . The height of the free surface wave

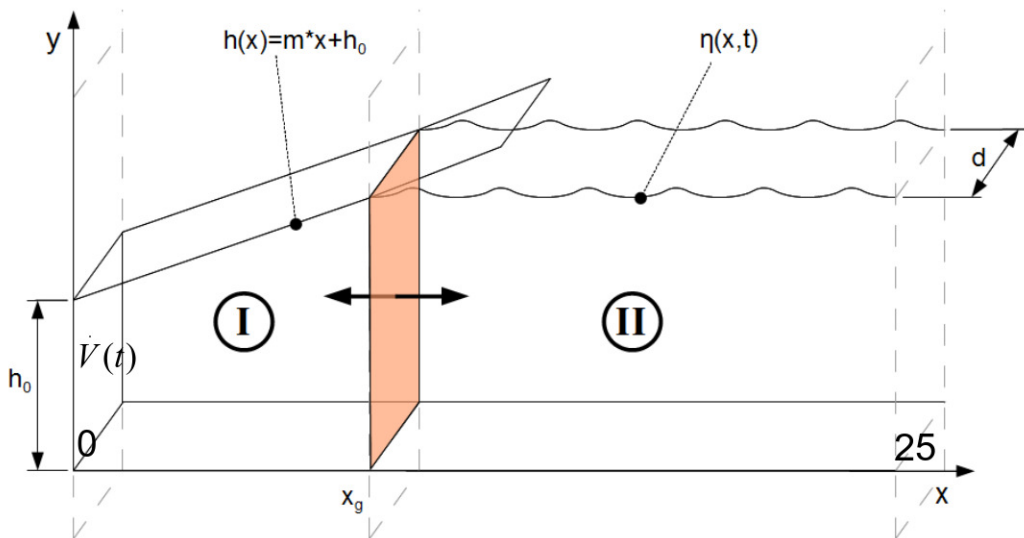


Figure 5.9.: Scheme of physical two-zone diffusor model of Steinbacher [132].

after the diffusor is given by its contour $\eta(x, t)$. By varying the inlet volume flow $\dot{V}(t)$, the flow velocity is changed. Accordingly, the impact of friction alters in the channel and hence the position of the break-off point of the free surface. This leads to surface waves varying in time.

An exhaustive derivation of the underlying equations describing both, the diffusor and the free surface, can be found in [132]. Hereafter, only the basic ideas are referred to. Providing a clear representation, unnecessary informations or restatements are omitted. The derivation can be divided into three parts. The first part describes the flow in the diverging channel, the second part deals with the model of the free surface and a last one treats the coupling between (I) and (II) by a time-varying boundary:

- The flow of the diverging channel is assumed to be two-dimensional (2D), laminar, incompressible and friction losses are proportional to the horizontal flow velocity. Based on the Navier-Stokes equations, following system of conservation equations for mass and momentum are given [132],

$$\begin{aligned}\frac{\partial u}{\partial x} + \frac{\partial v}{\partial y} &= 0, \\ \frac{\partial u}{\partial t} + u \frac{\partial u}{\partial x} &= -\frac{1}{\rho} \frac{\partial p}{\partial x} - Au + \frac{g}{2} \frac{\partial h}{\partial x},\end{aligned}$$

where ρ is the density of the fluid, g the gravitational force, u denotes the velocity component in x -direction and v the component in y -direction of the velocity vector \vec{v} , and p denotes the pressure. Note that the momentum conservation is derived by the complete set of momentum equations for a 2D, laminar and incompressible flow [132]. It corresponds to the Euler equation for a flow path with additional friction term Au . The mass conservation is simplified based on assumptions of: a linear y -velocity profile, the independence of the x -velocity component on y , a negligible boundary layer and parallel flow at the upper wall. An equation for $u = u(x, t)$ can then directly be given. Inserting this expression and the proportional factor A into the momentum equation, and integration over the complete diffusor, yields an equation for the pressure distribution. Due to the complexity of the underlying pressure relation and based on the associated parameter region for the applied sinusoidal volume flow excitation, Steinbacher [132] derived a simplified representation. Hereby, he neglects quantities having small impact and doing a further approximation of the remaining influence by a logarithmic function. He finally attained the following pressure relation:

$$p(x, t) = p_0(t) + \frac{1}{2} gm\rho x + A_p(t) \ln(F_{korr}x + 1) \quad (5.4)$$

where p_0 denotes the inlet pressure, m the gradient of the channel surface wall, $A_p(t)$ is a prefactor and F_{korr} a correction term within the logarithmic approximation.

- The free surface after the diffusor is modeled by the Kortweg-de-Vries (KdV) equation. The model derivation assumes an incompressible, rotational-free and inviscid flow. The underlying Navier-Stokes equation read

$$\begin{aligned}\nabla \cdot \vec{v} &= 0, \\ \frac{\partial \vec{v}}{\partial t} + \vec{v} \cdot \nabla \vec{v} &= -\frac{1}{\rho} \nabla p + \frac{1}{\rho} \vec{f},\end{aligned}$$

where \vec{v} denotes the velocity vector of the flow, \vec{f} the volume force acting on the fluid, ρ the density, p the pressure. In a next step, the volume force is expressed by the gravitation potential and boundary conditions for the velocity components are defined: The velocity yields zero

value at the bottom and at the surface it corresponds to its vertical movement. As the medium is incompressible, the pressure level can be chosen to be zero at the surface. Moreover, the surface tension is neglected. The channel geometry is assumed to be small which implies a 2D problem. Transformation in its non-dimensional form, further expansion in a potential series and reformulation yields the Kortweg-de-Vries (KdV) equation describing the elevation η :

$$\eta_\tau + \eta_\xi + \frac{3}{2}\alpha\eta\eta_\xi + \frac{1}{6}\delta^2\eta_{\xi\xi\xi} = 0.$$

For coupling the KdV equation with the pressure distribution in the diffusor part of the test geometry, a reformulation in terms of non-dimensional pressure π has been given:

$$\pi_t + D_1\pi_x\pi + D_2\pi_{xxx} = 0. \quad (5.5)$$

Hereby, a relation between water depth and pressure is applied. D_1 and D_2 are terms proportional to the chosen water depth h in zone II. The pressure in Eq. (5.4) is reformulated in non-dimensional form by defining

$$\pi = p - \frac{gH\rho}{6p_{system}}.$$

- The coupling of both equations, Eq. (5.4) and Eq. (5.5), manifests itself at the time-varying boundary x_g which can directly be derived. Provided that the channel pressure equals the ambient pressure in addition to the mean gravitational pressure, a free surface wave is released. The ambient pressure is set to zero throughout this section. The position x_g is hence depending on the inlet pressure p_0 , the ambient pressure p_U and the pressure losses in the channel. Figure 5.10 illustrates the dependency between the chosen inlet volume flow and the position of the break-off point.

5.2.2 FULL ORDER MODEL IMPLEMENTATION

Having all ingredients by hand, Eq. (5.4) in its non-dimensional form is coupled to Eq. (5.5) by a Heaviside function based on the temporal varying break-off point x_g . This system of equations is implemented in COMSOL[®]. A complete list of system parameters can be found in [132]. A

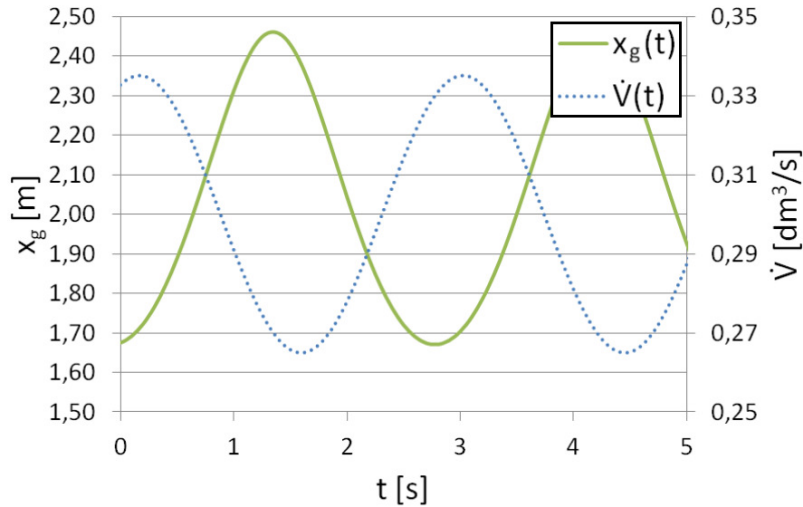


Figure 5.10.: Coupling of the two-zone diffusor model due to flow rate variation, Steinbacher [132].

three-region geometry is defined consisting of: the channel, a transition zone including the altering position of arising free surface waves, and the free surface zone itself. The mesh size is chosen to be $x_h = 0.025$ in the channel and free surface zone. A finer mesh size is selected in the transition zone having $x_h = 0.005$. The sinusoidal mass inlet flow is chosen to trigger the system, see Fig. 5.10.

5.2.3 PROPER ORTHOGONAL DECOMPOSITION ANALYSIS

Due to the chosen non-stationary mass inlet flow, a time-varying wave break-off point is triggered. The test geometry can therefore be divided into three regions: The channel, a transition and the free surface zone. Correspondingly, by applying the POD algorithm to the full problem, POMs must be suited to this division into zones. This is based on the properties of the algorithm where a correlation is realized by using the complete data set. This is illustrated by Fig. 5.11 showing the excluded mean and the first four dominant POMs. FOM data has been recorded for 35s on a properly chosen grid of $x_h = 0.005$ for a time step size of $t_h = 0.1s$, see [132]. The mean clearly shows the pressure drop and the average pressure level of the free surface. All modes show a strong jump within the transition zone. The pressure drop of the channel zone is visible in the beginning of each mode. Also, the sinusoidal wave in the free surface region after the transition zone is identified. The transition zone starts approximately at $x = 1.8$ and ends before $x = 2.5$. However, the location of the transition zone differs from mode to mode.

Applying the POD algorithm, a clearly assignment to one underlying physical system can only be realized by a separate treatment of the diffuser or the free surface zone. As the break-off point of the wave in the transition zone depends on time, snapshot data always refers to the channel pressure drop and/or the free surface model. Here, various POMs are necessary to fully describe the temporal break-off point in reconstructions, see [132]. This fundamental finding leads to the suggestion of a three zone treatment of the problem. Nevertheless, there is no equation for the transition zone hence only a two-zone setup can be realized.

Even having modes to the full domain as in Fig. 5.11 and additional knowledge about the time-varying boundary x_g , a two-zone model fails in simulations [132] without modifications. This is due to the present static transition zone within the modes. By solely installing a switch based on x_g -knowledge, only parts of the modes are used for each zone model. Nevertheless, the transition

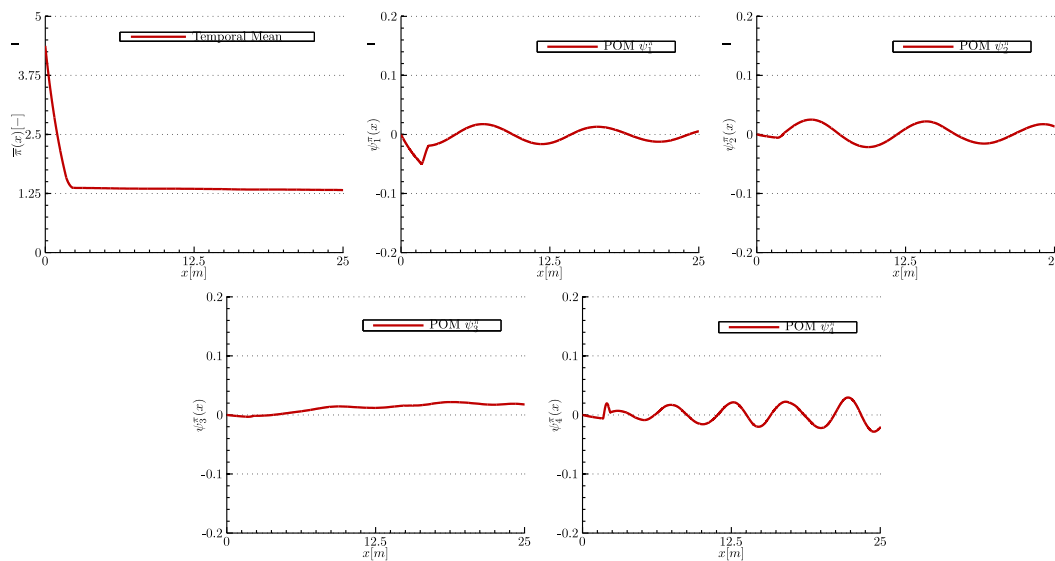


Figure 5.11.: Mean and four dominant proper orthogonal modes of pressure for the complete analysis of the two-zone diffuser model.

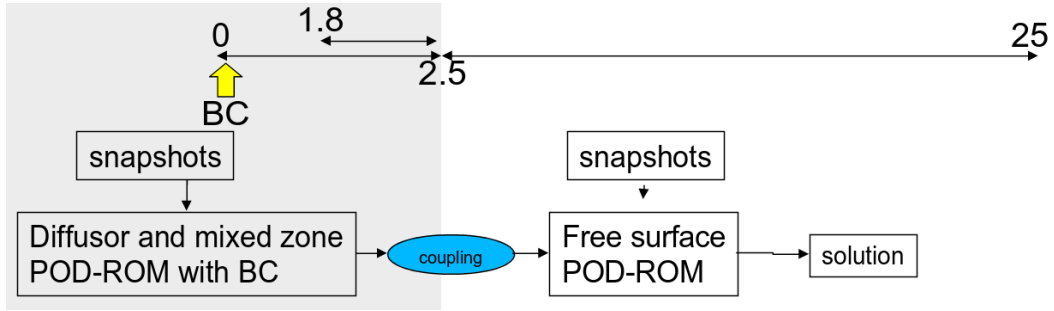


Figure 5.12.: Scheme of static two-zone diffusor coupling based on Steinbacher [132].

zone and especially the jump has influence in this type of modeling. As the two underlying physical equations have furthermore different character from a mathematical point of view, simulations diverge. Based on these findings, a constant two-zone setup was developed in [132] which is discussed hereafter.

5.2.4 TWO-ZONE REDUCED ORDER MODEL

CONSTANT COUPLING SCHEME

The coupling scheme is illustrated in Fig. 5.12. The complete domain is divided into two zones at $x = 2.5$. The first zone (shaded in gray) includes the channel and transition region, the second zone consists only of the free surface region. Based on FOM data belonging to separate regions, two POD based ROMs are derived, having different character:

- The first POD-ROM is based on the diffusor pressure loss equation with time-varying inlet volume flow. Due to the lack of a time derivative and the simple structure of the derived pressure loss Eq. (5.4) in its non-dimensional form, following system (of algebraic form) is attained:

$$A\alpha = f,$$

where A is the system matrix, α the vector of unknowns and f a source term.

- The second POD-ROM is solely based on the KdV Eq. (5.5) and coupled via boundary values available from the first system. The structure of the underlying physical equation has a time derivative which yields following ODE structure:

$$A\dot{\alpha} = f.$$

The first system inlet boundary condition is included by a penalty formulation with high penalty parameter $\Gamma = 1000$, necessary to preserve sufficient impact of the changing volume flow. Also a penalty parameter of same magnitude connects both derived ROM regimes. Accordingly, the coupling is realized via the inlet boundary of the POD-ROM in zone (II) and the terminus value of the obtained reduced system of zone (I).

REDUCED BASIS FOR TWO DIFFERENT ZONES

FOM is used to derive a POD basis within zone (I) and (II). Data for zone (I) consists of a transient of $t \in [0, 2s]$ for chosen grids of $x_h = 0.005$ and $t_h = 0.1s$. Numerical experiments demonstrate that a 2s transient is sufficient: The data set consists of more than half a period of the excited inlet volume flow

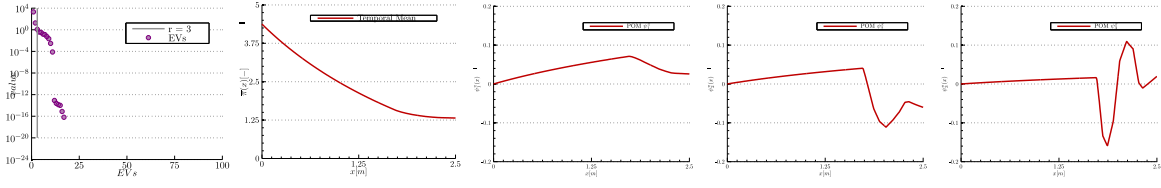


Figure 5.13.: Static two-zone diffuser coupled model - zone (I) : Eigenspectrum, mean and three dominant proper orthogonal modes.

and all details are contained, referring to the simple sinusoidal triggered dynamics of the pressure loss within the diffuser. Obtaining a reconstruction level of 99.99% requires three POMs for sufficiently reproducing main dynamics of the data set. Figure 5.13 illustrates the eigenspectrum, the mean and associated three dominant POMs. Note, that POMs contain information about the diffuser pressure loss and the dynamical behavior in the transition zone.

Zone (II) data is based on a transient of $t \in [0, 20s]$ for grids $x_h = 0.025$ and $t_h = 0.02s$. Here, a transient of $20s$ duration is needed until an excited wave completely passes through the domain. Taking less than $20s$ evokes wave dynamics that are only presented in parts of the free surface zone. Ten POMs are needed to reproduce the main dynamics, preserving 99.99% of its eigenspectrum. Figure 5.14 illustrates the eigenspectrum, the mean and associated ten dominant POMs.

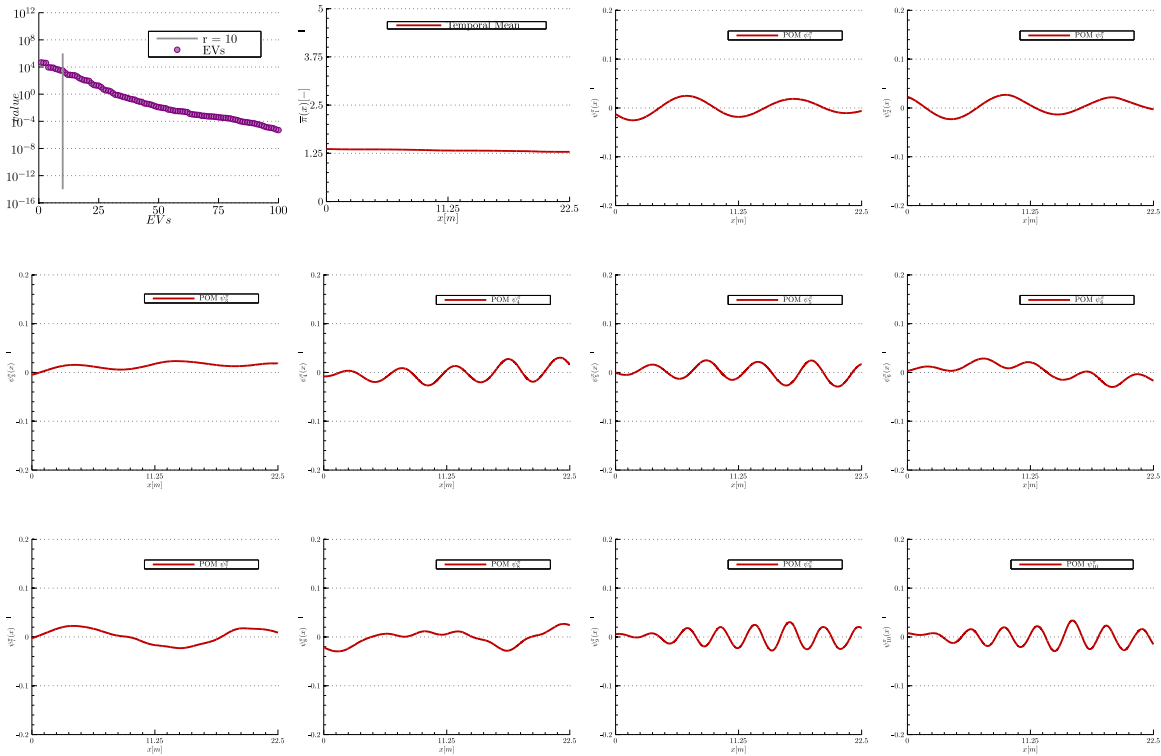


Figure 5.14.: Static two-zone diffuser coupled model - zone (II) : Eigenspectrum, mean and ten dominant proper orthogonal modes.

PERFORMANCE

A comparison of the attained *static two-zone diffuser* ROM solution versus the FOM is illustrated in Fig. 5.15. By four temporal snapshots, see Fig. 5.15(a), it is demonstrated that the dynamical

behavior is reproduced correctly. Fig. 5.15(b) shows that the overall root mean square error (RMSE) is approximately 12% and the correlation coefficient (CC) yields 88%.

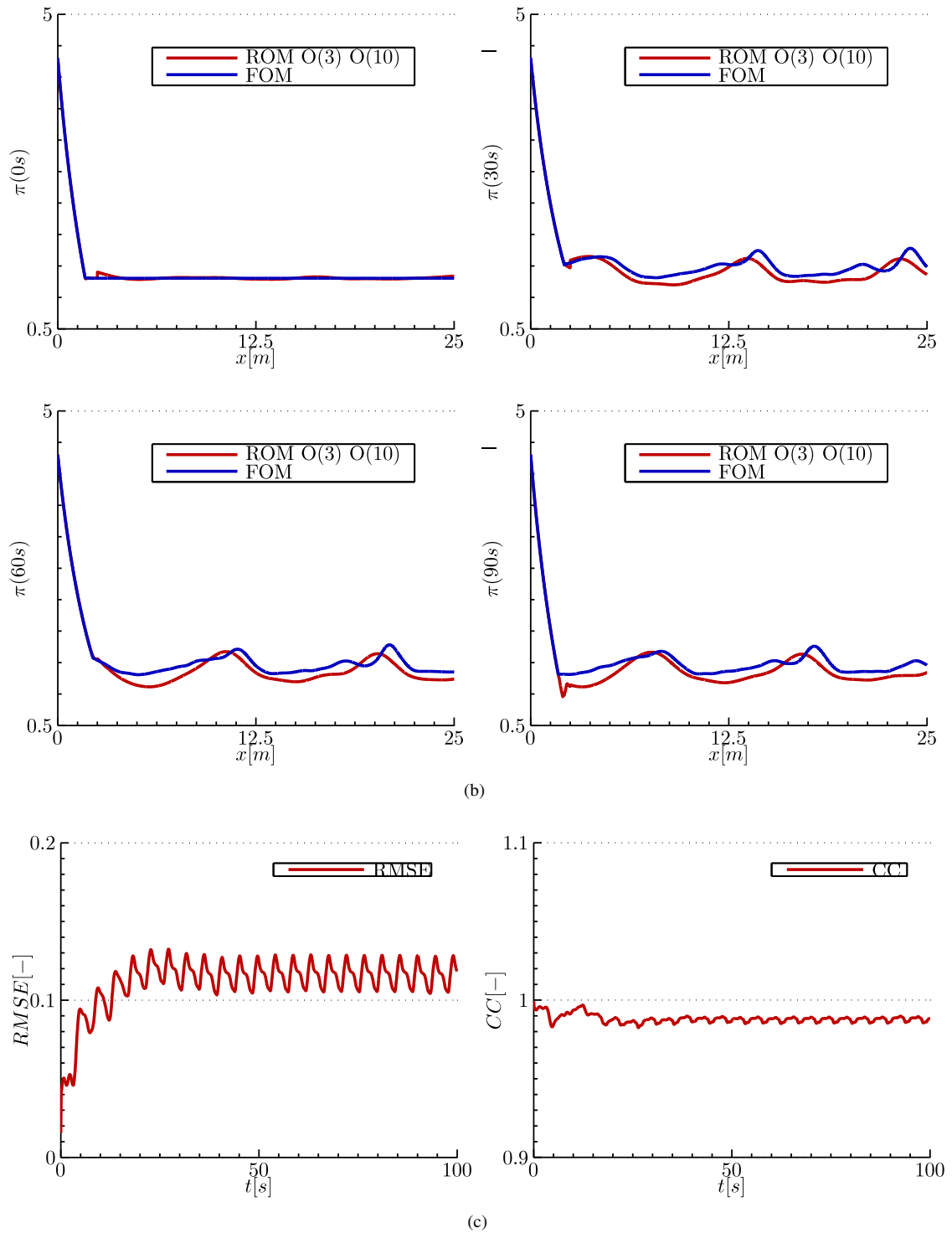


Figure 5.15.: Static two-zone diffusor coupled model: (a) temporal snapshots for $t = \{0, 30s, 60s, 90s\}$, (b) global root mean square error and correlation coefficient.

DISCUSSION

The *static two-zone diffusor* ROM is capable of handling time-varying interfaces separating regions obeying different PDEs. Note that the dynamical simulation of the ROM only consists of a small data basis of 2s and 20s duration. Induced errors are due to the modeling of the moving boundary. Improvements are expected for different modeling strategies:

Structure: The previous coupling strategy presented in Fig. 5.12 is based on the derivation of two equation systems having different character. In the diffusor region an algebraic equation has been derived. The free surface region has been approximated by a PDE of first order. Finding a similar character for both equations would lead to a reduced order system having at least the same structure. This can be realized by differentiation of the pressure equation obtained for the diffusor part.

Nevertheless, results would differ from the true solution as POMs have a static nature. Even by having knowledge about the time-varying boundary $x_g(t)$, parts of the transition zone represented in the POMs will influence the models of the two different zones.

Mapping: Problems of time-varying boundaries can be overcome by topological mappings. Conformal mappings yield a transformed problem having a stationary boundary [12].

5.3 NATURAL CONVECTION IN A CLOSED CIRCUIT

An interesting verification and validation example is given by an example of natural convection in a closed circuit (NCC). A BWR shows dynamical similarities since both systems consist of a closed circuit and are subject to strong non-linear effects. Both of them include a heat source and sink connected via pipes. Among other things, perturbation and stability investigations can be based on changes in heat input. This makes the NCC an adequate qualification example to verify and validate the derived enhanced POD-ROM methodology of Sec. 4.3.

Experiments and modeling for a single NCC are carried out by Ehrhard and Müller [40, 41]. Ehrhard not only investigated an isolated circuit but rather two coupled single circuits [40]. Aiming at suitable validation and verification examples, this section only refers to the single circuit configuration. The single-phase water circuit is heated in the lower and cooled in the upper part. It can be tilted by an angle δ . By making crucial assumptions, the authors derived an 1D physical model. Numerical processes in 2D and 3D are complex and only hardly lead to better knowledge about the physics behind processes in this case. This gives reasons for their further reduction of the system to a set of non-linear ODEs by pure analytical manipulation. The derived ROM, a coupled Lorenz-type system (of order three) with additional (i.e. 61) temperature adjusting equations, has been validated against experimental data. The used dimensionless variables are directly connected to the Fourier series approach which has been applied in advance.

This section starts with the derivation of the conservation equations in their dimensionless form and is essential for comparison purposes. The implemented model is subsequently discussed and compared to neutral stability maps in terms of the critical heat rate and the fluid-wall parameter for tilting angles of $\delta = \{0^\circ, 10^\circ\}$. This serves as a validation of the FOM data. The applied Fourier series approach of [40, 41] is appropriate for this individual setup. Regarding BWR applications, that have a more complex geometry among other things, efficient ROMs need to be utilized. With this focus, the POD based reduction is shown to attain the same results with less effort. Accordingly, the routine of POD-based decomposition of two expert-chosen transients are illustrated and discussed. The extraction of POMs and the reconstruction of the ROM is compared to results of bifurcation diagrams of [40, 41]. Perturbations are imposed by an abrupt change of heat input.

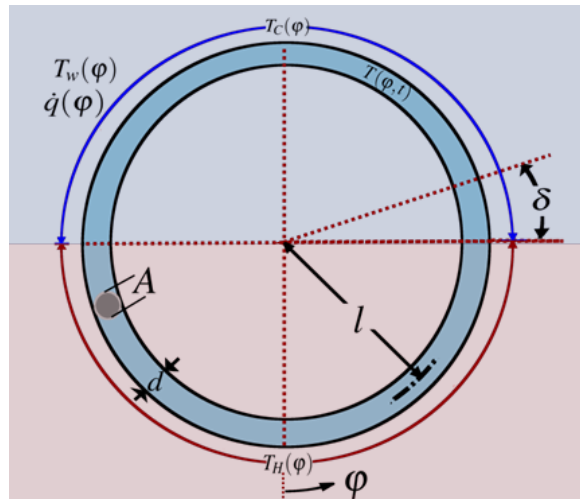


Figure 5.16.: Configuration of the natural convection in a closed circuit model (redrawn from [40, 41]).

5.3.1 CONFIGURATION

GEOMETRY

A single circular circuit with radius l , diameter d and constant flow cross-section A is investigated. Origins of the chosen coordinates and the flow velocity are defined according to Fig. 5.16. The cross-sectional averaged temperature is denoted by $T = T(\varphi, t)$. Space and time coordinates of the circuit are given by φ and t . The mean flow velocity is denoted by u . The circuit is subject to local gravitational acceleration g .

BOUNDARY CONDITIONS

Boundary conditions are imposed either by the wall temperature T_w or the volumetric power distribution \dot{q} . All experiments are subject to a dominant heat supply is in the lower part and the heat removal in the upper part. The symmetry plane between the heat source and sink, marked by a horizontal dash-dotted line, can be tilted by an angle of δ . There is a smooth transition between peak/lowest value, i.e. $T_H(\varphi)$ and $T_C(\varphi)$, of the heated/cooled region. This is marked in red/blue. The forcing temperature $\Delta T = T_H(\varphi) - T_C(\varphi)$ drives the system. Increasing this value will drive the system from an initial conductive state to a convective state. The situation of a possible symmetry brake is defined by the help of a cosine switch depending on the perimeter position and the shift δ ,

$$\cos(\varphi - \delta).$$

Due to the chosen cosine profile, a smooth heat input is ensured.

FLUID PROPERTIES

Let us assume an incompressible fluid within the circuit. Its properties are given by the density ρ_0 at temperature T_0 . The fluid has a kinematic viscosity ν_0 , a thermal conductivity λ_0 , a specific heat capacity c_p and a coefficient of thermal expansion α_0 . The fluid is further assumed to be in single-phase at all time.

5.3.2 CONSERVATION EQUATIONS

MOMENTUM EQUATION

The momentum equation for the 1D cross-sectional averaged circular pipe is given in differential form by

$$\rho_0 \left(\frac{\partial u}{\partial t} + u \frac{1}{l} \frac{\partial u}{\partial \varphi} \right) = -\frac{1}{l} \frac{\partial p}{\partial \varphi} - \rho(T) g \sin(\varphi) - \nu_0 \frac{1}{l^2} \frac{\partial^2 u}{\partial \varphi^2} - f_w.$$

The density is assumed to be constant, i.e. $\rho = \rho_0$, on the basis of the Boussinesq approximation. Buoyancy is an external force only. It results from modeling the density as a linear function of temperature:

$$\rho(T) := \rho_0 (1 - \alpha_0 (T - T_0)). \quad (5.6)$$

Due to the constant cross-sectional area and density, the continuation equation is defined by

$$\frac{\partial u}{\partial t} = \frac{du}{dt},$$

and all derivatives of the averaged flow velocity with respect to the spatial coordinate φ vanish

$$\frac{\partial u}{\partial \varphi} = \frac{\partial^2 u}{\partial \varphi^2} = 0.$$

The influence of the pipe wall friction onto the flow is given by the friction force f_w . Due to the 1D modeling approach, this function needs to be implemented in an empirical way, as no velocity gradients are available. The function is assumed to depend on the averaged velocity. Based on the stability of the flow under isothermal conditions only laminar flow profiles exist within experiments for water [40]. A linear correlation between the friction f_w and the velocity u is hence appropriate. It is defined by

$$f_w = \frac{1}{2} \rho_0 f_{w0} u, \quad (5.7)$$

where the friction transfer coefficient is denoted by f_{w0} . Note that turbulent flow only occurs at high heat inputs.

Aiming at an elimination of the pressure gradient $\partial p / \partial \varphi$ within the momentum equation, hereafter an integration along the circuit is realized. The momentum equation is reformulated by:

$$\begin{aligned} \rho_0 \frac{\partial u}{\partial t} &= -\frac{1}{l} \frac{\partial p}{\partial \varphi} - \rho(T)g \sin(\varphi) - f_w \\ \Leftrightarrow -\frac{\partial p}{\partial \varphi} &= l \left(+\rho_0 \frac{\partial u}{\partial t} + \rho(T)g \sin(\varphi) + f_w \right) \end{aligned}$$

An integration along the circuit leads to

$$\begin{aligned} -\frac{1}{l\rho_0} \int_0^{2\pi} \frac{\partial p}{\partial \varphi} d\varphi &= 2\pi \frac{du}{dt} + \int_0^{2\pi} \frac{1}{\rho_0} (\rho(T)g \sin(\varphi) + f_w) d\varphi \\ \Leftrightarrow 0 &\stackrel{(5.6)}{=} 2\pi \frac{du}{dt} + \int_0^{2\pi} (1 - \alpha_0(T - T_0))g \sin(\varphi) + \frac{1}{\rho_0} f_w d\varphi \\ \Leftrightarrow 0 &= 2\pi \frac{du}{dt} + \int_0^{2\pi} g \sin(\varphi) d\varphi - \int_0^{2\pi} \alpha_0(T - T_0)g \sin(\varphi) d\varphi + \int_0^{2\pi} \frac{1}{\rho_0} f_w d\varphi \\ \Leftrightarrow 0 &\stackrel{(5.7)}{=} 2\pi \frac{du}{dt} + g\alpha_0 T_0 \int_0^{2\pi} \sin(\varphi) d\varphi - g\alpha_0 \int_0^{2\pi} T(\varphi) \sin(\varphi) d\varphi + \int_0^{2\pi} \frac{1}{\rho_0} \left(\frac{1}{2} \rho_0 f_{w0} u \right) d\varphi \\ \Leftrightarrow 0 &= \frac{du}{dt} - \frac{g\alpha_0}{2\pi} \int_0^{2\pi} T(\varphi) \sin(\varphi) d\varphi + \frac{1}{2\pi} \int_0^{2\pi} \left(\frac{1}{2} f_{w0} \right) d\varphi \cdot u \\ \Leftrightarrow \frac{du}{dt} &= \frac{\alpha_0 g}{2\pi} \int_0^{2\pi} T(\varphi) \sin(\varphi) d\varphi - Ru. \end{aligned}$$

The integrated momentum equation is hence given by

$$\frac{du}{dt} = \frac{\alpha_0 g}{2\pi} \int_0^{2\pi} T(\varphi) \sin(\varphi) d\varphi - Ru, \quad (5.8)$$

where the friction factor is denoted by

$$R = \frac{1}{2\pi} \int_0^{2\pi} \left(\frac{1}{2} f_{w0} \right) d\varphi.$$

Due to the integration process over φ , the momentum equation is transformed to an ODE.

ENERGY EQUATION

The cross-section averaged energy equation for the 1D circular pipe is given in differential form by

$$\rho_0 c_p \left(\frac{\partial T}{\partial t} + u \frac{1}{l} \frac{\partial T}{\partial \varphi} \right) - \lambda_0 \frac{1}{l^2} \frac{\partial^2 T}{\partial \varphi^2} = \dot{q}(\varphi) + \frac{4h_w}{d} (T_w(\varphi) - T).$$

The volumetric heating $\dot{q}(\varphi)$ is only a function of φ . The interchange of heat with the pipe wall with constant wall temperature $T_w(\varphi)$ is modeled in a linear way. The local heat flow at the surface is proportional to the difference of mean fluid temperature $T(\varphi)$ and the wall temperature $T_w(\varphi)$ with a heat transfer coefficient h_w . The energy equation can be redefined by combining all source terms into \dot{Q} . It then reads as

$$\frac{\partial T}{\partial t} + u \frac{1}{l} \frac{\partial T}{\partial \varphi} - \Lambda \frac{1}{l^2} \frac{\partial^2 T}{\partial \varphi^2} = \dot{Q}(\varphi) - H \cdot T, \quad (5.9)$$

where following substitutions have been applied:

$$\Lambda = \rho_0 \frac{1}{\rho_0 c_p l^2}, \quad (5.10)$$

$$\dot{Q}(\varphi) = \frac{1}{\rho_0} c_p \left(\dot{q}(\varphi) + \frac{4h_w}{d} T_w(\varphi) \right), \quad (5.11)$$

$$H = \frac{4h_w}{d \rho_0 c_p}. \quad (5.12)$$

Note that in comparison to the momentum equation, the energy equation is a PDE of second order.

DIMENSIONLESS FORM

Before applying the POD-ROM methodology for yielding an efficient ODE system, a reformulation of the conservation equations in dimensionless form is given. Following normalization is used for time t , the cross-averaged flow velocity u , the temperature T and the source term \dot{Q} :

$$\begin{aligned} t &= \frac{\tau}{H_0}, \\ u &= H_0 l \tilde{u}, \\ T(\varphi) &= \frac{2H_0 l R}{\alpha_0 g} \tilde{T}(\varphi), \\ \dot{Q}(\varphi) &= \frac{2H_0^2 l R}{\alpha_0 g} \dot{\tilde{Q}}(\varphi), \end{aligned}$$

with given dimensionless parameters for the time τ , the flow velocity \tilde{u} , the temperature \tilde{T} and the source term $\dot{\tilde{Q}}$. Accordingly, the dimensionless system of integrated momentum equation (5.8) and

energy equation (5.9) reads:

$$\frac{d\tilde{u}}{d\tau} = \alpha \left(\frac{1}{\pi} \int_0^{2\pi} \tilde{T}(\varphi) \sin(\varphi) d\varphi - \tilde{u} \right), \quad (5.13a)$$

$$\frac{\partial \tilde{T}}{\partial \tau} = -u \frac{\partial \tilde{T}}{\partial \varphi} + \frac{\Lambda}{H_0} \frac{\partial^2 \tilde{T}}{\partial \varphi^2} - \frac{H}{H_0} \cdot T + \dot{Q}(\varphi). \quad (5.13b)$$

On the basis of the heat-transfer coefficient model introduced by Ehrhard [40], the following closure restriction for heat transfer is assumed:

$$H := H_0 \left(1 + K |\tilde{u}|^{1/3} \right). \quad (5.14)$$

DIMENSIONLESS NUMBERS, MEANING AND ASSUMPTIONS

Following dimensionless numbers are used:

(a)	material/wall parameter	$\alpha = \frac{R}{H_0},$
(b)	heating parameter	$\beta = \frac{\alpha_0 g}{2H_0^2 l R},$
(c)	symmetry angle	$\delta,$
(d)	heat transfer parameter	$\frac{\Lambda}{H_0},$
(e)	control parameter	$K.$

- (a) The parameter α relates the friction factor to the heat transfer coefficient at the wall. It is a parameter that only depends on properties of the fluid and the wall. Viscous fluids have parameters greater than one. Accordingly a parameter, that is smaller than one, denotes a good heat conductive material. In the following this parameter is assumed to be constant. Ehrhard points out the analogy to the Prandtl number [40].
- (b) The heating parameter β relates the density difference $\alpha_0 g R / H_0$ to dissipative mechanisms of the fluid (friction, heat losses, ...). Ehrhard notes the analogy to the Rayleigh-number within the Bénard problem.
- (c) The angle δ indicates whether the heat input is dominant at the bottom of the circuit ($\delta = 0^*$) or the symmetry is broken and the circuit is rotated. The profile of the source term \dot{Q} is defined by the symmetry angle: $\cos(\varphi - \delta)$.
- (d) The heat transfer parameter denotes the quotient of diffusive and convective transport heat. According to Ehrhard [40], the impact of this parameter is small as the heat conductance is expected to be low in comparison to convective heat transportation. This parameter is neglected in the following.
- (e) The control parameter of the fluid-wall relation model weights the constant part of the heat transfer coefficient to that part that is proportional to the flow velocity. For $K = 0$ the heat transfer coefficient is assumed to be constant irrespective of the the mean flow velocity. In the following $K = 0$ is assumed.

5.3.3 VERIFICATION OF THE IMPLEMENTATION

MODELING IN COMSOL

The dimensionless NCC model (5.13) was implemented in Comsol to obtain the FOM data. Both equations were included as general form PDEs. Quadratic Ansatz functions are applied in the FEM simulation. Moreover, modeling was realized on a 1D string of length 2π with periodic boundary conditions. The control parameter K vanishes, which leads to $H = H_0$ by Eq. (5.14), Λ/H_0 also tends to zero and the material/wall parameter is assumed to be constant $\alpha = 15$, referring to a viscous fluid. The implemented equation system reads

$$\frac{d\tilde{u}}{d\tau} = \alpha \left(\frac{1}{\pi} \int_0^{2\pi} \tilde{T}(\varphi) \sin(\varphi) d\varphi - \tilde{u} \right), \quad (5.15a)$$

$$\frac{\partial \tilde{T}}{\partial \tau} = -\tilde{u} \frac{\partial \tilde{T}}{\partial \varphi} + \beta \cos(\varphi - \delta) - \tilde{T}. \quad (5.15b)$$

The equation system is implemented in weak formulation. The integration in Eq. (5.15) is performed in Comsol using the internal integral modeling coupling expression. It is evaluated by integrating the argument over the whole domain with an integration order of 10. The spatial resolution is chosen to be $x_h = 2\pi/100$, such that EVs are independent of grid size.

VERIFICATION BY LINEAR STABILITY MAPS

The implementation is double-checked with results from [40, 41] for two linear stability maps of a non-tilted system ($\delta = 0^\circ$) and a tilted system of $\delta = 10^\circ$.

For this purpose, Comsol's internal EV solver is used and the frequency-domain method is applied. The frequency-domain method is a well-established method for stability analysis. Applying first order perturbation theory to a stationary solution, the original system is linearized. The perturbation is expressed by a modal approach and the resulting EV problem is solved by the FEM yielding conjugate complex EVs. The system becomes unstable if a real part of EVs becomes negative as the bifurcation parameter is increased. This method yields the linear neutral stability boundary.

A further Matlab routine is applied that searches for the minimum non-negative real part of EV by varying bifurcation parameters on a defined direction. This self-written routine checks the EV for the desired grid mesh of $x_h = 2\pi/100$ and a further refinement. It cross-correlates the EVs and erases non-physical values. It further distinguishes whether a linear stable (marked by a plus) operation point is present or a linear unstable point (marked by an asterix). The routine starts searching the linear stability boundary on two lines. Each new search line has a distinct interval to the former line and is chosen by walking on the normal to the previously found points of the linear stability map.

The main important quantities, having influence on stability in the NCC system, are the heat input β , the symmetry δ and the material parameter α . Fig. 5.17 illustrates the linear stability map in the α - β -plane for a symmetric (left) and a tilted systems (right). For a symmetric setup, there is a boundary of $\alpha = 2$ which separates the oscillatory stable region from the unstable region. This is indicated by a black line within Fig. 5.17(a). This boundary holds for both stationary solutions, i.e. for positive and negative velocities. For $\alpha < 2$ all EVs only have real parts and hence perturbations are asymptotically damped. The heat transfer capacity of the fluid is the physical mechanism behind. A high capacity dims temperature perturbations before a possible coupling after a complete circulation. In contrast, a lower heat capacity leads to oscillatory behavior, as perturbations have potential to couple. Changing the symmetry to $\delta = 10^\circ$ leads to two neutral stability boundaries, whereas the upper belongs to the preferred positive direction and the lower belongs to negative solutions. Between both curves, one

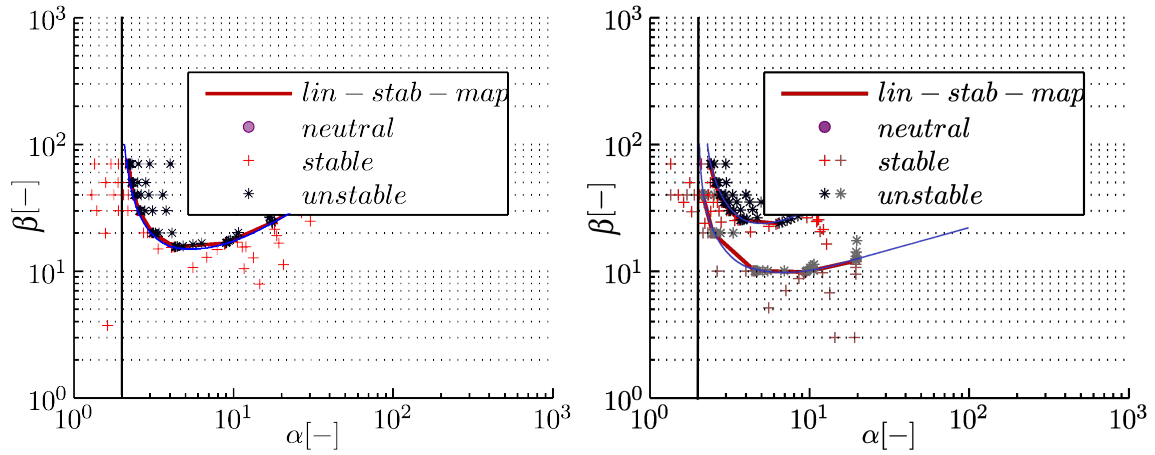


Figure 5.17.: Linear stability maps for configurations $\delta = 0^\circ$ as well as $\delta = 10^\circ$ represented in the α - β -plane. The curves (blue: Ehrhard & Müller, red: Prill) show the critical heat β as function of α .

of the solution is already unstable while the other stationary solution is still stable. The oscillatory stable region is located left of the black line within Fig. 5.17(b).

In both cases, blue curves show results of Ehrhard and Müller [40, 41]. Red curves belong to results attained by our implementation. A plus indicates a calculated stable point, an asterisk an unstable point. By an iterative minima search on lines, the neutral stability curves have been found. Note that results agree well. This underlines that linear dynamics of the implemented model are in agreement to the model of Ehrhard and Müller.

The frequency domain method is based on a linearization around the stationary solution, and only valid for perturbations with small amplitudes. In the neighborhood of the linear stability map or above, it is impossible to make a statement. Here, perturbations with finite amplitude might arise [40].

5.3.4 NON-LINEAR CHARACTERISTICS

The expert choice of two characteristic transients being employed within the later POD-ROM methodology will be explained in this subsection. For that purpose, bifurcation diagrams, attained by [40, 41] are discussed in terms of velocity u for an increasing asymmetry angle δ . They were derived by the consecutive analysis of a Fourier mode based ROM by: Steady-state analysis, linear stability analysis, weak non-linear perturbation analysis and a further numerical routine for solving, evaluation stability and persecution of periodic solution branches. This routine is based on the search of periodic solutions by non-linear problem treated as boundary/eigenvalue problem. By varying of the heat input β these solutions are tracked. Its stability character is calculated by Floquet theory.

SYMMETRIC BIFURCATION DIAGRAMS

The case of a symmetric heating, i.e. $\delta = 0^\circ$, is illustrated in Fig. 5.18 by the flow velocity versus the heating rate β . Results refer to setups with constant heat transfer $K = 0$ and constant fluid-wall parameter $\alpha = 15$ and are redrawn from [40, 41].

Starting from isothermal conditions at $\beta = 0$ for increasing heat inputs only the zero solution is found. The system features a solution without fluid flow. At $\beta = \beta^0 = 1$ two solutions branch off symmetrically. This is referred to as perfect forward or pitchfork bifurcation. It implies the loss of stability for the zero flow solution and an appearing of two convective stable solutions for $\beta > \beta^0$

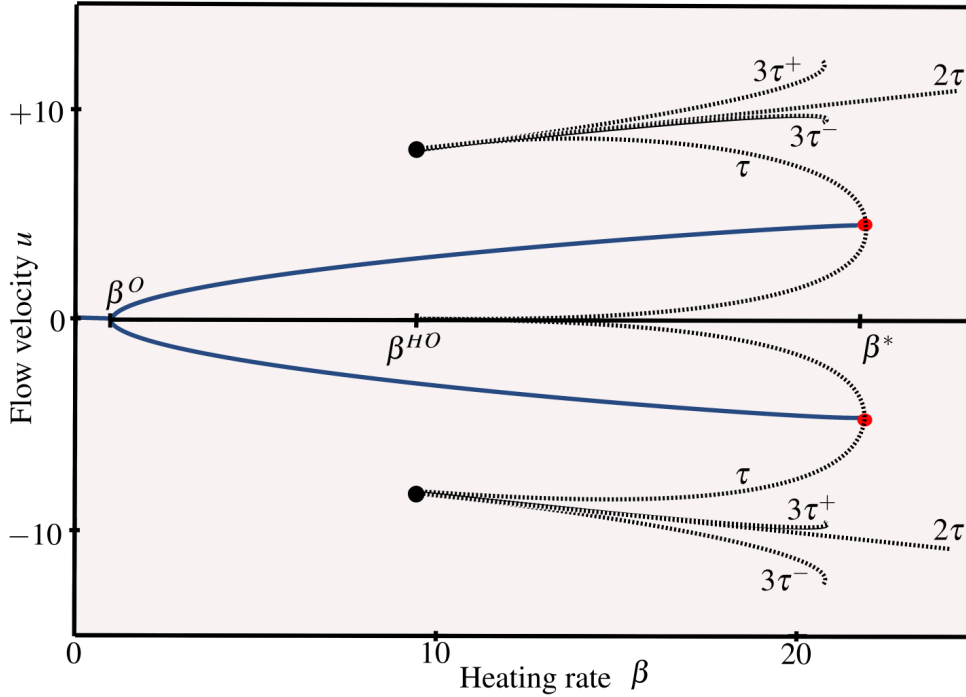


Figure 5.18.: Bifurcation diagram for a symmetric heating in terms of velocity ($\alpha = 15, K = 0$). Solid lines are stable steady branches, a circle marks the stability bounds and dotted lines represent amplitudes of periodic solutions (redrawn from [40, 41]).

where the fluid flows either clockwise or counterclockwise. These three solutions branches can be found by a steady-state analysis of the reduced system.

For even higher heat inputs the stable steady state solutions becomes unstable with respect to oscillatory disturbances. These behavior is marked by the Hopf bifurcation point at $\beta^* = 21.92$ and can be found by a linear analysis.

By the numerical analysis of the non-linear ROM and persecution of the periodic solutions, τ periodic solutions are found that have growing amplitudes for decreasing values of heat input β . Two types of periodic solutions can be found: symmetric periodic solutions e.g. τ , 2τ and mirror symmetric e.g. $3\tau^+$ and $3\tau^-$. A backward bifurcation is seen. A homoclinic orbit occurs at $\beta = 9.4$. The amplitude of the periodic solution approaches the stationary unstable conductive solution at $u = 0$. Approaching β^{HO} from higher values the period of the oscillation tends to infinity. This is denoted as homoclinic bifurcation point and homoclinic explosion.

As only the conductive solution exists between $0 \leq \beta \leq \beta^0$, the system acts absolutely stable. Since two stable solution coexists between $\beta^0 \leq \beta < \beta^{HO}$ a transition may only be implied by finite-amplitude perturbations. Between the homoclinic orbit and the Hopf bifurcation point, i.e. $\beta^{HO} \leq \beta \leq \beta^*$, a more complex system behavior is expected. Small perturbation are damped. If the value of a finite-amplitude perturbation exceed a certain value, more chaotic behavior is expected. This is related to the backward bifurcation and the sub-critical region. The perturbation leads to irregular behavior with flow reversal due to the time-dependent flow. The temporal behavior in this region is called transient-chaotic. The solution might behave strangely invariant but including rare events of spiraling into the stable steady solution branches. A strange attractor is formed when the duration of the chaotic wandering tends to infinity and is usually fulfilled just before the Hopf bifurcation point. A fully chaotic time behavior is expected for $\beta > \beta^*$ where multiple unstable periodic and aperiodic solutions coexists with unstable steady state solutions. The strange attractor is continued.

ASYMMETRIC BIFURCATION DIAGRAMS

Changing the non-symmetry angle δ of the NCC results in a change of the non-linear dynamical system and hence leads to a different bifurcation diagram. Two results are shown in Fig. 5.19.

As only the upper branch is directly connected to $\beta = 0$, the fluid will preferentially circulate with positive velocity in both rotated setups. The upper solution branch is the so-called preferred solution in contrast to the "isolated" non-connected solution. The latter can only be attained by a large initial perturbation on the system. This dynamical constellation is called an imperfect forward bifurcation. Increasing the asymmetry δ leads to a more pronounced preferred solution branch and shrinks the isolated one.

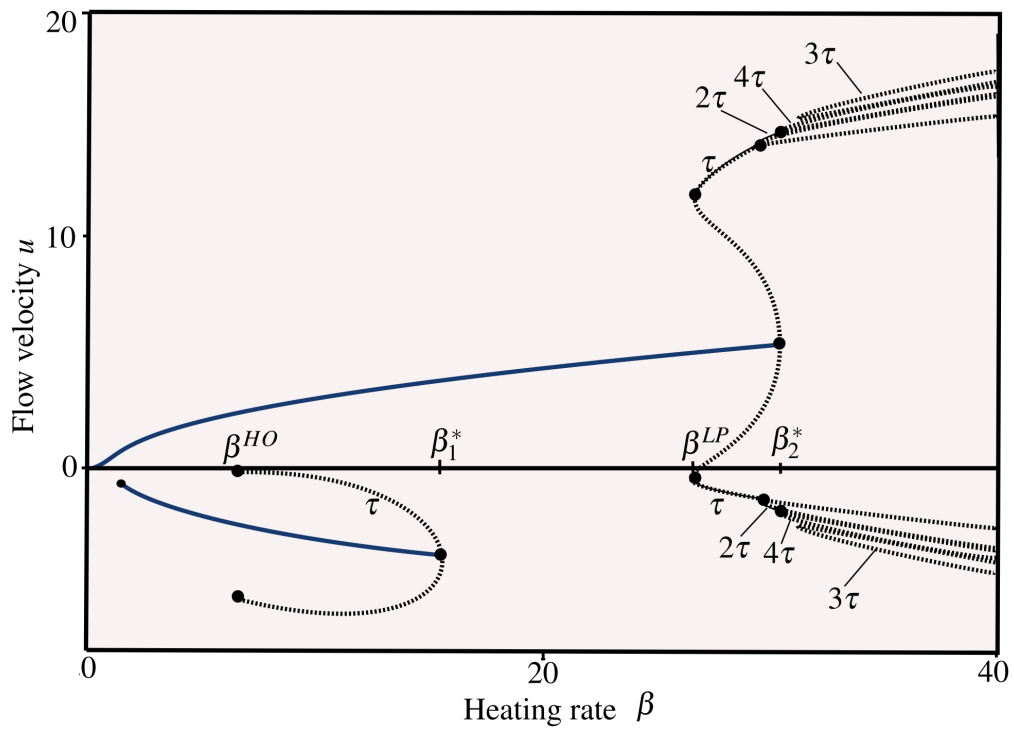
Both, the preferred and isolated steady state solutions lose their stability while increasing the heat input. This occurs at different values of β . The isolated solution loses its stability at β_1^* which occurs remarkably faster than the loss of stability of the preferred solution at β_2^* . The stability character of both bifurcation points is of periodic nature (Hopf points) and can be calculated by non-linear stability analysis (Floquet theory). The solutions for the preferred solution branch alter by growing rotations δ from branching off in backward Fig. 5.19(a) to forward Fig. 5.19(b) directions. In contrast, the backward bifurcation for the isolated branch remains in both cases. An homoclinic orbit exists at $\beta = \beta^{HO}$ where the amplitude of the τ -periodic solution, branching off from the isolated solution, approaches the unstable steady state solution. For decreasing values of β approaching the homoclinic orbit, the amplitude tends to infinity. Between β_1^* and β^{HO} the solution is locally unstable.

For small values of δ the backward bifurcation of the preferred steady state solution changes direction and at the limit point β^{LP} the former unstable periodic solution is stabilized on the forward part. The stable τ -periodic solution loses stability for higher heating values as a subharmonic 2τ -periodic solution, which is stable again, bifurcates off. By increasing β even more, $2^n\tau$ -periodic solutions are found. By increasing the asymmetry angle δ the backward bifurcation is pushed into a forward bifurcation.

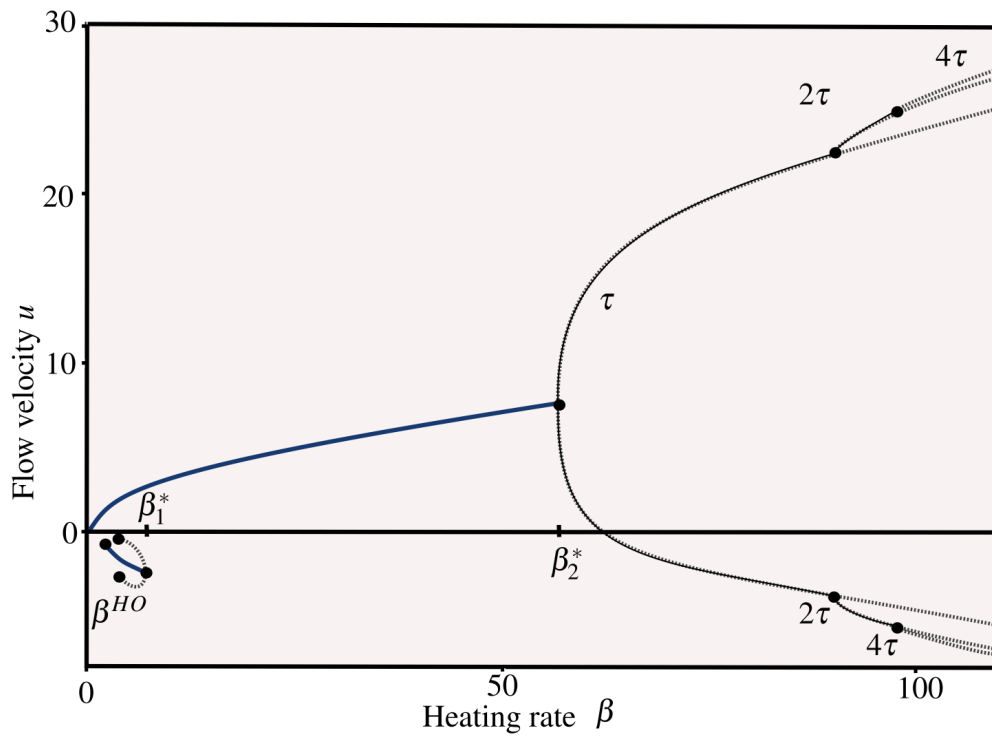
CHOICE OF TRANSIENTS

An expert choice of a transient consists of a complete representative extract of the dynamical response of a system. Having introduced the bifurcation diagrams, such an expert choice of a representative transient can be illustrated. This step is similar to an BWR expert that will choose representative transients that corresponds to important states of dynamical responses of a BWR. In the following two different kind of transients will be treated:

- A transient corresponding to a non-symmetric setup where system dynamics of the upper bifurcation branch are of forward bifurcation nature:
The NCC is not rotating when a heat input ramp is started. As the upper bifurcation branch is connected to the zero point, the system starts rotating clockwise. The heat input ramp drives the system into the super-critical region. By a rectangular perturbation a limit cycle is established while keeping the heat input constant afterwards. This is illustrated in Fig. 5.20(a).
- A transient corresponding to a symmetric setup:
By a small initial velocity perturbation and an increase of the heat input by a small ramp the system is pushed to the lower steady state branch. The flow rotates counter-clockwise. The heat input is increased just right before the Hopf bifurcation point. The heat input is then kept constant, undergoes a sinusoidal perturbation and is faded out to zero heat input. This is illustrated in Fig. 5.20(b).



(a)



(b)

Figure 5.19.: Bifurcation diagram for non-symmetric heating in terms of velocity: (a) $\delta = 5^\circ$ and (b) $\delta = 15^\circ$ ($\alpha = 15, K = 0$). Solid lines are stable steady branches, circ marks stability bounds and dotted lines represent amplitudes of periodic solutions and connected dots mark stable ranges of periodic solutions (redrawn from [40, 41]).

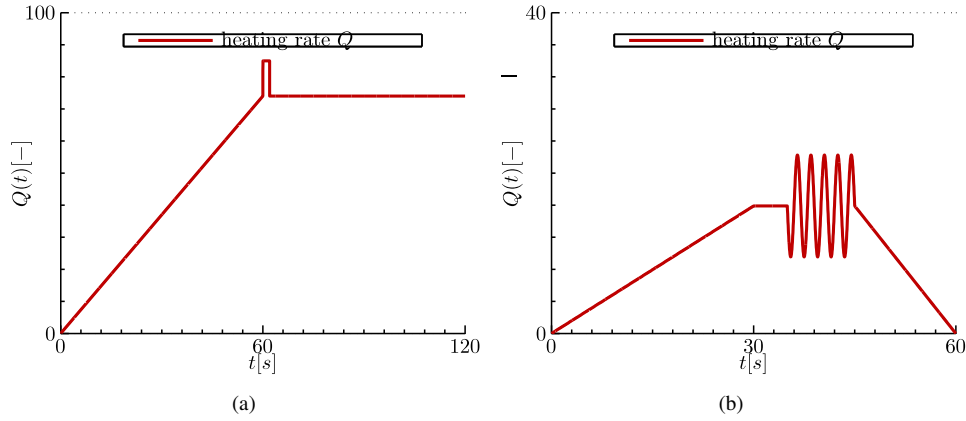


Figure 5.20.: Transient choices: (a) non-symmetric setup, (b) symmetric setup.

Both transients include main characteristic features of the dynamical response of the system and are used to predict different states of the NCC. Transient (a) is used for a prediction of system of different tilting and transient (b) is used for prediction of different heat input transient.

5.3.5 POD BASED ROM FOR THE NCC

This subsection illustrates the different steps towards a POD based ROM for the NCC. Following the explanation of Sec. 4.3, the derived equation system (5.15) is simplified to an ODE system by a consecutive application of the low modal approach and subsequent Galerkin projection step. The simulated NCC system that gives the data for the reduction, and always referred to as FOM, is subject to a constant chosen $K = 0$ and $\alpha = 15$. Only the tilting and the heat input transient are arbitrary parameters.

THE EQUATION SYSTEM

Here and in the following, φ is replaced by the state variable x . The corresponding equation system reads

$$\begin{aligned} \frac{\partial T}{\partial t} + u \frac{\partial T}{\partial x} + T - \beta_{all} &= 0, \\ \frac{du}{dt} - \frac{15}{\pi} \int_0^{2\pi} (T \sin(x)) dx - u &= 0. \end{aligned}$$

where $\beta_{all} = \beta \cos(x - \delta)$ is the heat input for a rotated or unrotated system. The system is subject to periodic boundary conditions

$$\begin{cases} T|_{x=0} = T|_{x=2\pi}, \\ u|_{x=0} = u|_{x=2\pi}. \end{cases}$$

In general, boundary conditions are imposed by a penalty formulation yielding

$$\frac{\partial T}{\partial t} + u \frac{\partial T}{\partial x} + T + \beta_{all} - \Gamma^T (T - T \delta|_{x=0}) \delta|_{x=2\pi} = 0, \quad (5.17a)$$

$$\frac{du}{dt} - \frac{15}{\pi} \int_0^{2\pi} (T \sin(x) - u) dx - \Gamma^u (u - u \delta|_{x=0}) \delta|_{x=2\pi} = 0, \quad (5.17b)$$

where δ denotes a Heaviside function.

Due to the periodic nature of the NCC system, both penalty parameter Γ^T and Γ^u can be chosen to vanish which can later be justified by a careful look at the POMs. They have already periodic shape which automatically guarantees periodic boundary conditions. Also, a further manipulation of the boundary is physically unreasonable due to the existence of a closed circuit.

PROPER ORTHOGONAL MODES

Let us assume that FOM transient data of the velocity and temperature fields are available. The correlated data, also so-called covariance matrix or kernel, is used by a singular value decomposition (SVD) for attaining the POMs. The chosen transients are sufficiently slow such that higher order derivatives play a minor role. The system response is also not expected to demand for higher order derivatives. The kernel of the NCC correspondingly consists only of the FOM data itself, i.e. generalized Sobolev weight $\varepsilon_0 = 1$ and higher order derivatives are disregarded.

Let us further assume that POMs, ϕ_i^T and ϕ_i^u , are constructed out of the FOM snapshot data for temperature or velocity fields separately, i.e.

$$T(x, t) = \sum_{i=1}^{r^T} \alpha_i^T(t) \phi_i^T(x),$$

$$u(x, t) = \sum_{i=1}^{r^u} \alpha_i^u(t) \phi_i^u(x).$$

The amplitudes for temperature and velocity modes are given by the temporal functions α_i^T and α_i^u . Truncation criteria for temperature and velocity are given by r^T and r^u . Note that this decomposition includes a variation of the mean to the different fields as it is represented within the first POM. This is of main importance for a transient application.

THE GALERKIN PROJECTION OF THE SYSTEM

Without loss of generality, let us further assume that the energy related truncation criterion yields two temperature POMs and one velocity mode: $r = (r^T, r^u) = (2, 1)$. The ROM is attained by projection of Eq. (5.17a) onto ϕ_i^T POMs in the L^2 -inner product for $i = \{1, \dots, r^T\} = \{1, 2\}$ and (5.17b) onto ϕ_i^u POMs for the same inner product choice for $i = \{1, \dots, r^u\} = \{1\}$. This leads to the following ROM with three unknown magnitudes of the POMs:

$$\dot{\alpha}_i^T \langle \phi_i^T, \phi_j^T \rangle = -\alpha_1^u \alpha_i^T \left\langle \frac{\partial \phi_i^T}{\partial \varphi}, \phi_j^T \right\rangle + \alpha_i^T \langle \phi_i^T, \phi_j^T \rangle + \langle \beta_{all}, \phi_i^T \rangle \quad , j = 1, 2 \quad (5.18a)$$

$$\begin{aligned} \dot{\alpha}_1^u \langle \phi_1^u, \phi_1^u \rangle = & -\frac{15}{\pi} \alpha_1^T \left\langle \int_0^{2\pi} \phi_1^T \sin(x) dx, \phi_1^u \right\rangle \\ & - \frac{15}{\pi} \alpha_2^T \left\langle \int_0^{2\pi} \phi_2^T \sin(x) dx, \phi_1^u \right\rangle - \alpha_1^u \langle \phi_1^u, \phi_1^u \rangle \end{aligned} \quad (5.18b)$$

In advance to the time integration of the ODE system, OFFLINE COSTS can be evaluated. This is in contrast to ONLINE costs, such as time-dependent source terms for instance, that need to be calculated at each time step. Note that inner products of POMs, the orthonormality of POMs as well as the integral can be invoked into Eq. (5.18). Inner products are calculated point-wise on the axial grid. Those inner products containing integrals are treated within the Mathematica script by an interpolation of the integrand and a further numerical integration. The NCC-POD-ROM with

highlighted OFFLINE/ONLINE COSTS in blue/red reads:

$$\begin{aligned}\dot{\alpha}_i^T &= -\alpha_1^\mu \alpha_i^T \left\langle \frac{\partial \phi_i^T}{\partial \phi}, \phi_j^T \right\rangle + \alpha_i^T \langle \phi_i^T, \phi_j^T \rangle + \langle \beta_{all}, \phi_i^T \rangle \quad , j = 1, 2, \\ \alpha_1^\mu &= -\frac{15}{\pi} \left\langle \int_0^{2\pi} \phi_1^T \sin(x) dx, \phi_1^\mu \right\rangle \alpha_1^T - \frac{15}{\pi} \left\langle \int_0^{2\pi} \phi_2^T \sin(x) dx, \phi_1^\mu \right\rangle \alpha_2^T - \alpha_1^\mu.\end{aligned}$$

The simplified matrix scheme of the system reads

$$A\dot{\alpha} = B\alpha + C\tilde{\alpha} + D, \quad (5.19)$$

where the vector of unknowns is denoted by

$$\alpha = \begin{pmatrix} \alpha_1^T \\ \alpha_2^T \\ \alpha_1^\mu \end{pmatrix},$$

and its first time-derivative by $\dot{\alpha}$. The vector containing non-linear products of unknowns is denoted by

$$\tilde{\alpha} = \begin{pmatrix} \alpha_1^\mu \alpha_1^T \\ \alpha_1^\mu \alpha_2^T \end{pmatrix},$$

the mass matrix by

$$A = \begin{pmatrix} 1 & 0 & 0 \\ 0 & 1 & 0 \\ 0 & 0 & 1 \end{pmatrix},$$

the stiffness matrix by

$$B = \begin{pmatrix} 1 & \langle \phi_2^T, \phi_1^T \rangle & 0 \\ \langle \phi_1^T, \phi_2^T \rangle & 1 & 0 \\ -\frac{15}{\pi} \langle \int_0^{2\pi} \phi_1^T \sin(x) dx, \phi_1^\mu \rangle & -\frac{15}{\pi} \langle \int_0^{2\pi} \phi_2^T \sin(x) dx, \phi_1^\mu \rangle & 1 \end{pmatrix},$$

C refers to the non-linear part of the system behavior

$$C = \begin{pmatrix} \langle \frac{\partial \phi_1^T}{\partial x}, \phi_1^T \rangle & 0 \\ \langle \frac{\partial \phi_2^T}{\partial x}, \phi_2^T \rangle & 0 \\ 0 & 0 \end{pmatrix},$$

and the source term is defined by

$$D = \begin{pmatrix} \langle \beta_{all}, \phi_1^T \rangle \\ \langle \beta_{all}, \phi_2^T \rangle \\ 0 \end{pmatrix}.$$

The initial conditions are chosen by

$$\alpha_{init} = \begin{pmatrix} \alpha_1^T \\ \alpha_2^T \\ \alpha_1^\mu \end{pmatrix} \Big|_{t=0} = \begin{pmatrix} \langle T_{FOM} \Big|_{t=0}, \phi_1^T \rangle \\ \langle T_{FOM} \Big|_{t=0}, \phi_2^T \rangle \\ \langle u_{FOM} \Big|_{t=0}, \phi_1^\mu \rangle \end{pmatrix}.$$

5.3.6 TWO NCC-POD-ROM TRANSIENTS

NON-SYMMETRIC TRANSIENT

In Fig. 5.21(a), our simulated data is superimposed on the full non-linear stability diagram (black). The simulation corresponds to a tilted system of $\delta = 15^\circ$ with a fluid-wall parameter $\alpha = 15$ relating the wall friction coefficient to the heat transfer coefficient at the wall. For this asymmetrical example, the positive flow direction solution is preferred over an isolated negative solution branch. The stability range of the positive flow solution becomes unstable at higher heating values β_2^* where super-critical bifurcation of periodic solutions is observed.

A transient NCC simulation ($\alpha = 15$, $\delta = 10^\circ$) of $t=120s$ duration is simulated. This data is referred to as FOM data (always illustrated in red) and is based on sufficiently fine spatial and temporal grids, i.e. $x_h = 2\pi/50$ and $t_h = 0.025$, such that long wave phenomena are completely resolved. The implemented model is validated by means of a linear stability map, see Sec. 5.3.3. Its heating rate transient is shown in Fig. 5.21(b). The FOM temporal velocity amplitude is illustrated in Fig. 5.21(c) together with the ROM results.

In the non-linear stability map, Fig. 5.21(a), the velocity amplitude is plotted versus the heating rate. Referring to the transient, see Fig. 5.21(b), the system heating rate is increased by a slow ramp which drives the system in stable positive flow direction with increasing speed. The ramp is driven for 60s such that the system reaches a terminal value above β_2^* of $\beta = 74$. After 60s a rectangular perturbation of $t = 2s$ duration is applied (peak value of $\beta = 85$) which is not illustrated within Fig. 5.21(a). The system responds unstable and a periodic limit circle is observed. The heating rate is afterwards kept constant at $\beta = 74$ for another 58s. Note that temporary reversed flow is observed.

A POD-ROM for the NCC is created based on this transient (monovariate) data. The calibration road map is applied with vanishing penalty parameter corresponding to periodic boundary conditions. Importance of higher order derivatives within the data set is negligible hence the generalized Sobolev weights vanish. For a reduction level of 99.9% there are two POMs for the temperature and one POM for velocity amplitude necessary (see Fig. 5.22). Due to the periodic nature of the NCC temperature modes have sinusoidal shape. Further on, the tilting of the setup is visible in the shifted sinusoidal modes. The periodicity is retained within the modes.

The ROM is applied to predict a dynamical behavior of a NCC system with a substantial higher tilting of $\delta = 15^\circ$ but same transient. Fig. 5.21(a) shows a comparison of limit cycles attained by [40, 41] in black and the NCC-POD-ROM in blue exhibiting same amplitudes.

SYMMETRIC TRANSIENT

Fig. 5.23(a) illustrates temporal velocity amplitudes versus the heating rate for a non-tilted system ($\delta = 0$) with a fluid-wall parameter $\alpha = 15$. By a small initial perturbation the negative flow direction is preferred over the positive solution branch for this symmetric setup. The transient is simulated for $t = 60s$. FOM is again based on well-chosen grids, i.e. $x_h = 2\pi/50$ and $t_h = 0.025$, and illustrated in red. A validation has been performed by a linear stability map already presented in Sec. 5.3.3.

The system heating rate is depicted in Fig. 5.23(c). A slow ramp drives the system in the sub-critical region within 30s. Right before the Hopf bifurcation point, the terminal value of $\beta = 15.9$ is reached. This heat input is kept constant for 5s until a sinusoidal perturbation is implied with amplitudes of 50% of the terminal value β . This perturbation continues for 10s. Then the heat input is faded out within 15s. Note that the perturbation leads to time-dependent flow spiraling around the negative branch.

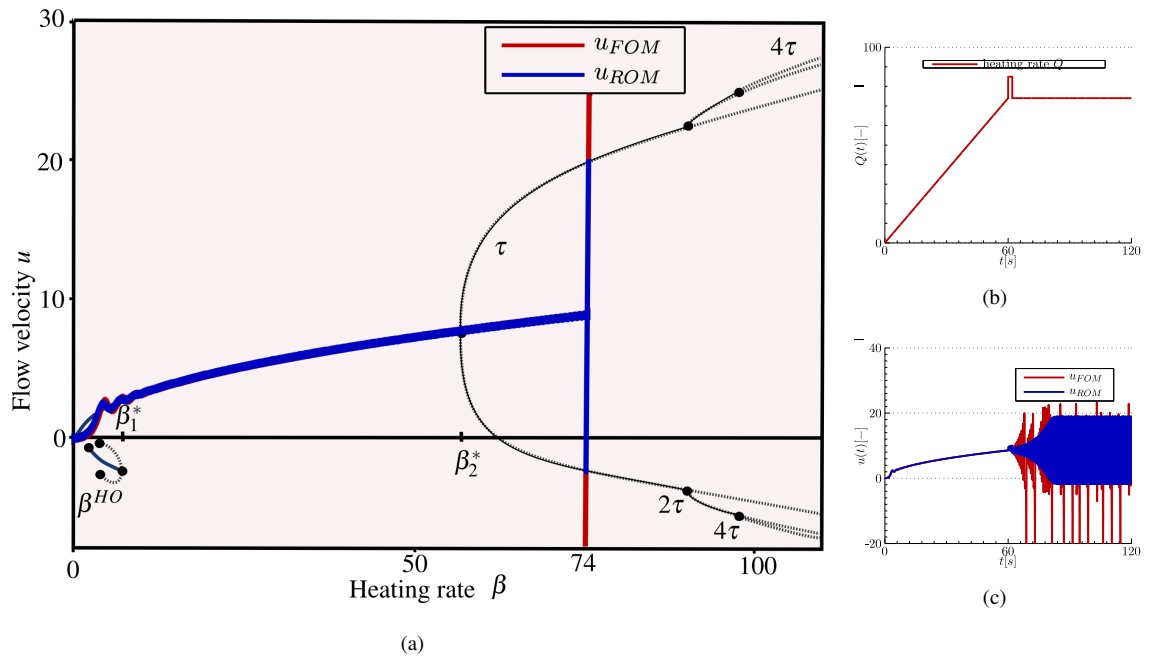


Figure 5.21.: Asymmetric transient representation: Non-linear stability map (a), heating rate (b) and flow velocity (c).

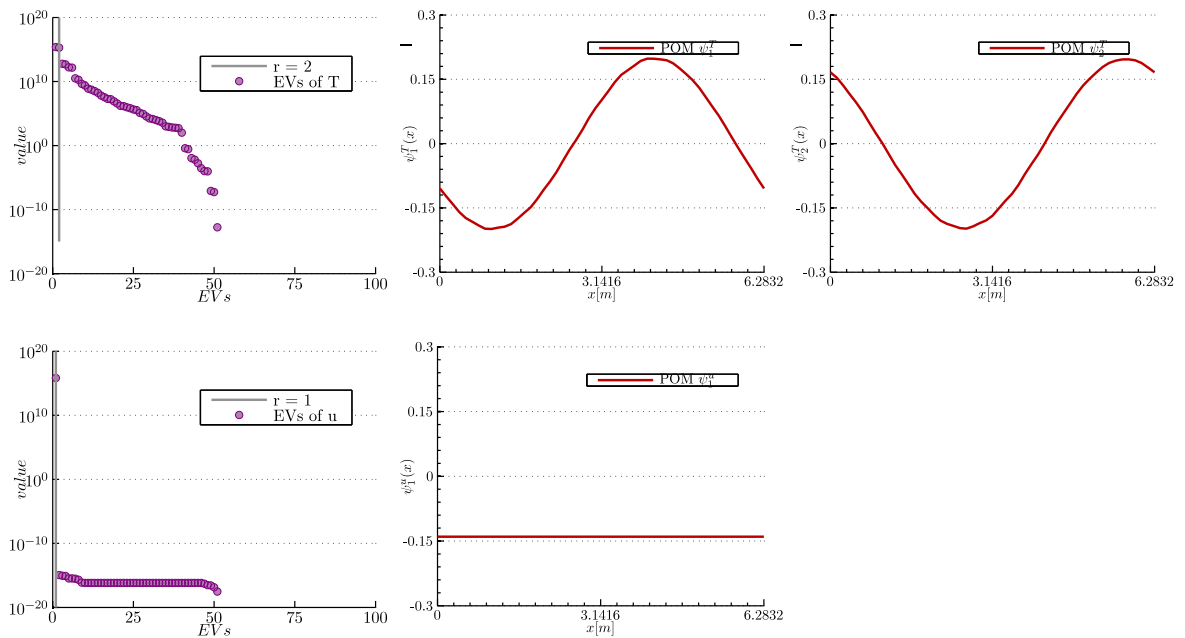


Figure 5.22.: Eigenspectra for temperature and velocity on a semi-logarithmic scale with inserted reduction level (1st column) and two dominant proper orthogonal modes for temperature and one for velocity.

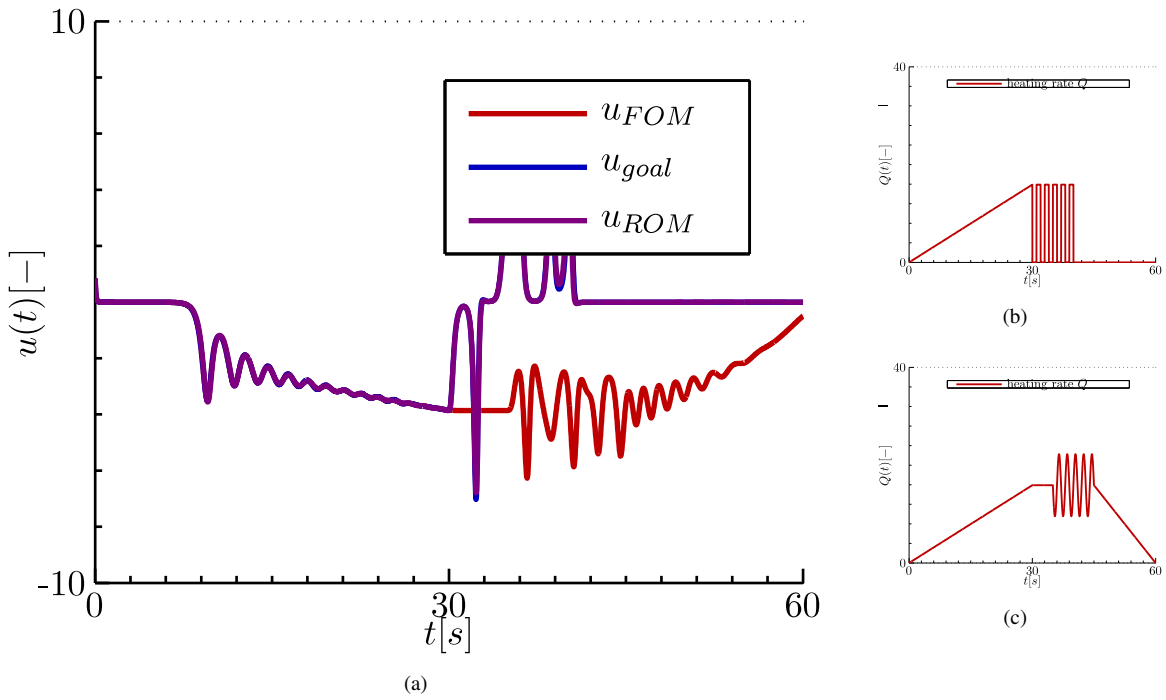


Figure 5.23.: Symmetric transient representation: flow velocity (a), heating rate of reduced order model (b) and full order model (c).

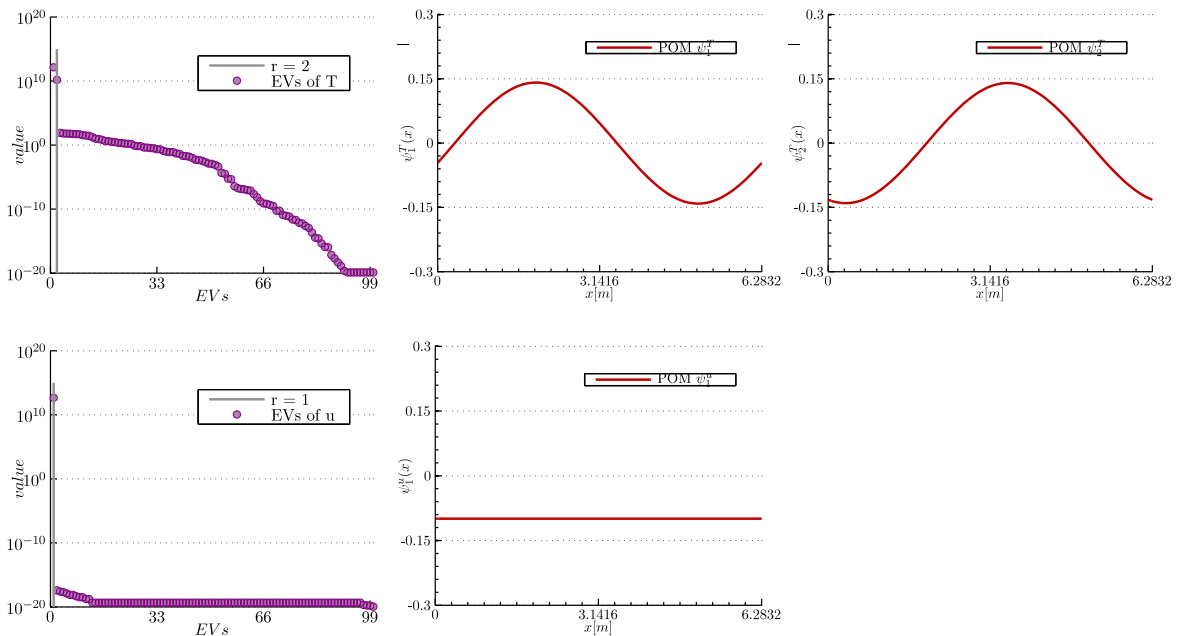


Figure 5.24.: Eigenspectra to temperature and velocity on a semi-logarithmic scale with inserted reduction level (1st column) and two dominant proper orthogonal modes for temperature and one for velocity.

The calibration road map for the derived NCC-POD-ROM consists of a vanishing penalty parameter and generalized Sobolev weights. A reduction level of 99.9% indicates that there are two POMs for the temperature and one POM for velocity amplitude necessary (see Fig. 5.24). Temperature modes have again sinusoidal shape.

The ROM is applied to predict the dynamical behavior of a NCC system for a different perturbation, see Fig. 5.23(b). The system ramp is driven for 30s, then a rectangular perturbation is applied and afterwards the heat input is switched off. The resulting "true" velocity transient for this perturbation is illustrated within Fig. 5.23(a) in blue, calculated by the FOM. Results by the POD based NCC ROM are marked in purple. Note that the true and the predicted solution match perfectly.

5.3.7 CONCLUSIONS

The POD-ROM methodology is successfully applied to a NCC problem with oscillating dynamics. The methodology reduces the complex PDE system to a coupled nonlinear system of ordinary equations with a very small number of degrees of freedom. A comparison of limit cycles attained by [40, 41] and the NCC-POD-ROM shows same amplitudes. A reduced system of Lorenz type was derived which predicts non-linear dynamics up to deterministic chaos in agreement with experimental results. The ROM not only reproduces the input data but is rather able to predict system dynamics at other operation states (different tilting, different perturbation).

5.4 TUBULAR REACTOR

This section considers a system featuring a complex non-linear dynamical behavior chosen for validation and verification purposes. It is identical to the applied setup of van Belzen et al. [136]. They tested their reduced ordering modeling strategies for this setup focusing on robustness, computational efficiency and sensitivities. A similar setup was chosen by Kalashnikova and Barone [62] to test their efficient non-linear POD-Galerkin ROM with stable penalty enforcement of boundary conditions. In contrast to the investigations of Belzen et al. they only deal with steady-state solutions.

This example is considered as an equivalent test case for perturbation investigations of the BWR system, i.e. against pump trips etc., violating the inlet and exit conditions. The derived methodology can be validated and verified for oscillating phenomena caused by external conditions.

This section treats the application of the derived methodology. It describes the "pathologic" tubular reactor (TR) system and its discretization. The number of snapshots is based on a convergence plot of EVs. Focus is put on important methodology steps. Effects of certain weighted Sobolev inner product choices on the eigenspectra are investigated. Increasing dissipation by the choice of inner product is shown to influence fine-scale structures. Moreover, by a comparison of ROMs, that are based on mean adjusted or non-adjusted fluctuation fields, the importance of included mean flows are underlined for transient applications. Different stabilized ROMs are reviewed and the road to an optimal ROM is given for both, mean excluded and included ROM types. Subsequently they are applied for answering questions regarding prediction capabilities. Analyses for mean excluded fields are always referred to as (ANA:a) and those for mean included field are denoted by (ANA:b).

5.4.1 FULL ORDER MODEL DATA

MODEL

A 1D non-isothermal formulation of a TR is considered where a first order irreversible exothermic reaction takes place. The geometry consists of a reactor of length $L_e = 1$ with temperature controllers along the reactor tube. The jacket wall temperature control is divided into three adjustable regions. Moreover, temperature and concentration distributions, T_i and C_i , can individually be regulated at the inlet. The TR can be modeled by a set of PDEs [136]:

$$\begin{aligned}\frac{\partial T}{\partial t} &= \frac{1}{\text{Pe}_h} \frac{\partial^2 T}{\partial x^2} - \frac{1}{L_e} \frac{\partial T}{\partial x} + \nu C e^{\gamma(1-\frac{1}{T})} + \mu (T_{wall} - T), \\ \frac{\partial C}{\partial t} &= \frac{1}{\text{Pe}_m} \frac{\partial^2 C}{\partial x^2} - \frac{\partial C}{\partial x} - \text{Da} C e^{\gamma(1-\frac{1}{T})},\end{aligned}$$

where x is the dimensionless axial distance, t is the dimensionless time, L_e is the length of the reactor, μ is the dimensionless heat transfer coefficient, ν is the dimensionless heat of reaction, γ is the dimensionless activation energy, Da is the Damköhler number, Pe_m and Pe_h are the Peclet numbers for mass and heat transfer, respectively. Physical parameters, chosen for this setup, are illustrated in Tab. 5.2. The setup is subject to the following boundary conditions at inlet and outlet:

$$\left\{ \begin{array}{l} \frac{\partial T}{\partial x} \Big|_{x=0} = \text{Pe}_h (T - T_i) \\ \frac{\partial C}{\partial x} \Big|_{x=0} = \text{Pe}_m (C - C_i) \end{array} \right. \quad \text{and} \quad \left\{ \begin{array}{l} \frac{\partial T}{\partial x} \Big|_{x=1} = 0 \\ \frac{\partial C}{\partial x} \Big|_{x=1} = 0 \end{array} \right. .$$

Note that the enforced boundary conditions are of mixed type: Neumann type at the right boundary ($x = 1$) and Robin type at the left boundary ($x = 0$).

Table 5.2.: Physical parameters selected for the tubular reactor setup.

property	symbol	value
Peclet number for mass transfer	Pe_m	5.000
Peclet number for heat transfer	Pe_h	5.000
length of channel	L_e	1.000
Damköhler number	Da	0.875
activation energy	γ	15.000
heat of reaction	ν	0.840
heat transfer coefficient	μ	13.000

STEADY-STATE CONDITION

Referring to van Belzen et al. [136], the optimal steady-state operating condition for this reactor is a result of a minimization procedure between minimal energy consumption and maximal production under the constraint of an upper temperature limit. The optimal steady-state jacket wall temperatures are

$$T_{wall}(x) = \begin{cases} 0.9970 & x \in [0, \frac{1}{3}) \\ 1.0475 & x \in [\frac{1}{3}, \frac{2}{3}) \\ 1.0353 & x \in [\frac{1}{3}, 1] \end{cases} .$$

The inlet conditions are given by $(T_i, C_i) = (1, 1)$. It turns out that the reactor is in an asymptotically stable operating condition for this setup.

PERTURBATION

For attaining the FOM data, a transient of $T_{end} = 20s$ is simulated which refers to a system where the inlet temperature and concentration are affected by a perturbation after 4s. The starting inlet concentration $C_i = 1$ and temperature $T_i = 1$ are chosen to be steady-state operating conditions. The temporal distribution of the perturbed inlet conditions are illustrated in Fig. 5.25 and given by:

$$T_i(t) = \begin{cases} 1 & , t \in [0, 4) \\ 1 + 0.04e^{0.045(t-4)} \sin(2(t-4)) \\ \quad + 0.01 \sin(5(t-4)) & , t \in [4, 18] \\ 1 & , t \in (18, 20] \end{cases}$$

$$C_i(t) = \begin{cases} 1 & , t \in [0, 4) \\ 1 + 0.015 \sin(5t) + 0.02 \sin(t) & , t \in [4, 18] \\ 1.02 & , t \in (18, 20] \end{cases}$$

The optimal steady-state jacket temperatures are slightly changed to a constant wall temperature $T_w = 1$. Note that this perturbation is exactly the one stated in [136] for a further comparison to single-variable ROM results.

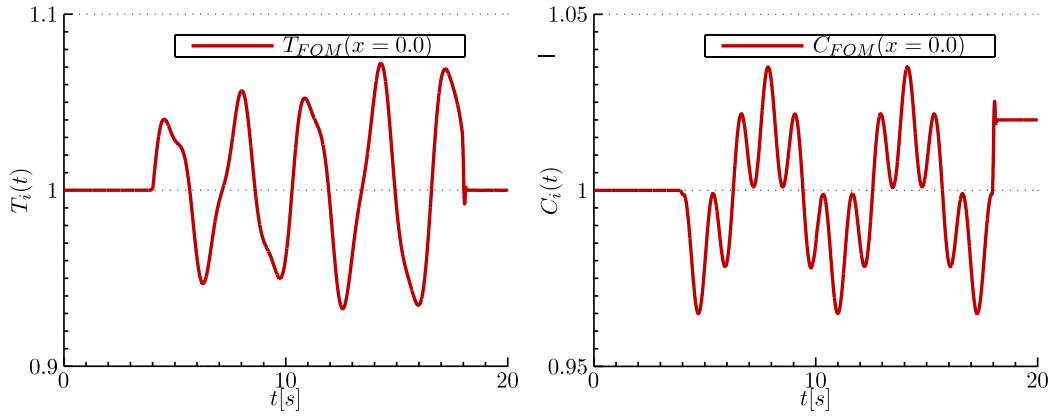


Figure 5.25.: Temporal distribution of the perturbed inlet conditions.

5.4.2 DISCRETIZATION

The POD algorithm is applied to an ensemble of snapshots for temperature and concentration fields for a time period of $t \in [0, 20s]$. The spatial grid is well resolved and fixed for all setups to $x_h = 0.01$, see [136]. The number of snapshots, necessary for attaining the correlation matrix is not a priori known. Figure 5.26 shows that dominant eigenvalues converge as the number of snapshots is increased. Based on Fig. 5.26, 5000 snapshots within 20s are equidistantly selected and results in a temporal step size of $t_h = 0.004$ which is applied throughout all ROM calculations. Note that grids within the FOM and ROM remain identical.

5.4.3 ANALYSIS OF DIFFERENT KERNEL CHOICES

A proper kernel choice is subject of the discussion below. For this purpose, exemplary plot sequences of the fluctuation energy, the POM shapes and how they are affected by different kernel choices are surveyed in Fig. 5.27-5.29 and Tab. 5.3. Qualitative results are based on mean adjusted temperature and concentration fields. However, findings generally also hold for mean non-adjusted equations but they are omitted here.

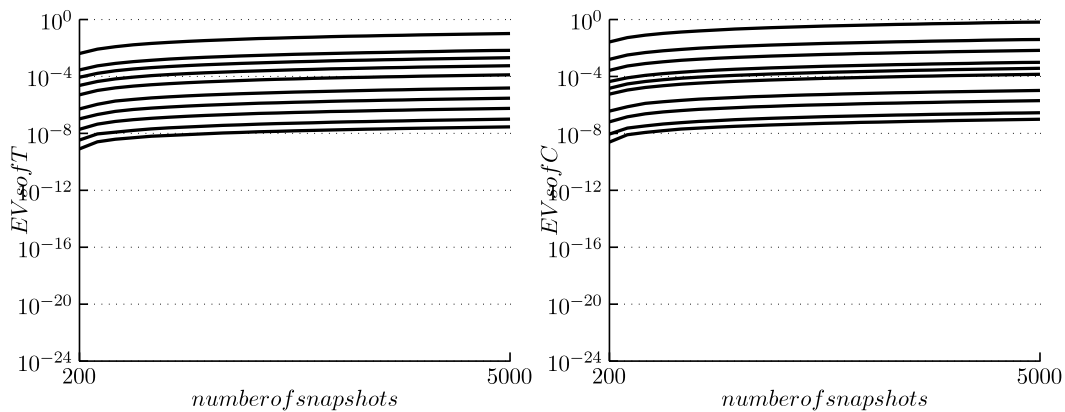


Figure 5.26.: Convergence plot of the first ten eigenvalues of the temperature and concentration fields as function of the number of snapshots for kernel $(\epsilon_0, \epsilon_1, \epsilon_2) = (1, 0, 0)$.

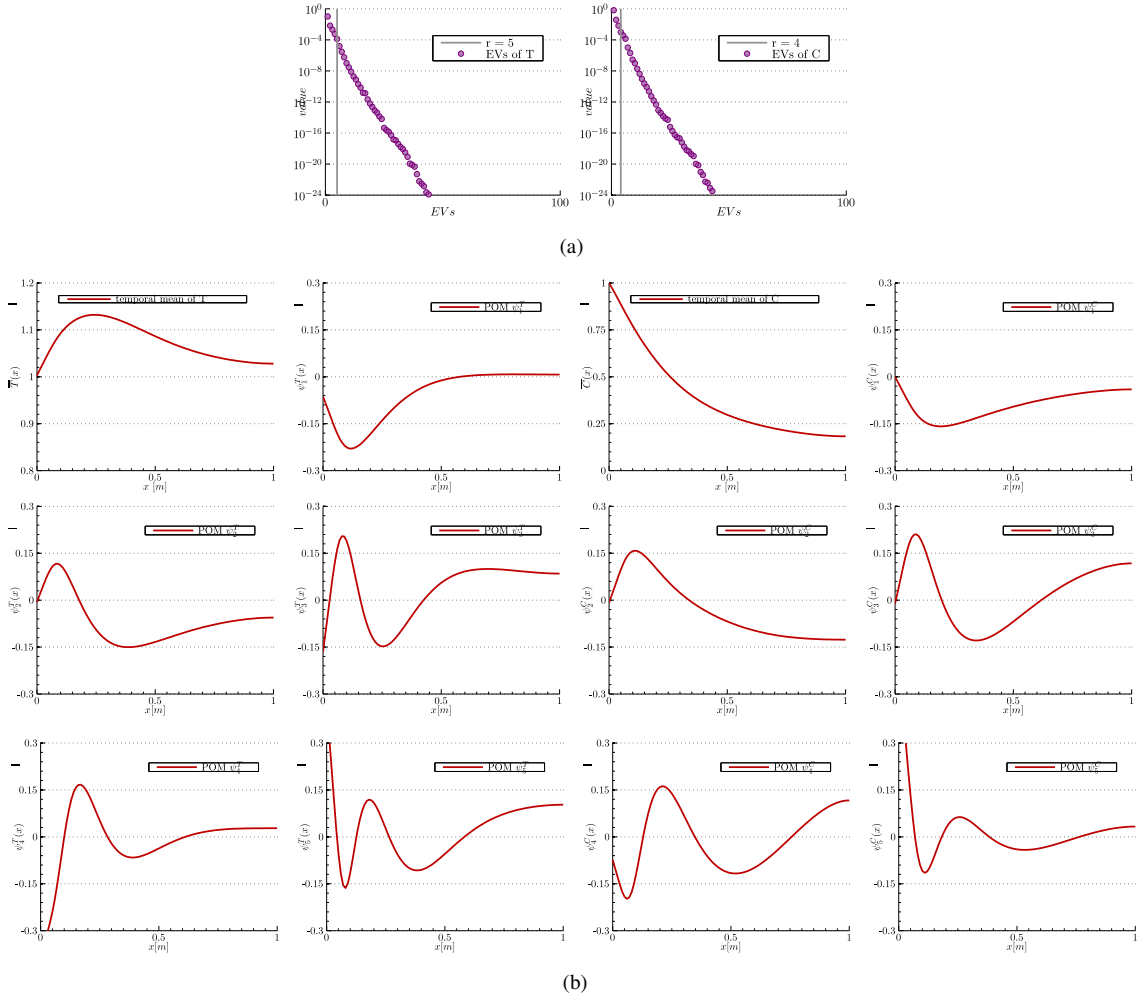


Figure 5.27.: Eigenspectra of temperature and concentration on a semi-logarithmic scale with inserted reduction level (a), temporal means and five dominant proper orthogonal modes (b): Kernel K_0 .

FLUCTUATION ENERGY

Part (a) of Figs. 5.27-5.29 show the eigenspectra of temperature and concentration fields on a semi-logarithmic scale for different kernels K_0 , K_1 , and K_s with $(\epsilon_0, \epsilon_1, \epsilon_2) = (1.00, 0.03, 0.00)$. For all eigenspectra, a rapidly decreasing impact of eigenvalues can be seen. The reduction level is set to

Table 5.3.: Total fluctuation energies in the first ten proper orthogonal modes for temperature fields of different kernels: K_0 , K_1 and K_s with $(\epsilon_0, \epsilon_1, \epsilon_2) = (1.00, 0.03, 0.00)$, and truncation limit colored in gray.

i	K_0 % kin. energy	K_1 % kin. energy	K_s % kin. energy
1	91.484823877575550	89.7434339736530	91.208576985334560
2	97.545017378764854	97.4817117842180	97.417083137735929
3	99.370317287560511	99.7943910139420	99.516451613119983
4	99.868628855151513	98.8098595505489	99.918421919532364
5	99.983231674355096	99.9588108751814	99.979882899477104
6	99.996767504158797	99.9875544954431	99.994984714888602
7	99.999376209589698	99.9951437785730	99.999038637074861
8	99.999876918165853	99.9987748329402	99.999778102675933
9	99.999965235187290	99.9996891368789	99.999937774343593
10	99.999990626544417	99.9998776885285	99.999980340164058

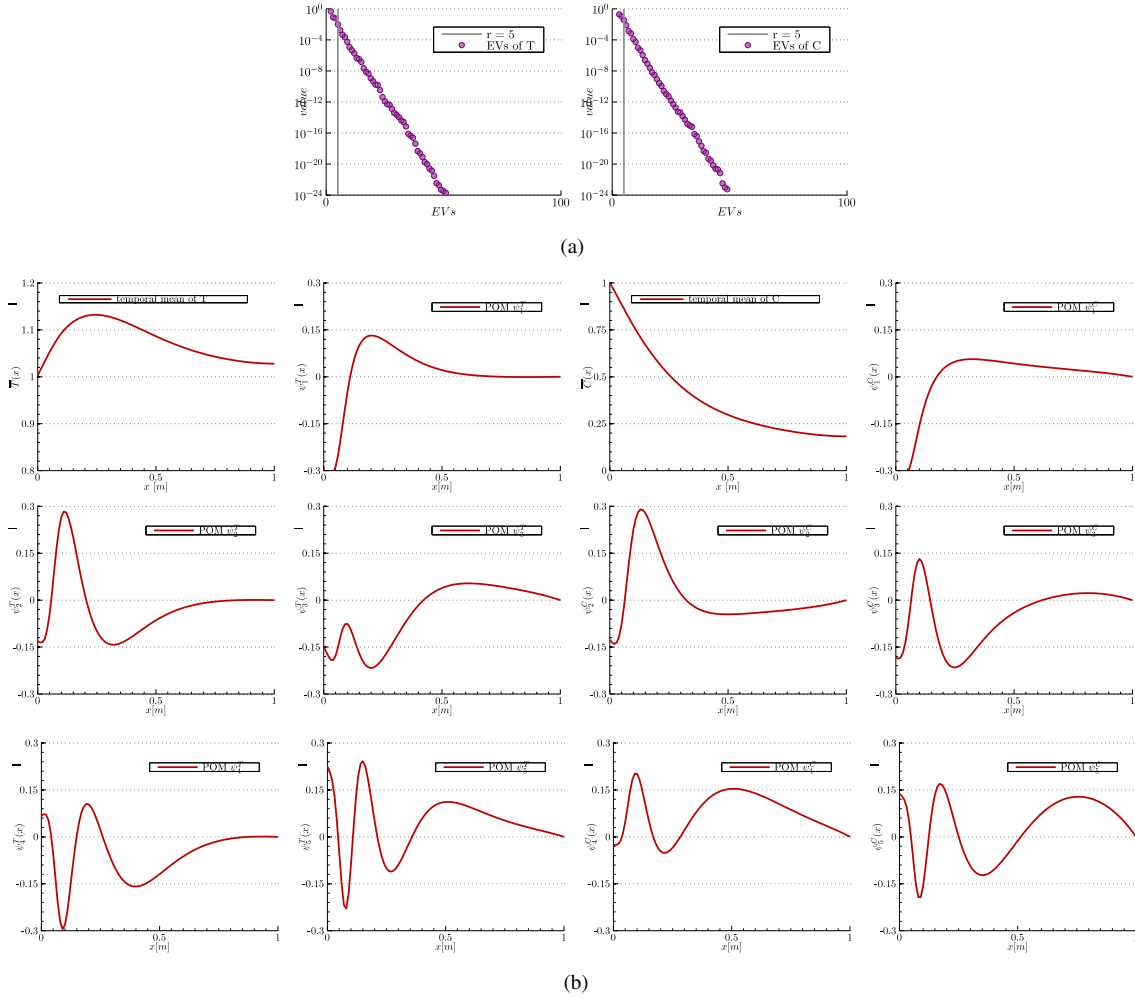


Figure 5.28.: Eigenspectra of temperature and concentration on a semi-logarithmic scale with inserted reduction level (a), temporal means and five dominant proper orthogonal modes (b): Kernel K_1 .

99.9% which leads to the truncation criteria for temperature and concentration (r^T, r^C) indicated in the figure labels.

Note that in case of kernel K_0 (r^T, r^C) = (5, 4) POMs are necessary for the reconstruction to preserve the energy level, in contrast to kernel K_S which needs less POMs (r^T, r^C) = (4, 4). By regarding first order derivatives within the kernel, fluctuation energy of the first two POMs is transferred to the third and fourth POM. This can be better visualized by the numerical values of fluctuation energy referring to the temperature spectra for the first ten POMs listed in Tab. 5.3. Fluctuation energy is equal to the corresponding sum of the first EVs λ_i . The first few eigenfunctions contain most of the temperature fluctuation energy.

PROPER ORTHOGONAL MODES

The mean and the first five POMs for temperature and concentrations are shown for different kernel choices in Fig. 5.27-5.29(b). The mean is not affected by the choice of different kernel functions as it is excluded before the decomposition and treated statically. Moreover, coherent structures do not appear in pairs regarding the POMs of temperature and concentration fields for kernels K_0 and K_S . This is due to the fact that the autocorrelation matrix is not invariant under translation. It not only depends on the difference between the snapshot fields which is in contrast to Fourier modes, leading

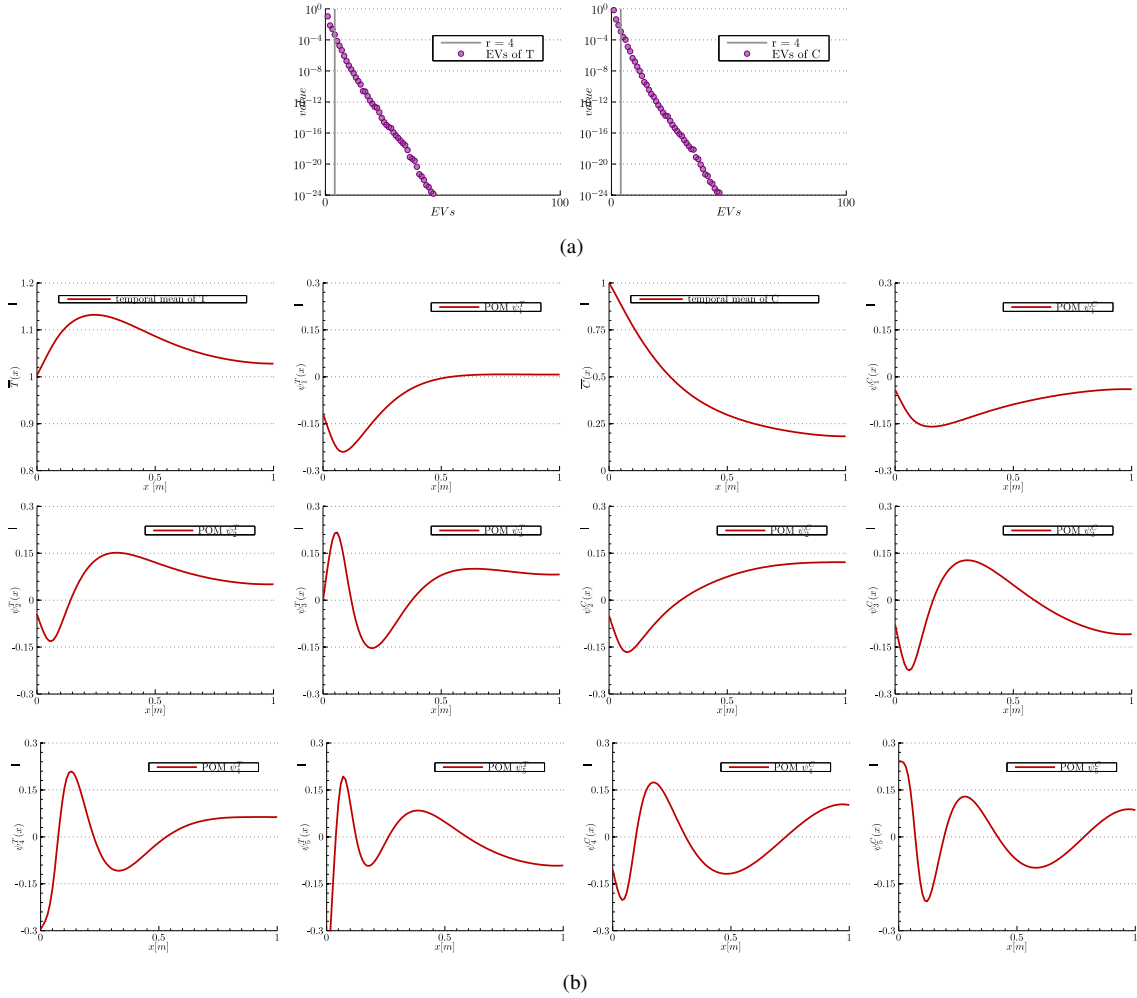


Figure 5.29.: Eigenspectra of temperature and concentration on a semi-logarithmic scale with inserted reduction level (a), temporal means and five dominant proper orthogonal modes (b): Kernel K_S , $\varepsilon_0 = 1.00$, $\varepsilon_1 = 0.03$.

POMs in lid-driven cavities or flat plate transitional boundary layer [16]. In particular, POMs of kernels K_0 and K_S have similar shape but for a kernel K_S the shape is more pronounced especially at the boundary.

REMARKS

Low-dimensional POD-ROMs lose fine-scale information due to the truncation. Obviously, considering first order derivatives within the kernel K_S leads to a better distribution of fluctuation energy. Small changes in mode shape appearing for kernel K_S are preferable as fluctuation energy is better distributed. ROMs having kernels consisting of higher order derivatives have potential to better match the underlying FOM solution. Note that gradients, playing decisive roles especially for time-varying inflow conditions, are expected to be of importance for the TR. In the following, this will be examined by reconstructions to mean adjusted fields (ANA:a).

5.4.4 RECONSTRUCTIONS: MEAN EXCLUDED (ANA:A)

Results of this analysis consist of temperature and concentration fields being mean adjusted before the calculation of correlation matrices and further ROM achievements. The goal of this section is

a comparison of TR-POD-ROMs with different kernel choices and ranks. Note, that the Arrhenius term has a strong exponential dependency on temperature. In the following, comparisons and optimizations are based on the most important quantity within the equation system, the temperature.

The comparisons are visualized by plotting the time evolution of the temperature at a reference location within the reactor ($x = 0.49$). Evolution of concentration shows similar behavior and therefore is omitted. So far only local data has been considered. An extension is given by a comparison of quantities referring to the entire domain, having introduced in Sec. 4.5. Finally, by a certain penalty parameter choice, reconstructions with different kernel choices are illustrated.

The RMSE between the POD-ROM and the true FOM solution at time levels t_j estimates the error of the projection. It is denoted by $RMSE$ and the average RMSE by \overline{RMSE} . For an optimal system the RMSE vanishes at all time. Another error quantity describing how the dynamical behavior of the reduced system behaves in comparison to the original system is given by the CC. It is denoted by CC . Its time averaged pendant, termed by \overline{CC} , is a measure for the averaged correlation. The maximum error (ME) indicates the maximum error on the whole temporal and spatial domain. Note that an optimal ROM has smallest \overline{RMSE} by a large as possible \overline{CC} and smallest ME.

Boundary conditions are imposed by the penalty formulation with two penalty parameters (Γ^T, Γ^C) for temperature and concentration boundaries. By an iteration loop they are calibrated: $(\Gamma^T, \Gamma^C) = (250, 125)$. Moreover, they are determined such that the system response is numerically stable. Higher penalty values result in unstable systems. The penalty parameter for concentration has a minimum stable value and the parameter for temperature is chosen to be twice as big. Note that due to the choice of constant penalty parameters, an error deviation in the steady-state and perturbed solutions is expected.

A comparison of errors regarding different TR-POD-ROMs are illustrated in Tab. 5.4. Errors are visualized by plotting ROMs consisting of three and four POMs for temperature and concentration fields. The first two rows of Tab. 5.4 have a kernel setup K_0 including no derivatives, rows three and four refer to ROMs including also first derivatives and an iteratively chosen optimal Sobolev weight ε_1 . Rows five and six show results of manually optimized kernel choices including first and second order derivatives.

KERNEL WITHOUT DERIVATIVES

Figure 5.30 shows results for the time evolution of the temperature fields referring to ROMs with kernel K_0 having orders $(r^T, r^C) = (3, 3)$ (left) or $(r^T, r^C) = (4, 4)$ (right). Both simulations fail to capture the maxima and minima values within the perturbed part of the transient. Note that dynamics are qualitatively reproduced. However, higher order derivatives have a dominant role and are not sufficiently approximated as the peak values are highly underestimated. A better comparison is given in terms of error results printed in Tab. 5.4. Both ROMs show similar results. The \overline{RMSE} is slightly decreased and the \overline{CC} is slightly increased for a ROM of order $(r^T, r^C) = (4, 4)$ compared to

Table 5.4.: Tubular Reactor Reduced Order Model Error Results.

(Γ^T, Γ^C)	(r^T, r^C)	ε_0	ε_1	ε_2	\overline{RMSE}	\overline{CC}	ME_T
(250, 125)	(3, 3)	1	0.0000	0.0000	0.0268	0.9135	0.5098
(250, 125)	(4, 4)	1	0.0000	0.0000	0.0254	0.9249	0.4814
(250, 125)	(3, 3)	1	0.0300	0.0000	0.0236	0.9322	0.4349
(250, 125)	(4, 4)	1	0.0375	0.0000	0.0249	0.9273	0.4766
(250, 125)	(3, 3)	1	0.0080	0.0025	0.0229	0.9569	0.4068
(250, 125)	(3, 3)	1	0.0077	0.0023	0.0193	0.9625	0.3960

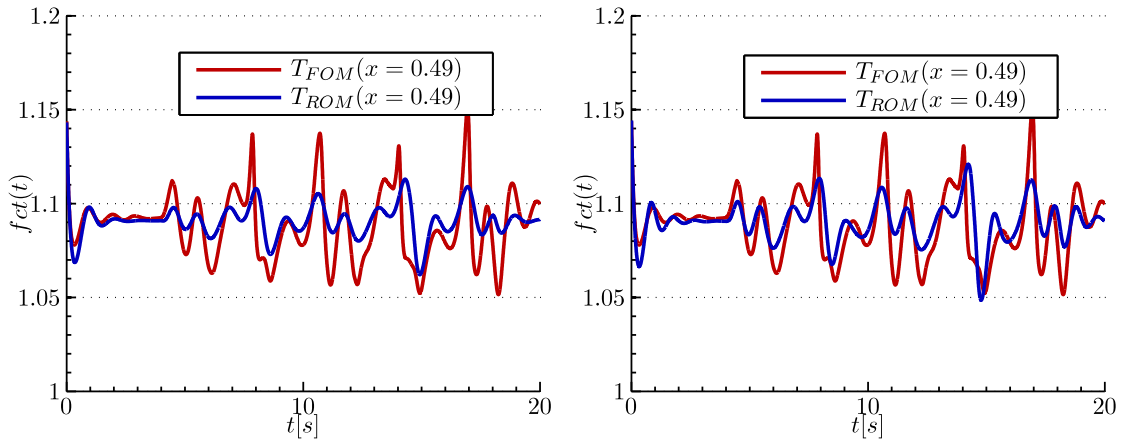


Figure 5.30.: Time evolution of temperature at $x = 0.49$ for K_0 with $(\varepsilon_0, \varepsilon_1, \varepsilon_2) = (1.0000, 0.0000, 0.0000)$: left $(r^T, r^C) = (3, 3)$, right $(r^T, r^C) = (4, 4)$.

order $(r^T, r^C) = (3, 3)$. Furthermore, the ME is decreased. Note that higher order ROMs only slowly better approximate the true solution.

KERNEL WITH FIRST ORDER DERIVATIVES

Due to the dominant role of higher order derivatives, an investigation is presented for kernels consisting of data with a varying amount of derivatives. Including first order derivatives within the kernel makes an iterative strategy necessary.

First of all we refer to a setup with order $(r^T, r^C) = (3, 3)$. Figure 5.31 shows how the kernel optimization routine works. Results are plotted regarding the time evolution of the temperature and concentration fields referring to kernel K_s with varying ε_1 and constant $\varepsilon_0 = 1$ and order $(r^T, r^C) = (3, 3)$. Finding a minimum optimal solution for a ROM needs a coarse variation of the Sobolev weight ε_1 and a fine variation for the region of interest. The first row shows the temporal RMSE and CC as function of a coarse variation of ε_1 in the range of 10^{-3} to 10^1 . This indicates that the region of interest, where the reduced model best fits the true solution, is the low \overline{RMSE} -range. Correspondingly, the second row shows the zoom into this region of interest. Note that there is a minimum temporal RMSE value such that the overall dynamical behavior of the ROM solution best fits the dynamics of the FOM solution. Having iteratively chosen an optimal calibration value for ε_1 , the third and fourth rows show temporal evolutions of important variables. The third row gives the evolution of CC and RMSE as function of time to the iteratively chosen optimal Sobolev weight ($\varepsilon_1 = 0.03$). The fourth row shows the local temperature distribution near the center position of the channel. During the period of perturbation the RMSE and CC is affected by rapidly changing inflow conditions. The temporal evolution of the temperature show that, due to the exploitation of first derivatives within the kernel, the temporal gradients are clearly better reproduced within this optimal ROM. This demonstrates the validity of the optimization concept. Error results, listed within Table 5.4, also underline this. Note that both, the RMSE and the CC give better results than for uncalibrated ROMs. Also the ME is decreased.

The second setup shows the performance of the kernel optimization routine to a higher order ROM. It is devoted to the question if even second or higher order derivatives are necessary within the data basis for decomposition to represent the dynamics or if a simple increase of order is sufficient.

Figure 5.32 refers to kernel K_s with varying ε_1 , constant $\varepsilon_0 = 1$ and $\varepsilon_2 = 0$ for ROM of order of $(r^T, r^C) = (4, 4)$. Again the first row shows the temporal RMSE and CC as function of a coarse

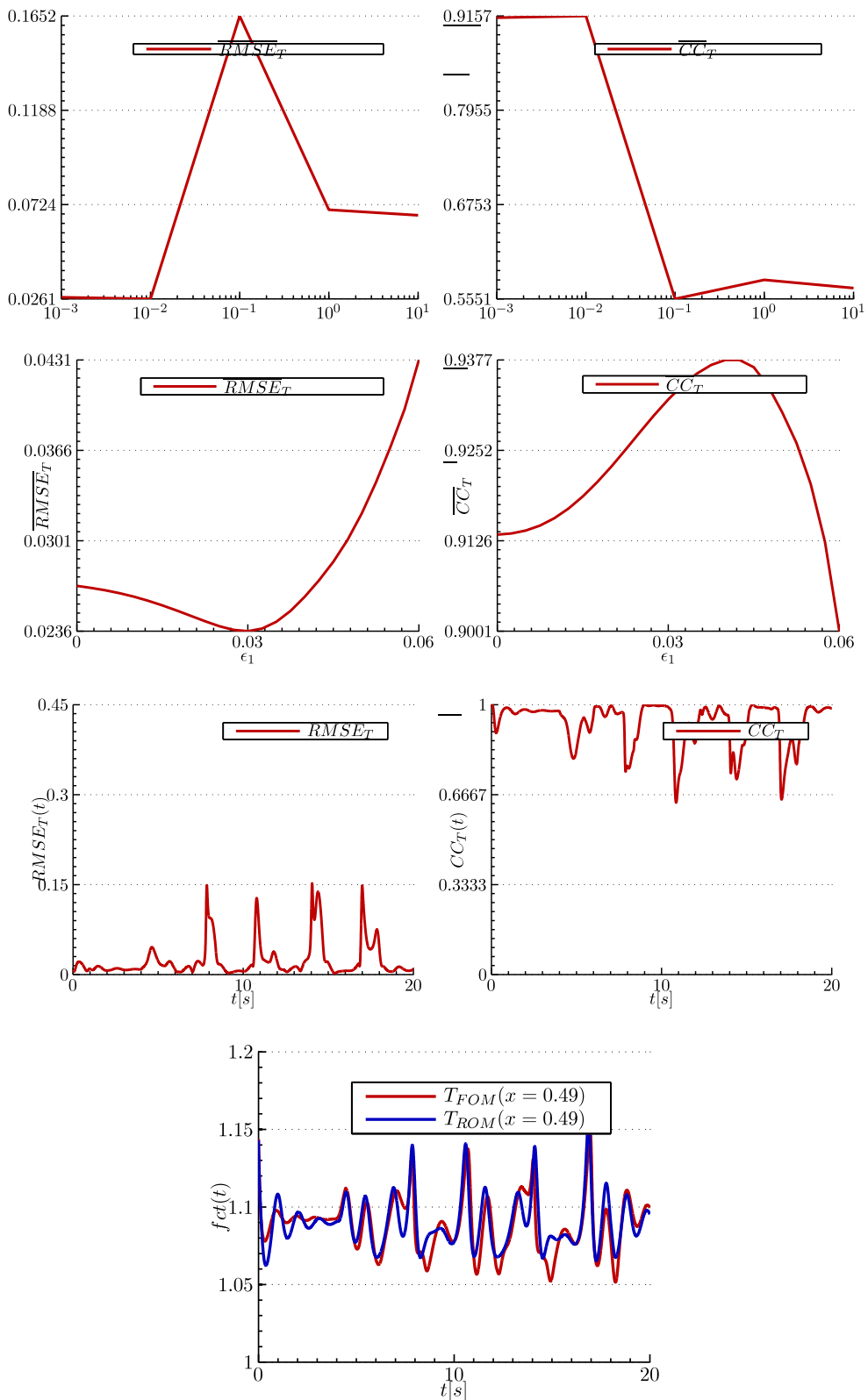


Figure 5.31.: Depicting intermediate steps and final result of kernel optimization for a TR-POD-ROM with order $(r^T, r^C) = (3, 3)$: Temporal mean of root mean square error and correlation coefficient as function of ϵ_1 for a coarse grid (1st row) and fine grid (2nd row), time evolution of root mean square error and correlation coefficient (3rd row) for the best result $(\epsilon_0, \epsilon_1, \epsilon_2) = (1.0000, 0.0300, 0.0000)$ and its time evolution of temperature at $x = 0.49$ (4th row).

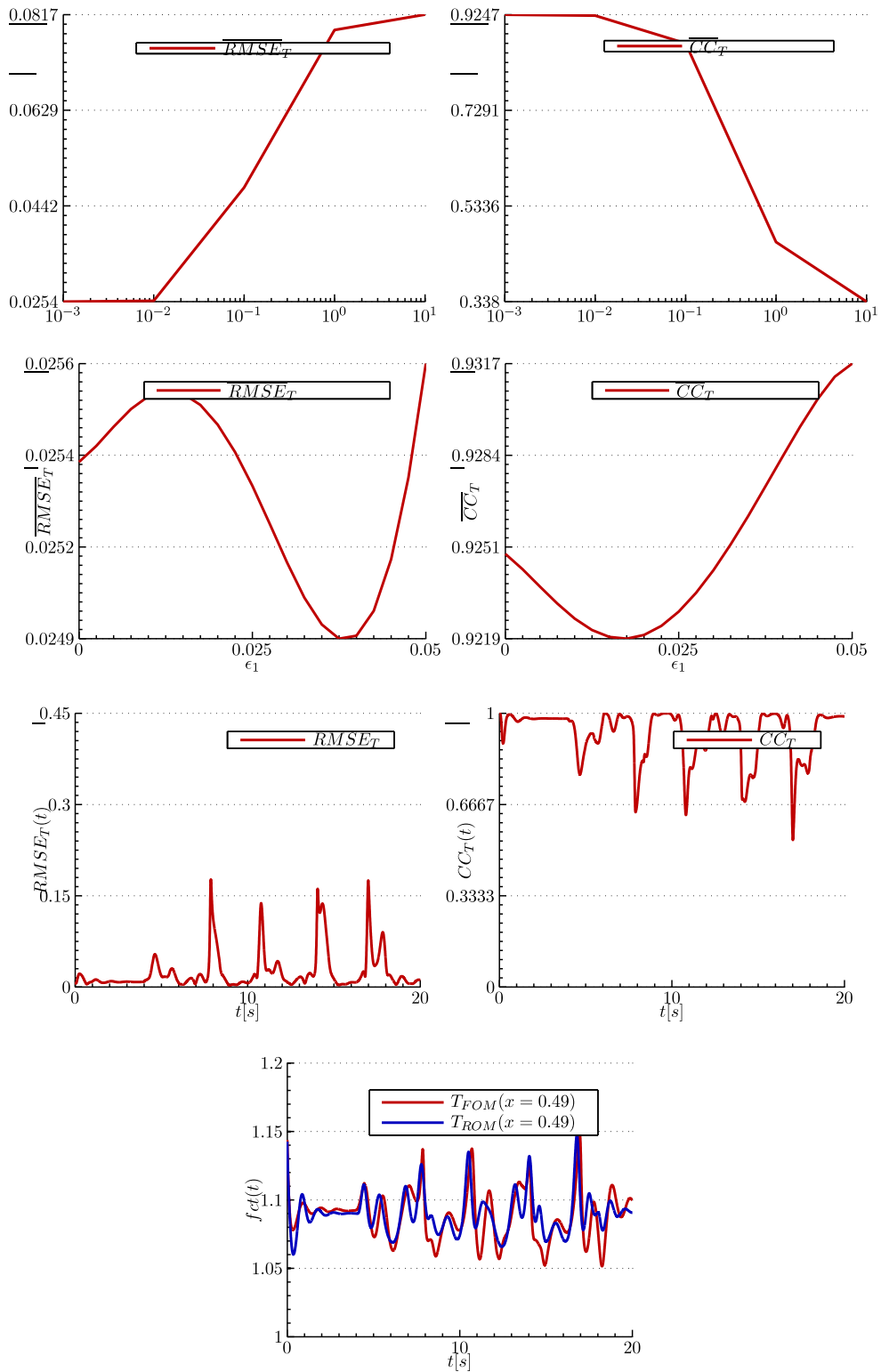


Figure 5.32.: Depicting intermediate steps and final result of kernel optimization for a TR-POD-ROM with order $(r^T, r^C) = (4, 4)$: Temporal mean of root mean square error and correlation coefficient as function of ϵ_1 for a coarse grid (1st row) and fine grid (2nd row), time evolution of root mean square error and correlation coefficient (3rd row) for the best result $(\epsilon_0, \epsilon_1, \epsilon_2) = (1.0000, 0.0375, 0.0000)$ and its time evolution of temperature at $x = 0.49$ (4th row).

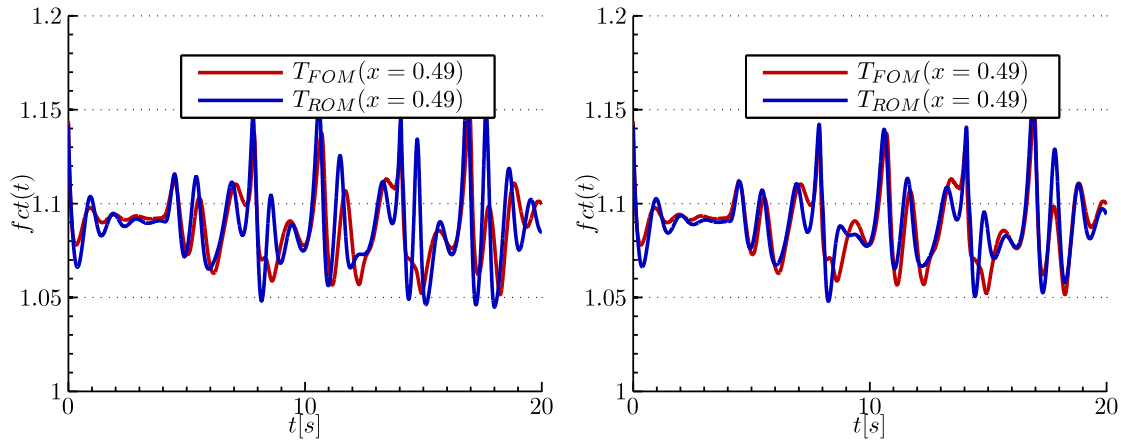


Figure 5.33.: Time Evolution of temperature at $x = 0.49$: left $(\varepsilon_0, \varepsilon_1, \varepsilon_2) = (1.00, 0.008, 0.0025)$, $(r^T, r^C) = (3, 3)$; right $(\varepsilon_0, \varepsilon_1, \varepsilon_2) = (1.00, 0.0077, 0.0023)$: $(r^T, r^C) = (3, 3)$.

variation of ε_1 in logarithmic scale. According to the low \overline{RMSE} -range, the second row shows its region of interest. The temporal RMSE has a minimum value such that the overall dynamical behavior of the ROM solution best maps the dynamics of the FOM solution. For the optimal Sobolev weights, $(\varepsilon_0, \varepsilon_1, \varepsilon_2) = (1.0000, 0.0375, 0.0000)$ (iteratively determined), the third row gives the best ROM evolution of CC and RMSE as function of time and the fourth row shows the local temperature distribution near the center position of the channel. Error results are listed within Table 5.4. Note that both, the RMSE and the CC give better results and also the ME is decreased in comparison to non-calibrated ROMs. Apparently only small improvements between orders of $(r^T, r^C) = (3, 3)$ and $(r^T, r^C) = (4, 4)$ can be achieved. This indicates that yet higher order derivatives are necessary to reproduce the dynamics of the original system.

KERNEL WITH FIRST AND SECOND ORDER DERIVATIVES

Given that increasing the order of the ROM only has small effect, manual optimization of a TR-POD-ROM for two Sobolev weight parameters ε_1 and ε_2 is illustrated in Figure 5.33 for order $(r^T, r^C) = (3, 3)$. Both graphs illustrate the time evolution of the temperature field referring to kernel K_s with varying ε_1 and ε_2 , and constant $\varepsilon_0 = 1$. The order is kept constant. Obviously, the dynamics of the FOM are better reproduced for both cases which confirms the previous speculation that higher order derivatives are important. Error results are listed within Table 5.4. Note that for both models, the RMSE and the CC give better results and also the ME is further decreased. The ROM with manually-calibrated Sobolev weights of $(\varepsilon_0, \varepsilon_1, \varepsilon_2) = (1.000, 0.0077, 0.0023)$ give best results (but not yet iteratively chosen).

5.4.5 PREDICTION CAPABILITIES: MEAN EXCLUDED (ANA:A)

Summing up the kernel optimization tests, it can be stated that for an optimal calibrated ROM at least second order derivatives are of importance. For a ROM consisting of a kernel with first derivatives the optimization routine was shown to work. For kernel choices with first and second order derivatives a manually-calibrated ROM underline the importance of even higher order derivatives. Note that increasing the number of derivatives need even better optimization strategies and hence also computational time.

The manually-calibrated model with first and second order derivatives is now referred to as the "optimal" ROM, i.e.

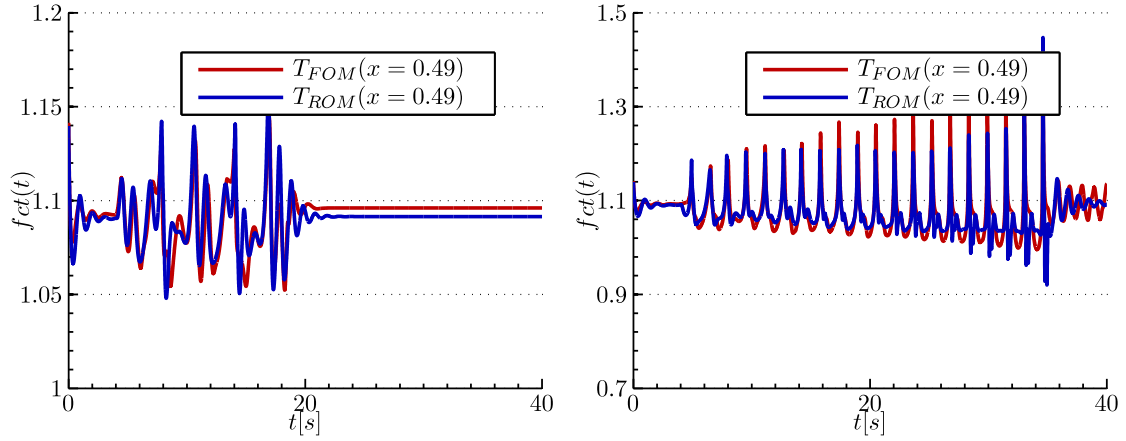


Figure 5.34.: Time Evolution of temperature at $x = 0.49$ for an optimal calibrated reduced order model. ROM predictions to setup (1) (left) and setup (2) (right).

- $(r^T, r^C) = (3, 3)$,
- $(\Gamma^T, \Gamma^C) = (250, 125)$,
- $(\varepsilon_0, \varepsilon_1, \varepsilon_2) = (1.00, 0.0077, 0.0023)$,

It has been attained by FOM data that belongs to a perturbed "pathologic" TR example for a time range of $t \in [0, 20s]$. Including data fields of temperature and concentration and also an "optimal" choice of first and second order contributions, this ROM has best performance in reconstruction of the FOM data. In comparison to van Belzen et al. [136], its ME is better conditioned for this single variable expansion setup and has lower rank: $(r^T, r^C) = (3, 3)$.

The "optimal" calibrated TR-POD-ROM is exploited to study prediction capabilities. Referring to BWR stability analysis, the prediction capabilities are essential since a BWR-POD-ROM will be based on sparse data. Accordingly, this subsection addresses the validity of the TR-POD-ROMs and is tested for two different setups:

- (1) identical perturbation but extension of simulation time: $t \in [0, 40s]$
- (2) prediction with a generic inflow perturbation:

$$T_i(t) = \begin{cases} 1 & , t \in [0, 4) \\ 1 + 0.057e^{0.07(t-2)} \cdot \sin(4(t-3)) + 0.015 \sin(7(t-3)) & , t \in [4, 35] \\ 1.02 & , t \in (35, 40] \end{cases}$$

$$C_i(t) = \begin{cases} 1 & , t \in [0, 4) \\ 1 + 0.025 \sin(3(t-2)) + 0.027 \sin(2t) & , t \in [4, 35] \\ 1.04 & , t \in (35, 40] \end{cases}$$

Figure 5.34 shows the results for the time evolution of the temperature at mid position for setup (1) and setup (2). Global error results are listed in Table 5.5. The dynamics are well represented for both setups.

Table 5.5.: Tubular Reactor Reduced Order Model Prediction Error Results.

Setup	(Γ^T, Γ^C)	(r^T, r^C)	ε_0	ε_1	ε_2	$RMSE$	CC	ME_T
(1)	(250, 125)	(3, 3)	1	0.0077	0.0023	0.0133	0.9770	0.3980
(2)	(250, 125)	(3, 3)	1	0.0077	0.0023	0.0610	0.8801	1.3462

It is expected that dynamics for the first 20 seconds of setup (1) are reproduced as this was already included in the input data for calibration. The ongoing prediction of the model maps a nearly identical steady-state which is due to the projection error of the model. Note that the system was reduced to a system of small order. The original system stability is preserved and no artificial numerical destabilization is observed. A steady-state is still a steady state and no instability effects due to numerics are visible. The ME for the first setup is of same order as for the tested calibrated model.

Setup (2) reproduces the perturbed dynamics of a system that is not represented in the data set. The dynamics of the reduced and original system fit, but peaks are sometimes over-predicted. No artificial numerical destabilizing effects are observed, but due to a completely different perturbation, the ME increases. This indicates that yet more POMs are necessary describing this generic perturbation or a further calibration to this kind of perturbation is necessary.

In both cases deviations to the FOM solution are still visible. Small errors will result in phase changes of oscillations and in slightly different dynamical results. We mostly address these errors to the static treatment of the mean value within the Galerkin projection step. Further errors are provoked by a defective derivative representation (see Sec. 4.3.6) within the POM construction and the Galerkin projection step.

5.4.6 RECONSTRUCTIONS: MEAN INCLUDED (ANA:B)

Results of this analysis consist of temperature and concentration fields without being mean adjusted before the calculation of correlation matrices and further ROM achievements. In all previous ROMs, the mean has been treated in a static way. Due to the modeling, only POMs were allowed to vary in time. The goal of this section is a comparison of TR-POD-ROMs keeping the mean in the data set. As described above, the Arrhenius term has a strong exponential dependency on temperature, hence it is sufficient to base comparisons and optimizations on the temperature variable. Visualization is again realized by plotting the time evolution of the temperature at a reference location within the reactor ($x = 0.49$) and global error quantities.

Part (a) of Fig. 5.35 show the eigenspectra of temperature and concentration fields on a semi-logarithmic scale. For all eigenspectra, a rapidly decreasing impact of eigenvalues can be seen.

Table 5.6.: Total energies in the first ten proper orthogonal modes for temperature fields: setup (ANA:b).

i	K_0 % kin. energy
1	99.8749795893212
2	99.9926922413126
3	99.9981331751913
4	99.9992858937321
5	99.9999491644390
6	99.9999902139982
7	99.9999984084791
8	99.9999997506735
9	99.9999999299476
10	99.9999999816133

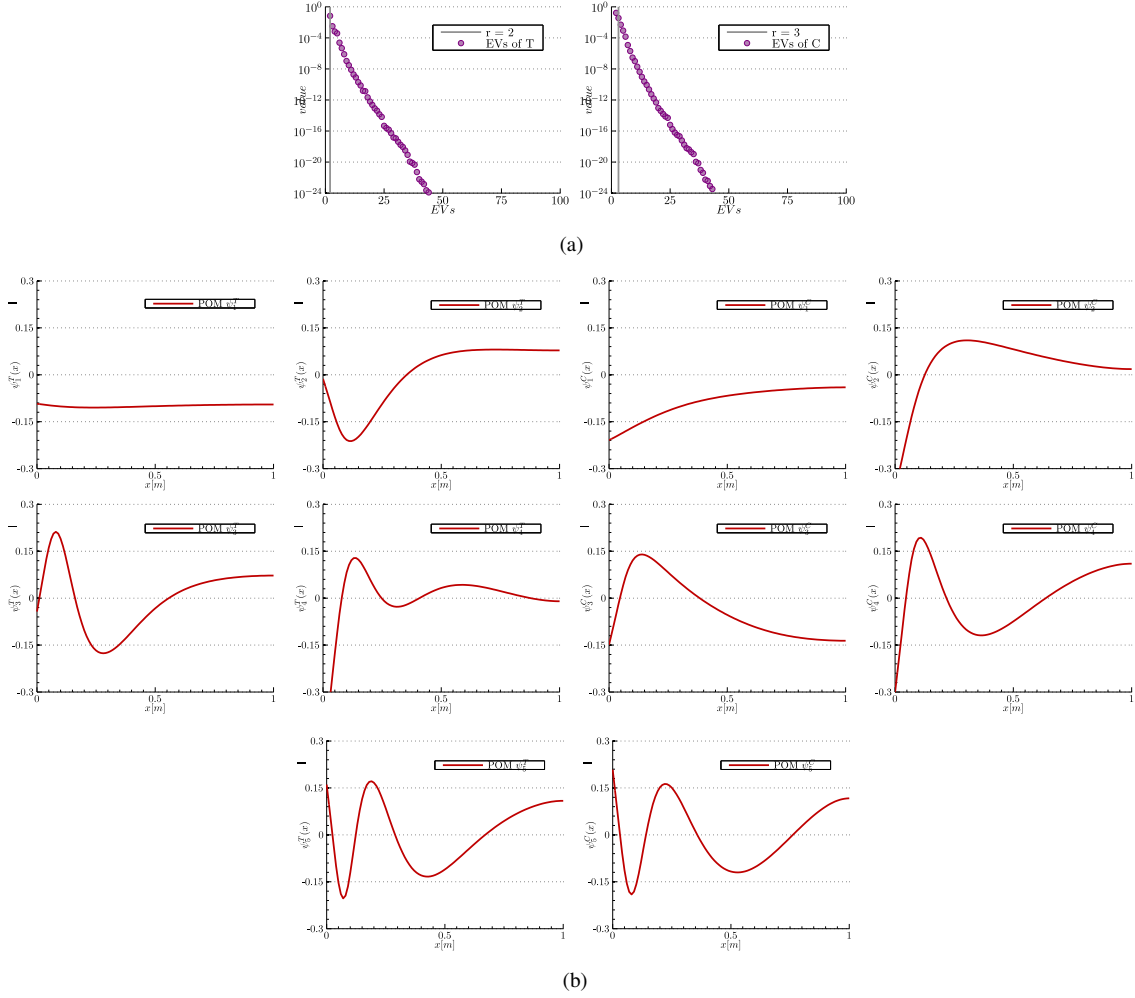


Figure 5.35.: Eigenspectra of temperature and concentration on a semi-logarithmic scale with inserted reduction level (a), five dominant proper orthogonal modes (b): setup (ANA:b).

Note that $(r^T, r^C) = (2, 2)$ POMs are necessary for the reconstruction to preserve the reduction level of 99.9%. The truncation criteria for temperature and concentration (r^T, r^C) is indicated in the figure labels. In contrast to a POD analysis of mean adjusted fields, the eigenspectra are increased due to the keeping of the most energetic modes (the means) within the data sets. This contributes to the chosen reduction level. A choice of 99.9% yields inaccurate ROMs. These facts are visualized by the numerical values of energy referring to the temperature spectra for the first ten POMs listed in Tab. 5.6. A more restrictive criterion is needed, e.g. 99.99%, keeping at least $(r^T, r^C) = (4, 4)$ POMs within the reduced system.

The first five POMs for temperature and concentrations are shown in Fig. 5.35(b). The first mode is related to the mean. Moreover, coherent structures do not appear in pairs regarding the POMs of temperature and concentration fields. POMs have similar shape as in POD analyses for mean adjusted fields.

Boundary conditions are imposed by the penalty formulation with two penalty parameters (Γ^T, Γ^C) for temperature and concentration boundaries. By keeping the mean mode (1st POM) varying, the penalty amplified weak formulation becomes increasingly important. Diffusion and convection terms are replaced by their equivalent integration by parts formulation where their boundary parts are amplified by a penalty parameter. By non-mean-adjusted data fields and the usage of a penalty amplified weak formulation, penalty parameters can be chosen considerably higher than for adjusted

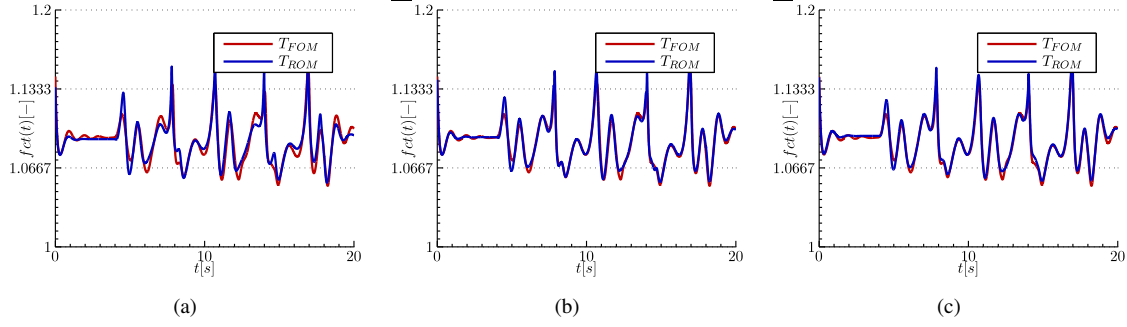


Figure 5.36.: Time evolution of temperature at $x = 0.49$ for K_0 with $(\varepsilon_0, \varepsilon_1, \varepsilon_2) = (1.0000, 0.0000, 0.0000)$: (a) $(r^T, r^C) = (4, 4)$, (b) $(r^T, r^C) = (5, 5)$, (c) $(r^T, r^C) = (6, 6)$: (ANA:b).

data fields. This has certainly influence on the exactness of the compliance of boundary conditions. Penalty parameters are chosen to be $(\Gamma^T, \Gamma^C) = (3 \cdot 10^6, 3 \cdot 10^6)$. They keep the system response numerically stable.

KERNEL WITHOUT DERIVATIVES

Figure 5.36 shows results for the time evolution of the temperature fields referring to ROMs with kernel K_0 having orders $(r^T, r^C) = (4, 4)$ (a), $(r^T, r^C) = (5, 5)$ (b) or $(r^T, r^C) = (6, 6)$ (c). The transient dynamical response is remarkably captured in all simulations in comparison to results of (ANA:a). Note that ROMs are constructed without a derivative representation in the kernel. However, maxima and minima values are better reproduced for setups with order $(r^T, r^C) = (5, 5)$ and higher. A better comparison can be given in terms of error results printed in Tab. 5.7. ROMs having order $(r^T, r^C) = (5, 5)$ and higher yield almost constant $\overline{RMSE} (\approx 0.003)$ and $\overline{CC} (\approx 0.9993)$. Only the maximum error varies. ROMs having order $(r^T, r^C) = (5, 5)$ sufficiently capture dynamics of the underlying FOM. Higher order derivatives, playing a dominant role in ROMs (ANA:a), are not necessarily needed for capturing the true dynamics.

5.4.7 PREDICTION CAPABILITIES: MEAN INCLUDED (ANA:B)

In contrast ROMs of excluded mean data (ANA:a), ROMs based on the complete data (ANA:b) yield accurate results saving time-consuming optimizations. For setups (ANA:b) an "optimal" ROM is referred to as consisting of

- $(r^T, r^C) = (5, 5)$,
- $(\Gamma^T, \Gamma^C) = (3 \cdot 10^6, 3 \cdot 10^6)$,
- $(\varepsilon_0, \varepsilon_1, \varepsilon_2) = (1, 0, 0)$,

This ROM has shown best performance in reconstruction of the FOM data. Note that this ROM yield similar or even better ME results in comparison to single, lumped or tensor POD approaches

Table 5.7.: Tubular Reactor Reduced Order Model Error Results for mean included.

(Γ^T, Γ^C)	(r^T, r^C)	ε_0	ε_1	ε_2	\overline{RMSE}	\overline{CC}	ME_T
$(3 \cdot 10^6, 3 \cdot 10^6)$	(4, 4)	1	0	0	0.0066	0.9977	0.1975
$(3 \cdot 10^6, 3 \cdot 10^6)$	(5, 5)	1	0	0	0.0031	0.9993	0.0710
$(3 \cdot 10^6, 3 \cdot 10^6)$	(6, 6)	1	0	0	0.0027	0.9993	0.0474

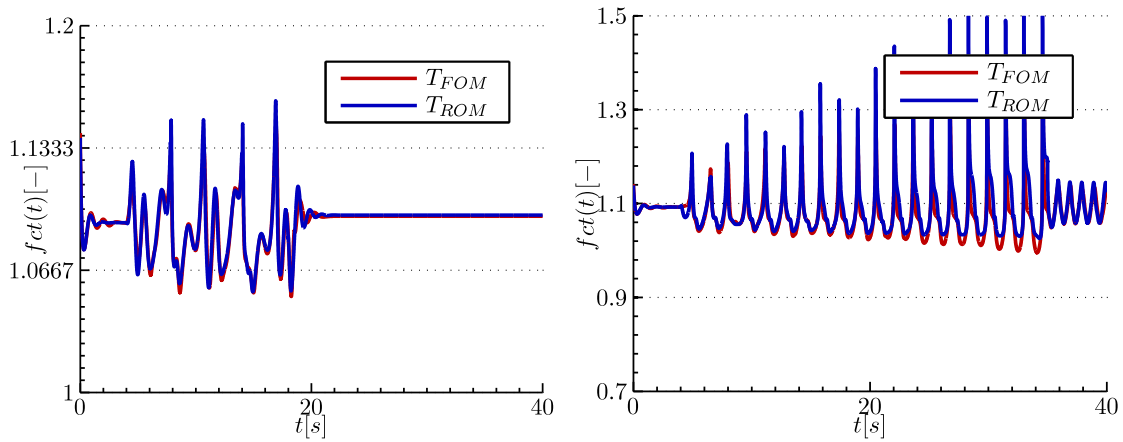


Figure 5.37.: Time Evolution of temperature at $x = 0.49$ for an optimal calibrated reduced order model. ROM predictions to setup (1) (left) and setup (2) (right) (umean included).

of [136]. In the following, this "optimal" TR-POD-ROM is exploited to study prediction capabilities setups already mentioned in Sec. 5.4.5. These setups are referred to as (1) and (2).

Figure 5.37 shows the time evolution of the temperature at mid position for setup (1) and setup (2). Global error results are listed in Table 5.8. The dynamics are well represented for both setups. In comparison to results of Sec. 5.4.5, the fundamental transient, being used for calibration, is also well-reproduced for setup (1). Further, the steady-state is now identically mapped. Error values underline these well-conditioned results in Tab. 5.8. All error results have same order as in the reconstruction. Setup (2) reproduces the perturbed dynamics of a system that is not represented in the data set. Dynamics fit to the original system, nevertheless peaks are sometimes over-predicted. Note that the achieved limit cycle at the end of the transient is now reproduced. The maximum error is reduced by approximately 50% in comparison to results of (ANA:a).

5.4.8 CONCLUSIONS

By the TR, a system featuring complex non-linear dynamics, different reduced ordering modeling strategies have been tested and compared with the goal to highlight the best strategy to find an "optimal" ROM. Validation and verification have been realized by comparing results to van Belzen et al. [136], having published results of an identical configuration. It was shown that the "optimal" ROM choice is comparable to results of [136].

Effects of certain weighted Sobolev inner product choices where illustrated and applied to ROMs, that are based on mean adjusted fluctuation fields. An optimization strategy has been presented yielding overall good results. Strategies including higher order derivatives have potential to better match the underlying FOM solution.

Comparing results to TR-POD-ROMs keeping the mean in the data set show a transient dynamical development that remarkable captures all details of the underlying data. Penalty parameters can

Table 5.8.: Tubular Reactor Reduced Order Model Prediction Error Results with mean included.

Setup	(Γ^T, Γ^C)	(r^T, r^C)	ε_0	ε_1	ε_2	\overline{RMSE}	\overline{CC}	ME_T
(1)	$(3 \cdot 10^6, 3 \cdot 10^6)$	(5,5)	1	0	0	0.0030	0.9992	0.1064
(2)	$(3 \cdot 10^6, 3 \cdot 10^6)$	(5,5)	1	0	0	0.0224	0.9830	0.6317

be chosen considerably higher than for adjusted data fields which influences the exactness of the compliance of boundary conditions. Note that these setups are not yet constructed with an optimal derivative representation in the kernel. Even better results might thus be attained.

Different stabilized ROMs are reviewed on the road to an optimal ROM. Questions regarding prediction capabilities underline that within an optimal methodology, the mean need to be included in the data set. If gradients still play a decisive roles, then a further optimization strategy of kernels, having various higher order terms, is needed.

6 TOWARDS BWR-APPLICATION

Dynamics of a boiling water reactor (BWR) are governed by a non-linear coupling of different physical disciplines, namely the thermal-hydraulics, neutronics, fuel dynamics and the recirculation loop. This chapter only focuses on elementary thermal-hydraulics. To this effect, a stability experiment of Solberg [130] is addressed who investigated thermally induced flow instabilities in a uniformly heated boiling channel. Various thermal-hydraulic calculations and experiments of authors such as Ishii, Saha and Zuber [59, 60, 115, 116] have chosen this experiment as adequate for comparison purposes. The dynamics of this experiment are of non-linear character. Given a distinct inlet sub-cooling and stepwise increasing the axially constant heat flux into the channel, an unstable density wave oscillation can be observed [98].

The hereby considered thermal-hydraulic equation system is the homogeneous equilibrium model (HEM) which assumes a disperse two-phase-mixture. Both phases move with the same velocity, i.e. the slip ratio equals one. They are moreover considered to be in thermodynamic equilibrium [126].

Regarding the applied methodology for attaining a reduced model, this system has been chosen for investigations demonstrating the advantages of the proper orthogonal decomposition (POD)-reduced order model (ROM) methodology compared to state-of-the-art model reduction applied in the BWR community, see Sec. 2. Although this system is physically rather simplistic and not the most sophisticated model to apply for BWR thermal-hydraulics, from a mathematical point of view it already consists of certain hurdles.

A mathematical derivation of the underlying thermal-hydraulic system is given in the following. The coolant flow will be characterized, the governing equations are introduced, constitutive equations for pressure losses due to friction and local devices like spacers or orifices are given. The final equation system will then be derived and representative non-dimensional parameters introduced.

The implementation of the underlying equation system is discussed afterwards. The spatial resolution is chosen such that eigenvalues (EVs) attained by COMSOL[®]'s eigenvalue solver are fully converged. The implementation is further verified by a comparison to experimental results of Solberg [130] within a linear stability map.

Based on one transient that passes through the boundary of this linear stability map, a POD based ROM is derived. Different proper orthogonal modes (POMs) based on a single variable expansion are discussed. It is further analyzed whether appropriate transients for POD based ROMs can robustly be chosen without defining a specific transient history. In contrast to systems, being chosen for validation and verification of the methodology, the HEM features a missing transport equation for the pressure variable. This necessitates a reformulation to derive the intended POD-based ROM. Continuity of mass is further achieved by a semi-implicit method for pressure linked equations (SIMPLE)-like iterative scheme. A HEM-POD-ROM is presented that represents main characteristics of the underlying transient.

6.1 THERMAL-HYDRAULIC SYSTEM

Physics are modeled by a thermal-hydraulic system, namely the homogeneous equilibrium model (HEM). The conservation equations are given by the mass, momentum and energy equation that are governing the flow of a coolant in a one-dimensional (1D) channel. The system is closed by an equation of the thermodynamic state which essential is a function depending on pressure and temperature or enthalpy. The fluid within the HEM is characterized by three independent variables and the state variable: Namely the pressure p , enthalpy h , mass flux G and density ρ .

From a physical point of view this system is rather simplistic, nevertheless from a mathematical point of view it consists certain hurdles. Three different partial differential equations (PDEs) govern this system. The mass equation is rewritten in terms of mass flux and a time-derivative with respect to pressure is missing. The amount of energy referring to pressure variation is negligible and hence pressure related terms, and in particular a time-derivative, are missing in the energy equation. On the one hand, the state equation is modeled by spline fitted data of the water steam table (WST) [139] as function of enthalpy, on the other hand the friction term is modeled as a function of enthalpy and mass flux [22, 51]. Further inlet and exit orifices have only regional influence [58]. Similar mathematical features certainly also emerge in more sophisticated thermal-hydraulic models.

The homogeneous equilibrium model (HEM) is derived in this section based on literature of [68, 93, 98]. The coolant flow will be characterized, the governing equations are introduced, constitutive equations for pressure losses due to friction and local devices like spacers or orifices are given for the mixture. The final equation system will then be derived and representative non-dimensional parameters introduced.

6.1.1 CHARACTERIZATION OF THE FLUID

MACROSCOPIC EFFECTS

Many types of instabilities are known that can contribute to unstable behavior of a fluid within a channel, see Sec. 2.2.1. For instance, fluctuations and oscillations within different flow regimes, transition pattern, or large scale fluctuations caused by density-wave oscillations (DWOs) or pressure-drop oscillations (PDOs). Only macroscopic phenomena instabilities are of interest and fluctuations of microscopic scale are neglected throughout this chapter, although they may also provide triggers for large scale instabilities.

1D APPROACH

Focusing on future stability analysis of a BWR, a 1D approach is justified on the basis of well-predicted stability limits by numerical calculations with 1D codes in comparison to three-dimensional (3D) computational fluid dynamics (CFD) codes. Complete fuel assemblies (FAs) can be treated as a 1D flow channel [68]. A further argument for a 1D approach is the high ratio to length scale within a BWR. Typically the axial height of a FA of a BWR is approximately about $4m$, by having hydraulic diameters of around $D_H \approx 5mm$.

DENSITY-WEIGHTED CROSS-SECTION AVERAGED QUANTITIES

All quantities used within this chapter are based either on density weighted cross-sectional averaged or the related Favre averaged [93] procedure. An arbitrary density-weighted cross-sectional averaged

quantity f , is defined according to

$$\tilde{f} := \frac{\overline{\rho f}}{\bar{\rho}},$$

and always denoted by a tilde \sim . An overlined variable, always indicated by $\overline{}$, symbolizes a cross-sectional averaged quantity referring to the cross-sectional flow area of a FA given by A_{x-s} :

$$\overline{\rho f} := \frac{1}{A_{x-s}} \iint_{A_{x-s}} (\rho f) dA_{x-s}.$$

In case of $f = 1$, the cross-sectional averaged density is given by:

$$\bar{\rho} := \frac{1}{A_{x-s}} \iint_{A_{x-s}} \rho dA_{x-s}.$$

At cross-sections of one FA, only **homogenized** profiles are assumed for quantities such as the fluid temperature, the static pressure and the velocity.

MACH NUMBER

The dimensionless Mach number relates the density-weighted cross-sectional averaged velocity \tilde{u} to the speed of sound u_s :

$$\text{Ma} = \frac{\tilde{u}}{u_s}.$$

For a BWR the speed of sound of water is given by the WST [139]. For the maximum designed temperatures of approximately $T = 286.4^\circ\text{C}$ till $T = 310^\circ\text{C}$, the speed of sound yields values of $\mathcal{O}(10^3)$. The density-weighted cross-sectional averaged velocity is given between $1 - 10\text{m/s}$. This results in Mach numbers of orders $\mathcal{O}(10^{-2}) - \mathcal{O}(10^{-3})$. The low Mach approximation [93] is therefore justified and the liquid phase is considered to be **incompressible** whereas the gas phase is treated compressible.

REYNOLDS NUMBER

The Reynolds number gives information about the flow pattern of a fluid. Based on the Reynolds number, laminar and turbulent flow can be distinguished. It is defined by:

$$\text{Re} = \frac{\tilde{u} D_H}{\nu},$$

and describes the ratio of inertial forces to viscous forces by the help of the hydraulic diameter D_H , the cross-sectional averaged kinematic viscosity ν and the density-weighted cross-sectional averaged velocity \tilde{u} . The hydraulic diameter is given by:

$$D_H = \frac{4A_{x-s}}{P_f},$$

where P_f denotes the wetted perimeter. For a BWR the density-weighted cross-sectional averaged velocity is expected to vary between $1 - 10\text{m/s}$, the hydraulic diameter is a small constant and the kinematic viscosity varies according the expected temperatures and is approximately $\mathcal{O}(10^{-7})$. This underlines that the expected flow is of **turbulent** character.

FROUDE NUMBER

The Froude number relates inertial forces to gravitational forces:

$$\text{Fr} = \frac{\text{inertial forces}}{\text{gravitational forces}} = \frac{\tilde{u}_{in}^2}{gL_H},$$

where L_H is the length of the heated flow channel, \tilde{u}_{in} is the inlet velocity of the fluid and g is the gravitational acceleration. The Froude number is expected to be greater than one at stationary conditions which indicates a **drifted flow** and perturbation stream in all directions.

PRANDTL NUMBER

The local Prandtl number relates momentum and thermal diffusivity:

$$\text{Pr} = \frac{\text{momentum diffusion rate}}{\text{thermal diffusion rate}} = \frac{\bar{c}_p \bar{\mu}}{\bar{\lambda}_{th}},$$

where c_p is the heat capacity at BWR pressure, μ is the dynamic viscosity and the thermal conductivity is given by λ_{th} . As the transport of momentum is defined by the velocity field and the heat transport is defined by the temperature fields, it relates both fields and is a measure of the ratio of thicknesses between flow and temperature boundary layers. Only **small Pr variation** is expected for a BWR.

6.1.2 FLUID PROPERTIES

As the conservation equations are under-determined, so-called state equations need to be introduced. A state equation relates two or more state functions like pressure, density, volume or enthalpy. It is a constitutive equation describing a thermodynamic equation under a given set of conditions. The used state equation that relates the specific volume v as function of pressure p and enthalpy h is given by:

$$v = v(p, h).$$

Material properties, like the dynamic viscosity denoted by μ , can also be determined as functions of pressure and enthalpy:

$$\mu = \mu(p, h).$$

$$v = \frac{\mu}{\rho} = \mu v.$$

Within normal system BWR pressure conditions only marginal fluctuations of the density can be observed and the low Mach approximation is valid. In case of transients, there is only a small pressure fluctuation from approximately 20 – 50 kPa and hence the dependency with respect to pressure can be neglected. Figure 6.1 illustrates state and material properties with respect to enthalpy and pressure. All quantities are included by data of the WST of the National Institute of Standards and Technology [139] within a enthalpy range of $h = 0 - 4.5 \cdot 10^6 \text{ J/kg}$ and for three pressure levels $p = \{6.9 \text{ MPa}, 7.0 \text{ MPa}, 7.1 \text{ MPa}\}$. The function representation is calculated by MATLAB[®]'s internal spline fit *pchip*. Only small variations with respect to pressure are visible. In the following, state and material equations are assumed to be given according to a defined system pressure, i.e.

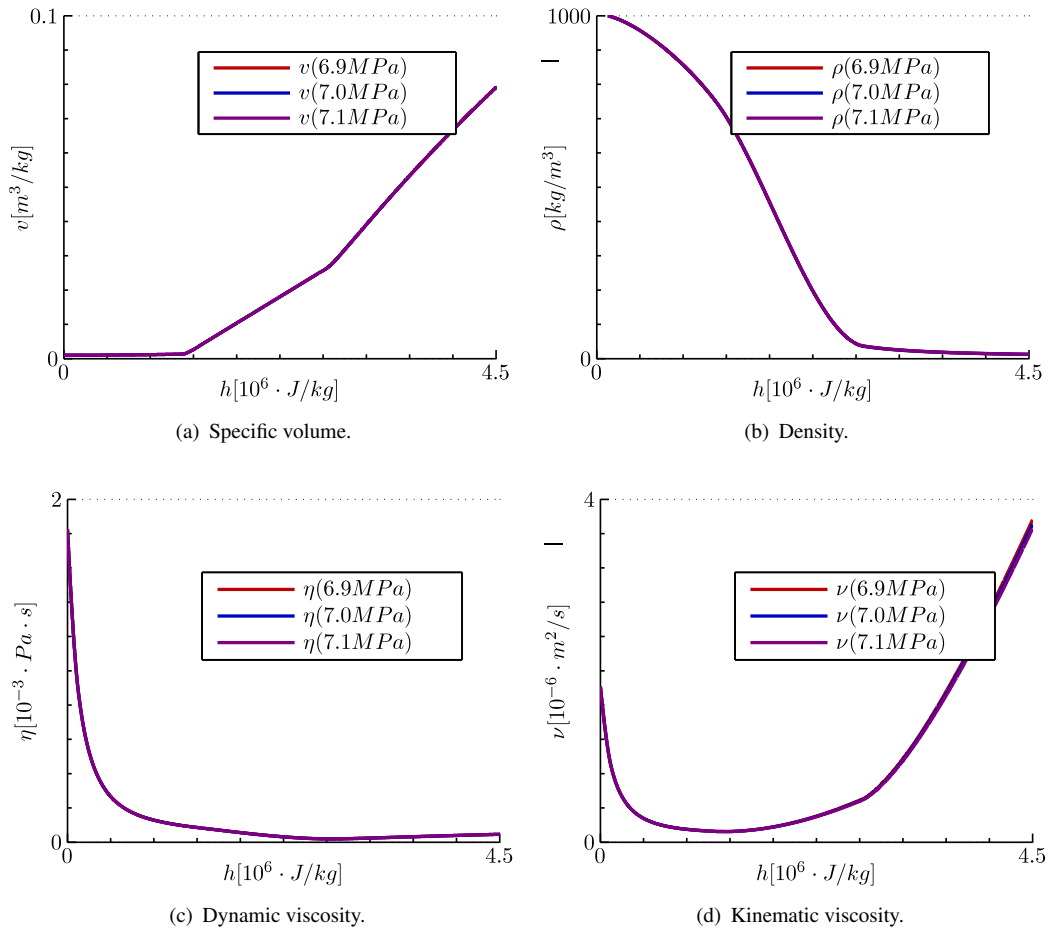


Figure 6.1.: Material properties with respect to enthalpy and pressure.

$p = const$:

$$v = v(h)_p, \quad (6.1a)$$

$$\mathbf{v} = \mathbf{v}(h)_p. \quad (6.1b)$$

6.1.3 DERIVATION OF THE EQUATION SYSTEM

The coolant flow is characterized by the governing equations of mass, momentum and energy. In the following, the derivation of the system is derived based on [93] and other technical literature.

AVERAGING PROCESS

Velocity components in x , y and z -directions are denoted by u, v, w . They can be separated into their density weighted cross-sectional averaged part and their local deviation:

$$u = \tilde{u} + u'', \quad (6.2a)$$

$$v = \tilde{v} + v'', \quad (6.2b)$$

$$w = \tilde{w} + w''. \quad (6.2c)$$

Density ρ and pressure p are expressed into cross-sectional weighted parts and their local deviation, marked by a single prime $'$:

$$\rho = \bar{\rho} + \rho', \quad (6.3a)$$

$$p = \bar{p} + p'. \quad (6.3b)$$

By Oertel et al. [93], it can be shown that following rules hold for quantities f and l :

$$\frac{\overline{\partial f}}{\partial s} = \frac{\partial \bar{f}}{\partial s}, \quad (6.4a)$$

$$\overline{f+l} = \bar{f} + \bar{l}, \quad (6.4b)$$

$$\overline{f'} = 0, \quad (6.4c)$$

$$\overline{\rho f''} = 0. \quad (6.4d)$$

MASS CONSERVATION

The temporal variation of mass within a control volume element equals the sum of inflow mass rate minus the sum of outflow mass rate:

$$\left[\begin{array}{c} \text{rate of} \\ \text{creation of} \\ \text{mass} \end{array} \right] \hat{=} \left[\begin{array}{c} \text{mass} \\ \text{outflow} \\ \text{rate} \end{array} \right] - \left[\begin{array}{c} \text{mass} \\ \text{inflow} \\ \text{rate} \end{array} \right] + \left[\begin{array}{c} \text{mass} \\ \text{storage} \\ \text{rate} \end{array} \right] = 0,$$

This balancing over in and out flowing mass rates leads to the conservation of mass:

$$\frac{\partial \rho}{\partial t} + \frac{\partial(\rho u)}{\partial x} + \frac{\partial(\rho v)}{\partial y} + \frac{\partial(\rho w)}{\partial z} = 0. \quad (6.5)$$

The density is given by ρ and the velocity components in x , y and z -direction are denoted by u, v, w . The mass conservation equation is transferred into cross-sectional averaged form by:

$$\frac{1}{A_{x-s}} \iint \left(\frac{\partial \rho}{\partial t} + \frac{\partial(\rho u)}{\partial x} + \frac{\partial(\rho v)}{\partial y} + \frac{\partial(\rho w)}{\partial z} \right) dA_{x-s} = 0.$$

Its compact notation is given by:

$$\overline{\frac{\partial \rho}{\partial t} + \frac{\partial(\rho u)}{\partial x} + \frac{\partial(\rho v)}{\partial y} + \frac{\partial(\rho w)}{\partial z}} = 0.$$

Applying definitions and rules of Eq.(6.2)-(6.4) leads to

$$\frac{\partial \bar{\rho}}{\partial t} + \sum_{i=1}^3 \frac{\partial \overline{\rho(\tilde{u}_i + u_i'')}}{\partial x_i} = 0$$

where the index i is related to the spatial coordinates and $u = u_1$, $v = u_2$ and $w = u_3$. Again using the defined rules of Eq.(6.4), this yields

$$\frac{\partial \bar{\rho}}{\partial t} + \sum_{i=1}^3 \frac{\partial \bar{\rho} \tilde{u}_i}{\partial x_i} = 0. \quad (6.6)$$

By assuming an expansion in x -direction only and neglecting expansions in y - and z -direction, components $i = 2$ and $i = 3$ in Eq.(6.6) yield vanishing values. The axial direction of vertical coolant

channels is hence only denoted by the x -direction.

The 1D mass conservation equation is hence given by

$$\frac{\partial \bar{\rho}}{\partial t} + \frac{\partial \bar{\rho} \tilde{u}}{\partial x} = 0.$$

As the cross-sectional averaged mass flux G is defined by

$$\bar{G} = \overline{\rho u} = \bar{\rho} \tilde{u},$$

a reformulation yields:

$$\frac{\partial \bar{\rho}}{\partial t} + \frac{\partial \bar{G}}{\partial x} = 0. \quad (6.7)$$

Moreover, the state-equation is given with respect to a defined system pressure:

$$\rho = \rho(h)_p, \quad p = \text{const.}$$

Employing the chain rule and inserting the relation between density and specific volume yields

$$\frac{\partial \bar{\rho}}{\partial t} = \frac{\partial \bar{\rho}}{\partial h} \frac{\partial h}{\partial t} = \frac{\partial^{1/v}}{\partial h} \frac{\partial h}{\partial t} = -\frac{1}{\bar{v}^2} \frac{\partial \bar{v}}{\partial h} \frac{\partial h}{\partial t},$$

which is included into Eq. (6.7). The 1D cross-sectional averaged mass equation is hence given by:

$$\frac{\partial \bar{h}}{\partial t} = \bar{v}^2 \frac{\partial \bar{G}}{\partial x} \left(\frac{\partial \bar{v}}{\partial \bar{h}} \right)^{-1}. \quad (6.8)$$

MOMENTUM CONSERVATION

The temporal change of momentum within a control volume equals the sum of outflow momentum rates, minus inflow momentum rates, plus the sum of momentum that is stored. This represents the sum of acting shear forces and normal stresses on the control volume [134]:

$$\left[\begin{array}{c} \text{rate of} \\ \text{creation of} \\ \text{momentum} \end{array} \right] \hat{=} \left[\begin{array}{c} \text{momentum} \\ \text{outflow} \\ \text{rate} \end{array} \right] - \left[\begin{array}{c} \text{momentum} \\ \text{inflow} \\ \text{rate} \end{array} \right] + \left[\begin{array}{c} \text{momentum} \\ \text{storage} \\ \text{rate} \end{array} \right] = \left[\begin{array}{c} \text{sum of forces} \\ \text{on the} \\ \text{control volume} \end{array} \right].$$

Assuming no spatial expansion in y - and z -direction, those momentum equations, formulated for y - and z -directions, can be neglected. The momentum equation, for the x -direction only, is given by:

$$\frac{\partial \rho u}{\partial t} + \frac{\partial (\rho u u)}{\partial x} + \frac{\partial (\rho u v)}{\partial y} + \frac{\partial (\rho u w)}{\partial z} = k_x - \frac{\partial p}{\partial x} + \frac{\partial \sigma_{xx}}{\partial x} + \frac{\tau_{xy}}{\partial y} + \frac{\partial \tau_{zx}}{\partial z}. \quad (6.9)$$

The volume force in x -direction (i.e gravitational, electrical or magnetical forces) is given by k_x . Newton's law of friction postulates a linear modeling approach between shear stresses τ and velocity gradients. Accordingly, shear stresses on x components are given by:

$$\tau_{yx} = \mu \left(\frac{\partial v}{\partial x} + \frac{\partial u}{\partial y} \right),$$

$$\tau_{zx} = \mu \left(\frac{\partial w}{\partial x} + \frac{\partial u}{\partial z} \right).$$

Normal stresses denoted by σ , referring to friction effects, are defined by:

$$\sigma_{xx} = 2\mu \frac{\partial u}{\partial x} - \frac{2}{3}\mu \left(\frac{\partial u}{\partial x} + \frac{\partial v}{\partial y} + \frac{\partial w}{\partial z} \right),$$

where μ denotes the dynamic viscosity. The pressure p is defined as:

$$\tau_{xx} = \sigma_{xx} - p.$$

Note that cross-sectional averaged τ_{xy} and τ_{xz} vanish. Moreover, due to rule Eq. (6.4), components in y - and z -direction also become zero:

$$\frac{\partial(\overline{\rho u u_i})}{\partial x_i} = \frac{\partial}{\partial x_i} \frac{1}{A_{x-s}} \iint_{A_{x-s}} (\rho u u_i) dA_{x-s} \equiv 0.$$

Again, lateral directions are denoted by $i = 2, 3$.

The cross-sectional averaged momentum Eq.(6.9) in x -direction hence yields:

$$\frac{\partial(\overline{\rho u})}{\partial t} + \frac{\partial(\overline{\rho u^2})}{\partial x} = \bar{k}_x - \frac{\partial \bar{p}}{\partial x} + \frac{\partial \overline{\sigma_{xx}}}{\partial x}. \quad (6.10)$$

Taking the second term of the left hand side and applying rules Eq. (6.2)-(6.3) yields:

$$\frac{\partial(\overline{\rho u^2})}{\partial x} = \frac{\partial(\overline{\rho(\tilde{u} + u'')^2})}{\partial x} = \frac{\partial}{\partial x}(\overline{\rho \tilde{u}^2}) + \frac{\partial}{\partial x}(\overline{\rho u''^2}) + \underbrace{(2\tilde{u}) \frac{\partial}{\partial x}(\overline{\rho u''}) + (2\overline{\rho u''}) \frac{\partial}{\partial x}(\tilde{u})}_{=0}.$$

The gravitational force is given by

$$\bar{k}_x = -g\bar{\rho} \sin \theta,$$

with vertical gravitational component g_{eff} :

$$g_{eff} = g \sin \theta.$$

Joining all ingredients together, the 1D cross-sectional averaged momentum equation is derived:

$$\frac{\partial(\overline{G})}{\partial t} + \frac{\partial(\overline{G^2/\bar{\rho}})}{\partial x} = -\bar{\rho} g_{eff} - \underbrace{\frac{\partial \bar{p}}{\partial x} + \frac{\partial \overline{\sigma_{xx}}}{\partial x} - \frac{\overline{\rho u''^2}}{\partial x}}_{\text{friction losses}}.$$

The last two terms refer to frictional losses that will be described in the following in addition to not yet mentioned local pressure losses.

FRICIONAL PRESSURE LOSSES

Within the homogeneous equilibrium model (HEM) the single- and the two-phase are assumed as an disperse mixture. Blended variables for the single-(mixture-)phase are solely available. However, frictional pressure in boiling channels is significant higher compared to single-phase channels. This can be explained by bubbles establishing at the heated surface, leading to an abruptly increase in surface roughness, and the increase of flow velocity. Standard approaches for modeling two-phase frictional losses are based on saturated liquid and a multiplying by an empirical correlation factor, the so-called two-phase multiplier. Modeling, of the mixture state-equation by WST data, inherently

includes a two-phase-multipliers-like behavior. It is similar to the functional form of the two-phase multiplier derived by the assumption of a homogeneous flow. Here, the increase of friction loss is solely modeled due to the increase in velocity.

The single-phase frictional head loss can be defined through the Darcy-Weisbach friction factor ξ [89]:

$$\frac{\partial \overline{\sigma_{xx}}}{\partial x} - \frac{\overline{\rho u'^2}}{\partial x} = \Delta p = -\frac{\xi}{2D_H} \frac{\overline{\rho} \bar{u}^2}{2} = -\frac{\xi}{2D_H} \frac{\bar{G}^2}{\bar{\rho}}.$$

Since the Moody's chart, various friction factor correlations have been derived. Colebrook derived an implicit form, combining experimental data of underlying laminar and turbulent circular pipe flow experiments [22]:

$$\frac{1}{\sqrt{\xi}} = -2 \log \left(\frac{\varepsilon}{3.7D_H} + \frac{2.51}{\text{Re} \sqrt{\xi}} \right).$$

Note, that this equation is developed for fully developed and isothermal flow. It relates the Reynolds number Re to the relative pipe roughness ε/D_H , where the mean height of the roughness of the underlying steel is denoted by ε . It is chosen to be 0.000035 throughout calculations in this chapter. Haaland proposed in 1983 an explicit approximation of the Darcy-Weisbach friction factor [51]:

$$\xi = \left(-1.8 \log \left(\left(\frac{\varepsilon}{3.7D_H} \right)^{1.11} + \left(\frac{6.9}{\text{Re}} \right) \right) \right)^{-0.5}.$$

Note that the Colebrook formula is developed for a single circular pipe but still yields reasonable results for rod bundles. For instance, a more accurate single-phase friction factor for rod bundles is available by Rehme [84].

LOCAL PRESSURE LOSSES

Pressure losses due to local flow obstructions at different axial point of interests (POIs) can be expressed by [58]:

$$\Delta p = -\delta(x = x_{poi}) K_{poi} \frac{1}{2} \bar{\rho} \bar{u}^2 = -\delta(x = x_{poi}) K_{poi} \frac{\bar{G}^2}{2\bar{\rho}},$$

with

$$\delta(x) = \begin{cases} 1 & , x = x_{poi}, \\ 0 & , \textit{else}. \end{cases}$$

The representative local loss coefficient for inlet and outlet orifices, as well as lower and upper tie plates, and spacers are denoted by K_{poi} . The spatial position of local losses is indicated by $x_{poi} = \{x_{in}, x_{out}, x_{spacer}, x_{uplate}, x_{lplate}\}$. Two-phase local pressure loss effects are inherently modeled by state-equations depending on enthalpy and hence on axial position.

MOMENTUM EQUATION WITH INSERTED PRESSURE LOSSES

Applying the relation between density and specific volume, the momentum equation with pressure losses due to friction, and an inlet and outlet orifice reads:

$$\frac{\partial(\bar{G})}{\partial t} + \frac{\partial(\bar{v}\bar{G}^2)}{\partial x} = -\frac{g_{eff}}{\bar{v}} - \frac{\partial\bar{p}}{\partial x} - \left(\frac{\xi}{D_H} + \delta(x=x_{in})K_{in} + \delta(x=x_{out})K_{out} \right) \frac{\bar{v}\bar{G}^2}{2}. \quad (6.11)$$

ENERGY EQUATION

The energy conservation equation is given by the composition of energy in a volume element based on temporal changes of inner and kinetic energies. Energy of a volume element can be changed by flow transport, heat conduction, work per time due to pressure, shear and normal stress forces, supplied energy and acting volume forces such as gravitation, electric and/or magnetic forces [92]:

$$\left[\begin{array}{c} \text{rate of} \\ \text{creation of} \\ \text{energy} \end{array} \right] \triangleq \left[\begin{array}{c} \text{energy} \\ \text{outflow} \\ \text{rate} \end{array} \right] - \left[\begin{array}{c} \text{energy} \\ \text{inflow} \\ \text{rate} \end{array} \right] + \left[\begin{array}{c} \text{energy} \\ \text{storage} \\ \text{rate} \end{array} \right] = 0.$$

The conservation equation for energy reads after balancing:

$$\rho \left(\frac{\partial h}{\partial t} + u \frac{\partial h}{\partial x} + v \frac{\partial h}{\partial y} + w \frac{\partial h}{\partial z} \right) = \left(\frac{\partial p}{\partial t} + u \frac{\partial p}{\partial x} + v \frac{\partial p}{\partial y} + w \frac{\partial p}{\partial z} \right) + \left(\frac{\partial}{\partial x} \left[\lambda_{th} \cdot \frac{\partial T}{\partial x} \right] + \frac{\partial}{\partial y} \left[\lambda_{th} \cdot \frac{\partial T}{\partial y} \right] + \frac{\partial}{\partial z} \left[\lambda_{th} \cdot \frac{\partial T}{\partial z} \right] \right) + \mu \phi,$$

where the enthalpy h is defined by

$$h = e + \frac{p}{\rho},$$

the temperature is denoted by T and the thermal heat conductivity is given by λ_{th} . Inner energy is denoted by e . Energy changes due to shear and normal stresses are combined in $\mu\phi$. Here, μ denotes the dynamic viscosity and ϕ represents the dissipation function:

$$\phi = 2 \left[\left(\frac{\partial u}{\partial x} \right)^2 + \left(\frac{\partial v}{\partial y} \right)^2 + \left(\frac{\partial w}{\partial z} \right)^2 \right] + \left(\frac{\partial v}{\partial x} + \frac{\partial u}{\partial y} \right)^2 + \left(\frac{\partial w}{\partial y} + \frac{\partial v}{\partial z} \right)^2 + \left(\frac{\partial u}{\partial z} + \frac{\partial w}{\partial x} \right)^2 - \frac{2}{3} \left(\frac{\partial u}{\partial x} + \frac{\partial v}{\partial y} + \frac{\partial w}{\partial z} \right)^2.$$

No energy is considered due to radiation or combustion, hence $\rho\dot{q}_s$ yields vanishing value, just like energy due to acting volume forces.

Following the averaging procedures in the derivations of mass and momentum equations, the 1D cross-sectional averaged energy equation reads:

$$\rho \frac{\partial \bar{h}}{\partial t} + \rho u \frac{\partial \bar{h}}{\partial x} = \frac{q'' P_H}{A_{x-s}} + \frac{\partial}{\partial x} \left[\lambda_{th} \cdot \frac{\partial T}{\partial x} \right].$$

The equation contains a number of simplifications. The heat transfer due to the pressure is negligible compared to nuclear energy heat input:

$$\overline{\left(\frac{\partial p}{\partial t} + u \frac{\partial p}{\partial x} + v \frac{\partial p}{\partial y} + w \frac{\partial p}{\partial z}\right)} \approx 0.$$

Thermal energy, generated due to dissipation $\mu\phi$, has no practical relevance and is hence omitted. Further, radial heat conduction, in y - and z -directions, is combined into one quantity:

$$\frac{q'' P_H}{A_{x-s}} = \frac{\partial}{\partial y} \left[\lambda_{th} \cdot \frac{\partial T}{\partial y} \right] + \frac{\partial}{\partial z} \left[\lambda_{th} \cdot \frac{\partial T}{\partial z} \right].$$

Applying rules, stated in Eq.(6.2)-(6.4), moreover yields

$$\bar{\rho} \frac{\partial \tilde{h}}{\partial t} + \bar{\rho} \tilde{u} \frac{\partial \tilde{h}}{\partial x} = \frac{q'' P_H}{A_{x-s}} + \underbrace{\frac{\partial}{\partial x} \left[\lambda_{th} \cdot \frac{\partial T}{\partial x} \right] - \rho u'' \frac{\partial h''}{\partial x}}_{\text{heat transfer in } x\text{-direction}}.$$

The last two terms are regarded as heat transfer in x -direction. As the wall of a FA is thin, the heat conductivity is high and approximately independent of temperature [68]. The heat transfer is dominated by the heat transfer through the cladding and the convective part. Accordingly,

$$\frac{\partial}{\partial x} \left[\lambda_{th} \cdot \frac{\partial T}{\partial x} \right] - \rho u'' \frac{\partial h''}{\partial x} \approx 0.$$

Applying the relation between density and specific volume, the derived 1D cross-sectional averaged energy equation reads

$$\frac{\partial \tilde{h}}{\partial t} + \bar{G} \tilde{v} \frac{\partial \tilde{h}}{\partial x} = \bar{v} \frac{q'' P_H}{A_{x-s}}. \quad (6.12)$$

THERMAL-HYDRAULIC EQUATION SYSTEM

Within this chapter all flow and state-variables are given by cross-sectional averaged quantities. For reasons of simplification overbars and overtilde are dropped in the following. The derived thermal-hydraulic equation system is summarized in the following:

Mass conservation equation:

$$\boxed{\frac{\partial h}{\partial t} = v^2 \frac{\partial G}{\partial x} \left(\frac{\partial v}{\partial h} \right)^{-1}}. \quad (6.13a)$$

Momentum conservation equation:

$$\boxed{\frac{\partial G}{\partial t} + \frac{\partial (vG^2)}{\partial x} = -\frac{g_{eff}}{v} - \frac{\partial p}{\partial x} - \left(\frac{\xi}{D_H} + \delta(x = x_{in})K_{in} + \delta(x = x_{out})K_{out} \right) \frac{vG^2}{2}}. \quad (6.13b)$$

Energy conservation equation:

$$\boxed{\frac{\partial h}{\partial t} + Gv \frac{\partial h}{\partial x} = v \frac{q'' P_H}{A_{x-s}}}. \quad (6.13c)$$

State equation:

$$\boxed{v = v(h)_p}. \quad (6.13d)$$

6.1.4 NON-DIMENSIONAL GROUPS

In general, stability characteristics of a BWR can be quantified by several non-dimensional groups [68]. The capability of model predictions in comparison to plant conditions can be illustrated by three classes of variables [27]: Those that directly quantify stability and safety margins (at a reactor level) such as average power range monitor (APRM) or local power range monitor (LPRM) signals; quantities that can allow comparing to measurements such as pressure and velocity distributions; and those suitable for physical representation of the system such as the slip ratio and heat transfer coefficients among others.

The physical representation of simplified BWR descriptions consists of single- or multi-boiling-channel setups. Their operation are specified by various, usually predefined parameters: the fluid properties, the channel geometry (i.e. length, hydraulic diameter, heated perimeter, frictional and pressure drop characteristics), the system pressure and the axial heat input distribution [98].

Dimensionless groups help to reduce the number of independent parameters. Stability characterizing quantities based on scaled models simplify the comparison between experiment and simulation. Only non-dimensional quantities related to stability are mentioned in this subsection. By assuming a uniform power profile \bar{q}'' , a distinct inlet velocity \tilde{u}_{in} and an inlet sub-cooling Δh_{SUB} , following dimensional groups can be stated [98] that are relevant within this chapter:

- The already introduced Froude number (see Sec. 6.1.1) relates inertial to gravitational forces:

$$Fr = \frac{\tilde{u}_{in}^2}{gL_H}.$$

- The Euler number, or so-called friction number Λ_{EU} , is a measure for friction losses through components:

$$\Lambda_{EU} = \frac{\xi L_H}{2D_H}.$$

- The phase-change number (NPCH) ensures that a phase change has progressed equally in two systems [59]. If the number is not equal, both systems are subject to different dynamics. It is given by the specific volume ratio $(v_g - v_f)/v_f$ to the latent heat $h_g - h_f$ multiplied by the ratio of power $\bar{q}'' P_H L_H$ to reduced velocity in the flow channels GA_{x-s} :

$$NPCH = \frac{v_g - v_f}{v_f(h_g - h_f)} \frac{\bar{q}'' P_H L_H}{GA_{x-s}}.$$

Here, specific volumes and enthalpy of saturated liquid and steam are denoted by indices f and g . The axial heat flux is given by \bar{q}'' , G denotes the mass flux, P_H the heated perimeter and A_{x-s} the cross-sectional flow area.

- The sub-boiling number (NSUB) defines the rate of sub-cooling of the fluid at the inlet Δh_{SUB} to the latent heat $(h_g - h_f)$, weighted by the specific volume ratio $(v_g - v_f)/v_f$:

$$NSUB = \frac{v_g - v_f}{v_f(h_g - h_f)} \Delta h_{SUB}.$$

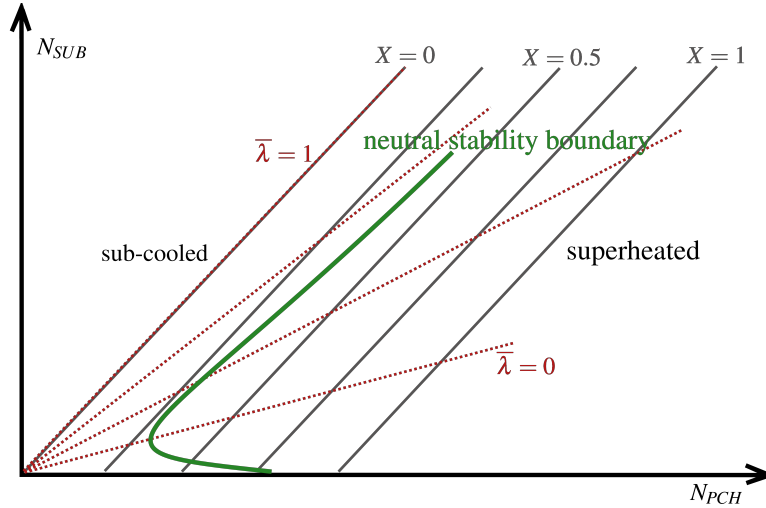


Figure 6.2.: Scheme of an Ishii-Zuber-stability map, redraw of [27, 59, 98, 112].

The inlet sub-cooling is defined by the inlet enthalpy h_{in} :

$$\Delta h_{SUB} = h_f - h_{in}.$$

Within this chapter, stability maps are always based on the sub-boiling number (NSUB)-phase-change number (NPCH) plane. It is a classical two-dimensional (2D) map for single channel thermal-hydraulic instabilities [27]. Ishii introduced first those dimensionless variables within his PhD thesis [60] (see also [59, 116]). Accordingly, this stability map is also called Ishii-Zuber-stability-plane. Ortega Gómez used a similar plane for supercritical equivalent formulations for two hydraulically identical coupled channels [98].

The basic characteristics of the stability plane are illustrated in Fig. 6.2 which is based on [27, 59, 98, 112]. Constant quality lines are indicated in black. The first bisectrix (i.e. quality $X = 0$) indicates an operation where the boiling boundary is reached at the exit. Before, there is only sub-cooled liquid at the exit. Parallel constant quality lines indicate a boiling boundary within the channel and vapor at the exit ($0 < X < 1$). The quality increases until there is saturated steam ($X = 1$) at the exit. Above, the iso-quality line for saturated steam ($X = 1$) there is superheated vapor. Neutral stability boundary curves (green) can be derived by linear theory. It separates linear stable from unstable operation conditions. The neutral stability boundary for DWOs lies between the iso-quality lines. It has asymptotic behavior to constant quality for high NSUB and a trend to bigger NPCH for moderate sub-cooling [98]. Moreover, lines of constant boiling boundary positions (dashed, red) are given by

$$\bar{\lambda} = \frac{\lambda}{L_H}.$$

6.2 IMPLEMENTATION AND VERIFICATION

Validation against experimental data of the implemented HEM model within COMSOL[®] is based on a DWO stability experiment of Solberg [59, 130]. This step is essential since the proceeding ROM-POD analysis consists of snapshots calculated by time-domain calculations. Reliable statements

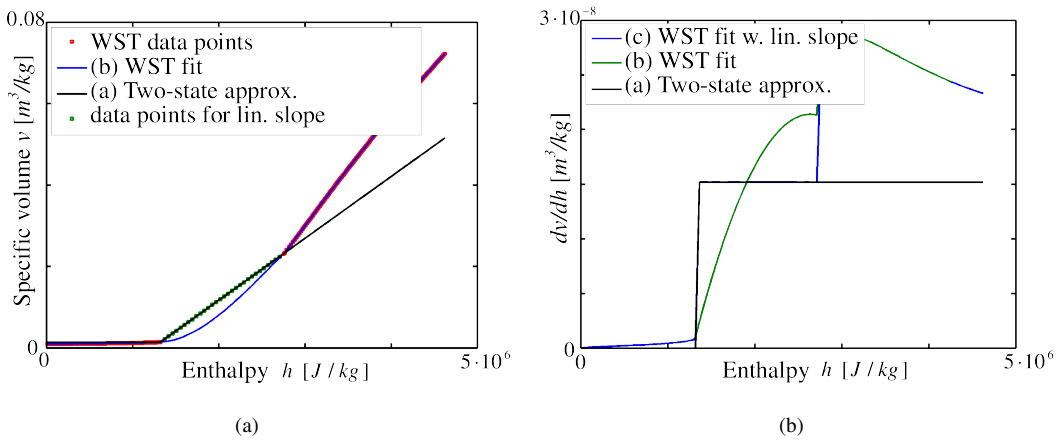


Figure 6.3.: Comparison of state equation approximations: (a) specific volume, (b) derivative of specific volume with respect to enthalpy.

of the reduced system strongly depends on the underlying data. This section considers the model implementation and its validation by means of a linear stability analysis derived in [102]. Validation aims at reproducing the experimentally derived stability behavior.

6.2.1 SOLBERG EXPERIMENT

Experimental studies of thermally induced flow instabilities in a uniformly heated boiling channel has been studied by Solberg [130]. For a given inlet temperature the essentially uniform heat flux into the flow channel was increased in small steps until sustainable flow instabilities could be observed. Waiting a sufficiently long time period reveals the true character of this response: either oscillatory or of steady-state.

The two-phase system is studied at $p = 80 \text{ atm}$. A 1D calculation is performed representing the vertical round tube in the experiment. The length of the channel is $L = 2.90 \text{ m}$ and its diameter is given by $D_h = 0.00525 \text{ m}$. It consists of an inlet and outlet exit orifice with pressure loss coefficients of $K_{in} = 17.8$ and $K_{out} = 0.03$. A parallel channel boundary condition is applied by assuming a constant pressure drop of $\Delta p = p_{loss} = 47.8 \text{ kPa}$ [98]. The flow Reynolds number is given by $Re_{fs} = 4.78 \cdot 10^4$ and permits conclusions regarding the inlet velocity u_{in} and hence the inlet mass flux G_{in} . The friction factor is calculated by the Darcy-Weisbach friction correlation and is doubled according to [59] to account for two-phase losses. The mean height of the roughness of the underlying steel is given by $\varepsilon = 0.000035$. Three different formulations of the state equation are tested in the following:

- (a) a two-state formulation,
- (b) an approximation based on cubic spline fitted WST data only,
- (c) an approximation based on cubic spline fitted WST data with a linear slope assumption.

Figure 6.3 illustrates the state functions and its derivatives with respect to enthalpy. Note the region between saturated liquid and vapor enthalpy. High deviations are notable for spline fitted data without considering an additional linear slope. If enthalpy rises above saturated vapor enthalpy h_g an approximation, based on spline fitted WST data with a linear slope assumption, gives best results.

6.2.2 IMPLEMENTATION

According to [98], a fast convergence of the momentum Eq. (6.13b) is realized by a transformation of fast changing components into the boundary condition. A dynamic pressure p_d is defined which

is given by the sum of the static pressure p and the dynamic head G^2v :

$$p_d = p + G^2v.$$

Moreover, terms related to local pressure losses are substituted into the boundary conditions:

$$\begin{aligned} 0 &= -p + p_{in} + G^2v_{in} + 1/2K_{in}G^2v_{in}, \\ 0 &= -p + p_{in} - p_{loss} + G^2v_{in} + 1/2K_{out}G^2v_{in}, \end{aligned}$$

where the enforced constant pressure drop of the channel is given by p_{loss} .

The momentum conservation equation is hence given by

$$\boxed{\frac{\partial G}{\partial t} = -\frac{g_{eff}}{v} - \frac{\partial p_d}{\partial x} - \frac{\xi}{D_H} \frac{vG^2}{2}}. \quad (6.14)$$

The setup is subject to a given distinct inlet enthalpy h_{in} . The spatial resolution is chosen such that EVs, attained by COMSOL[®]'s eigenvalue solver, are fully converged. This results in a chosen mesh size of $x_h = 0.0145$ at maximum. Also Ortega Gómez [98] applied mesh sizes in the same range. The momentum equation is solved by shape functions that are one order smaller than those for mass and energy conservation (order five). Fluid properties are given by WST data of the national institute of standards and technology [139]. Spline fits consisting of at least 100 control points give their algebraic forms. Different formulations are tested, particularly noteworthy is the spline fit with a linear slope between saturated fluid and steam enthalpy.

6.2.3 VALIDATION

Figure 6.4 illustrates the results of the linear stability analysis of the HEM where the phase-change number (NPCH) is plotted against the sub-boiling number (NSUB). The computed two-dimensional stability plane is compared to experimental unstable data points (green) that have been derived by stability tests of Solberg. For a certain inlet sub-cooling the heat flux was continuously increased until an unstable oscillation has been observed. The investigation of the HEM with a two-state formulation (black) of specific volume is satisfactory describing the experiment of Solberg. Employing the state-equation based on spline fitted WST data (red), yields large deviations from experimental data.

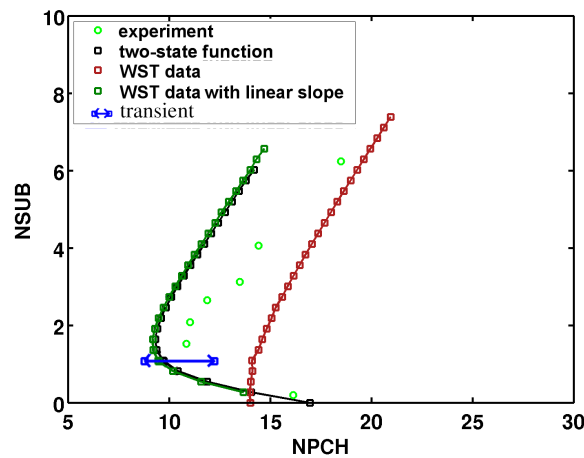


Figure 6.4.: Comparison of linear neutral stability boundaries predicted by the HEM model for equation of state (a)-(c) and investigated transient line (blue).

The error is accounted to the under- and overestimation of specific volume in the two-phase region (see Fig. 6.3). Investigations using a linear slope assumption (dark green) gives satisfying results. The impact of higher specific volume (beyond saturated vapor enthalpy) on the stability boundary can be neglected. Ortega Gómez [98] remarked that two-step state equations for supercritical water based reactors lead to over restricting operation conditions.

Keeping track on a general methodology applicable to various system setups, within this chapter, a spline fitted state equation is complemented by a linear slope assumption. This assumption diminishes for a super critical setups. It is moreover applied within the later derived POD based ROM.

6.3 APPLICATION OF THE POD-ROM METHODOLOGY

Based on the implemented and adjusted homogeneous equilibrium model (HEM) model, the validation experiment of Solberg (Sec. 6.2), and a suitable transient choice, its proper orthogonal decomposition (POD)-reduced order model (ROM) is derived in this section. Focus is put on the distinct steps of the POD-ROMing strategy to derive a suitable reduced version of the thermal-hydraulic system.

Since the methodology is mostly automated, the most essential input provided by an expert user is the choice of transients. This section starts by illustrating a selection of transients which cross the linear stability boundary. Moreover, questions concerning a suitable snapshot basis are treated, as well as further issues regarding how appropriate transients for POD based ROMs can robustly be chosen. Having a reliable reduced basis, a further hurdle is given by the missing transport equation for the pressure variable. It is taken by a reformulation of the underlying HEM equation system. The pressure equation is then given by a Poisson equation. Finally, by including boundary conditions with an appropriate choice of penalty parameters, the POD based ROM is derived.

6.3.1 PERTURBATION OF A LINEAR STABLE OPERATION POINT

Let us consider a linear stable operation point (*) of the HEM with an inlet sub-cooling of $\Delta h = 10^5 J/kg$ and a net heat input of $\dot{Q} = 9000W$. A POD analysis of a stationary operation point would identify precisely this fixed spatial distribution as POM of most importance for each system variable. The POD eigenspectra to each system variable would reveal negligible contribution of additional modes to this state. POD's strength is to reveal coherent structures to a given data set. Hence, analyzing a stationary operation point with the ROM-POD methodology gives insufficient information about system dynamics. This implies investigations with respect to a distinct time-varying transient.

Corresponding parameter values of four transient choices are pictured by the blue line in Fig. 6.4. Note that all power excursions start after 3 seconds. The analyzed transients are:

- (A1) A power excursion of (*) with $\Delta Q = 2000W$ and returning to the initial power after 0.5s.
- (A2) A power excursion of (*) with $\Delta Q = 2000W$ and returning to the initial power after 2.0s.
- (B1) A power excursion of (*) with $\Delta Q = 1000W$ and returning to the initial power after 2.0s.
- (B2) A power excursion of (*) with $\Delta Q = 1000W$.

Figures 6.5-6.8 depict the temporal mass flux evolution due to these power excursions at distinct positions within the channel. As all transients cross the linear stability boundary, oscillating behavior is developed following the power excursion. Corresponding full order model (FOM) data has been generated on the basis of the calibrated HEM model of Sec. 6.2 using a non-linear fully coupled implicit solver routine of COMSOL®.

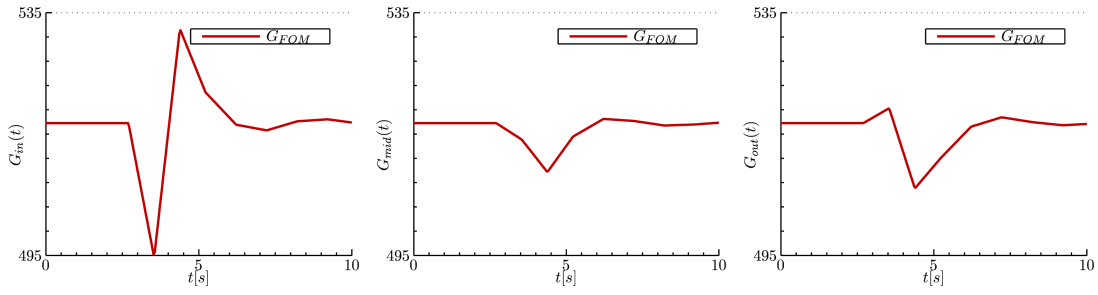


Figure 6.5.: Transient (A1): Time evolution of the mass flux (FOM): (a) inlet, (b) mid position and (c) outlet.

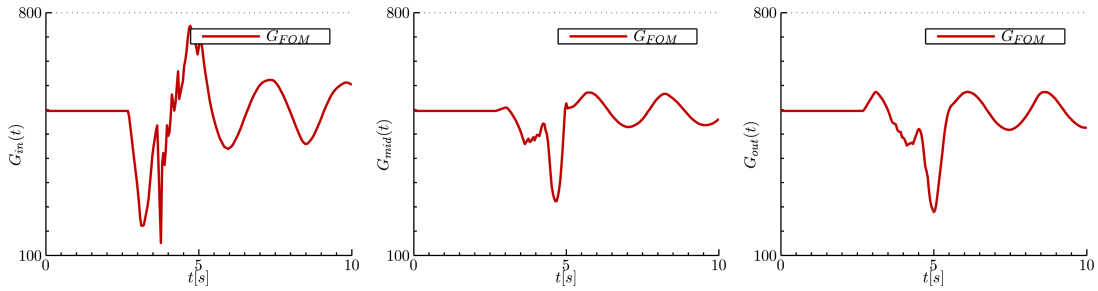


Figure 6.6.: Transient (A2): Time evolution of the mass flux (FOM): (a) inlet, (b) mid position and (c) outlet.

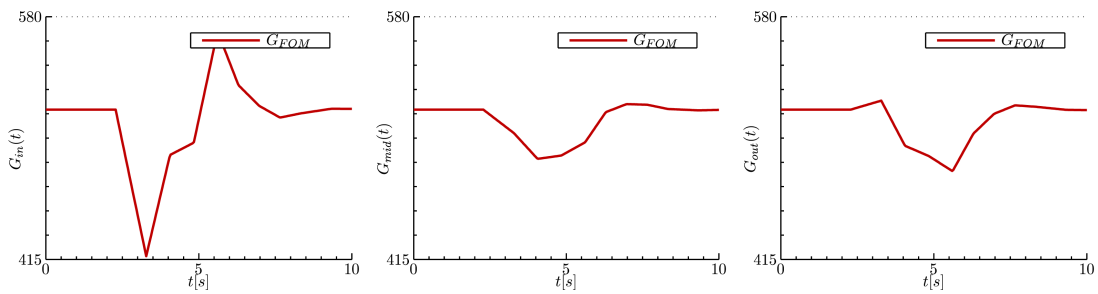


Figure 6.7.: Transient (B1): Time evolution of the mass flux (FOM): (a) inlet, (b) mid position and (c) outlet.

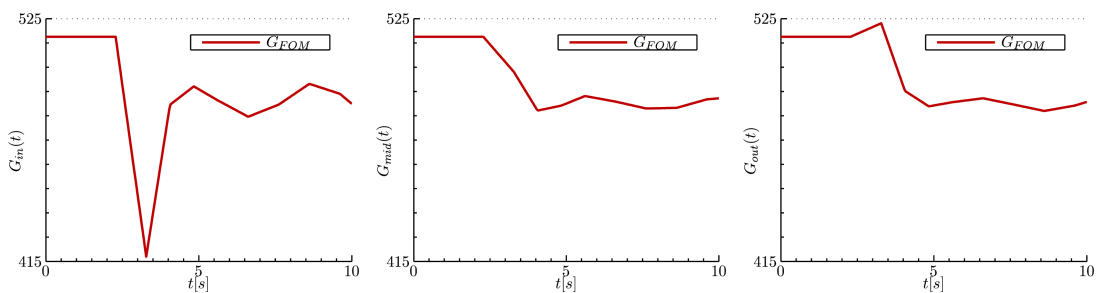


Figure 6.8.: Transient (B2): Time evolution of the mass flux (FOM): (a) inlet, (b) mid position and (c) outlet.

The system response is highly sensitive regarding the type of perturbation. Although transient (A1) yields the same heat input level after perturbation as compared to (A2), the duration of the pulsed disturbance has impact on the generation of a limit cycle. Note that only the transient (A2) is subject to a self-contained limit cycle. Keeping the energy level at a high value after perturbation leads to a small limit cycle in case of transient (B2). In contrast, the transient (B1) gets back to the steady-state.

This investigation implies that underlying FOM data is highly sensitive against the defined transient. It reveals that an expert choice of transient is mandatory. As the POD is a completely data-dependent

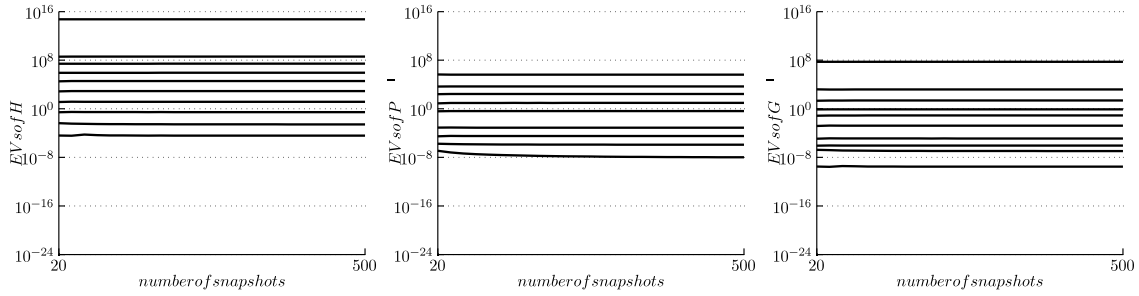


Figure 6.9.: Convergence plot of the first ten eigenvalues of the enthalpy, pressure and mass flux fields as a function of the number of snapshots.

method, this has impact on POM shape.

6.3.2 SNAPSHOT BASIS

By the experience of the tubular reactor (TR), highly accurate ROMs are achieved by non-mean-adjusted snapshot fields. Higher-order derivative information within the kernel yields an even more accurate result. Nevertheless, as this section mainly focuses on the strategy to derive the HEM-ROM, small inaccuracy is accepted by treating non-mean-adjusted snapshot fields and kernels consist of data that are not constructed using derivatives, i.e. K_0 with $\varepsilon_0 = 1$.

Spatial grids within the ROM remain well resolved and identical chosen for all setups to be $x_h = 0.0145$, see [98]. The number of snapshots, necessary for attaining the correlation matrix, is not a priori known. For this purpose, different ensemble of snapshots, i.e. for enthalpy, pressure and mass flux fields, are recorded by an exemplary transient (A1) for a duration of $t \in [0, 10s]$. Convergence plots of the dominant EVs are presented in Fig. 6.9.

No significant variation indicates that relevant transient dynamics are not hidden between the time steps and fine-scale information is captured. The figure underlines that grid-independent eigenvalue spectra are achieved by only a small amount of snapshots (which differs in comparison to experiments of Chapter 5). A snapshot basis of approximately 250 is sufficient for fully resolving long-wave phenomena. Hence, the time step size is fixed to $t_h = 0.04s$ such that for each oscillation in the transient response of the system, multiple snapshots are recorded. This step size is applied throughout this section. Note that different transient choices, i.e. transients (A2), (B1) and (B2) for instance, lead to the same conclusion (which is not shown here).

6.3.3 COMPARISON OF OSCILLATION MODES

Figures 6.10 and 6.11 illustrate the dominant proper orthogonal EVs on a semi-logarithmic scale and the first three POMs for the two transients (B1) and (B2). The truncation criteria is indicated in the corresponding eigenspectra labels. Moreover, Tab. 6.1 visualizes the numerical values of energies referring to enthalpy, pressure and mass flux spectra for the first ten POMs. For all eigenspectra, a rapidly decreasing impact of EVs can be seen. An extremely high chosen reconstruction level of 99.99999% yields a reduction level suggestion less or equal to five for a corresponding ROM-POD. Note that decent results might be obtained by a lower number of modes. The non-linear dynamics of the HEM can be described by a superposition of a very small number of POMs where the methodology is based on a single variable expansion. This yields ROMs with a slightly higher number of degrees of freedom in comparison to a coupled variable approach [101] but still an overall small ROM is attained. Specifically, the number of needed modes is 4 for h , 1 for P and 5 for the variable G for transient (B1) and, accordingly, $G = 4$ for transient (B2). One explanation for this

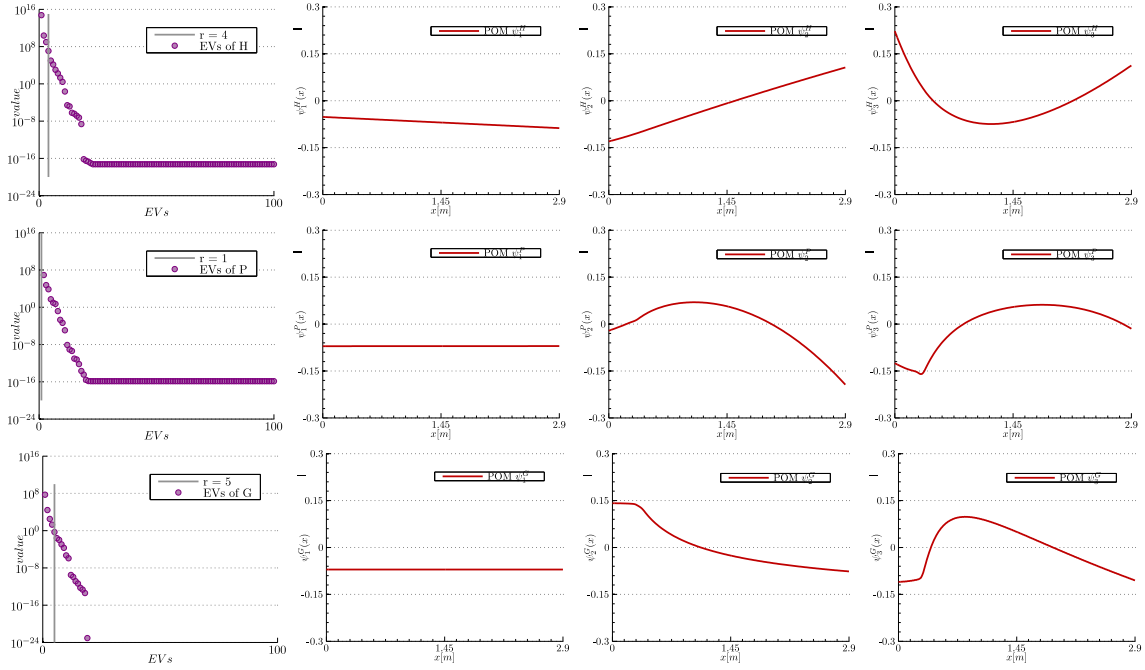


Figure 6.10.: Eigenspectra of enthalpy (1st row), pressure (2nd row) and mass flux (3rd row) on a semi-logarithmic scale with inserted reduction level and three dominant proper orthogonal modes: transient (B1).

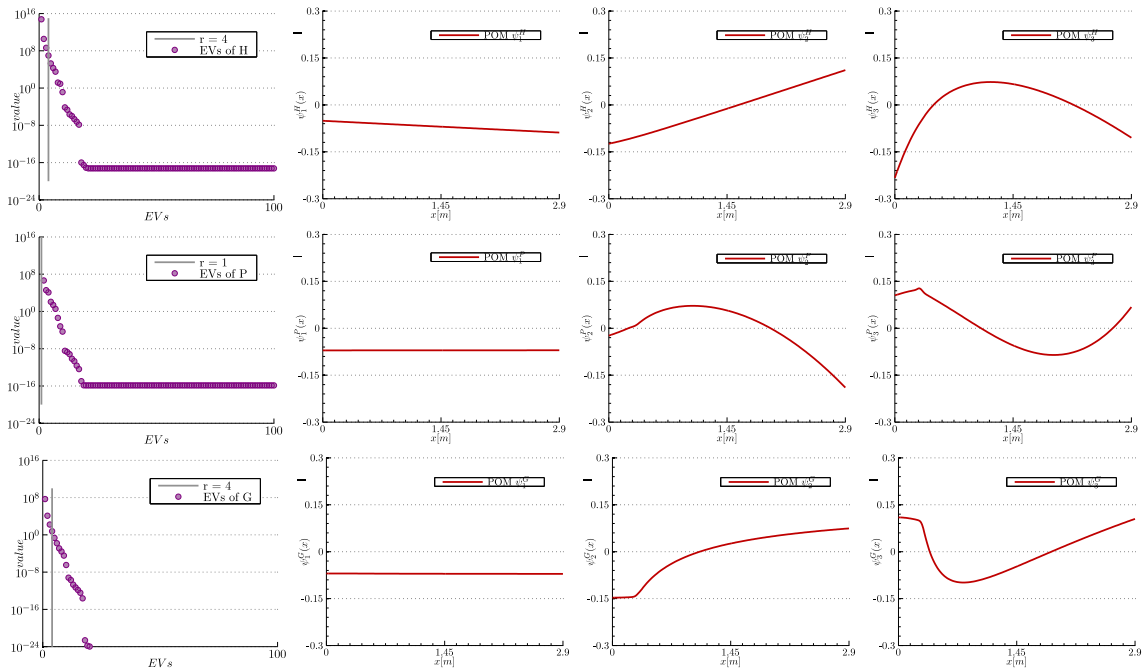


Figure 6.11.: Eigenspectra of enthalpy (1st row), pressure (2nd row) and mass flux (3rd row) on a semi-logarithmic scale with inserted reduction level and three dominant proper orthogonal modes: transient (B2).

Table 6.1.: Total kinetic energies in the first ten proper orthogonal modes for enthalpy, pressure and mass flux fields: transient (B1) and (B2).

i	transient (B1)			transient (B2)		
	$K_0 \%E_{kin}^H$	$K_0 \%E_{kin}^P$	$K_0 \%E_{kin}^G$	$K_0 \%E_{kin}^H$	$K_0 \%E_{kin}^P$	$K_0 \%E_{kin}^G$
1	99.9955088419680	99.9999999353999	99.9480316009672	99.9936641562539	99.9999999658792	99.9735176247214
2	99.9998277419670	99.999999994987	99.9993395374976	99.9999218371644	99.999999996301	99.9996598279342
3	99.9999978666134	99.999999999429	99.9999618169553	99.9999982937581	99.999999999068	99.9999873977040
4	99.9999999795152	99.999999999995	99.9999989814338	99.9999999631681	99.999999999989	99.9999995119912
5	99.999999971915	99.999999999999	99.999999294858	99.999999959510	99.999999999998	99.999999640442
6	99.99999997756	100.000000000000	99.999999775217	99.999999994188	100.000000000000	99.999999968507
7	99.99999999638	100.000000000000	99.999999974454	99.999999999959	100.000000000000	99.999999993940
8	99.99999999957	100.000000000000	99.999999996014	99.999999999985	100.000000000000	99.999999999274
9	99.99999999995	100.000000000000	99.999999999885	100.000000000000	100.000000000000	99.999999999993
10	100.000000000000	100.000000000000	99.999999999977	100.000000000000	100.000000000000	100.000000000000

could be the spatial course of pressure across the channel that is only slightly affected by the heat perturbation. In contrast, enthalpy and mass flux change heavily during perturbation. Accordingly, the difference can be explained by the pronounced impact of oscillations on mass flux and enthalpy due to two-phase phenomena.

Note that the number of modes for transients (A1) and (A2) (not shown) increases for h and G since both transients penetrate deeper into the linear unstable region.

The two different transients (B1) and (B2) yield nearly identical number of modes. Note that (B1) and (B2) only differ in the duration of the power excursion while possessing identical extreme states. Corresponding modes in Figs. 6.10 and 6.11 show similar qualitative properties. Note that in some cases the sign of modes is inverted (e.g. second POM for P) while exhibiting similar shape. As POMs build the basis for the ROM, both would be capable to achieve the same dynamics as the fundamentals are identical. This demonstrates the robustness against details of otherwise similar transients. Analogous to modes from conventional EV analysis, higher modes correspond to higher frequencies so that a larger number of extrema is found.

This investigation demonstrates that details of the transient, such as duration, have minor effects on the POMs. It can be assumed that to some extent, the POD basis is insensitive regarding the input data. This suggests that appropriate transients for POD based ROMs can robustly be chosen without defining a specific transient history as the ROMs contain almost identical number of modes.

In the following, all simulation results are based on FOM data attained by transient (B2).

6.3.4 A REFORMULATION OF THE HEM

The HEM is characterized by a transport equation for mass flux and enthalpy respectively and a still missing transport equation for the pressure variable. As POMs are orthogonal to each other, a natural choice of projection is given by mapping the momentum equation onto mass flux modes which yields the time evolution of mass flux in a spectral sense. In exactly the same manner, the projection of the energy equation onto enthalpy modes describes the evolution of enthalpy, also in a spectral sense. Considering the remaining projection of the mass conservation equation onto pressure modes, the resulting pressure field should be mass conserving. However, the time evolution is only indirectly given by the enthalpy dependence in the state variable and a pressure variable is missing. Enthalpy and pressure modes, within a single variable expansion, are not orthogonal. This actually results in small driving forces for systems with a low number of pressure modes which violate the requirements of mass conservation. This hurdle is taken by a reformulation of the underlying HEM equation system and is outlined below.

Taking the spatial derivative of the momentum Eq. (6.14) that have been implemented in COMSOL[®],

$$\frac{\partial}{\partial x} \left(\frac{\partial G}{\partial t} + \frac{g_{eff}}{v} + \frac{\partial p_d}{\partial x} + \frac{\xi}{D_H} \frac{vG^2}{2} \right) = 0,$$

interchanging the time and space derivative of the mass flux,

$$\frac{\partial}{\partial t} \left(\frac{\partial G}{\partial x} \right) + \frac{\partial}{\partial x} \left(\frac{g_{eff}}{v} + \frac{\partial p_d}{\partial x} + \frac{\xi}{D_H} \frac{vG^2}{2} \right) = 0,$$

and applying the mass conservation Eq. (6.13a) leads to a Poisson formulation of the pressure equation:

$$\frac{\partial^2 p_d}{\partial x^2} + \underbrace{\frac{\partial}{\partial t} \left(\frac{\partial v / \partial h}{v^2} \frac{\partial h}{\partial t} \right)}_{(*)} + \underbrace{\frac{\partial}{\partial x} \left(\frac{g_{eff}}{v} + \frac{\xi}{D_H} \frac{vG^2}{2} \right)}_{(**)} = 0. \quad (6.15)$$

This transport equation now includes the pressure variable and includes the formulation of mass conservation. Mathematical terms of (*) and (**) are well-known. However, taking the time derivative of (*) leads to an inefficient formulation as all terms directly depend on enthalpy,

$$\frac{\partial}{\partial t} \left(\frac{\partial v}{\partial h} \frac{1}{v^2} \frac{\partial h}{\partial t} \right) = \frac{\partial^2 h}{\partial t^2} \left(\frac{1}{v^2} \frac{\partial v}{\partial h} \right) + \left(\frac{\partial h}{\partial t} \right)^2 \left(\frac{\partial^2 v}{\partial h^2} \frac{1}{v^2} - 2 \left(\frac{\partial v}{\partial h} \right)^2 \frac{1}{v^3} \right),$$

and especially $\partial^2 v / \partial h^2$ is not given. This problem can be dealt with a non-physical pressure equation but also with an auxiliary equation for $(\partial h / \partial t) \cdot (\partial v / \partial h / v^2)$ which is not focused here. Appendix C outlines the latter approach.

NON-PHYSICAL PRESSURE EQUATION:

A non-physical-based pressure equation can be established but necessitates a SIMPLE-like iterative pressure correction scheme [99]:

$$\frac{\partial^2 p_d}{\partial x^2} - \chi \cdot error + \frac{\partial}{\partial x} \left(\frac{g_{eff}}{v} + \frac{\xi}{D_H} \frac{vG^2}{2} \right) = 0, \quad (6.16a)$$

$$\text{where } error := \frac{\partial G}{\partial x} - \frac{\partial h}{\partial t} \frac{\partial v / \partial h}{v^2}. \quad (6.16b)$$

The correction of the mass error is defined by χ . The pressure correction is based on the mass conservation error: A positive *error*, corresponding to a local mass source, requires a positive $\partial^2 p / \partial x^2$ which tends to drive the flow towards the mass source. As the mass equation is only approximately fulfilled within each time-step, an iterative scheme is necessary. The speed of convergence depends on χ .

On the one hand, achieving a mass conserving pressure field requires iterations and hence additional costs. However, in general only a few iterations are sufficient. On the other hand, this method benefits of a non-physical pressure equation that has simple structure which obviously saves costs.

REFORMULATED HEM

The POD-based ROM consists of the pressure formulation of Eq. (6.16), the momentum equation Eq. (6.14), the derived energy Eq. (6.13c) and a state formulation based on cubic spline fitted WST

data with a linear slope assumption (see Sec. 6.2.1). In the following, the d within the dynamic pressure p_d is dropped for convenience:

$$\begin{aligned} \frac{\partial h}{\partial t} + Gv \frac{\partial h}{\partial x} - v \frac{q'' P_H}{A_{x-s}} &= 0, & (6.17a) \\ \frac{\partial G}{\partial t} + \frac{g_{eff}}{v} + \frac{\partial p}{\partial x} + \frac{\xi}{D_H} \frac{vG^2}{2} &= 0, & (6.17b) \\ \frac{\partial^2 p}{\partial x^2} - \chi \cdot error + \frac{\partial}{\partial x} \left(\frac{g_{eff}}{v} + \frac{\xi}{D_H} \frac{vG^2}{2} \right) &= 0, & (6.17c) \end{aligned}$$

where $v = v(h)_p$.

Note that inlet and outlet local pressure losses as well as the convection term are substituted into the boundary condition. The model is subject to the following boundary conditions at inlet and outlet:

$$\begin{cases} p|_{x=0} = p_{in} + G^2v + 1/2K_{in}G^2v, \\ p|_{x=L} = p_{in} - p_{loss} + G^2v + 1/2K_{out}G^2v, \\ h|_{x=0} = h_{in}. \end{cases} \quad (6.18)$$

6.3.5 HEM-POD-ROM SYSTEM

This subsection outlines the derived ROM of the HEM. The boundary conditions given by Eq. (6.18) are imposed in the HEM-ROM version of Eq. (6.17) by a penalty formulation. Five constraints are formulated with the help of five penalty parameters ($\Gamma_{in}^h, \Gamma_{in}^p, \Gamma_{out}^p, \Gamma_{in}^G, \Gamma_{out}^G$) representing the inlet enthalpy, inlet and outlet pressure as well as deduced inlet and outlet mass flux boundaries. A penalty amplified weak formulation is applied as the mean mode is kept varying. Diffusion terms are in the projection replaced by their equivalent integration by parts formulation where their boundary parts are amplified by a penalty parameter. Penalty parameters are chosen such that exactness of the compliance of boundary conditions is guaranteed. This keeps the system response numerically stable.

$$\begin{aligned} \frac{\partial h}{\partial t} + Gv \frac{\partial h}{\partial x} - v \frac{q'' P_H}{A_{x-s}} - \Gamma^h (h - h_{in}) \delta|_{x=0} &= 0, & (6.19a) \\ \frac{\partial G}{\partial t} + \frac{g_{eff}}{v} + \frac{\partial p}{\partial x} + \frac{\xi}{D_H} \frac{vG^2}{2} & & \\ - \Gamma^G \left(G - ((p - p_{in})/v(1 + 1/2K_{in}))^{0.5} \right) \delta|_{x=0} & & \\ - \Gamma^G \left(G - ((p - p_{in} + p_{loss})/v(1 + 1/2K_{out}))^{0.5} \right) \delta|_{x=L} &= 0, & (6.19b) \\ \frac{\partial^2 p}{\partial x^2} - \chi \cdot error + \frac{\partial}{\partial x} \left(\frac{g_{eff}}{v} + \frac{\xi}{D_H} \frac{vG^2}{2} \right) & & \\ - \Gamma_{in}^p (p - p_{in} - G^2v - 1/2K_{in}G^2v) \delta|_{x=0} & & \\ - \Gamma_{in}^p (p - p_{in} + p_{loss} - G^2v - 1/2K_{out}G^2v) \delta|_{x=L} &= 0, & (6.19c) \end{aligned}$$

where $v = v(h)_p$.

Approximations of the variables h , G and p are given by a superposition of the temporal variation of their POMs:

$$\begin{aligned} h_{ROM} &= \sum_{i=1}^{r^h} \alpha_i^h \phi_i^h, \\ G_{ROM} &= \sum_{i=1}^{r^G} \alpha_i^G \phi_i^G, \\ p_{ROM} &= \sum_{i=1}^{r^p} \alpha_i^p \phi_i^p. \end{aligned}$$

Insertion of these approximations into Eq. (6.19) and a Galerkin projection leads to a fully-coupled non-linear ordinary differential equation (ODE) system, the so-called HEM-POD-ROM. Note that the mass conservation equation is projected onto pressure modes, the momentum equation is mapped onto mass flux modes and the energy equation onto enthalpy modes:

$$\left\langle \frac{\partial h_{ROM}}{\partial t} + G_{ROM} v(h_{ROM}) \frac{\partial h_{ROM}}{\partial x} - v(h_{ROM}) \frac{q'' P_H}{A_{x-s}} - \Gamma^h (h_{ROM} - h_{in}) \delta \Big|_{x=0}, \phi_j^h \right\rangle = 0, \quad j = 1, \dots, r^h \quad (6.20a)$$

$$\left\langle \frac{\partial G_{ROM}}{\partial t} + \frac{g_{eff}}{v(h_{ROM})} + \frac{\partial p_{ROM}}{\partial x} + \frac{\xi(h_{ROM}, G_{ROM}) v(h_{ROM}) G_{ROM}^2}{2 D_H} - \Gamma^G \left(G_{ROM} - ((p_{ROM} - p_{in}) / v(h_{ROM})^{(1+1/2K_{in})})^{0.5} \right) \delta \Big|_{x=0} - \Gamma^G \left(G_{ROM} - ((p_{ROM} - p_{in} + p_{loss}) / v(h_{ROM})^{(1+1/2K_{out})})^{0.5} \right) \right\rangle = 0, \quad j = 1, \dots, r^G \quad (6.20b)$$

$$\left\langle \frac{\partial^2 p_{ROM}}{\partial x^2} - \chi \cdot error + \frac{\partial}{\partial x} \left(\frac{g_{eff}}{v(h_{ROM})} + \frac{\xi(h_{ROM}, G_{ROM}) v(h_{ROM}) G_{ROM}^2}{2 D_H} \right) - \Gamma_{in}^p (p_{ROM} - p_{in} - G_{ROM}^2 v(h_{ROM}) - 1/2 K_{in} G_{ROM}^2 v(h_{ROM})) \delta \Big|_{x=0} - \Gamma_{in}^p (p_{ROM} - p_{in} + p_{loss} - G_{ROM}^2 v(h_{ROM}) - 1/2 K_{out} G_{ROM}^2 v(h_{ROM})) \delta \Big|_{x=L} \right\rangle = 0, \quad j = 1, \dots, r^p \quad (6.20c)$$

where $v = v(h)_p$.

For reasons of simplification the derived system is here only given without removing of offline costs. The HEM-POD-ROM is solved within MATLAB[®] by ODE15I, an ODE multistep solver for fully implicit differential equations of variable ODE order.

6.3.6 RESULTS

Results illustrated within this section underline that the fundamentals of the POD-ROM methodology can be applied to achieve drastically reduced versions of a thermal-hydraulic system while keeping main characteristics. Regarding the HEM in the formulation with a non-physical pressure equation, a finely-tuned pressure correction scheme is required. Note, that solver strategies applied to the FOM problem need to be used to solve the ROM.

The pressure correction scheme, applied for attaining upcoming results, is an extremely simplified routine and can only be used for demonstration purposes at this stage. Pressure correction is realized

by a distinct choice of pressure correction weight χ . It acts on the pressure field by sensing the mass error. As this scheme is coupled to an iterative ODE routine, the mass flux is only corrected in the consecutive time step. Results are achieved by a pressure correction weight of $\chi = 11.5$.

Penalty parameters are chosen such that the impact of the boundary conditions are guaranteed. Note that constraints have been included into the equation system, thus the system order of a small system is not blown up. Due to the simple pressure correction scheme, exactness cannot be guaranteed at this stage but can in general be fulfilled for more sophisticated iterative schemes. Within calculations the system response is kept numerically stable by the parameter values of $(\Gamma_{in}^h, \Gamma_{in}^p, \Gamma_{out}^p, \Gamma_{in}^G, \Gamma_{out}^G) = (2.9 \cdot 10^5, 10^2, 3.5 \cdot 10^4, 1, 1)$.

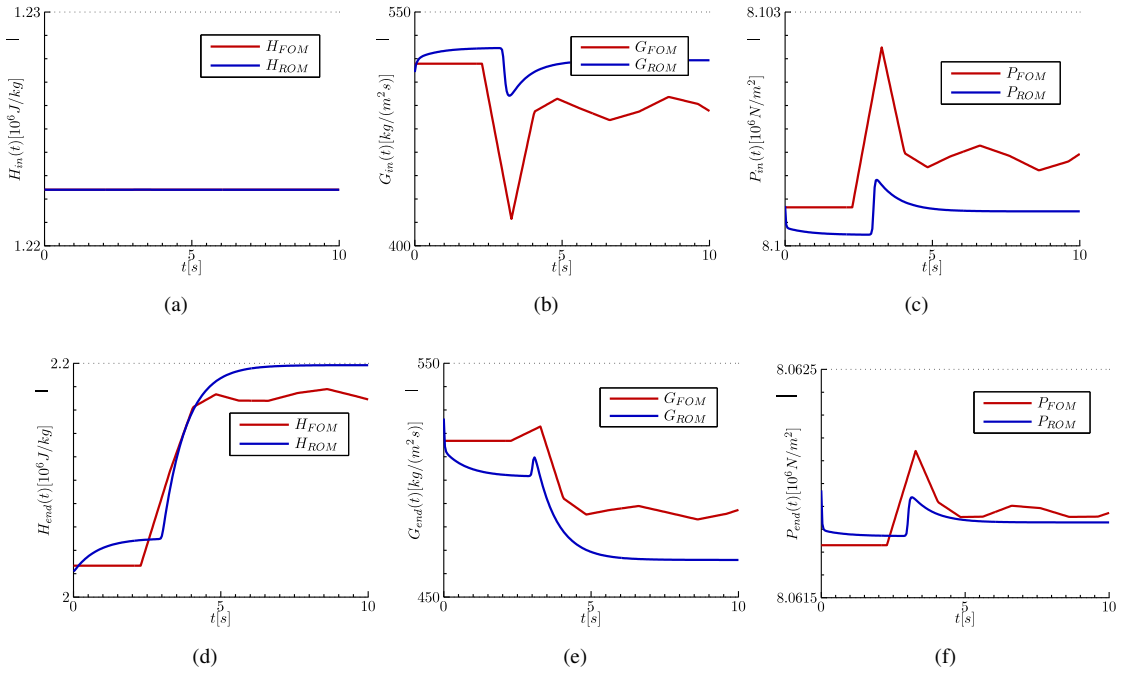


Figure 6.12.: Transient (B2): Comparison of the temporal evolution of the enthalpy, mass flux, and pressure (FOM versus ROM): inlet (first row), outlet (second row).

Fig. 6.12 shows results for the temporal evolution of the three different fields of the HEM: enthalpy, mass flux and pressure. It compares FOM against ROM results at the inlet (first row) and outlet (second row) of the heating channel. Note, that the ROM only consists of a kernel choice of K_0 . Moreover, based on a reconstruction level of 99.999% the order for the ROM-POD is suggested to be less or equal to two. Accordingly, the ROM has order $(r^h, r^p, r^G) = (2, 2, 2)$, i.e. an order of overall 6 degrees of freedom. In comparison, the FOM consists of 200 finite elements of order 5 and 4 resulting in 2803 degrees of freedom.

The simulation fails to capture the correct temporal evolution. This is not surprising as the HEM system is a strongly non-linear coupled system, and even small deviations of one single variable provoke a mismatch in other variables and vice versa. The simple structure of the pressure correction scheme contributes to these results. A mass conserving system can not be justified and the mass flux always notices a slightly wrong pressure. Nevertheless, due to the iterative ODE scheme this error is small. Note, that the temporal trends of all three variables within the perturbation are represented well.

In particular, the penalty parameter for the inlet enthalpy is of high value such that the boundary condition is fulfilled. This issue is represented in Fig. 6.12(a). The mismatch at the outlet, presented

in Fig. 6.12(d), is due to by the error in mass flux G .

The same is true for the feedbacks and interactions between mass flux and pressure evolutions illustrated in Fig. 6.12(b,c,e,f). It is not expected that the peak values in the perturbation can be represented by this minimal system. However, even this simple ROM represents main features such as the decrease of the mass flux or increase of the pressure within the perturbation. A drift is seen in the first part of the transient for pressure as well as mass flux. This is due to the simple pressure iteration scheme.

6.3.7 DISCUSSION

It has been shown that the HEM system needs a reformulation due to a missing transport equation for pressure. The attained pressure equation needs to be treated by a pressure correction scheme. First results with a simple correction scheme have been shown and discussed.

The POD based ROM of the HEM can be shown to describe the underlying transient characteristics in good agreement. An analysis reveals that a deviation can mostly be addressed to the simple pressure correction scheme. A more sophisticated scheme would surely avoid the mass drift and ensure mass conservation. Nevertheless, still one additional parameter needs constantly to be adjusted, namely the pressure correction weight χ . Appendix C outlines how a pressure correction scheme can be avoided by introducing an auxiliary equation.

Having introduced the correct pressure correction scheme or a precise formulation based on an auxiliary equation, the mass can be conserved in a spectral sense within each time step. Further studies regarding the order of the HEM-POD-ROM can then be pursued.

7 CONCLUSIONS AND RECOMMENDATION FOR FUTURE WORK

In the present thesis, a general and self-contained non-linear model order reduction (MOR) methodology has been derived which is based on a systematic procedure. It is applicable for several classes of dynamical problems, and in particular to boiling water reactors (BWRs).

Expert knowledge defines its fundamentals and can be given either by operational, experimental or numerical transient data. The methodology is mostly automated and provides the framework for the reduction of various different systems of any level of complexity. It efficiently couples sophisticated commercial software packages COMSOL[®], MATLAB[®] and MATHEMATICA[®]. For any system, only little effort is necessary to attain a reduced version within this self-written code developed by the author. The methodology reduces a complex system in a grid-free manner to a small system able to capture even non-linear dynamics. It is based on an optimal choice of basis functions given by the so-called proper orthogonal decomposition (POD). The resulting system can be deployed in the non-linear regime, which allows insight into the physical mechanisms behind complex dynamical behavior, for instance using bifurcation tools.

In summary, this thesis contains the following major contributions:

- The framework of an automated and general non-linear MOR methodology based on POD provided by a self-written code structure.
- Its adaptability to any system's degree of detail with limited effort.
- Its flexibility of exchanging distinct components within this framework, for instance the choice of basis functions.

The BWR system is marked by various involving physical disciplines. It is subject to thermally induced two-phase flow instabilities due to the boiling process. High-power low-flow conditions in connection with unfavorable power distributions can drive the BWR system into unstable regions where power oscillations can be triggered. This important threat to operational safety requires careful analysis for proper understanding. BWR's oscillating behavior is addressed by operating companies and vendors, as well as scientific institutions. In general, oscillating behavior is avoided by design and additional appropriate operating precepts based on time-domain or frequency-domain codes. Nevertheless, depending on the level of regarded BWR details, time-domain codes can be rather time-consuming procedures. Moreover, frequency-domain codes reduce the analysis complexity enormously. The scientific community hence has recently focused on low-dimensional simplified reduced BWR models that allow fast computation and where the stability character can be studied by bifurcation analysis tools. This allows additional insight into stability mechanisms.

Presently within reactor dynamics, no general and automatic predictions of high-dimensional reduced order models (ROMs) based on detailed BWR models are available. This thesis is the very first work on a general and systematic MOR technique within the scope of BWR systems. It can be applied to BWR models of any degree of details, is completely adjustable and yields BWR-ROMs of a prescribed accuracy goal.

As a very first step in this thesis, transient data is produced by an implementation of an equation system within the commercial software COMSOL[®]. Further, they are checked to be independent of the defined grid. A major advantage is that solutions can fully be derived using MATLAB[®] routines. An implementation can hence be validated by self-written code that creates linear stability maps. Regarding the MOR methodology, the POD has been identified as an optimal decomposition method within the applied spectral approach. POD projections converge faster than any other spatial or temporal basis with the same number of modes. The POD-ROM methodology is automated by a coupling to a MATHEMATICA[®] script that derives the analytical reformulation of any system. Required steps to achieve reliable and numerical stable ROMs are given by a distinct calibration road-map. Proper orthogonal modes (POMs) are selected based on grid-independent eigenspectra which guarantee fully resolved long-wave phenomena. In general, single variable expansions of fields are applied. For time-dependent systems, the mean flow plays an important role and is considered in the decomposition and reconstruction. Due to the truncation, in general, energy dissipation mechanisms and long-term stability are getting lost. Within this thesis, long-term stabilization is derived by a penalty formulation of boundary parameters. Moreover, energy dissipation mechanisms can artificially be imposed by another inner product choice leading to a calibration of the POMs.

Within the scope of the envisioned BWR-POD-ROM for stability analysis, a wide spectrum of verification and qualification examples has been explored. A Kortweg-de-Vries (KdV)-POD-ROM has been derived due to involved non-linearities and dispersive terms. Instationary transition between two different regions has been treated by a generic two-zone model. A ROM of a natural convection loop has been considered due to its dynamical similarities to BWRs. ROMs of the tubular reactor (TR), that includes Arrhenius reaction and heat losses, have been shown to represent the system's sensitive response on transient boundary conditions. All derived ROMs have in common that a small number of modes are sufficient to represent their dynamics. Examples show that the principal systematic procedure within the methodology is sufficiently mature to be applied for BWR systems. In particular, the methodology is shown to be capable of handling time-varying interfaces separating regions. Moreover, non-linear dynamics up to deterministic chaos are predicted in agreement with experimental results for a distinct range of validity. Oscillating phenomena caused by external conditions are shown to yield overall good results. Problems, including time-varying interfaces separating regions of different physics, need well-defined topological mappings.

Moreover, this thesis covers a first mandatory step towards a BWR-POD-ROM focusing on elementary thermal-hydraulics described by the homogeneous equilibrium model (HEM). This setup already consists of certain important hurdles. For instance, the state equation is modeled as a cubic spline function depending on enthalpy, the friction term is a highly non-linear function, local pressure losses have been modeled by a Dirac delta function and further it features a missing transport equation for the pressure variable. Within its derived POD-ROM, the latter is overcome by a reformulation of the underlying homogeneous equilibrium model (HEM) equation system. It is then treated by a simple pressure correction scheme. The POD based ROM of the HEM can be shown to describe the underlying transient characteristics in good agreement. A mismatch can mostly be addressed to the premature pressure correction scheme. This highlights that problems arising for the detailed simulation are also reflected in the reduced version. In particular, solver know-how from detailed simulations needs to be transferred to simulations of their ROMs.

This mostly automated non-linear methodology for deriving ROMs can be used in the near future with the goal to attain a BWR-ROM and stability analysis in the complete non-linear parameter space. This necessarily implies following further steps:

- To describe the non-linear stability behavior of the two-phase flow within a fuel assembly (FA) of a BWR, the derived thermal-hydraulic ROM needs to be extended to a more sophisticated thermal-hydraulic system. Additional reliable heat transfer and neutronics models need to be considered.

-
- Sophisticated physical and geometrical information, like the impact of grid spacers, should be included.
 - Regarding the complex stability behavior of a BWR, multiple FA connected via a plenum should be considered.
 - A recirculation loop finally needs to be considered.

The model needs further qualification, for example based on KATHY (multi-function thermal-hydraulic test loop in Karlstein) measurements or via a code-to-code comparison to TOBI (time domain analysis of BWR instability).

However, even more sophisticated models might be regarded using the POD-ROM-methodology. Models might also include three-dimensional (3D) non-linear phenomena. For instance, a grid-free pool model of future Gen-IV reactors using POD based ROMs [110]. Coupling between natural convection and heat transfer in large pool type reactors may result in strongly non-linear dynamical responses. Safety considerations require maintaining a minimal flow rate in any transient situation to provide core cooling. State-of-the-art (SOTA) analysis of the 3D non-linear behavior requires numerical integration with detailed models. Due to the high level of numerical costs, these computational fluid dynamics (CFD) simulations must be restricted to representative cases which holds a risk of missing critical cases. Reduced-order-modeling of convective pool flow regimes based on decomposition methods can be used as an alternative to conventional CFD.

Regarding a BWR application this implies that models not necessarily need to be based on one-dimensional (1D) formulations. For instance, the neutron diffusion equation, modeling the neutron population within a BWR, can be considered on a two-dimensional (2D) or even 3D geometry. This enables to include higher dimensional non-linear phenomena and allows utilizing measurements directly given by real BWR transients.

A IMPLEMENTATION OF THE DYNAMIC MODE DECOMPOSITION

The following explains the implementation of the dynamic mode decomposition (DMD) within MATLAB[®] and is based on [18, 133].

Assume that for a distinct problem, n snapshots $\{v_i, i = 1, \dots, n\}$ at equidistantly chosen time instances are given. The temporal grid size is chosen to be Δt . This ensemble of snapshots can be combined in the so-called snapshot matrix $X = [v_1, \dots, v_n]$ which is divided into two parts for forming two matrices:

$$\begin{aligned} V_1^{n-1} &= [v_1, v_2, v_3, \dots, v_{n-1}], \\ V_2^n &= [v_2, v_3, v_4, \dots, v_n]. \end{aligned}$$

The calculation of the companion matrix C can be realized by two different approaches

(a) **QR decomposition:**

QR decomposition in economy mode needs to be performed:

$$[Q, R] = qr(V_1^{n-1}).$$

The companion matrix C is calculated by:

$$C = R^{-1}Q^H V_2^n$$

where Q^H symbolized the conjugate transpose of Q . The spectrum λ_j is computed by the eigenvalues of the companion matrix:

$$[X, D] = eig(C).$$

and is given by:

$$\lambda_j = \frac{\log D_j}{\Delta t},$$

where Δt is the time interval between the snapshots. Dynamic modes are given according to

$$DMD = V_1^{n-1} X.$$

(b) **SVD decomposition:**

SVD decomposition in economy mode needs to be performed:

$$[U, S, V] = svd(V_1^{n-1}).$$

The companion matrix C is calculated by:

$$C = U^H V_2^n V S^{-1}$$

where U^H symbolized the conjugate transpose of U . The spectrum λ_j is computed again by the eigenvalues of the companion matrix:

$$[X, D] = \text{eig}(C).$$

and is given by:

$$\lambda_j = \frac{\log D_j}{\Delta t},$$

where Δt is the time interval between the snapshots. Dynamic modes are given according to

$$DMD = UX.$$

A scaling can be achieved by the complex scalars.

B FURTHER ENHANCEMENTS OF PROPER ORTHOGONAL DECOMPOSITION REDUCED ORDER MODELS

B.1 MULTI VARIABLE EXPANSION BY TENSOR DECOMPOSITION

Construction of data-based expansions for multi variables $u^{(a)}(x,t), \dots, u^{(q)}(x,t)$, with space coordinates x and time variables t , can be realized in different ways. Fig. 4.3 illustrates different methods and is extended by tensor approaches in Fig. B.1.

Having a multi variable system, another choice of expansion applies tensor decomposition. Here, the decomposition is derived by applying higher-order singular value decomposition (HOSVD) or Tensor singular value decomposition (SVD). Note that the computation of the orthonormal bases is not straightforward. For the tensor approach of a decomposition of an order three tensor we refer to [136]. HOSVD is often applied in signal processing and considers an extension of the matrix SVD treating all possible unfoldings of tensors [74]. The multi-linear structure of the tensor is replaced by its unfoldings, e.g. a SVD is computed to each of these bilinear structures. The Tensor SVD [135] is an alternative for constructing a SVD for tensors using successive rank approximations and orthonormality constraint of the basis vectors. Note that the multi-linearity of the original tensor is retained during the decompositions. Both methods are computationally beneficial. They are independent of the choice of the inner product for each variable. The methods are less sensitive to the scaling of physical variables. Variable fields are not separated and hence their coupling are preserved.

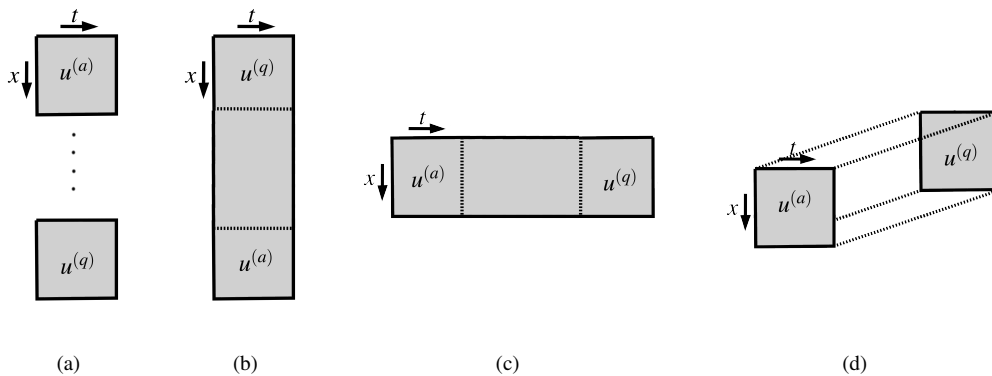


Figure B.1.: Different multivariable approaches: (a) single variable expansion, (b) lumped-variable expansion, (c) coupled variable expansion, (d) tensor approach of order three.

B.2 BOUNDARY CONDITIONS WITHIN A VARIATIONAL PROBLEM

Different forcing conditions can be included into a variational or Galerkin projected formulation by different ways. Preferred approaches are those leading to no additional unknowns within the system [143]:

Lagrange multiplier method The method of Lagrange multiplier is used generally in variational formulations but by the disadvantage of having additional unknowns.

Penalty method Loosing forcing conditions by including constitutive equations is well-known called "penalty method". This equals the idea of a regularization of the functional with penalty parameters having impact on the exactness of the contact. On the one hand, no additional unknown are included in the system, but on the other hand having penetration of i.e. normal conditions, leading to physically non-suitable conditions for small contact (penalty) parameters. Note that higher penalty parameters lead to ill-conditioned problems with numerical problems. A proportional-integral-derivative (PID)-controller-based penalty formulation might adapt the stiffness of the system matrix.

Augmented Lagrange method Having higher numerical effort, this method respects the forcing condition exactly.

Perturbed Lagrange method Stiff-contact laws can also be included by the perturbed Lagrange method. Also additional unknowns need to be treated due to the Lagrange multiplier.

Concludingly, with the attention of exact contact problems (forcing functions), one has the choice of treating the problems by additional Lagrange multiplier unknowns by the method of Lagrange multiplier respectively the perturbed Lagrange method or by additional computational effort using the Augmented-Lagrange-Method.

B.3 INNER PRODUCT CHOICES

Barone et al. [5], Kalashnikova and Barone [62] emphasized that for compressible Euler or Navier-Stokes equations the preferable inner product choice is of Sobolev inner product type. Tests need to be conducted if the standard L^2 inner product needs to be changed to a particular Sobolev norm H^1 within the Galerkin projection step to preserve stability for each equation system.

Stabilization might be achieved by Sobolev type inner products $\langle \cdot, \cdot \rangle_{H^1}$ with a Sobolev weight ε_1 and another weight ε_0 . The continuous Sobolev inner product will then be approximated by

$$\langle u, v \rangle_{H^1} = \varepsilon_0 \int_{\Omega} uvd\Omega + \varepsilon_1 \int_{\Omega} \nabla u \nabla v d\Omega \approx \varepsilon_0 \sum_{k=0}^N u(x_k)v(x_k) + \varepsilon_1 \sum_{k=0}^N \frac{du(x_k)}{dt} \frac{dv(x_k)}{dt},$$

where $x_0, \dots, x_N \in \Omega$ are spatial discretization points.

B.4 ALIASING

We suggest to include an error control checking non-linear terms projections at certain time-steps. Note that the following error control is a suggestion and not included yet. For a non-linear term

$\mathcal{N}(u, u, \dots)$ check whether

$$\langle \mathcal{N}(u, u, \dots), \phi_l \rangle = \langle \mathcal{N}(\sum_{i=1}^r \alpha_i \phi_i, \sum_{j=1}^r \alpha_j \phi_j, \dots), \phi_l \rangle \approx \langle \mathcal{N}(\sum_{i=1}^{r-1} \alpha_i \phi_i, \sum_{j=1}^{r-1} \alpha_j \phi_j, \dots), \phi_l \rangle \text{ for } l \leq r-1$$

If this criteria is violated than the low order approach will be limited such that higher order contributions will be set to zero:

$$\langle \mathcal{N}(\sum_{i=1}^r \alpha_i \phi_i, \sum_{j=1}^r \alpha_j \phi_j, \dots), \phi_l \rangle = \begin{cases} \langle \mathcal{N}(\sum_{i=1}^{r-1} \alpha_i \phi_i, \sum_{j=1}^{r-1} \alpha_j \phi_j, \dots), \phi_l \rangle & \text{for } l \leq r-1 \\ 0 & \text{for } l \leq r \end{cases}$$

For the anti-aliased Fourier Galerkin approach the criteria can be calculated to be $2/3$ of the reduction level. In case of the proper orthogonal decomposition (POD), this need to be checked more carefully due to their more general shape.

C REFORMULATION OF THE HOMOGENEOUS EQUILIBRIUM MODEL BASED ON AN AUXILIARY EQUATION

Taking the spatial derivative of the momentum Eq. (6.14) that have been implemented in COMSOL[®], interchanging the time and space derivative of the mass flux, and applying the mass conservation Eq. (6.13a) leads to a Poisson formulation of the pressure equation. This transport equation now includes the pressure variable and includes the formulation of mass conservation. Mathematical terms are well-known, however taking the time derivative leads to an inefficient formulation as all terms directly depend on enthalpy and especially $\frac{\partial^2 v}{\partial h^2}$ is not being given. In contrast of solving a non-physical pressure equation, this problem can also be dealt with an auxiliary equation for $(\partial h / \partial t) \cdot (\partial v / \partial h / v^2)$.

(1) **Non-physical pressure equation:**

Section 6.3.4 outlines the non-physical pressure equation.

(2) **Auxiliary equation:**

The right hand side of the mass conservation equation $(\partial h / \partial t) \cdot (\partial v / \partial h / v^2)$ is treated as supplementary variable \tilde{p}_d in an auxiliary equation. This gives the time transport of this supplementary variable.

$$\begin{aligned} \tilde{p}_d - \frac{\partial v / \partial h}{v^2} \frac{\partial h}{\partial t} &= 0, \\ \frac{\partial^2 p_d}{\partial x^2} + \frac{\partial}{\partial t} \tilde{p}_d + \frac{\partial}{\partial x} \left(\frac{g_{eff}}{v} + \frac{\xi}{D_H} \frac{v G^2}{2} \right) &= 0. \end{aligned}$$

An implicit solver, offering up to first order derivatives, is required for solving. However, this can be overcome with the help of the energy conservation:

$$\tilde{p}_d - \frac{\partial v / \partial h}{v^2} \left(-Gv \frac{\partial h}{\partial x} + v \frac{q'' P_H}{A_{x-s}} \right) = 0 \quad (C.1a)$$

$$\frac{\partial^2 p_d}{\partial x^2} + \frac{\partial}{\partial t} \tilde{p}_d + \frac{\partial}{\partial x} \left(\frac{g_{eff}}{v} + \frac{\xi}{D_H} \frac{v G^2}{2} \right) = 0 \quad (C.1b)$$

REFORMULATED HEM

The reformulation (2) has some favorable properties. The mass conservation is completely fulfilled in a spectral sense and additional iterations are not required. Moreover, this approach not necessarily needs proper orthogonal modes (POMs) of the auxiliary variable \tilde{p}_d that can be projected onto pressure modes. Hence, this approach is additionally to the pressure correction approach of the main Sec. 6.3.4 outlined here.

It consists of the pressure formulation with an auxiliary equation, the momentum equation Eq. (6.14),

the derived energy Eq. (6.13c) and a state formulation (see Sec. 6.2.1). In the following, the d within the dynamic pressure p_d is dropped for convenience:

$$\frac{\partial h}{\partial t} + Gv \frac{\partial h}{\partial x} - v \frac{q'' P_H}{A_{x-s}} = 0, \quad (\text{C.2a})$$

$$\frac{\partial G}{\partial t} + \frac{g_{eff}}{v} + \frac{\partial p}{\partial x} + \frac{\xi}{D_H} \frac{vG^2}{2} = 0, \quad (\text{C.2b})$$

$$\tilde{p} - \frac{\partial v / \partial h}{v^2} \left(-Gv \frac{\partial h}{\partial x} + v \frac{q'' P_H}{A_{x-s}} \right) = 0, \quad (\text{C.2c})$$

$$\frac{\partial^2 p}{\partial x^2} + \frac{\partial}{\partial t} \tilde{p} + \frac{\partial}{\partial x} \left(\frac{g_{eff}}{v} + \frac{\xi}{D_H} \frac{vG^2}{2} \right) = 0, \quad (\text{C.2d})$$

where $v = v(h)_p$.

Note that inlet and outlet local pressure losses as well as the convection term are substituted into the boundary condition. The model is subject to the following boundary conditions at inlet and outlet:

$$\begin{cases} p|_{x=0} = p_{in} + G^2 v + 0.5 \cdot K_{in} G^2 v, \\ p|_{x=1} = p_{in} - p_{loss} + G^2 v + 0.5 \cdot K_{out} G^2 v, \\ h|_{x=0} = h_{in}. \end{cases} \quad (\text{C.3})$$

HEM-POD-ROM SYSTEM

This subsection outlines the derived reduced order model (ROM) of the homogeneous equilibrium model (HEM).

The boundary conditions of Eq. (C.3) are imposed in the HEM-ROM version of Eq. (C.2) by a penalty formulation. Five constraints are formulated with the help of five penalty parameters ($\Gamma_{in}^h, \Gamma_{in}^p, \Gamma_{out}^p, \Gamma_{in}^G, \Gamma_{out}^G$) representing the inlet enthalpy, inlet and outlet pressure as well as deduced inlet and outlet mass flux boundaries. A penalty amplified weak formulation is applied as the mean mode is kept varying. Diffusion terms are in the projection replaced by their equivalent integration by parts formulation where their boundary parts are amplified by a penalty parameter. Penalty parameters are chosen such that exactness of the compliance of boundary conditions is guaranteed. This keep the system response numerically stable.

$$\begin{aligned} \frac{\partial h}{\partial t} + Gv \frac{\partial h}{\partial x} - v \frac{q'' P_H}{A_{x-s}} - \Gamma^h (h - h_{in}) \delta|_{x=0} &= 0, & (C.4a) \\ \frac{\partial G}{\partial t} + \frac{g_{eff}}{v} + \frac{\partial p}{\partial x} + \frac{\xi}{D_H} \frac{vG^2}{2} \\ - \Gamma^G \left(G - ((p-p_{in})/v(1+0.5 \cdot K_{in}))^{0.5} \right) \delta|_{x=0} \\ - \Gamma^G \left(G - ((p-p_{in}+p_{loss})/v(1+0.5 \cdot K_{out}))^{0.5} \right) \delta|_{x=L} &= 0, & (C.4b) \\ \tilde{p} - \frac{\partial v / \partial h}{v^2} \left(-Gv \frac{\partial h}{\partial x} + v \frac{q'' P_H}{A_{x-s}} \right) &= 0, & (C.4c) \\ \frac{\partial^2 p}{\partial x^2} + \frac{\partial}{\partial t} \tilde{p} + \frac{\partial}{\partial x} \left(\frac{g_{eff}}{v} + \frac{\xi}{D_H} \frac{vG^2}{2} \right) \\ - \Gamma_{in}^p (p - p_{in} - G^2 v - 0.5 K_{in} G^2 v) \delta|_{x=0} \\ - \Gamma_{in}^p (p - p_{in} + p_{loss} - G^2 v - 0.5 K_{out} G^2 v) \delta|_{x=L} &= 0, & (C.4d) \\ & \text{where } v = v(h)_p. \end{aligned}$$

Approximations of the variables h , G , p and \tilde{p} are given by a superposition of the temporal variation of their POMs:

$$\begin{aligned} h_{ROM} &= \sum_{i=1}^{r^h} \alpha_i^h \phi_i^h, \\ G_{ROM} &= \sum_{i=1}^{r^G} \alpha_i^G \phi_i^G, \\ p_{ROM} &= \sum_{i=1}^{r^p} \alpha_i^p \phi_i^p, \\ \tilde{p}_{ROM} &= \sum_{i=1}^{r^{\tilde{p}}} \alpha_i^{\tilde{p}} \phi_i^{\tilde{p}}. \end{aligned}$$

Insertion of these approximations into Eq. (C.4) and a Galerkin projection leads to a fully-coupled non-linear ordinary differential equation (ODE) system, the so-called HEM-proper orthogonal decomposition (POD)-ROM. Note that the mass conservation equation and the auxiliary equation is projected onto pressure modes, the momentum equation is mapped onto mass flux modes and the

energy equation onto enthalpy modes:

$$\begin{aligned}
 & \left\langle \frac{\partial h_{ROM}}{\partial t} + G_{ROM} v(h_{ROM}) \frac{\partial h_{ROM}}{\partial x} - v(h_{ROM}) \frac{q'' P_H}{A_{x-s}} \right. \\
 & \quad \left. - \Gamma^h (h_{ROM} - h_{in}) \delta \Big|_{x=0}, \phi_j^h \right\rangle = 0, \\
 & \quad j = 1, \dots, r^h \quad (C.5a)
 \end{aligned}$$

$$\begin{aligned}
 & \left\langle \frac{\partial G_{ROM}}{\partial t} + \frac{g_{eff}}{v(h_{ROM})} + \frac{\partial p_{ROM}}{\partial x} + \frac{\xi(h_{ROM}, G_{ROM}) v(h_{ROM}) G_{ROM}^2}{D_H} \right. \\
 & \quad \left. - \Gamma^G \left(G_{ROM} - ((p_{ROM} - p_{in}) / v(h_{ROM}) (1 - 0.5 \cdot K_{in}))^{0.5} \right) \delta \Big|_{x=0} \right. \\
 & \quad \left. - \Gamma^G \left(G_{ROM} - ((p_{ROM} - p_{in} + p_{loss}) / v(h_{ROM}) (1 - 0.5 \cdot K_{out}))^{0.5} \right) \right\rangle = 0, \\
 & \quad j = 1, \dots, r^G \quad (C.5b)
 \end{aligned}$$

$$\begin{aligned}
 & \left\langle \tilde{p}_{ROM} - \frac{\partial v(h_{ROM}) / \partial h_{ROM}}{v(h_{ROM})^2} \left(-G_{ROM} v(h_{ROM}) \frac{\partial h_{ROM}}{\partial x} + v(h_{ROM}) \frac{q'' P_h}{A_{x-s}} \right) \right\rangle = 0, \\
 & \quad j = 1, \dots, r^p \quad (C.5c)
 \end{aligned}$$

$$\begin{aligned}
 & \left\langle \frac{\partial^2 p_{ROM}}{\partial x^2} - \frac{\partial}{\partial t} \tilde{p}_{ROM} + \frac{\partial}{\partial x} \left(+ \frac{g_{eff}}{v(h_{ROM})} + \frac{\xi(h_{ROM}, G_{ROM}) v(h_{ROM}) G_{ROM}^2}{D_H} \right) \right. \\
 & \quad \left. - \Gamma_{in}^p (p_{ROM} - p_{in} + G_{ROM}^2 v(h_{ROM}) + K_{in} G_{ROM}^2 v(h_{ROM})) \delta \Big|_{x=0} \right. \\
 & \quad \left. - \Gamma_{in}^p (p_{ROM} - p_{in} + p_{loss} + G_{ROM}^2 v(h_{ROM}) + K_{out} G_{ROM}^2 v(h_{ROM})) \delta \Big|_{x=L} \right\rangle = 0, \\
 & \quad j = 1, \dots, r^p \quad (C.5d)
 \end{aligned}$$

where $v = v(h)_p$.

For reasons of simplification the derived system is only given without removing of offline costs.

This HEM-POD-ROM can now be solved within MATLAB[®] by ODE15I, an ODE multistep solver for fully implicit differential equations of variable ODE order, without an additional pressure correction scheme.

BIBLIOGRAPHY

- [1] F-Cobra-TF 1.7 Theory Manual.
- [2] Jean-Luc Achard, Donald A. Drew, and Richard T. Lahey. The analysis of nonlinear density-wave oscillations in boiling channels. Journal of Fluid Mechanics, 155:213–232, 1985. ISSN 1469-7645. doi: 10.1017/S0022112085001781. URL <http://dx.doi.org/10.1017/S0022112085001781>.
- [3] W. E. Arnoldi. The principle of minimized iterations in the solution of the matrix eigenvalue problem. Quarterly of Applied Mathematics, 9(17):17–29, 1951.
- [4] Nadine Aubry. On the hidden beauty of the proper orthogonal decomposition. Theoretical and Computational Fluid Dynamics, 2:339–352, 1991. ISSN 0935-4964. doi: 10.1007/BF00271473. URL <http://dx.doi.org/10.1007/BF00271473>.
- [5] Matthew F. Barone, Irina Kalashnikova, Daniel J. Segalman, and Heidi K. Thornquist. Stable Galerkin reduced order models for linearized compressible flow. Journal of Computational Physics, 228(6):1932 – 1946, April 2009. doi: 10.1016/j.jcp.2008.11.015. URL <http://dx.doi.org/10.1016/j.jcp.2008.11.015>.
- [6] A. Beisiegel, J. Kronenberg, and D. Kreuter. Expanding the Test Capabilities of the Multifunction Thermal Hydraulic Test Loop KATHY. In Annual Meeting on Nuclear Technology, pages 131 – 134, May 2006.
- [7] A.E. Bergles. Review of instabilities in two-phase systems. Two-phase flow and heat transfer, 2:382–422, 1977.
- [8] Christopher M. Bishop. Pattern Recognition and Machine Learning (Information Science and Statistics). Springer-Verlag New York, Inc., Secaucus, NJ, USA, 2006.
- [9] J.A. Bouré, A.E. Bergles, and L.S. Tong. Review of two-phase flow instability. Nuclear Engineering and Design, 25(2):165 – 192, 1973. doi: DOI:10.1016/0029-5493(73)90043-5. URL <http://www.sciencedirect.com/science/article/B6V4D-4816XW0-PW/2/e67d66dd77b0beb0154236f86b41f9ab>.
- [10] C. Bruneau and M. Saad. The 2D lid-driven cavity problem revisited. Computers and Fluids, 35(3):326–348, 2006. doi: 10.1016/j.compfluid.2004.12.004. URL <http://dx.doi.org/10.1016/j.compfluid.2004.12.004>.
- [11] A.G. Buchan, C.C. Pain, Fang F., and I.M. Navon. A POD reduced order model for eigenvalue problems with application to Reactor Physics. International Journal for Numerical Methods in Engineering, 2013.
- [12] C. Canuto. Spectral methods in fluid dynamics. Springer series in computational physics. Springer-Verlag, 1988. URL <http://books.google.de/books?id=SwgbAQAIAAJ>.

- [13] Yanhua Cao, Jiang Zhu, Zhendong Luo, and I.M. Navon. Reduced-Order Modeling of the Upper Tropical Pacific Ocean Model using Proper Orthogonal Decomposition. Computers & Mathematics with Applications, 52(8-9):1373 – 1386, 2006. doi: <http://dx.doi.org/10.1016/j.camwa.2006.11.012>. URL <http://www.sciencedirect.com/science/article/pii/S0898122106003245>.
- [14] Michael Cardiff and Peter K. Kitanidis. Efficient solution of nonlinear, underdetermined inverse problems with a generalized PDE model. Computers and Geosciences, 34(11):1480 – 1491, November 2008. doi: 10.1016/j.cageo.2008.01.013. URL <http://portal.acm.org/citation.cfm?id=1401275.1401597>.
- [15] Kevin Thomas Carlberg. Model Reduction of Nonlinear Mechanical Systems via Optimal Projection and Tensor Approximation. Stanford University, 2011.
- [16] W. Cazemier, R. W. C. P. Verstappen, and A. E. P. Veldman. Proper orthogonal decomposition and low-dimensional models for driven cavity flows. Physics of Fluids, 10(7):1685 – 1699, 1998. URL <http://scitation.aip.org/getabs/servlet/GetabsServlet?prog=normal&id=PHFLE600001000007001685000001&idtype=cvips&gifs=yes>.
- [17] Anindya Chatterjee. An introduction to the proper orthogonal decomposition. 2000. URL <http://www.iisc.ernet.in/currsci/apr102000/tutorial2.pdf>. Department of Engineering Science and Mechanics, Penn State University, University Park, Pennsylvania, PA, 16802, USA.
- [18] Kevin K. Chen, Jonathan H. Tu, and Clarence W. Rowley. Variants of Dynamic Mode Decomposition: Boundary Condition, Koopman and Fourier Analyses. Journal of nonlinear science, 22(6):887–915, 2012.
- [19] A.G. Class. Zellulare Strukturen laminarer Staupunktflammen. PhD thesis, Forschungszentrum Karlsruhe, 1995.
- [20] A.G. Class and D.P. Prill. Semi-automatic reduced order models from expert defined transients. In American Physical Society: 66th Annual Meeting of the APS Division of Fluid Dynamics, November 24-26 2013.
- [21] Alejandro Clausse and Lahey. The Analysis of Periodic and Strange Attractors during Density-wave Oscillations in Boiling Flows. Journal of Chaos, Solitons and Fractals, 1(2): 167 – 178, 1991.
- [22] C. Colebrook. Turbulent flow in pipes, with particular reference to the transition region between smooth and rough pipe laws. Journal of the Institution of Civil Engineers, 1939.
- [23] AB COMSOL. COMSOL Multiphysics - LiveLink for Matlab User’s Guide, COMSOL 4.3 edition, 2012.
- [24] AB COMSOL. COMSOL Multiphysics - Reference Guide, COMSOL 4.3 edition, 2012.
- [25] AB COMSOL. COMSOL Multiphysics - User’s Guide, COMSOL 4.3 edition, 2012.
- [26] C. Cuvelier, A. Segal, and A.A. van Steenhoven. Finite Element Methods and Navier-Stokes Equations. Mathematics and Its Applications. Springer, 1986. URL <http://books.google.de/books?id=cM4XYJ39mjAC>.

- [27] F. D'Auria, W. Ambrosini, T. Anegawa, J. Blomstrand, J. In De Betou, S. Langenbuch, T. Lefvert, and K. Valtonen. State of the Art Report on Boiling Water Reactor Stability. OECD/CSNI report (97) 13, OECD/GD, 1997. URL <http://www.oecd-nea.org/html/nsd/docs/1996/csni-r1996-21.pdf>.
- [28] A. Dhooge, W. Govaerts, and Yu. A. Kuznetsov. MatCont: A MATLAB package for numerical bifurcation analysis of ODEs. *ACM TOMS*, 29:141–164, 2003.
- [29] A. Dhooge, W. Govaerts, Yu. A. Kuznetsov, H.G.E. Meijer, and B. Sautois. New features of the software MatCont for bifurcation analysis of dynamical systems. *Mathematical and Computer Modelling of Dynamical Systems*, 14(2):147–175, 2008. doi: 10.1080/13873950701742754. URL <http://www.tandfonline.com/doi/abs/10.1080/13873950701742754>.
- [30] P. DiMarco, A. Clausse, and R.T. Lahey. An analysis of nonlinear instabilities in boiling systems. *Dynamics and Stability of Systems*, 6(3):191–216, 1991. URL <http://www.informaworld.com/10.1080/02681119108806116>.
- [31] E.J. Doedel and B.E. Oldeman. AUTO-07P: continuation and bifurcation software. 2012.
- [32] A. Dokhane. *BWR stability and bifurcation analysis using a novel reduced order model and the system code RAMONA*. PhD thesis, IPEP Institut de physique de l'énergie et des particules, Lausanne : EPFL, 2004. URL <http://library.epfl.ch/theses/?nr=2927>.
- [33] A. Dokhane, D. Hennig, R. Chawla, and Rizwan-uddin. Semi-analytical bifurcation analysis of two-phase flow in a heated channel. *International Journal of Bifurcation and Chaos*, 15(8):2395–2409, 2005. doi: 10.1142/S0218127405013381.
- [34] A. Dokhane, D. Hennig, Rizwan-uddin, and R. Chawla. Interpretation of in-phase and out-of-phase BWR oscillations using an extended reduced order model and semi-analytical bifurcation analysis. *Annals of Nuclear Energy*, 34(4):271 – 287, 2007. ISSN 0306-4549. doi: 10.1016/j.anucene.2006.12.005. URL <http://www.sciencedirect.com/science/article/pii/S0306454906002398>.
- [35] P.G. Drazin. *Solitons*. London Mathematical Society Lecture Note Series. Cambridge University Press, 1983. ISBN 9780521274227. URL <http://books.google.de/books?id=k77FbwAACAAJ>.
- [36] Juan Du, I.M. Navon, J.L. Steward, A.K. Alekseev, and Z. Luo. Reduced order modeling based on POD of a parabolized Navier-Stokes equations model I : Forward Model. *International Journal for Numerical Methods in Fluids*, 69(3):710–730, 2012.
- [37] V. Dykin, C. Demazière, C. Lange, and D. Hennig. Investigation of global and regional BWR instabilities with a four heated-channel Reduced Order Model. *Annals of Nuclear Energy*, 53(0):381 – 400, 2013. doi: 10.1016/j.anucene.2012.09.007. URL <http://www.sciencedirect.com/science/article/pii/S030645491200357X>.
- [38] M.Ö. Efe and H. Özbay. Proper orthogonal decomposition for reduced order modeling: 2D heat flow. In *2003 IEEE Conference on Control Applications (CCA)*, volume 2, pages 1273–1277, 2003. doi: 10.1109/CCA.2003.1223194.
- [39] M.Ö. Efe and H. Özbay. Low dimensional modelling and Dirichlet boundary controller design for Burgers equation. *International Journal of Control*, 77(10):895–906, 2004. doi: 10.1080/00207170412331270532. URL <http://www.tandfonline.com/doi/abs/10.1080/00207170412331270532>.

- [40] P. Ehrhard. Dynamisches Verhalten der Naturkonvektion in geschlossenen Kreisläufen. Number 4373 in KfK. Kernforschungszentrum Karlsruhe, April 1988. URL <http://books.google.de/books?id=dMpvGwAACAAJ>.
- [41] P. Ehrhard and U. Müller. Dynamical behaviour of natural convection in a single-phase loop. Journal of Fluid Mechanics, 217:487–518, 1990.
- [42] M. Farawila and D. W. Pruitt. A study of nonlinear oscillation and limit cycles in boiling water reactors - II: The regional mode. Nuclear Science and Engineering, 154:316–327, 2006.
- [43] Y. M. Farawila and D. W. Pruitt. A study of nonlinear oscillation and limit cycles in boiling water reactors - I: The global mode. Nuclear Science and Engineering, 154:302–315, 2006.
- [44] Dirk Klaus Feßler. Modellbasierte On-Board-Diagnoseverfahren für Drei-Wege-Katalysatoren. PhD thesis, Karlsruhe, 2011. URL <http://digbib.ubka.uni-karlsruhe.de/volltexte/1000020627>.
- [45] C. S. Gardner, J. M. Greene, M. D. Kruskal, and R. M. Miura. Korteweg-deVries equation and generalizations. VI. Methods for exact solution. Communications on Pure and Applied Mathematics, 27(1):97–133, 1974. ISSN 1097-0312. doi: 10.1002/cpa.3160270108. URL <http://dx.doi.org/10.1002/cpa.3160270108>.
- [46] C.S. Gardner, C.S. Greene, M.D. Kruskal, and R.M. Miura. Method for solving the korteweg-de vries equation. Physical Review Letters, 19:1095–1097, 1967.
- [47] X. Gloerfelt. Compressible proper orthogonal decomposition/Galerkin reduced-order model of self sustained oscillations in a cavity. Physics of Fluids, 20:0–0, 2008.
- [48] L. Gorbauch. Untersuchung eines HPLWR-Brennelements auf gekoppelte Thermohydraulische/ neutronische Stabilität. Master’s thesis, University of Karlsruhe, 2008.
- [49] P. Grandclément. Introduction to spectral methods. EAS Publications Series, 21:153–180, 1 2006. doi: 10.1051/eas:2006112. URL http://www.eas-journal.org/article_S1633476006001128.
- [50] Anne Greenbaum. Iterative methods for solving linear systems. Frontiers in applied mathematics. Society for industrial and applied mathematics, Philadelphia (US), 1997. URL <http://opac.inria.fr/record=b1103102>. Index.
- [51] S. Haaland. Simple and explicit formulas for the friction factor in turbulent flow. Trans. ASIVIE: Journal of Fluids Engineering, 103:89–90, 1983.
- [52] B. D. Hassard. A code for Hopf bifurcation analysis of autonomous delay differential systems. Oscillations, Bifurcations and Chaos, 8:447–463, 1987.
- [53] Sabrina Herkt. Model Reduction of Nonlinear Problems in Structural Mechanics: Towards a Finite Element Tyre Model for Multibody Simulation. PhD thesis, TU Kaiserslautern, 2008. URL <https://kluedo.ub.uni-kl.de/frontdoor/index/index/docId/2061>.
- [54] P. Holmes, J. L. Lumley, and Berkooz G. Turbulence, Coherent Structures, Dynamical Systems and Symmetry. Cambridge University Press, 1998.
- [55] E. Hopf. Abzweigung einer periodischen lösung von einer stationären lösung eines differential-systems. Berichte der mathematisch-physischen Klasse der sächsischen Akademie der Wissenschaften zu Leipzig, 94:1 – 22, 1942.

- [56] P. Hänggi. Investigating BWR stability with a new linear frequency-domain method and detailed 3D neutronics. PhD thesis, Swiss Federal Institute of Technology, Zurich ETHZ, 2001. URL <http://e-collection.ethbib.ethz.ch/view/eth:24620>.
- [57] S. Höttges. Numerische Untersuchung eines fluidischen Rückleitungssoszillators. PhD thesis, Universität Karlsruhe (TH), Fakultät für Maschinenbau, 2010.
- [58] Verein Deutscher Ingenieure. VDI-Wärmeatlas. Verlag des Vereins Deutscher Ingenieure (VDI-Verlag GmbH), 1900. URL <http://books.google.de/books?id=1FS81QEACAAJ>.
- [59] M. Ishii and N. Zuber. Thermally induced flow instabilities in two phase mixtures. In Heat Transfer Conference, volume 5 of Heat Transfer Conference, September 1970.
- [60] Mamoru Ishii. Thermally induced flow instabilities in two-phase mixtures in thermal equilibrium. Dissertation, Georgia Institute of Technology, August 1971. URL <http://smartech.gatech.edu/handle/1853/16452>.
- [61] S. Kakac and B. Bon. A review of two-phase flow dynamic instabilities in tube boiling systems. International Journal of Heat and Mass Transfer, 51(3-4):399 – 433, 2008. doi: DOI:10.1016/j.ijheatmasstransfer.2007.09.026. URL <http://www.sciencedirect.com/science/article/B6V3H-4RB5BNW-2/2/553fb38d8b5e4ec02b12d2887e7b414b>.
- [62] I. Kalashnikova and M. F. Barone. Efficient non-linear proper orthogonal decomposition/Galerkin reduced order models with stable penalty enforcement of boundary conditions. International Journal for Numerical Methods in Engineering, 90(11):1337–1362, 2012. doi: 10.1002/nme.3366. URL <http://dx.doi.org/10.1002/nme.3366>.
- [63] A.A. Karve, Rizwan-uddin, and J.J. Dorning. On spatial approximations for liquid enthalpy and two-phase quality during density-wave oscillations. Transactions of the American Nuclear Society, 22:533–535, 1994.
- [64] Atul A. Karve, Rizwan-uddin, and J.J. Dorning. Stability analysis of BWR nuclear-coupled thermal-hydraulics using a simple model. Nuclear Engineering and Design, 177(1-3):155 – 177, 1997. doi: 10.1016/S0029-5493(97)00192-1. URL <http://www.sciencedirect.com/science/article/pii/S0029549397001921>.
- [65] Michael Kirby. Minimal dynamical systems from pdes using sobolev eigenfunctions. Physica D: Nonlinear Phenomena, 57(3-4):466 – 475, 1992. ISSN 0167-2789. doi: 10.1016/0167-2789(92)90014-E. URL <http://www.sciencedirect.com/science/article/pii/016727899290014E>.
- [66] D.J. Korteweg and G. de Vries. On the change of form of long waves advancing in a rectangular canal, and on a new type of long stationary waves. Philosophical Magazine, 5(39): 422–443, 1895.
- [67] R. T. Lahey Jr. An application of fractal and chaos theory in the field of two-phase flow & heat transfer. Wärme - und Stoffübertragung, 26:351–363, 1991. ISSN 0042-9929. doi: 10.1007/BF01591668. URL <http://dx.doi.org/10.1007/BF01591668>.
- [68] R.T. Lahey Jr. and F.J. Moody. The thermal-hydraulics of a boiling water nuclear reactor. American Nuclear Society, La Grange Park, III, 2. ed. edition, 1993.
- [69] R.T. Lahey Jr., D.A. Drew, U.S. Nuclear Regulatory Commission. Division of Systems Safety, and Rensselaer Polytechnic Institute. Dept. of Nuclear Engineering. An Assessment of the Literature Related to LWR Instability Modes. Number v. 88. The Commission, 1980. URL <http://books.google.de/books?id=RubWtgAACAAJ>.

- [70] Carsten Lange. Remarks to a novel nonlinear BWR stability analysis approach (RAM-ROM methology). In Advances in Nuclear Fuel Management IV, Hilton Head Island, South Carolina, USA, April 12-15 2009. American Nuclear Society. URL http://tu-dresden.de/die_tu_dresden/fakultaeten/fakultaet_maschinenwesen/iet/wket/texte/Full_Paper_ANFM_Lange.pdf.
- [71] Carsten Lange. Advanced nonlinear stability analysis of boiling water nuclear reactors. PhD thesis, Technische Universität Dresden, 2009. URL <http://nbn-resolving.de/urn:nbn:de:bsz:14-qucosa-24954>.
- [72] Carsten Lange, D. Hennig, G. Verdu, and V. Garcia I Llorens. Advanced BWR stability analysis with a reduced order model and system code. In 15th International Conference on Nuclear Engineering, Nagoya, Japan, April 22-26 2007. URL http://tu-dresden.de/die_tu_dresden/fakultaeten/fakultaet_maschinenwesen/iet/wket/texte/Paper_ICONE15_Lange.pdf.
- [73] Carsten Lange, D. Hennig, and A. Hurtado. A new approach for BWR stability analysis. In Annual Meeting on Nuclear Technology, Dresden, Mai 12-14 2009. URL http://tu-dresden.de/die_tu_dresden/fakultaeten/fakultaet_maschinenwesen/iet/wket/texte/Lange_Jahrestagung_2009_neueVers1.pdf.
- [74] Lieven De Lathauwer, Bart De Moor, and Joos Vandewalle. A multilinear singular value decomposition. SIAM J. Matrix Anal. Appl., 21:1253–1278, 2000.
- [75] E. Laurien and H. Oertel. Numerische Strömungsmechanik : Grundgleichungen und Modelle Lösungsmethoden Qualität und Genauigkeit. Vieweg+Teubner Verlag / GWV Fachverlage GmbH, Wiesbaden, Wiesbaden, 3., vollständig überarbeitete und erweiterte Auflage edition, 2009.
- [76] Jianping Li. General explicit difference formulas for numerical differentiation. Journal of Computational and Applied Mathematics, 183(1):29–52, November 2005. doi: 10.1016/j.cam.2004.12.026. URL <http://dx.doi.org/10.1016/j.cam.2004.12.026>.
- [77] D.M. Luchtenburg, B.R. Noack, and M. Schlegel. An introduction to the POD Galerkin method for fluid flows with analytical examples and MATLAB source codes. Technical report, Berlin Institute of Technology, 2009. URL <http://berndnoack.com/publications/Luchtenburg2009romfc.PDF>.
- [78] J.L. Lumley. Stochastic Tools in Turbulence. Academic Press, 1971.
- [79] J. March-Leuba. Dynamic behavior of boiling water reactors. PhD thesis, Univ. of Tennessee, Knoxville, USA, 1984. URL http://www.osti.gov/energycitations/product.biblio.jsp?query_id=0&page=0&osti_id=5387978.
- [80] J. March-Leuba. Density wave instabilities in boiling water reactors. Technical report, NUREG/CR- 6003 ORNL/TM-12130, Oak Ridge National Laboratory, 1992.
- [81] J. March-Leuba and J. M. Rey. Coupled thermohydraulic-neutronic instabilities in boiling water nuclear reactors: a review of the state of the art. Nuclear Engineering and Design, 145(1-2):97 – 111, 1993. doi: DOI:10.1016/0029-5493(93)90061-D. URL <http://www.sciencedirect.com/science/article/B6V4D-4810YWT-1D9/2/9c26d4679b5845c8333cfa7903700ea2>.

- [82] J. March-Leuba, D.G. Cacuci, and R.B. Perez. Nonlinear dynamics and stability of boiling water reactors: Part1 - qualitative analysis. Nuclear Science and Engineering, 93:111–123, 1986.
- [83] J. March-Leuba, D.G. Cacuci, and R.B. Perez. Nonlinear dynamics and stability of boiling water reactors: Part 2-quantitative analysis. Nucl. Sci. Eng.:(United States), 93(2), 1986.
- [84] J. Marek, K. Rehme, and K. Maubach. Heat transfer and pressure drop performance of rod bundles arranged in square arrays. International Journal of Heat and Mass Transfer, 16(12):2215 – 2228, 1973. URL <http://www.sciencedirect.com/science/article/B6V3H-481MSKD-S3/2/bfcf408e8a069e9a6b6340e1388353ba>.
- [85] Matlab. R2012a. The MathWorks Inc., Natick, Massachusetts, 2012.
- [86] E. Merzari and H. Ninokata. Proper Orthogonal Decomposition of the flow in a tight lattice rod-bundle. Nuclear Engineering and Design, 241:4621–4632, 2011. doi: DOI:10.1016/j.nucengdes.2010.12.005. URL <http://www.sciencedirect.com/science/article/B6V4D-5230KJ9-1/2/15e07c8f8a6df9a9a1a4e7cdb23d61f7>.
- [87] E. Merzari, W. D. Pointer, and P. Fischer. Proper Orthogonal Decomposition of the Flow in a T-Junction. In International Congress on Advances in Nuclear Power Plants, volume 1, San Diego, California, USA, May 2010.
- [88] R. Miró, D. Ginestar, G. Verdú, and D. Hennig. A nodal modal method for the neutron diffusion equation. Application to BWR instabilities analysis. Annals of Nuclear Energy, 29(10):1171 – 1194, 2002. doi: 10.1016/S0306-4549(01)00103-7. URL <http://www.sciencedirect.com/science/article/pii/S0306454901001037>.
- [89] L.F. Moody. An approximate formula for pipe friction factors. Transactions of the ASME, 69:1005–1006, 1947.
- [90] Marek Morzyński, Bernd R. Noack, and Gilead Tadmor. Global flow stability analysis and reduced order modeling for bluff-body flow control. journal of theoretical and applied mechanics, 45:621, 2007.
- [91] Bernd R Noack, Konstantin Afanasiev, Marek Morzynski, Gilead Tadmor, and Frank Thiele. A hierarchy of low-dimensional models for the transient and post-transient cylinder wake. Journal of Fluid Mechanics, 497(1):335–363, 2003.
- [92] H. Oertel, M. Böhle, and L. Prandtl. Prandtl - Führer durch die Strömungslehre: Grundlagen und Phänomene. Studium und Praxis. Vieweg, Friedr., & Sohn Verlagsgesellschaft mbH, 2002. ISBN 9783528482091. URL <http://books.google.de/books?id=a2qVAAAAAAAJ>.
- [93] H. Oertel, M. Böhle, and U. Dohrmann. Strömungsmechanik : Grundlagen - Grundgleichungen - Lösungsmethoden - Softwarebeispiele. Studium. Vieweg + Teubner, Wiesbaden, 5., überarb. und erw. Aufl. edition, 2009.
- [94] T. Ortega Gómez, A. Class, R.T. Lahey Jr., and T. Schulenberg. Stability analysis of a uniformly heated channel with supercritical water. In 14th International Conference on Nuclear Engineering (ICONE-14), July 17-20 2006.
- [95] T. Ortega Gómez, A. Class, R.T. Lahey Jr., and T. Schulenberg. Density wave oscillations in coupled parallel channels under supercritical pressure conditions. Number 97, pages 867–68. Transactions of the American Nuclear Society, American Nuclear Society Winter Meeting, November 11-15 2007.

- [96] T. Ortega Gómez, A. Class, R.T. Lahey Jr., and T. Schulenberg. Stability analysis of heated flow channels with supercritical water. Shanghai, China, March 12-15 2007. 3rd International Symposium on Supercritical Water-Cooled Reactors - Design and Technology.
- [97] T. Ortega Gómez, A. Class, R.T. Lahey Jr., and T. Schulenberg. Stability analysis of a uniformly heated channel with supercritical water. Nuclear Engineering and Design, 238(8):1930 – 1939, 2008. doi: DOI:10.1016/j.nucengdes.2007.10.031. URL <http://www.sciencedirect.com/science/article/B6V4D-4S0PX97-1/2/5716d88ac27e058642574ec73c843893>.
- [98] Tino Ortega Gómez. Stability analysis of the high performance light water reactor. Technical Report FZKA 7432, Forschungszentrum Karlsruhe, 2009. URL <http://bibliothek.fzk.de/zb/berichte/FZKA7432.pdf>; <http://d-nb.info/994365624/34>; <http://nbn-resolving.de/urn:nbn:de:0005-074321>.
- [99] S.V. Patankar. Numerical Heat Transfer and Fluid Flow. Series in computational methods in mechanics and thermal sciences. Taylor & Francis, 1980. ISBN 9780891165224. URL <http://books.google.de/books?id=5JMYZMX30VcC>.
- [100] P. Pohl and F. Wehle. BWR stability: analysis of cladding temperature for high amplitude oscillations. In American Nuclear Society, Pittsburgh, Pennsylvania, USA, May 2010.
- [101] D.P. Prill and A.G. Class. Analysis of Non-linear BWR Stability Behavior Applying Proper Orthogonal Decomposition. In Annual Meeting on Nuclear Technology, Stuttgart, Germany, May 2012.
- [102] D.P. Prill and A.G. Class. Application of reduced order modeling to BWR fuel assemblies. In The 9th International Conference on Nuclear Thermal Hydraulics, Operations and Safety (NUTHOS-9), Kaohsiung, Taiwan, September 2012.
- [103] D.P. Prill and A.G. Class. Progress of non-linear proper orthogonal decomposition reduced order modeling for BWR fuel assemblies. In European Nuclear Conference (ENC), Manchester, United Kingdom, December 2012. URL <http://www.euronuclear.org/events/enc/enc2012/transactions/ENC2012-transactions-plant-operations.pdf>.
- [104] D.P. Prill and A.G. Class. Non-linear Proper Orthogonal Decomposition Reduced Order Modeling: Bifurcation Study of a Natural Convection Circuit. Proceedings in Applied Mathematics and Mechanics (PAMM), 13, 2013.
- [105] D.P. Prill and A.G. Class. Semi-automated POD-ROM non-linear analysis for future BWR stability analysis. Annals of Nuclear Energy, 2013. URL <http://www.sciencedirect.com/science/article/pii/S0306454913006063>.
- [106] D.P. Prill and A.G. Class. Predictions by the Proper Orthogonal Decomposition reduced order methodology regarding non-linear BWR stability. In Annual Meeting on Nuclear Technology, Berlin, Germany, May 2013.
- [107] D.P. Prill and A.G. Class. Verification of non-linear Proper Orthogonal Decomposition Reduced Order Modeling for BWR Fuel Assemblies. In 21th International Conference on Nuclear Engineering (ICONE21), number 16434, Chengdu, China, July 29- August 2 2013.
- [108] D.P. Prill, A.G. Class, and M. Stokmaier. Methodology of reduced order modeling applying proper orthogonal decomposition of BWR fuel assemblies applied to introductory examples. Proceedings in Applied Mathematics and Mechanics (PAMM), 12 (1), 2012. URL <http://onlinelibrary.wiley.com/doi/10.1002/pamm.201210109/abstract;jsessionid=A83C749FD1BEA6E9C1DBFB1826530167.d04t03>.

- [109] D.P. Prill, A.G. Class, and M.J. Stokmaier. Report on grid-free pool model. In Thermal Hydraulics of Innovative Nuclear Systems (THINS) WP2 - Deliverable D2.1.07, 2013.
- [110] D.P. Prill, A.G. Class, and M.J. Stokmaier. On Grid-free pool models using proper orthogonal decomposition based reduced order models. In International Workshop on Thermal Hydraulics of Innovative Nuclear Systems (THINS), Modena, Italy, January 20-22 2014. (abstract accepted).
- [111] Muruhan Rathinam and Linda R. Petzold. A new look at proper orthogonal decomposition. SIAM Journal on Numerical Analysis, 41(5):1893–1925, 2003.
- [112] Rizwan-Uddin and Dorning. Some Nonlinear Dynamics of a Heated Channel. Nucl. Eng. Des., 93:1–14, 1986.
- [113] Clarence W. Rowley, I. Mezic, Shervin Bagherin, Philipp Schlatter, and Dan S. Hennigson. Spectral analysis of nonlinear flows. Journal of Fluid Mechanics, 641:115–127, 2009. doi: 10.1017/S0022112009992059. URL <http://journals.cambridge.org/action/displayFulltext?type=1&fid=6837880&jid=FLM&volumeId=641&issueId=-1&aid=6837872&bodyId=&membershipNumber=&societyETOCSession=>.
- [114] J. Scott Russell. Report on waves. Report of the fourteenth meeting of the British Association for the Advancement of Science, pages 311–390, September 1844.
- [115] P. Saha and N. Zuber. An analytical study of the thermally induced two-phase flow instabilities including the effect of thermal non-equilibrium. International Journal of Heat and Mass Transfer, 21(4):415 – 426, 1978. ISSN 0017-9310. doi: DOI:10.1016/0017-9310(78)90075-3. URL <http://www.sciencedirect.com/science/article/B6V3H-47YS98J-9Y/2/9f2ec42f0ddb457bf600e2a858296424>.
- [116] P. Saha, M. Ishii, and N. Zuber. An experimental investigation of the thermally induced flow oscillations in two-phase systems. Journal of Heat Transfer, 98(4):616–622, 1976. doi: 10.1115/1.3450609. URL <http://link.aip.org/link/?JHR/98/616/1>.
- [117] Wilhelmus H. Schilders, Henk A. van der Vorst, and Joost Rommes. Model Order Reduction: Theory, Research Aspects and Applications. Mathematics in Industry, The European Consortium for Mathematics in Industry ; 13. Springer, Berlin, Heidelberg, 2008. URL <http://dx.doi.org/10.1007/978-3-540-78841-6>.
- [118] P. Schmid, L. Li, M. Juniper, and O. Pust. Applications of the dynamic mode decomposition. Theoretical and Computational Fluid Dynamics, pages 1–11, 2010. URL <http://dx.doi.org/10.1007/s00162-010-0203-9>. 10.1007/s00162-010-0203-9.
- [119] P.J. Schmid. Dynamic Mode Decomposition of experimental data. 8th international symposium on particle image velocimetry, 2009.
- [120] P.J. Schmid. Dynamic mode decomposition of numerical and experimental data. Journal of Fluid Mechanics, 656:5–28, 2010. doi: 10.1017/S0022112010001217. URL <http://dx.doi.org/10.1017/S0022112010001217>.
- [121] P.J. Schmid and O. Pust. Stability Analysis of Experimental Data using Dynamic Mode Decomposition. Fachtagung Lasermethoden in der Strömungsmesstechnik, September 2009. URL http://www.oliver-pust.de/Veroffentlichungen/Pust_GALA_2009.pdf.
- [122] P.J. Schmid and O. Pust. PIV- and image-based flow analysis of a steady and pulsed jet using Dynamic Mode Decomposition. 8th international symposium on particle image velocimetry, 2009. URL http://www.oliver-pust.de/PIV09-0129_Schmid_Pust.pdf.

- [123] P.J. Schmid, K. E. Meyer, and O. Pust. Dynamic Mode Decomposition and Proper Orthogonal Decomposition of flow in a lid-driven cylindrical cavity. 8th international symposium on particle image velocimetry, 2009. URL http://www.oliver-pust.de/PIV09-0186_Schmid_Meyer_Pust.pdf.
- [124] P.J. Schmid, D. Violato, O. Pust, and F. Scarano. Decomposition of time-resolved tomographic PIV. 15th International Symposium on applications of laser techniques to fluid mechanics, 2010. URL http://ltces.dem.ist.utl.pt/lxllaser/lxllaser2010/upload/1647_bufbvd_3.7.1.Full_1647.pdf.
- [125] A. Schmidt, F. Wehle, S. Opel, and R. Velten. Advanced methods for BWR transient and stability analysis. In International Youth Nuclear Congress (INYC), Interlaken, Switzerland, September 2008.
- [126] T. Schulenberg. Kernkraftwerkstechnik. lecture notes, 2010.
- [127] F. Selimefendigil and W. Polifke. Non-Linear, Low-Order Model of Heat Transfer in Pulsating Flow based on Proper Orthogonal Decomposition. SFB-TR40 Jahresbericht, 2009.
- [128] Jonathon Shlens. A Tutorial on Principal Component Analysis. Technical report, Center for Neural Science, New York University and Systems Neurobiology Laboratory, Salk Institute for Biological Studies La Jolla, 2009. URL <http://www.sn1.salk.edu/~shlens/pca.pdf>.
- [129] L. Sirovich. Turbulence and the dynamics of coherent structures. i - coherent structures. ii - symmetries and transformations. iii - dynamics and scaling. Quarterly of Applied Mathematics, 45:561–571, 1987.
- [130] K. Solberg. Resultats des essais d'instabilités sur la boucle culine et comparaisons avec code de calcul. Technical Report 225, Centre d'Etudes Nucleaires de Grenoble, 1966.
- [131] Stefan J. Spronkman and P.P.J. van den Bosch. Comsol and Model Order Reduction by Proper Orthogonal Decomposition. Technical report, Technical University of Eindhoven, 2010. URL <http://alexandria.tue.nl/repository/books/708983.pdf>.
- [132] Thomas Steinbacher. Entwicklung und Simulation eines reduzierten Modells zur Beschreibung strömungsinduzierter Oberflächenwellen mittels der Proper Orthogonal Decomposition. Master's thesis, Karlsruhe Institute of Technology, 2012.
- [133] S. Tirunagari, V. Vuorinen, O. Kaario, and M. Larmi. Analysis of Proper Orthogonal Decomposition and Dynamic Mode Decomposition on LES of Subsonic Jets. CSI Journal of Computing, 1(3):20–26, 2012.
- [134] Mujid S. Todreas, Neil E. ; Kazimi. Nuclear systems, volume 1: Thermal hydraulic fundamentals. Taylor & Francis, New York [u.a.], 1990.
- [135] F. van Belzen, S. Weiland, and J. de Graaf. Singular value decompositions and low rank approximations of multi-linear functionals. Proceedings of the 46th Conference on Decision and Control, pages 3751–3756, December 2007.
- [136] F. van Belzen, S. Weiland, and L. Ozkan. Model reduction of multi-variable distributed systems through empirical projection spaces. In Joint 48th IEEE Conference on Decision and Control and 28th Chinese Control Conference, pages 5351–5356, Shanghai, China, December 2009. doi: 10.1109/CDC.2009.5400940. URL <http://dx.doi.org/10.1109/CDC.2009.5400940>.

-
- [137] S. Volkwein. Proper orthogonal decomposition and singular value decomposition. Technical report, University of Graz, 1999.
- [138] S. Volkwein. Numerische Verfahren der restringierten Optimierung. scriptum, 2009. URL <http://www.uni-graz.at/imawww/volkwein/Optimierung2.pdf>.
- [139] Wolfgang Wagner and Hans-Joachim Kretzschmar. International steam tables : properties of water and steam based on the industrial formulation IAPWS-IF97; tables, algorithms, diagrams, and CD-ROM Electronic steam tables; all of the equations of IAPWS-IF97 including a complete set of supplementary backward equations for fast calculations of heat cycles, boilers, and steam turbines. Springer, Berlin, 2. ed. edition, 2008.
- [140] F. Wehle, S. Opel, and R. Velten. Framatome ANP's experience in european BWRs with 3D transient analyses. In NURETH-11, number 541, Avignon, France, October 2005.
- [141] F. Wehle, A. Schmidt, S. Opel, and R. Velten. Non-Linear BWR Stability Analysis. In 16th International Conference on Nuclear Engineering (ICONE16), pages 121–128, Orlando, Florida, USA, May 2008. doi: <http://dx.doi.org/10.1115/ICONE16-48395>. URL <http://link.aip.org/link/abstract/ASMECP/v2008/i48140/p121/s1>.
- [142] F. Wehle, R. Velten, J. Kronenberg, A. Beisiegel, D. Pruitt, K. Greene, and Y. Farawila. Full Scale Stability and Void Fraction Measurements for the Atrium-10XM BWR Fuel Bundle. In Annual Meeting on Nuclear Technology, May 2011.
- [143] K. Willner. Kontinuums- und Kontaktmechanik: Synthetische und analytische Darstellung. Engineering online library. Springer, 2003. ISBN 9783540435297. URL <http://books.google.de/books?id=R8HXIEjRHHUC>.
- [144] Martin Wlotzka. Modellreduktion instationärer Strömungsvorgänge mit der Proper Orthogonal Decomposition Methode. Master's thesis, Karlsruhe Institute of Technologie, 2010.
- [145] Inc. Wolfram Research. Mathematica. Version 8.0. Wolfram Research Inc., Champaign, Illinois, 2010.
- [146] Frank Wols. Transient analyses of accelerator driven systems using modal expansion techniques. Master's thesis, Delft University of Technology, 2010.
- [147] D. Xiao, F. Fang, J. Du, C.C. Pain, I.M. Navon, A.G. Buchan, A.H. ElSheikh, and G. Hu. Non-Linear Petrov-Galerkin Methods for Reduced Order Modelling of the Navier-Stokes Equations using a Mixed Finite Element Pair. Computer Methods in Applied Mechanics and Engineering, (0):–, 2012. ISSN 0045-7825. doi: 10.1016/j.cma.2012.11.002. URL <http://www.sciencedirect.com/science/article/pii/S0045782512003404>.
- [148] Bill Hu Xinya Li, Xiao Chen and I.M. Navon. Model Reduction of A Coupled Numerical Model Using Proper Orthogonal Decomposition. Submitted to Water Resources Research, 2011.
- [149] N. J. Zabusky and M. D. Kruskal. Interaction of "solitons" in a collisionless plasma and the recurrence of initial states. Physical Review Letters, 15:240–243, 1965.